



UNIVERSITEIT VAN PRETORIA
UNIVERSITY OF PRETORIA
YUNIBESITHI YA PRETORIA

**INVESTIGATING THE RELATIONSHIP BETWEEN
SUCTION IN CEMENT PASTE AND SPECIFIC
CONCRETE PROPERTIES**

MARIESA SCHOEMAN

A dissertation submitted in partial fulfilment of the requirements for the degree of

MASTER ENGINEERING (STRUCTURAL ENGINEERING)

In the

FACULTY OF ENGINEERING

UNIVERSITY OF PRETORIA

PROJECT REPORT SUMMARY

**INVESTIGATING THE RELATIONSHIP BETWEEN
SUCTION IN CEMENT PASTE AND SPECIFIC
CONCRETE PROPERTIES**

M.SCHOEMAN

Supervisor: Professor EP Kearsley

Department: Civil Engineering

University: University of Pretoria

Degree: Masters of Engineering (Structural Engineering)

Summary

The Soil Water Retention Curve (SWRC) of different soils has been researched thoroughly by multiple Geotechnical Engineers. The interpretation of the SWRC for a specific soil leads to the identification of certain properties of the soil. The SWRC typically involves a plot of suction measurements (on a logarithmic scale) against the volumetric water content or degree of saturation of the soil. This project aims to determine a manner in which concrete properties (such as durability, porosity, shrinkage, strength and stiffness) can be estimated through suction measurements.

The Dew Point Potential Meter (WP4C) apparatus was used to measure the suctions of different concrete mixtures, as well as to derive the water retention curve of concrete. A cement paste study was first conducted to determine whether this apparatus is able to deliver representative results, which it is. It was discovered that the water retention curve of concrete is similar to a bimodal SWRC identified by Geotechnical Engineers. Thereafter, a mortar study was completed to determine if the water retention curves can be used to estimate different concrete properties. Three different porosity tests were investigated during this research study, namely the X-ray test, the Mercury Intrusion Porosimetry (MIP) test and a simple test method described in the durability index testing procedure manual assembled by

M.Schoeman

University of Cape Town, University of the Witwatersrand and CoMSIRU. It was concluded that the MIP test and the simple test method described in the durability index testing procedure manual gave the most comparable results with regards to literature. The shrinkage of the concrete mixture was investigated to determine a relationship between the suctions and the shrinkage of the concrete. Different strength tests of all the concrete mixtures were also investigated, namely the flexural test, the compressive test, the splitting cylinder test and the E-value test (stiffness).

It was concluded that there was a definite trend between the suction measurements and the specific concrete properties tested. The water retention curve has the potential to describe various properties of different concrete mixtures.


DECLARATION

I, the undersigned hereby declare that:

- I understand what plagiarism is and I am aware of the University's policy in this regard;
- The work contained in this thesis is my own original work;
- I did not refer to work of current or previous students, lecture notes, handbooks or any other study material without proper referencing;
- Where other people's work has been used this has been properly acknowledged and referenced;
- I have not allowed anyone to copy any part of my thesis;
- I have not previously in its entirety or in part submitted this thesis at any university for a degree.

DISCLAIMER:

The work presented in this report is that of the student alone. Students were encouraged to take ownership of their projects and to develop and execute their experiments with limited guidance and assistance. The content of the research does not necessarily represent the views of the supervisor or any staff member of the University of Pretoria, Department of Civil Engineering. The supervisor did not read or edit the final report and is not responsible for any technical inaccuracies, statements or errors. The conclusions and recommendations given in the report are also not necessarily that of the supervisor, sponsors or companies involved in the research.

Signature of student: 

Name of student: MARIESA SCHOEMAN

Student number: 15001335

Date: 23/08/2020

Number of words in report: 32603 words

ACKNOWLEDGEMENTS

I wish to express my appreciation to the following organisations and persons who made this project report possible:

- a) My supervisor, Professor EP Kearsley for the guidance and support. Permission to use the materials are gratefully acknowledged.
- b) Dr. Frikkie de Beer for making it possible to perform porosity tests and analysis at the South African Nuclear Energy Corporation (NECSA).
- c) The University of Pretoria for the use of the laboratory facilities during the course of the research study.
- d) The following persons are gratefully acknowledged for their assistance during the course of the study:
 - Mr. Scholtz
 - Mr. Mostert
 - And all other workers in the laboratory who assisted
- e) My family for their encouragement and support during the study.

TABLE OF CONTENTS

1	INTRODUCTION	1-1
1.1	Background.....	1-1
1.2	Objectives of the study	1-2
1.3	Scope of the study.....	1-3
1.4	Methodology.....	1-4
1.5	Organisation of the report.....	1-5
2	LITERATURE REVIEW.....	2-1
2.1	Introduction	2-1
2.2	Geotechnical background on suction measurements	2-1
2.2.1	Pore-water suction in soils.....	2-6
2.2.2	Shear strength and the Soil Water Retention curve	2-7
2.2.3	Humidity control.....	2-11
2.3	Current research on suction in concrete.....	2-12
2.4	Concrete properties.....	2-16
2.5	Pore structure of concrete	2-19
2.5.1	Scanning electron microscopy (SEM).....	2-24
2.5.2	X-ray microtomography	2-26
2.5.3	Mercury intrusion porosimetry (mip)	2-31
2.5.4	Gas adsorption technique for measuring porosity	2-33
2.5.5	Concrete sorptivity and porosity test	2-35
2.6	Shrinkage of concrete	2-36
2.6.1	Drying shrinkage	2-37
2.7	Strength of concrete.....	2-40
2.7.1	Flexural tests.....	2-43
2.7.2	Compressive tests	2-44
2.7.3	Splitting test.....	2-45
2.8	SUMMARY.....	2-45
3	EXPERIMENTAL WORK	3-1
3.1	Introduction	3-1
3.2	Dew point potentiometer.....	3-1
3.3	Cement paste testing.....	3-3

3.3.1	Cement paste testing Methodology.....	3-3
3.3.2	Sample preparation and suction measurements	3-4
3.3.3	Cement paste results	3-6
3.3.4	Cement paste study conclusions	3-12
3.4	Mortar study methodology	3-13
3.4.1	Concrete slump flow.....	3-17
3.4.2	Suction measurements	3-18
3.4.3	Porosity analysis	3-19
3.4.4	Shrinkage test	3-25
3.4.5	Mechanical properties.....	3-26
4	RESULTS AND DATA ANALYSIS.....	4-1
4.1	Introduction	4-1
4.1.1	Concrete slump flow.....	4-1
4.2	Water retention curves (wrc) / suction results	4-2
4.2.1	Discussion of the water retention curves	4-9
4.3	Porosity results	4-10
4.3.1	X-ray microtomography results.....	4-10
4.3.2	Mercury intrusion porosimetry (mip) results.....	4-18
4.3.3	Simple sorptivity and porosity test results	4-19
4.3.4	Discussion of the porosity results	4-22
4.4	Shrinkage results.....	4-23
4.5	Mechanical properties.....	4-27
4.5.1	Flexural test results.....	4-27
4.5.2	Compressive test results	4-29
4.5.3	Splitting cylinder test results	4-32
4.5.4	E-value test results.....	4-33
4.5.5	Discussion of the mechanical property results	4-35
4.6	Discussion of the overall combined results	4-35
4.6.1	Relationship between suctions & slump flow.....	4-36
4.6.2	Relationship between suctions & porosity.....	4-37
4.6.3	Relationship between suctions & shrinkage	4-38
4.6.4	Relationship between suctions, strength and stiffness.....	4-39
4.7	Summary of observed trends	4-42
5	CONCLUSIONS AND RECOMMENDATIONS.....	5-1
5.1	Conclusions	5-1

5.2	Recommendations.....	5-2
6	REFERENCES	6-1

APPENDIX A: CEMENT PASTE STUDY SUCTION RESULTS

APPENDIX B: PARTICLE SIZE DISTRIBUTION INFORMATION

APPENDIX C: DETAILED PROCEDURE OF THE X-RAY TEST SAMPLE ANALYSIS

APPENDIX D: MORTAR STUDY SUCTION RESULTS

APPENDIX E: X-RAY RESULTS (IMAGES)

APPENDIX F: X-RAY RESULTS (GRAPHS)

APPENDIX G: X-RAY RESULTS (MATLAB SCRIPT)

APPENDIX H: MIP RESULTS

APPENDIX I: SHRINKAGE RESULTS

APPENDIX J: GRAPHS ILLUSTRATING THE E-VALUES

LIST OF TABLES

Table 2-1: Summary of the different concrete mixtures (Pap et al., 2018).....	2-12
Table 2-2: Concrete mix design (Li and Yao, 2001).	2-39
Table 3-1: Mix design used in the cement paste testing.	3-4
Table 3-2: Average flexural and compressive strength after 7 Days.	3-12
Table 3-3: Mix design used for mortar mixtures.	3-13
Table 4-1: Results of the slump flow test.	4-1
Table 4-2: Sample names and description used in all the graphs.	4-2
Table 4-3: Porosity results from the X-Ray tests.	4-11
Table 4-4: Fitted function and parameters of oversize air void diameter distribution at 7 days.....	4-17
Table 4-5: Fitted function and parameters of oversize air void diameter distribution at 28 days.....	4-18
Table 4-6: Porosity results obtained for the MIP test.	4-18
Table 4-7: Dry and wet samples sorptivity results.	4-19
Table 4-8: Dry and wet samples porosity results.	4-20
Table 4-9: Correlation coefficient R^2 of the dry and wet samples.	4-20
Table 4-10: Porosity % results of three wet samples at 28 days.....	4-22
Table 4-11: Mortar prism beams flexural strength after 7 days.....	4-28
Table 4-12: Mortar prism beams flexural strength after 14 days.....	4-28
Table 4-13: Mortar prism beams flexural strength after 28 days.....	4-28
Table 4-14: Mortar prism beams compressive strength after 7 days.	4-30
Table 4-15: Mortar prism beams compressive strength after 14 days.	4-30
Table 4-16: Mortar prism beams compressive strength after 28 days.	4-30
Table 4-17: Dry cylinders compressive strength after 28 days.....	4-31
Table 4-18: Splitting cylinder tensile strength results at 28 days.	4-33
Table 4-19: Modulus of elasticity at 28 days for the cylindrical samples.	4-34
Table 4-20: Suction measurements of sample number 3 for all w/c ratios.....	4-36

LIST OF FIGURES

Figure 2-1: SWRC for a sandy, silty and clayey soil (Fredlund and Xing, 1994b).....	2-1
Figure 2-2: Features of the SWRC (Fredlund and Xing, 1994b).....	2-2
Figure 2-3: Three distinct zones of a typical water retention curve (Fredlund et al., 2011).....	2-3
Figure 2-4: Characteristics of a bimodal water retention curve (Satyanaga et al., 2013).....	2-3
Figure 2-5: Bimodal and unimodal pore size distribution and structure characteristics (Satyanaga et al., 2013).....	2-4
Figure 2-6: SWRC of the volumetric water content versus the matric suction (Lu and Likos, 2006).	2-5
Figure 2-7: Soil Water Retention Curves of volumetric water content and matric suction versus suction stress (Lu and Likos, 2006).	2-5
Figure 2-8: Matric suction against degree of saturation (Fredlund et al., 1995).....	2-8
Figure 2-9: Matric suction against the shear strength of a soil (Fredlund et al., 1995).	2-9
Figure 2-10: SWRC for compacted till sample (Fredlund et al., 1995).....	2-10
Figure 2-11: Shear strength with matric suction, comparison of different experimental models (Fredlund et al., 1995).	2-10
Figure 2-12: The fitted Water Retention Curves (Pap et al., 2018).....	2-14
Figure 2-13: The predicted and measured relative permeability function for light clay by Fredlund et al. (2012), data from Moore (1939).....	2-15
Figure 2-14: Relative permeability function for C1 concrete mixture (Pap et al., 2019).	2-16
Figure 2-15: Illustration of the hydration process of a single grain of Portland cement (Domone and Illston, 2010).....	2-17
Figure 2-16: The typical rate of reaction of hydration in cement paste at constant temperatures (Forester, 1970).....	2-18
Figure 2-17: Volumetric composition of hydrated hardened cement paste after storage in water (Hansen, 1970).....	2-18
Figure 2-18: Schematic representation of the structure of hardened concrete (Atahan et al., 2009).	2-19
Figure 2-19: Stable and unstable menisci in a pore by Martys and Ferraris (1997).	2-20

Figure 2-20: Penetration profiles for water, during capillary suction after storage at RH between 50 and 80% (Rucker-Gramm, 2010).	2-22
Figure 2-21: Effect of initial degree of saturation on water uptake of concrete (Rucker-Gramm, 2010).	2-23
Figure 2-22: Multilayer adsorption and capillary condensation in graded cylindrical pores schematic illustration (Zeng and Xu, 2015).....	2-24
Figure 2-23: The original Haley grain (Diamond, 1999).....	2-25
Figure 2-24: Secondary electron SEM analysis on a 1 day old, w/c ratio 0.5 cement paste (Diamond, 1999).....	2-25
Figure 2-25: Secondary electron SEM analysis showing the early stage with a thicker shell generated of hollow shell hydration (Diamond, 1999).....	2-25
Figure 2-26: Backscatter SEM showing the pores derived from the hollow shell hydration after 3 days by Diamond (1999).....	2-26
Figure 2-27: X-ray machine at the MIXRAD facility (De_Beer, 2012).....	2-27
Figure 2-28: Tomographic process of the X-Ray machine at the MIXRAD facility (De_Beer, 2012).	2-28
Figure 2-29: Tomographic slice of a small mortar sample (Lu et al., 2006).	2-28
Figure 2-30: 3D Representation of tomographic data (Lu et al., 2006).....	2-29
Figure 2-31: Pixel intensity of the images (Lu et al., 2006).	2-30
Figure 2-32: Greyscale images (Lu et al., 2006).	2-30
Figure 2-33: Comparison between a slow and fast scan on the void size of a concrete sample (Du Plessis et al., 2016).	2-31
Figure 2-34: Void diameter as a function of sphericity (Du Plessis et al., 2016).....	2-31
Figure 2-35: Porosity of different cement pastes determined with MIP (Hou et al., 2019).....	2-33
Figure 2-36: Illustration of the gas adsorption technique (Norcross, 1877).	2-34
Figure 2-37: Types of isotherms (left graph) and hysteresis loops (right graph) by Sing (1985).....	2-35
Figure 2-38: Filter paper test setup (University of Cape Town et al., 2017).	2-36
Figure 2-39: Vacuum saturation setup (University of Cape Town et al., 2017).....	2-36
Figure 2-40: Schematic of types of water within calcium silica hydrate (Feldman and Sereda, 1970)..	2-37

Figure 2-41: Effect of the cement, water content and w/c ratio on shrinkage of concrete – moist curing for 28 days followed by drying for 450 days (Shoya, 1979).	2-38
Figure 2-42: Drying shrinkage test results (Li and Yao, 2001).	2-39
Figure 2-43: Development of the hydration products of Portland cement (Soroka, 1979b).....	2-40
Figure 2-44: Development of strength of compounds in Portland cement on hydration (Bogue, 1955).	2-40
Figure 2-45: Demonstration of the Stefan effect (Wang et al., 2009).	2-41
Figure 2-46: Compressive strength versus porosity (Chen et al., 2013).....	2-42
Figure 2-47: Flexural strength versus porosity (Chen et al., 2013).	2-42
Figure 2-48: Splitting tensile strength versus porosity (Chen et al., 2013).	2-43
Figure 2-49: Three and four point bending tests.....	2-43
Figure 2-50: Cracking patterns during testing of concrete samples in compression (Soutsos and Domone, 2017).	2-44
Figure 2-51: Cylinder splitting tensile strength test setup.	2-45
Figure 3-1: The WP4C apparatus measuring suction.	3-1
Figure 3-2: WP4C view of the inside block.	3-3
Figure 3-3: PSD plot of the cement used in the cement paste study.....	3-4
Figure 3-4: Sample preparation steps before suction measurements.	3-5
Figure 3-5: Suction measurements for w/c ratio 0.3 cement paste (1).	3-7
Figure 3-6: Suction measurements for w/c ratio 0.35 cement paste (2).	3-7
Figure 3-7: Suction measurements for w/c ratio 0.4 cement paste (3).	3-8
Figure 3-8: Suction measurements for w/c ratio 0.45 cement paste (4).	3-8
Figure 3-9: 95% Confidence interval for w/c ratio 0.3 cement paste (1).....	3-9
Figure 3-10: 95% Confidence interval for w/c ratio 0.35 cement paste (2).....	3-9
Figure 3-11: 95% Confidence interval for w/c ratio 0.4 cement paste (3).....	3-10
Figure 3-12: 95% Confidence interval for w/c ratio 0.45 cement paste (4).....	3-10
Figure 3-13: Combined 95% confidence intervals for the different w/c ratio cement paste samples.	3-11
Figure 3-14: Average suction measurements for the different w/c ratio cement pastes.	3-11

Figure 3-15: Strength developed after 7 days versus the suction.	3-12
Figure 3-16: PSD for the silica sand and cement used in the mix design.....	3-14
Figure 3-17: Size sieve used to sieve the cement before mixing.	3-14
Figure 3-18: Humidity and temperature measuring apparatus.	3-16
Figure 3-19: AdafruitIO dashboard accessed on a smartphone.	3-16
Figure 3-20: Flow table test setup.....	3-17
Figure 3-21: Measuring the slump flow.	3-18
Figure 3-22: Suction samples and porosity analysis samples.	3-18
Figure 3-23: Two samples scanned at the same time.	3-19
Figure 3-24: Diamond cutting machine used to cut samples.....	3-20
Figure 3-25: Samples sliced in four to be used in the MIP test.	3-21
Figure 3-26: Tools required for the sample assembly.	3-21
Figure 3-27: Sealing the pipet before placing it into the machine.	3-22
Figure 3-28: Inserting sample into the MIP testing machine.....	3-22
Figure 3-29: MIP testing machine and mercury metal.	3-23
Figure 3-30: Vacuum saturated tank.....	3-24
Figure 3-31: Test setup using filter paper.....	3-24
Figure 3-32: Vacuum saturated facility.	3-25
Figure 3-33: Shrinkage beams with anvils on each side.....	3-25
Figure 3-34: Shrinkage beams testing apparatus.	3-26
Figure 3-35: Sample failure under TPBT.	3-27
Figure 3-36: Compressive testing machine.	3-27
Figure 3-37: E-Value testing machine setup.....	3-28
Figure 3-38: Fracture of the split cylinder test sample.	3-29
Figure 4-1: Slump flow for the different w/c ratio mortar mixtures.....	4-1
Figure 4-2: Suction versus time plot for the 0.3 w/c ratio mixture.....	4-3
Figure 4-3: Suction versus time plot for the 0.4 w/c ratio mixture.....	4-3
Figure 4-4: Suction versus time plot for the 0.5 w/c ratio mixture.....	4-4

Figure 4-5: Suction versus time plot for the 0.6 w/c ratio mixture.....	4-4
Figure 4-6: Suction versus time plot for the 0.7 w/c ratio mixture.....	4-5
Figure 4-7: Suction versus the age of the samples number 3 (partially wet).....	4-5
Figure 4-8: Environmental data logged throughout the duration of testing.....	4-6
Figure 4-9: Humidity and temperature readings for the first 530 hours.	4-6
Figure 4-10: Water Retention Curve of the partially wet sample (3), 0.3 w/c ratio.	4-7
Figure 4-11: Water Retention Curve of the partially wet sample (3), 0.4 w/c ratio.	4-7
Figure 4-12: Water Retention Curve of the partially wet sample (3), 0.5 w/c ratio.	4-8
Figure 4-13: Water Retention Curve of the partially wet sample (3), 0.6 w/c ratio.	4-8
Figure 4-14: Water Retention Curve of the partially wet sample (3), 0.7 w/c ratio.	4-8
Figure 4-15: Combined water retention plot for all the w/c ratios.	4-9
Figure 4-16: Turning points suction for the different w/c ratio samples.	4-10
Figure 4-17: Porosity versus w/c ratio after 7 and 28 days.....	4-11
Figure 4-18: Histogram of the porosity for the different w/c ratio samples after 7 and 28 days.	4-12
Figure 4-19: Enlarged top view image presenting the pore sizes of the sample.....	4-12
Figure 4-20: Enlarged side view image presenting the pore sizes of the sample.	4-13
Figure 4-21: Visual representation of the pores for the dry samples after 7 and 28 days.....	4-13
Figure 4-22: Visual representation of the pores for the wet samples after 7 and 28 days.	4-14
Figure 4-23: Void diameter versus the sphericity for the 0.3 dry w/c ratio sample after 7 days.	4-14
Figure 4-24: Void volume count for the 0.3 dry w/c ratio sample after 7 days.	4-15
Figure 4-25: Pore diameter frequency and cumulative percentage for the 0.3 dry w/c ratio sample after 7 days.	4-16
Figure 4-26: Pore diameter cumulative percentage exponential fit for the 0.3 dry w/c ratio sample after 7 days.	4-16
Figure 4-27: Cumulative pore area versus pore size for the different w/c ratio samples.....	4-19
Figure 4-28: Sorptivity versus w/c ratio after 7, 14 and 28 days.	4-21
Figure 4-29: Porosity versus w/c ratio after 7, 14 and 28 days.....	4-21
Figure 4-30: Histogram of the porosity for the different w/c ratio after 7, 14 and 28 days.....	4-22

Figure 4-31: Shrinkage versus the test age in days of the 0.3 w/c ratio samples.....	4-23
Figure 4-32: Shrinkage versus the test age in days of the 0.4 w/c ratio samples.....	4-24
Figure 4-33: Shrinkage versus the test age in days of the 0.5 w/c ratio samples.....	4-24
Figure 4-34: Shrinkage versus the test age in days of the 0.6 w/c ratio samples.....	4-25
Figure 4-35: Shrinkage versus the test age in days of the 0.7 w/c ratio samples.....	4-25
Figure 4-36: Shrinkage versus the test age in days of all the w/c ratio dry samples.	4-26
Figure 4-37: Shrinkage versus the test age in days of all the w/c ratio wet samples.....	4-26
Figure 4-38: Dry shrinkage versus the w/c ratio of the dry and wet samples after 60 days.	4-27
Figure 4-39: Flexural strength of all five mixtures at 7, 14 and 28 days.	4-29
Figure 4-40: Compressive strength of all five mixtures at 7, 14 and 28 days.	4-31
Figure 4-41: Compressive strength of cylindrical samples at 28 days.	4-32
Figure 4-42: Splitting cylinder tensile strength for all the w/c ratios.	4-33
Figure 4-43: E-Value of cylindrical samples at 28 days.....	4-34
Figure 4-44: Suctions developed within 28 days for samples number 3.	4-35
Figure 4-45: Slump flow versus suction from 7 to 28 days.....	4-36
Figure 4-46: Porosity (%) versus suction of the different tests performed.....	4-37
Figure 4-47: Drying shrinkage versus suctions from 7 to 28 days.....	4-38
Figure 4-48: Flexural strength versus suctions from 7 to 28 days.....	4-39
Figure 4-49: Compressive strength versus suctions of the dry samples from 7 to 28 days.....	4-40
Figure 4-50: Compressive strength versus suctions of the wet samples from 7 to 28 days.....	4-40
Figure 4-51: Splitting cylinder tensile strength versus suctions at 28 days.....	4-41
Figure 4-52: Modulus of elasticity versus suctions at 28 days.....	4-41

LIST OF SYMBOLS

Symbol	Description	Units
T	absolute temperature	K
g	aggregate volumetric content	
AE	air entrapped	
Ψ_{aev}	air-entry value, air-entry pressure	kPa
ϕ^b	angle of shearing resistance with respect to matric suction	kPa
σ_{CO}	apparent tensile stress at saturated state	kPa
σ_{cap}	capillary stress	kPa
u_g	cavitation pressure	kPa
n	constant depending on aggregate stiffness	
f_s	cylinder splitting strength	MPa
S	degree of saturation	%
θ'	derivative of the water retention curve equation	
v_w	dry air	$\text{m}^3/(\text{k}\cdot\text{mol})$
y	dummy variable of integration representing the logarithm of suction	
ϕ'	effective angle of shearing resistance	kPa
c'	effective cohesion	kPa
σ'	effective cohesion intercept	kPa
S_e	effective saturation	%
χ	effective stress parameter	

r	equivalent pore radius	m
a, n, m	fitting parameters of the water retention curve	
a_f, n_f, m_f	fitting parameters of the water retention curve for non-soil materials	
σ_c	intergranular stress	kPa
r_{eq}	kelvin radius (in equilibrium)	
σ_t	macroscopic stresses	kPa
$(u_a - u_w)$	matric suction	kPa
Ψ_m	matric suction pressure	kPa
f_b	maximum tensile strength	MPa
M	molecular mass of water	g/mol
e^y	natural number raised to the dummy variable power	
u_v	partial vapour pressure	kPa
PSD	particle size distribution	
k_r	permeability	k (m/s)
$\Delta\sigma_{pc}$	physicochemical stress	kPa
u_a	pore-air pressure	kPa
u_w	pore-water pressure, water pressure	kPa
P	pressure	kPa
RH	relative humidity	
S_r	residual degree of saturation	%
θ_r	residual volumetric water content	%
u_{vo}	saturated vapour pressure	kPa

θ_s	saturated volumetric water content	%
p_o	saturation vapor pressure at sample temperature	$\text{kg}\cdot\text{m}^{-1}\cdot\text{s}^{-2}$
ε_c	shrinkage strain of concrete	
ε_p	shrinkage strain of paste	
SWRC	soil water retention curve	
G_s	specific gravity	kg/m^3
ν	specific volume	m^3/kg
Ψ	suction pressure	kPa
σ'_s	suction stress	kPa
T_s	surface tension	N/m
γ	surface tension of liquid	
σ_s	uncorrected suction stress	kPa
C_u	uniformity coefficient	
R	universal gas constant	J/(mol·K)
b	upper limit of integration	
Ψ_r	value of suction to the residual volumetric water content	
p	vapor pressure of air	$\text{kg}\cdot\text{m}^{-1}\cdot\text{s}^{-2}$
e	void ratio	
θ	volumetric water content	%
$\theta(\Psi)$	volumetric water content at a given suction value	kPa
w	water content	%
w	water content	%

1 INTRODUCTION

1.1 BACKGROUND

Suction can be defined as powerful forces that cause water to be drawn into empty pores of a soil, similarly how water is drawn upwards into a small bore tube by capillary attraction forces (Ridley, 2015). Thus, suction is dependent on the surface tension at the pore water meniscus where small pores will have a larger suction force compared to a bigger pores. Therefore, the pore volume, hydration and drying will have an effect on the internal forces or suction (negative pore water pressure).

Suction measurements on different soil types is a well-researched topic within the field of Geotechnical studies. When soil suction is plotted against the degree of saturation or volumetric water content, it is known as the Soil Water Retention Curve (SWRC). The SWRC is used to indicate various properties of different soils within the Geotechnical field, including the air-entry value of a soil, the shear strength and the grain size of different soils can be predicted. It would be useful to relate the suction measurements of different cementitious materials to the properties used in the building industry. Examples of such properties include the compressive and tensile strength of the concrete, as well as the durability, porosity and the shrinkage of the concrete.

Concrete is a three phase composite material which usually consists of a cement paste medium, the aggregates added to the mixture and the interface between the aggregates and the cement paste (Macphee and Lachowski, 1998). The water cement ratio affects the durability and the strength of the concrete mixture. An increase in the water cement ratio decreases the durability and the strength of the concrete.

In Geotechnical studies the grain size of a material is commonly compared to the suction of the material. Research shows that the suction of a soil will increase with a decrease in grain size of the soil (Lu and Likos, 2006). In contrast to soil, concrete cannot necessarily be classified with only one grain size. The chemical reaction taking place when water and cement are mixed together could also play a significant role in the suction measurements obtained, which is not the case with soil measurements. The pore structure of cement has been studied for many years to understand the nature of the complex material prominently used in the building industry (Atahan et al., 2009). Winslow and Liu (1990), believed that the pore structure (formation of the pores within a cement paste sample) of cement paste within a concrete mixture (excluding aggregates) is the most important pore structure in the material. This structure significantly influences the concrete's properties such as durability, shrinkage, strength and permeability. Pores within a cementitious material are essential (Vydra et al., 2007). Individual pores found within a concrete structure can be classified into one of two categories based on size. These two

categories are known as gel pores and air voids which are typically measured in nanometres and millimetres respectively. According to Bhattacharjee (2003) the different pores can be categorised within the following sizes:

- 1) Gel pores, also known as micro-pores are characterised by dimension 0.5 nm to 10 nm.
- 2) Capillary pores also defined as meso-pores have an average radius of 5 nm to 5000 nm.
- 3) Larger macro-pores or entrapped air could develop due to inadequate compaction.

According to Gao et al. (2014) the durability of the concrete paste is closely related to the capillary pores within the cement paste. These pores are believed to contribute to the overall transport property of concrete (Zhang and Zhang, 2014).

If a strong correlation could be found between the measured suctions of concrete and the pore volume and size distribution, it may be possible to estimate concrete properties based on measured suctions.

Obtaining an overall understanding of the influence suctions may have on cementitious material properties will contribute to minimise the amount of concrete testing currently done on a building site in South Africa.

1.2 OBJECTIVES OF THE STUDY

The purpose of this study is to determine whether there is a relationship between the water retention curve of different cement mix designs and their basic properties.

The study can be subdivided into the following sub-objectives:

- 1) To determine whether the Dew Point PotentiaMeter (WP4C) apparatus derives representable results before continuing with the study.
- 2) To obtain a reliable test method for measuring the porosity of the concrete.
- 3) To determine whether environmental change will have an impact on the suction measurements. Including the temperature and humidity.
- 4) To determine if the water retention curve obtained for concrete is similar to the SWRC.

The study can be subdivided into the following main-objectives:

- 5) To determine the relationship between the suction of concrete and the following properties:
 - Durability of concrete.
 - Porosity (pore sizes and shapes) of concrete.
 - Shrinkage of concrete.
 - Strength of concrete.

Stiffness of concrete.

- 6) To obtain an overall relationship between the suction of concrete mixtures with varying water cement ratios.
- 7) To determine if the water retention curve can be used to determine the properties mentioned above.

1.3 SCOPE OF THE STUDY

A study was conducted to ensure that the WP4C apparatus used to measure the suctions are reliable and give representative results. Cement paste with varying water cement ratios were tested in the cement paste study and different concrete properties measured. Thereafter, the behaviour of mortar samples (cement paste including silica sand) were studied using five different water cement ratio mix designs. The suction of each sample was measured and compared to the durability, porosity, shrinkage, strength and stiffness of the concrete. Porosity is a difficult parameter to determine. Therefore, different porosity tests were conducted and compared to determine the best representation of the porosity for the concrete samples. Thereafter, the suction measurements were compared to the porosity obtained in the concrete samples.

The literature study entails the test procedures used for the purpose of this study. An overview of research related to this topic is discussed. A background of the suction measurements used in soil mechanics is also given.

Limitations of the research include:

- Suction measurements on different soil types are a well-researched topic within the field of Geotechnical studies. However, suction in concrete is a new research field being explored and there is limited work to compare results with.
- There is limited literature related to suction measurements for cementitious materials. Therefore, a trial test was undertaken to ensure that the suction measurements obtained for the concrete in this research project is reliable.
- Specialized machinery and equipment used to measure porosity is limited and facilities other than that of the university were used to carry out necessary porosity tests. The sample was transported to NECSA to complete different porosity tests.

Aspects that have not been covered during the study:

- No mathematical relationships were established during this research.
- Environmental impact of the samples being transported to other facilities for testing was not taken into account.
- Only one set of water cement ratios was used with one source of cement and one type of aggregate. The observed trends may differ from trends for concrete manufactured using different materials.
- Only fine aggregate (<5 mm) was used in all the mixtures and the effect of aggregate size was not taken into account in this investigation.

1.4 METHODOLOGY

Different laboratory tests were carried out to gather results for this research project.

The methodology followed in this study can be listed as follows:

- A literature review with regards to the test procedures used in this study and the reason behind the research study was provided.
- In the study of cement paste, multiple suction measurements of different w/c ratio cement pastes were determined to ensure that the WP4C apparatus was a reliable test for the determination of the suctions and the water retention curves of concrete.
- The study of cement based mortars, included various suction measurements on different mortar mixtures as well as different tests to determine specific concrete properties namely; durability, porosity, shrinkage, strength and stiffness.
- The different results obtained from the research were investigated and discussed in full.
- An overall comparison between the suctions and the concrete properties determined was made to conclude whether the suctions can be used to describe the different properties.
- Trends/patterns obtained from the study were formulated and future recommendations for the research project are also stated.

1.5 ORGANISATION OF THE REPORT

The report consists of the following chapters and appendices:

- Chapter 1 serves as an introduction to the report.
- Chapter 2 contains a technical introduction based on a literature study. A literature survey is conducted to form the basis of the research. The last section in this chapter includes a summary of further investigations to be done in this project based on the guidance from the literature.
- Chapter 3 describes the experimental observations undertaken during the study. All procedures followed to obtain specific results are discussed in this chapter.
- Chapter 4 describes the analysis of the experimental observations obtained in this study.
- Chapter 5 contains the conclusions and recommendations for future research projects in the same field of study.
- Chapter 6 lists all the references utilized in this research.
- Appendix A contains all the cement paste study suction results obtained from the WP4C test.
- Appendix B shows the particle size distribution information used in the study.
- Appendix C shows a detailed procedure of the X-Ray test for analysing the samples.
- Appendix D contains all the mortar study suction results and calculations required in the study.
- Appendix E to H present all the porosity results.
- All the shrinkage results are tabulated in Appendix I.
- Appendix J shows all the graphs illustrating the E-values determined during the stiffness test.

2 LITERATURE REVIEW

2.1 INTRODUCTION

The literature survey presents a short background on how Geotechnical Engineers obtain and utilise the SWRC of different soil types. Current research regarding suction measurements of concrete was investigated and the WP4C apparatus measuring technique discussed. Different concrete properties were examined and the concrete pore structure studied. Various methods used in the industry to measure porosity were considered and compared to one another. The drying shrinkage of concrete was investigated together with different strength tests commonly used in the industry. Relevant researchers' results discussed within the literature survey were compared to the results obtained during this research study. At the end of this chapter a small summary is provided, explaining what investigations were undertaken in this project based on guidance from the literature.

2.2 GEOTECHNICAL BACKGROUND ON SUCTION MEASUREMENTS

According to Fredlund and Xing (1994b) the soil water retention curve for a sandy, silty and clayey soil differs based on their grain size variances (see Figure 2-1). As the grain size for a soil decreases the saturated water content, the air-entry value and the residual state of the water content normally increase as well.

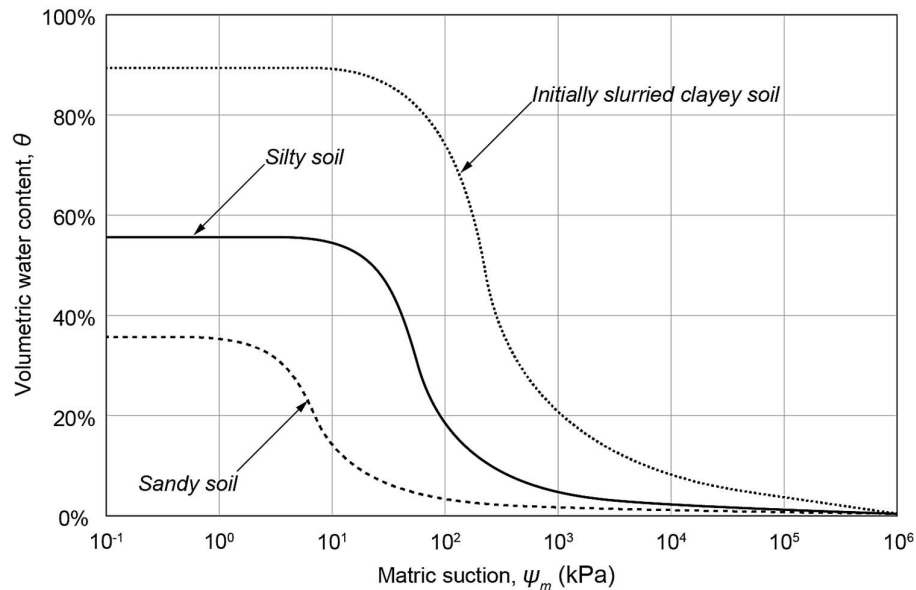


Figure 2-1: SWRC for a sandy, silty and clayey soil (Fredlund and Xing, 1994b).

The SWRC is usually plotted on a semi-logarithmic scale of the water content or the degree of saturation against the soil suction. Figure 2-2 illustrates how the SWRC curve is plotted according to Fredlund and Xing (1994b). The SWRC differs depending on whether the soil sample is wetted or dried. In Figure 2-2, θ_s represents the saturated volumetric water content and is related to the water content assuming all the pores in the soil are completely saturated (before drying). The volumetric water content at the end of the wetting curve (θ'_s) is typically different from the water content at the start of the drying curve. According to Fredlund and Xing (1994b) this is because of the air entrapment in the pores of the soil. The conditions at which the pore-water is in the form of isolated menisci surrounding the particle interface, is described as the residual volumetric water content (θ_r). The starting point for desaturation takes place when air enters the largest pores of the soil, and is known as the air-entry value (Ψ_{aev}).

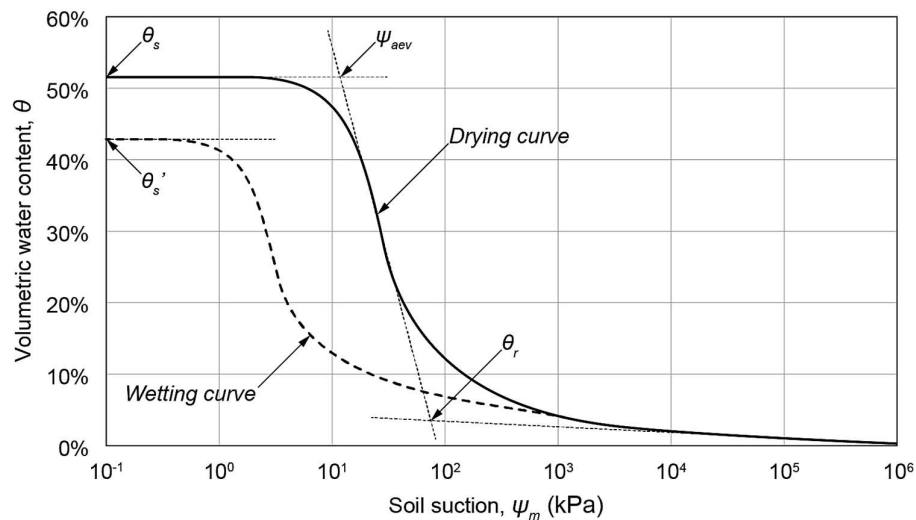


Figure 2-2: Features of the SWRC (Fredlund and Xing, 1994b).

According to Fredlund et al. (2011) the soil water retention curve can be divided into three distinct zones as depicted in Figure 2-3. In the boundary zone the soil is described to be practically saturated and this section is almost parallel to the x-axis of the graph. The transition zone depicts a gradual increase of the suction while the water content is largely reduced and the air content is increased. Then, in the residual zone the water content reduces until the water content is zero. The shape of the SWRC shown in Figure 2-3 represents a soil with only one pore size range and is described as a unimodal water retention curve. However, when a soil has more than one pore size range the curve will change to a bimodal water retention curve (see Figure 2-4). In Figure 2-5 the two different curves' pore size distribution and structure are shown.

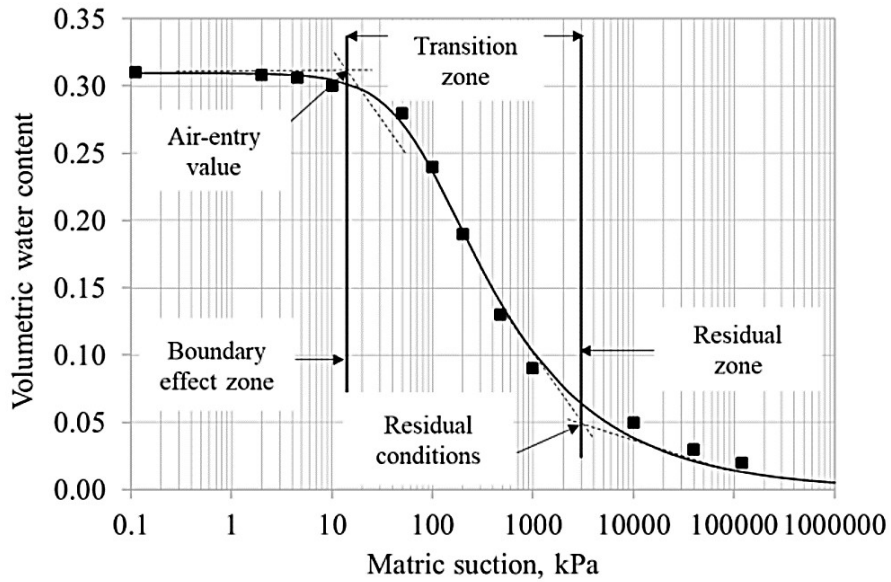


Figure 2-3: Three distinct zones of a typical water retention curve (Fredlund et al., 2011).

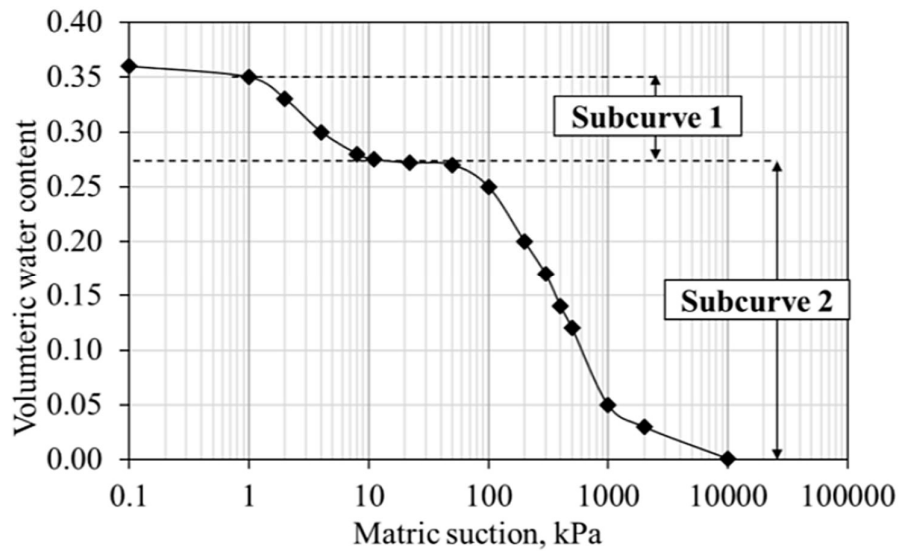


Figure 2-4: Characteristics of a bimodal water retention curve (Satyanaga et al., 2013).

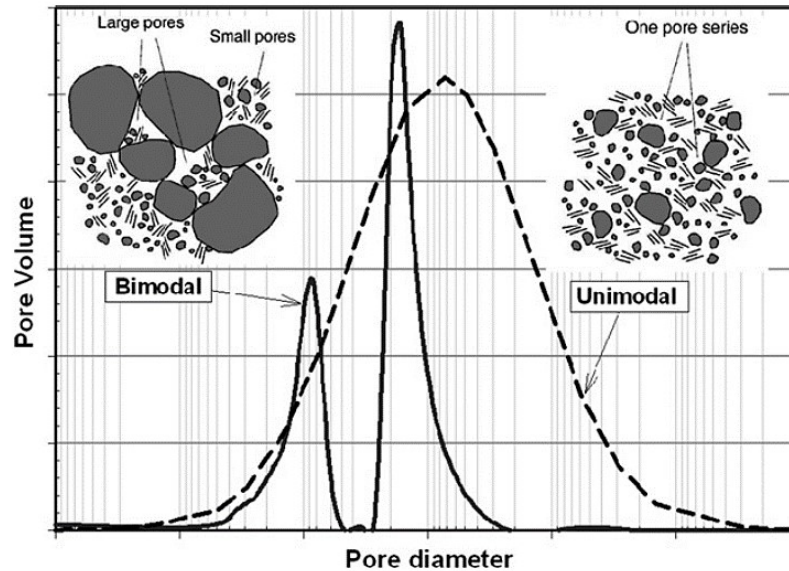


Figure 2-5: Bimodal and unimodal pore size distribution and structure characteristics (Satyanaga et al., 2013).

In Figure 2-6 the SWRC ranges from the saturated volumetric water content, at zero matric suction and the residual water content, as the upper bound of matric suction is reached. Figure 2-7 shows the corresponding suction stress curve in the form of the suction stress ($\sigma'_s(\theta)$) versus the matric suction ($\sigma'_s(u_a - u_w)$) (Lu and Likos, 2006). In region I the soil remains saturated under negative pore pressure and the upper bound of this section is the air-entry pressure. In this section the interparticle stress remains constant and due to surface tension no capillary stress between the particles are present. There is also no air-water interfaces in this section.

In region II the capillary menisci between the soil particles are retaining the pore-water. The pore size and pore size distribution both play a determining role in how much water will be retained in region II. As the matric suction becomes larger than the air-entry value (region II), capillary stresses develop and the soil becomes desaturated. In region III the amount of water retained becomes similar to the amount of water retained under the short range of the hydration mechanisms, at the soil particle surface. Region IV, the residual section, occurs where pore-water is retained primarily on the particle surface as water of hydration. The specific moisture content becomes smaller as the matric suction increases. The capillary stresses also change depending on the soil type. Sandy soil particles are larger compared to clayey soil particles. Therefore, for sandy soils the suction stress varies slightly and in clayey soil it varies gradually.

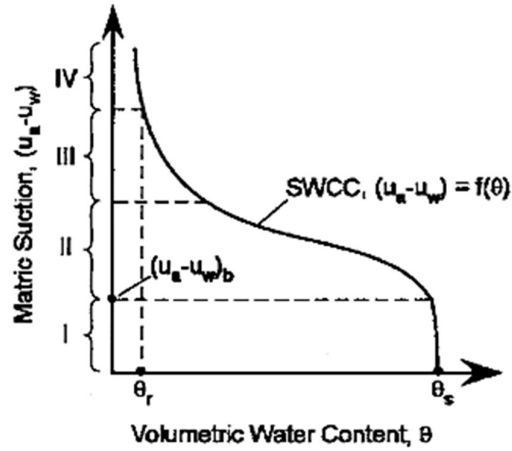


Figure 2-6: SWRC of the volumetric water content versus the matric suction (Lu and Likos, 2006).

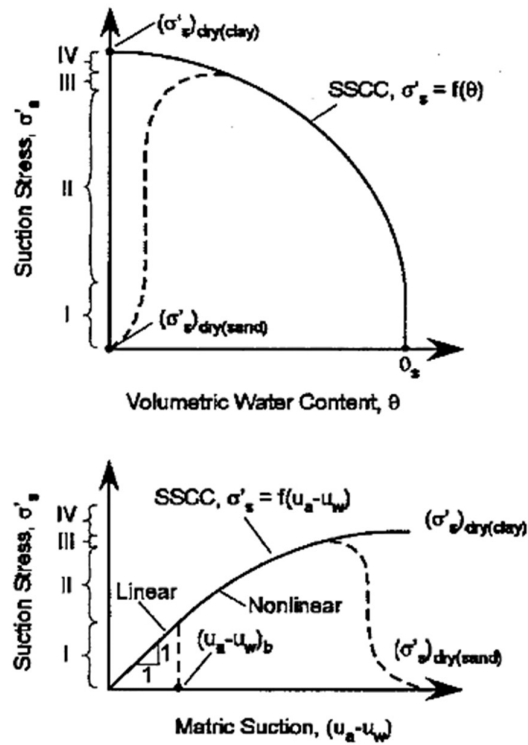


Figure 2-7: Soil Water Retention Curves of volumetric water content and matric suction versus suction stress (Lu and Likos, 2006).

2.2.1 PORE-WATER SUCTION IN SOILS

Unlike saturated soils, unsaturated soils have additional attractive forces appearing from surface tension at the air-water-interface and from negative pore-water pressure (Lu and Likos, 2006). The pore pressures in an unsaturated soil disintegrates into three forces. These forces act through the air phases of the soil water air system and through liquid. The first force is caused by the air pressure acting on the dry zone or portion of grain surface, the second force is a result of the water pressure acting on the wetted zone of the grain surface and the third force is due to the surface tension acting alongside the air-water-interface.

According to Lu and Likos (2006) the intergranular stress in unsaturated soils can be expressed as shown in Equation 2-1:

$$\sigma_c = \sigma' = \sigma_t - u_a + \sigma'_s + \sigma_{CO} \quad \text{Equation 2-1}$$

Where:

σ_c = intergranular stress

σ' = effective cohesion intercept

σ'_s = suction stress

σ_{CO} = apparent tensile stress at saturated state

σ_t = macroscopic stresses

u_a = pore-air pressure

The suction stress (σ'_s) is described as the resultant of interparticle stresses attributable to van der Waals attraction, capillary stress emerging from surface tension, cementation, double layer repulsion and negative pore-water pressure. Suction stress can be calculated as indicated in Equation 2-2 and Equation 2-3:

$$\sigma'_s = \Delta\sigma_{pc} + \sigma_{cap} + \chi * (u_a - u_w) \quad \text{Equation 2-2}$$

$$\sigma'_s = \sigma_{pc} + \sigma_{cap} + \chi * (u_a - u_w) - \sigma_{CO} \quad \text{Equation 2-3}$$

Where:

$\Delta\sigma_{pc}$ = physicochemical stress

σ_{cap} = capillary stress

χ = effective stress parameter

$(u_a - u_w)$ = matric suction

If the effective stress parameter (χ) is equal to zero it corresponds to completely dry conditions and if it is equal to unity it corresponds to saturated conditions (Lu and Likos, 2006).

The suction stress is a function of the degree of saturation and the water content or matric suction. Thus suction stress is a function of the soil water retention curve as indicated in Equation 2-4 and Equation 2-5:

$$\sigma'_s = f(u_a - u_w) = f(S) = f(\theta) \quad \text{Equation 2-4}$$

And,

$$\sigma'_s = \sigma_s - \sigma_{CO} \quad \text{Equation 2-5}$$

Where:

σ'_s = suction stress

σ_s = uncorrected suction stress

σ_{CO} = apparent tensile stress at saturated state

2.2.2 SHEAR STRENGTH AND THE SOIL WATER RETENTION CURVE

Shear strength plays an important role in the behaviour of unsaturated soils. The unsaturated interface is the contact zone between the soil and the structure where stresses are transferred. During shearing the interface acts as a stress concentrated zone and these behaviours are difficult to represent or to model mathematically. Unsaturated soils cannot only be described with a single stress state variable, but in terms of two stress state variables, namely the net normal stress, $(\sigma_n - u_a)$ and the matric suction $(u_a - u_w)$. According to Fredlund et al. (1995) the equation is as indicated in Equation 2-6:

$$\tau_f = c' + (\sigma_n - u_a) * \tan\phi' + (u_a - u_w) * \tan\phi^b \quad \text{Equation 2-6}$$

Where:

c' = effective cohesion

ϕ^b = angle of shearing resistance with respect to matric suction

ϕ' = effective angle of shearing resistance

Figure 2-8 shows the typical relationship between shear strength and soil suction. As the matric suction increases, the shear strength of the soil also increases through the water inter-aggregate contact area. However, above the air-entry value the shear strength of the soil decreases non-linearly with respect to suction. The air-entry value of a soil is determined by using the SWRC. Therefore, a strong correlation between the SWRC and the shear strength behaviour of a soil can be classified.

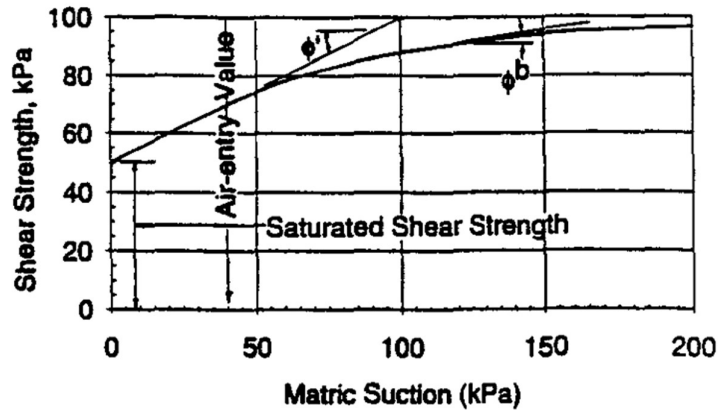


Figure 2-8: Matric suction against degree of saturation (Fredlund et al., 1995).

The SWRC is mostly plotted as the variation of volumetric water content (θ) or degree of saturation (S), with either matric or total suction of the soil. At suctions greater than about 2,500 kPa the matric and total suction can generally be assumed to be the same. In Figure 2-9 the degree of saturation is plotted against matric suction. The air-entry value of the soil and the residual degree of saturation (S_r) can be seen and the zone where the soil desaturates is also pointed out.

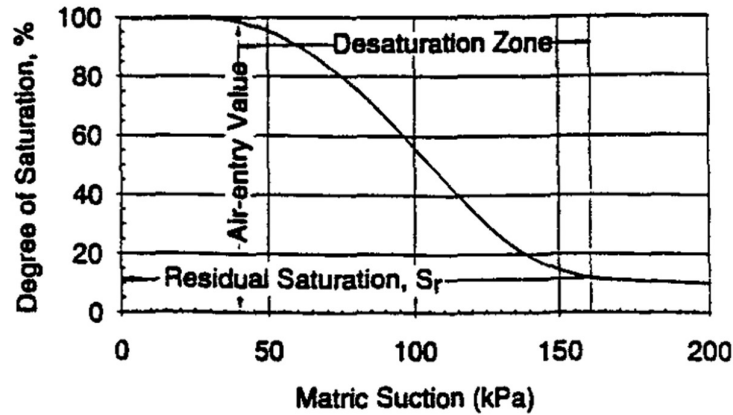


Figure 2-9: Matric suction against the shear strength of a soil (Fredlund et al., 1995).

Different formulas have been derived in the past through the use of the SWRC data and have been used to calculate the shear strength of an unsaturated soil. According to Fredlund et al. (1995), Brooks and Corey (1964) derived Equation 2-7 to define the effective saturation (S_e) from the SWRC:

$$S_e = \left(\frac{(u_a - u_w)_b}{\Psi} \right)^{b_2} \quad \text{Equation 2-7}$$

Where b_2 is the fitting parameter.

The effective saturation is only valid for matric suctions greater than the air-entry value. The shear strength may be derived using Equation 2-8 or Equation 2-9:

$$\begin{aligned} \tau = c' + (\sigma_n - u_a) \tan \phi' + (u_a - u_w)_b \tan \phi' + \frac{(u_a - u_w)_b^{b_2}}{b_2 - 1} \\ * \left(\frac{1}{(u_a - u_w)_b^{b_2 - 1}} - \frac{1}{(u_a - u_w)^{b_2 - 1}} \right) \tan \phi' \end{aligned} \quad \text{Equation 2-8}$$

(for $b_2 \neq 1$)

$$\begin{aligned} \tau = c' + (\sigma_n - u_a) \tan \phi' + (u_a - u_w)_b \tan \phi' + (u_a - u_w)_b \\ * \ln \left(\frac{(u_a - u_w)}{(u_a - u_w)_b} \right) \tan \phi' \end{aligned} \quad \text{Equation 2-9}$$

(for $b_2 = 1$)

Fredlund et al. (1995), tested Equation 2-8 and Equation 2-9 to investigate whether the predicted shear strengths are reliable. Glacial till was compacted to different densities and the direct shear test was conducted under different levels of net normal stress and matric suction. The plate apparatus was used to develop the SWRC shown in Figure 2-10. A good interrelationship was established between the predicted values and the measured values of the shear strength. In Figure 2-11 different equations used to conduct the SWRC of the same soil are presented. It is clear that the different methods used to derive the SWRC are not identical and variable answers could easily be obtained. Therefore, it is important that all parameters are known or chosen with certainty when utilizing different methods in determining the SWRC.

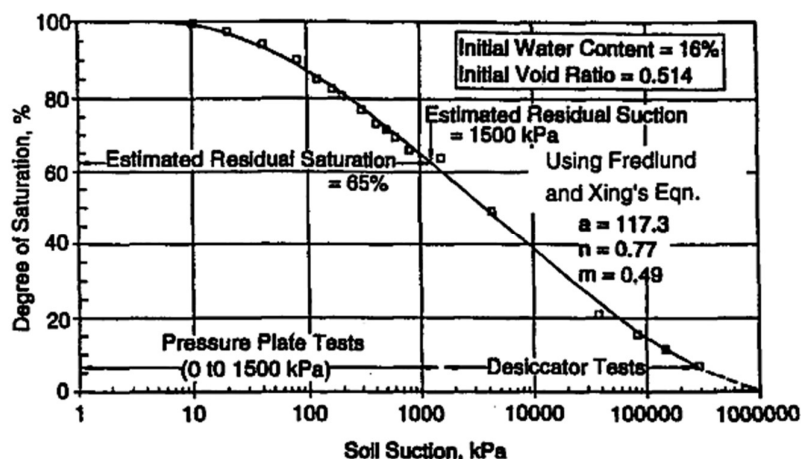


Figure 2-10: SWRC for compacted till sample (Fredlund et al., 1995).

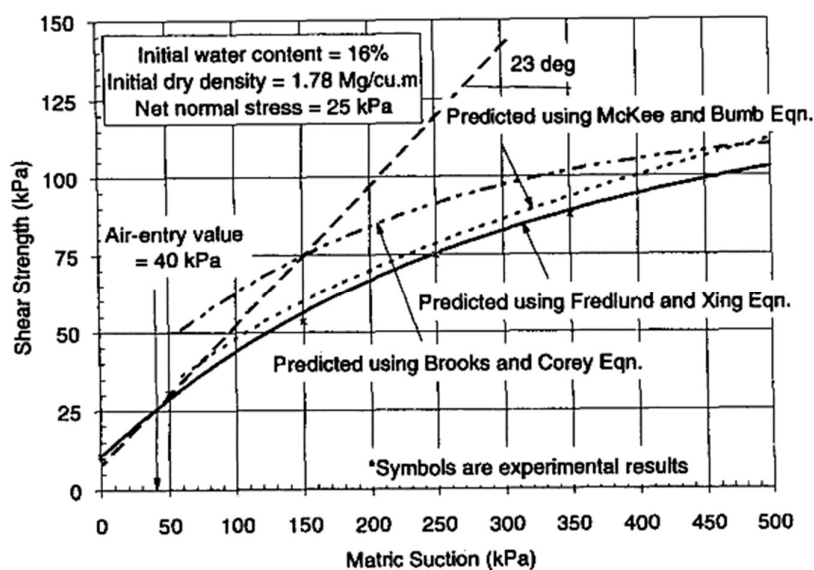


Figure 2-11: Shear strength with matric suction, comparison of different experimental models (Fredlund et al., 1995).

2.2.3 HUMIDITY CONTROL

When using techniques that rely on measurements of total suction with controlled water contents, for example the filter paper test method and the psychrometer test method, humidity control is not necessary. However, when the total suction is controlled and the test relies on the measurement of the water content of the soil sample, humidity control is important. The total suction can be controlled when controlling the relative humidity. According to Likos and Lu (2003) a closed environment chamber could be used to control the relative humidity through the aid of Kelvin's equation. This can be done by placing the samples in a closed environment where the humidity is controlled, by measuring whether equilibrium is reached as the water is desorbed or adsorbed. Kelvin's equation as derived by Likos and Lu (2003) is described in Equation 2-10:

$$-\frac{RT}{v_w} \ln \frac{u_v}{u_{vo}} = \frac{2T_s}{r} = u_a - u_w \quad \text{Equation 2-10}$$

Where:

u_a = total air pressure

u_w = total water pressure

u_v = vapour pressure

u_{vo} = saturated vapour pressure

v_w = dry air

r = equivalent pore radius

T_s = surface tension

T = absolute temperature

R = universal gas constant

When measuring the SWRC for soils with a relatively high total suction pressure (greater than 4000 to 10 000 kPa) humidity control techniques are relevant. The isopiestic (same pressure) traditional method for controlling relative humidity relies on accomplishing vapour pressure equilibrium for acid or salt solutions in a closed environment (Likos and Lu, 2003). The two pressure method relies on the active influence of relative humidity by mixing vapour saturated gas with dry gas or by varying pressure.

2.3 CURRENT RESEARCH ON SUCTION IN CONCRETE

Understanding the water flow through a concrete sample matrix has become a relatively large topic for the life-span analysis and modelling of concrete. Research done by Pap et al. (2018) aimed to estimate the main characteristic of the drying water retention curve of concrete as well as to determine whether there are a significant difference between different concrete types. Table 2-1 tabulates the different concrete mixtures used in the study undertaken by Pap et al. (2018).

Table 2-1: Summary of the different concrete mixtures (Pap et al., 2018).

Mixture No.	Amount of cement, kg/m ³	w/c ratio	Fibre reinforcement	Waterproofing admixture
C1	360	0.50	-	-
C2	400	0.45	Polymer	-
C3	360	0.50	-	Penetron
C4	400	0.45	-	-

Two different models were used to plot the water retention curve of the different concrete types. The first model by Van Genuchten (1980) is commonly used to fit the water retention curve for a series of data points and is written as can be seen in Equation 2-11:

$$\theta(\Psi) = \frac{\theta_s}{[1 + (a\Psi)^n]^m} \quad \text{Equation 2-11}$$

Where;

θ_s = saturated water content

Ψ = suction

a, n, m = fitting parameters

This method is limited to the range between the air-entry value and the residual suction value, due to the asymptotic characteristics of the equation (Pap et al., 2018).

The second model was developed by Fredlund and Xing (1994a) and according to Park and Fleming (2006) this method is suitable for fitting the water retention curve of a non-soil material as well. A natural logarithmic equation is used with a correction factor to extend the suction series from the residual suction to the fully dry state. The equation is described in Equation 2-12 and Equation 2-13 (Fredlund and Xing, 1994a):

$$\theta(\Psi) = C(\Psi) * \frac{\theta_s}{\{\ln(e + (\Psi/a_f)^{n_f})\}^{m_f}} \quad \text{Equation 2-12}$$

The correction factor is defined as:

$$C(\Psi) = 1 - \frac{\ln\left(1 + \left(\frac{\Psi}{\Psi_r}\right)\right)}{\ln\left(1 + \left(\frac{10^6}{\Psi_r}\right)\right)} \quad \text{Equation 2-13}$$

Where;

$\theta(\Psi)$ = volumetric water content at a given suction value (Ψ)

θ_s = saturated water content

a_f, n_f, m_f = fitting parameters

Ψ_r = value of suction to the residual volumetric water content

Figure 2-12 presents the different water retention curves of concrete C1 described in Table 2-1, Pap et al. (2018), stated that the complex pore structure of the concrete can be described by the characteristics of the water retention curve. The complex pore structure consists of macro-pores and capillary pores. On the low suction side water movement is caused by gravity and the water is quickly removed out of the opened macro-pores. The high suction side depends on the surface tension of the material matrix. The water only leaves the structure during water evaporation if the surface tension within the capillary pores, generated through concrete solidification, is low enough.

This study concluded that the characteristics of the pores and the capillary system are not significantly influenced by the exact composition of the concrete, for example by adding admixtures or fibre reinforcement. Pap et al. (2018) also stated that this is in good agreement with a study done by Pap (2015) related to the water retention curve of different concrete samples.

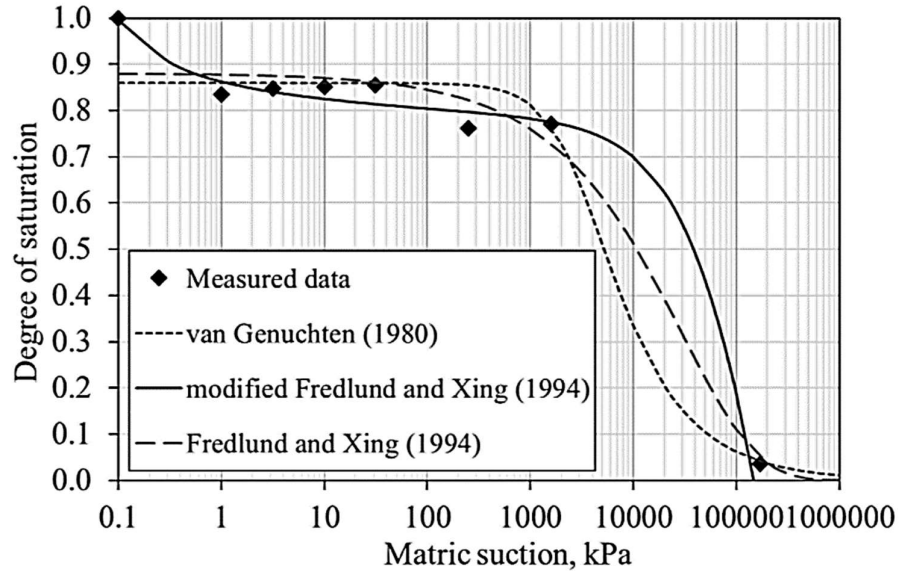


Figure 2-12: The fitted Water Retention Curves (Pap et al., 2018).

Pap et al. (2019), also tried to determine the permeability function of concrete through the water retention curve and the saturated coefficient of permeability. There are different estimation techniques to determine the permeability function which can be divided into four categories namely: empirical models, correlation models, regression models and statistical models. The Van Genuchten (1980) model to estimate the permeability function can be expressed using Equation 2-14:

$$k_r = \frac{\{1 - (a\Psi)^{n-1}[1 + (a\Psi)^n]^{-m}\}^2}{[1 + (a\Psi)^n]^{m/2}} \quad \text{Equation 2-14}$$

With the same parameters used to fit the water retention curve as defined above, Huang (1998) used the water retention curve of Fredlund and Xing (1994a) to determine the permeability function, which involves numerical integration along the water retention curve, as given by Equation 2-15:

$$k_r(\Psi) = \frac{\int_{\ln(\Psi)}^b \frac{\theta(e^y) - \theta(\Psi)}{e^y} \theta'(e^y) dy}{\int_{\ln(\Psi_{aev})}^b \frac{\theta(e^y) - \theta_s}{e^y} \theta'(e^y) dy} \quad \text{Equation 2-15}$$

Where;

b = upper limit of integration

y = dummy variable of integration representing the logarithm of suction

θ' = derivative of the water retention curve equation

e^y = natural number raised to the dummy variable power

These models assume that the water retention curve and the permeability function are closely related to the pore-size distribution of the material. Figure 2-13 presents the coefficient of permeability that was measured and also predicted with the different models.

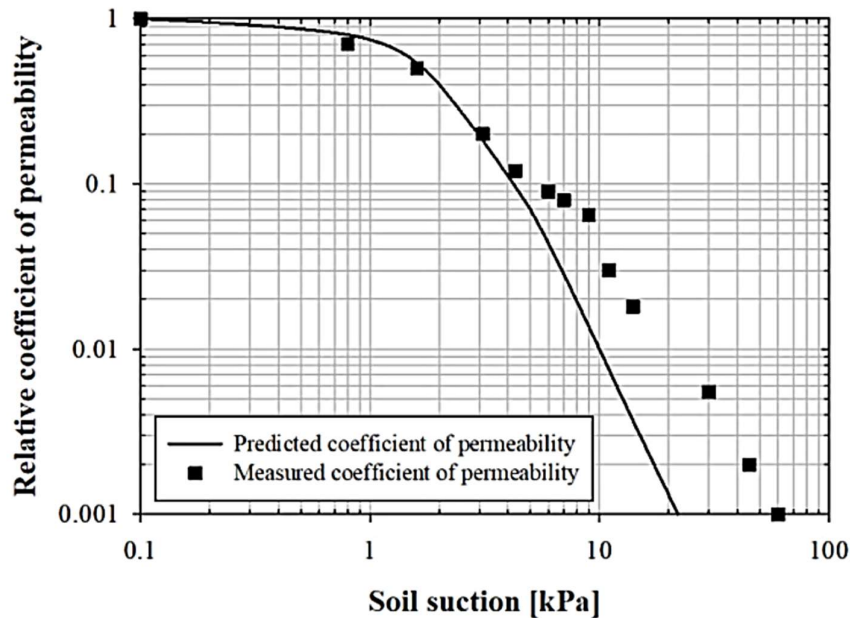


Figure 2-13: The predicted and measured relative permeability function for light clay by Fredlund et al. (2012), data from Moore (1939).

The relative coefficient of permeability functions for concrete are presented in Figure 2-14. The investigation concluded that the permeability function determined by both Fredlund and Xing (1994a) and Pap et al. (2018) are in good agreement with water retention models. However, the permeability functions determined through the Van Genuchten (1980) and Huang (1998) models are significantly different, compared to the other methods used. According to Pap et al. (2019) the fitting methods used for these two models shifts the function of unsaturated permeability, which means that more measured points at the low suction range as well as the transition zone is needed, hence indicating that the water retention property is important.

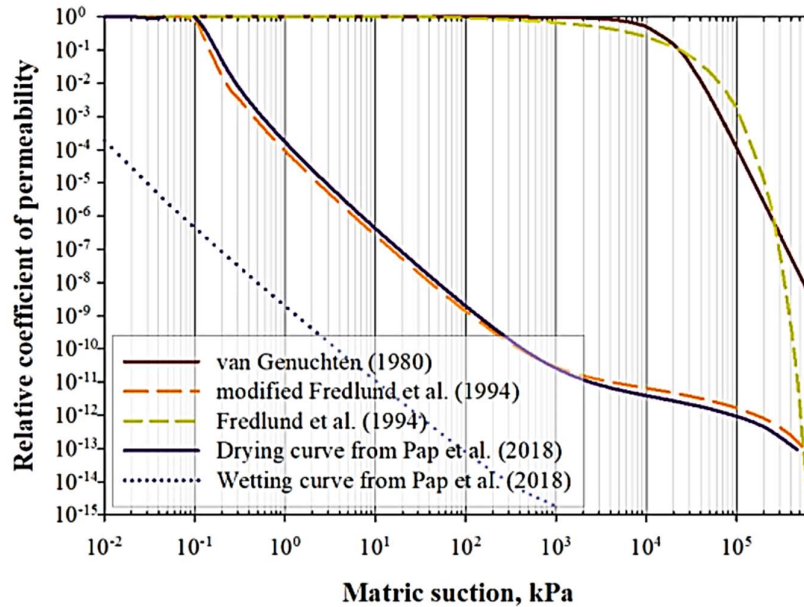


Figure 2-14: Relative permeability function for C1 concrete mixture (Pap et al., 2019).

2.4 CONCRETE PROPERTIES

Concrete can be described as a mixture of cement and water which binds together with sand and or aggregate particles to form a monolithic whole (Domone and Illston, 2010). Figure 2-15 illustrates how a single grain of Portland cement hydrates within a few weeks. According to Domone and Illston (2010) the important features are as follows:

- a) Solid products are deposited around the core of the un-hydrated cement within each cement grain and this process takes place at the solid liquid interface.
- b) A surface layer on the cement grain forms within the first hour (early products) and this acts as a barrier to further reactions taking place during the dormant period (before the concrete starts to harden).
- c) The dormant period stops as soon as it is broken down by either the internal pressure built-up (by osmosis), portlandite (Ca(OH)_2) or both. This enables the hydration process to proceed more rapidly.
- d) There are different properties of hydration products (also known as the gel) which include; needle like crystals of ettringite deposited in the early hydration process, large hexagonal crystals of Ca(OH)_2 which is scattered in the matrix and an amorphous (formless/shapeless) mass mainly consisting of C-S-H (Rayment and Majumdar, 1982, Soroka, 1979b).

- e) As the hydration process continues, gel pores within the gel are generated (with sizes between 0.5 nm and 5 nm wide) and while new products are being deposited within the matrix the gel porosity decreases.

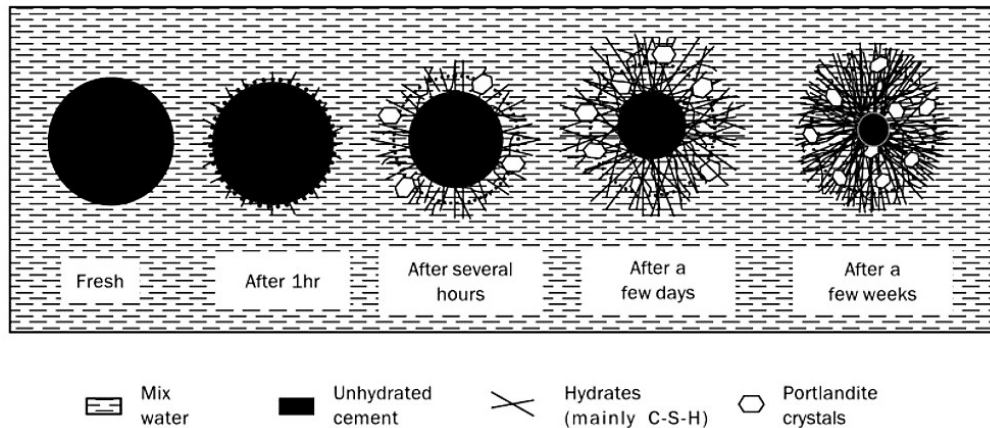


Figure 2-15: Illustration of the hydration process of a single grain of Portland cement (Domone and Illston, 2010).

The hydration reaction of concrete is an exothermic reaction which means that heat is discharged during the setting time and early hardening period (Bye et al., 2011). The heat discharged during this process can reach temperatures up to 100°C (or even more) if the concrete is kept in conditions where there is zero heat loss during hydration. Figure 2-16 presents a typical diagram explaining the rate of heat output during the hydration process in concrete paste. Directly after mixing the concrete, a high peak is detected (A) which only lasts for a few minutes and then the peak declines to a lower rate for a longer period (the dormant period). In the dormant period the cement is relatively inactive and it can take up to three hours to complete this period. Suddenly the rate of heat output will start to increase rapidly (assumed to be the initial setting time) until it reaches the maximum peak at B (after the final setting time). The reaction will then gradually start to slow down, but sometimes have a narrow peak (C) after one or two days.

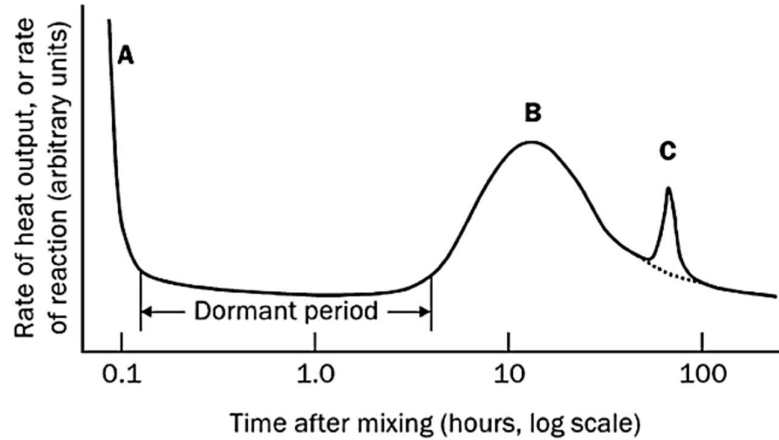


Figure 2-16: The typical rate of reaction of hydration in cement paste at constant temperatures (Forester, 1970).

Figure 2-17 illustrates that the volume of hydration products (gel) at a water cement (w/c) ratio of 0.38 precisely matches the fresh cement and water. At w/c ratios below 0.38 the hydration process will stop before completely finished, even if another source of water is available. This phenomena is called the condition of insufficient volume. When the w/c ratio is above 0.38 the amount of unfilled pores (named capillary pores) between the grains will increase.

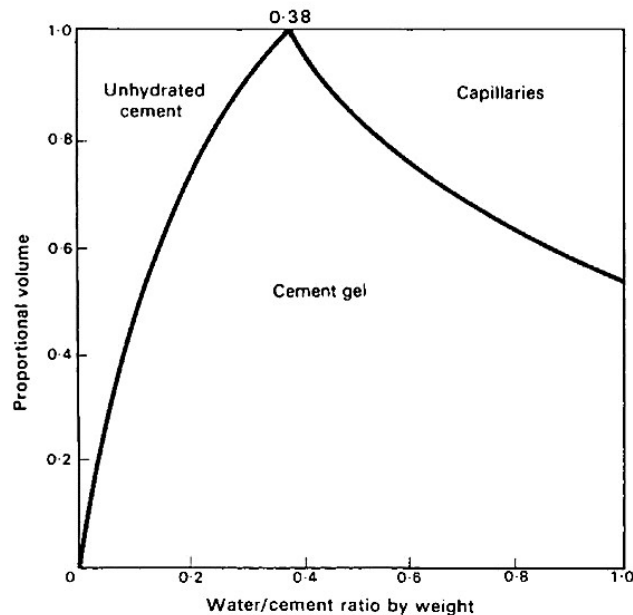


Figure 2-17: Volumetric composition of hydrated hardened cement paste after storage in water (Hansen, 1970).

2.5 PORE STRUCTURE OF CONCRETE

The simplified model of hardened cement paste consist of the gel formation which occurs from the surface of the cement particles, the capillary pores between the cement particles (these pores will be dry or partially filled with water) and entrapped air within the matrix, presented in Figure 2-18 (Oktar et al., 1996). According to Bhattacharjee (2003) the different pores can be categorised within the following sizes:

- a) Gel pores, also known as micro-pores are characterised by dimension 0.5 nm to 10 nm.
- b) Capillary pores also defined as meso-pores have an average radius of 5 nm to 5000 nm.
- c) Larger macro-pores or entrapped air could develop due to inadequate compaction.

The pore fluid composition of concrete can be affected by the curing technique (Zhang et al., 2018), the aggregate and the sand type used, the binder composition and type, sample preparation procedure used, as well as the period it is stored (Hewlett, 2004). The strength of concrete is one of the most important properties which is governed by the pore system of the concrete (Därr and Ludwig, 1973, Jivkov et al., 2013, Bu and Tian, 2016). The large pores such as capillary pores and entrapped air are responsible for the reduction in overall strength and elasticity (Mehta (1986); Neville and Brooks (1987)). The gel pores do not influence the strength of concrete. Therefore, when dealing with the strength-porosity relationship of concrete these small pores can be neglected in the overall porosity and pore size distribution.

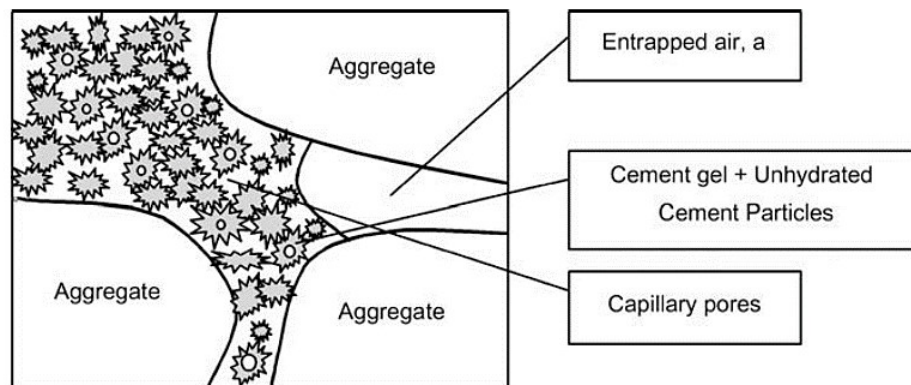


Figure 2-18: Schematic representation of the structure of hardened concrete (Atahan et al., 2009).

The w/c ratio plays an important role in the capillary porosity of hardened cement paste and also governs the transition zone porosity in the concrete (Soroka (1979a); Kim et al. (2014)). According to Martys and Ferraris (1997) the meniscus subjected to a small pressure from below is unstable in a narrow pore opening but stable in the neighbouring pore (see Figure 2-19). This capillary suction only applies when

the porous medium is initially dry. The flow through concrete is much more complicated due to the water reacting with the solid matrix causing the pore structure to change over time. Thus, the water uptake of concrete depends on the capillary suction which is dependent on the surface tension at the pore water meniscus, as well as the resistance to viscous flow of the penetrating water. The relationship between the meniscus radius of curvature (r) and the equivalent vapour pressure (p) is expressed by the Kelvin's equation as indicated in Equation 2-16:

$$\ln\left(\frac{p}{p_0}\right) = \frac{2T}{R\theta\rho r} \quad \text{Equation 2-16}$$

Where;

p_0 = vapour pressure over a plane surface

T = surface tension of the liquid

R = gas constant

θ = absolute temperature

ρ = density of the liquid

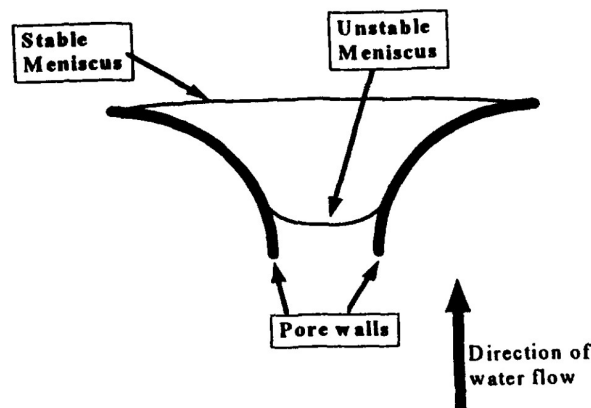


Figure 2-19: Stable and unstable menisci in a pore by Martys and Ferraris (1997).

A study was conducted by Rucker-Gramm (2010) to investigate the effect of moisture content of concrete on the water uptake. Portland cement CEM I 42.5 R (515 kg/m³) together with Munich sand was used to cast a 700x150x150 mm³ mortar slab with a water cement ratio of 0.6. Prisms (240x45x45 mm³) were sawn from the centre of the slab after the slab was demoulded (after 24 hours) and immersed in water for 3 days. After three months the prisms were oven-dried also for three months at 50 degree calcium (°C). Thereafter, the samples were stored in desiccators to a constant weight over saturated salt

solutions at a controlled temperature of 23°C, at relative humidities (RH) of 50, 65, 75 and 80%. The prism sides were coated with epoxy resin to limit the moisture exchange to the atmosphere, a few weeks before measurements started. The penetration of water through the prisms with different initial moisture contents were investigated using the Nuclear Magnetic Resonance (^1H NMR). According to Rucker-Gramm and R.E. Beddoe, the NMR scans were performed by placing the prism on a carriage moving the sample in 1 mm steps through the sensitive region of a 0.47T magnetic field across the width of the sample. Step scans of ^1H signal strength along the length of each prism were recorded. An initial NMR scan (on dry concrete) was performed on each prism and then the samples were placed in water and then NMR scans were performed at different time periods. The weight was recorded before and after each scan and this procedure took up to 10 minutes.

Figure 2-20 shows that water inside the pores conclusively affects the transport of water in larger capillaries and that the depth of water penetration increases as the preconditioning relative humidity (RH) is increased from 50 to 75%. The graph seen in the right hand corner shows that the water uptake and penetration depths (when the preconditioning RH is 80%) decreases, compared to the graph in the left hand corner. The maximum water uptake occurs at a critical degree of saturation (ϕ_c). The values indicated on each line describes the time at which data was recorded. The suctions were recorded up to 509 hours.

Figure 2-21 was used to represent the phenomena behind the effect of water content of concrete on water uptake. Firstly, when the initial degree of saturation is below (ϕ_c) water rapidly enters capillaries of dry concrete and moderately redistributes into the gel pores, which can be described as immobile water. Therefore, less water is available to transport into the larger capillary pores. In more moist concrete less penetrating water can be transported into the gel pores which is already filled with water. Therefore, the large capillaries are filled with water which result in a higher uptake of water. When the maximum water uptake is reached, insufficient pore space is available for redistribution of water. This investigation showed that the critical degree of saturation corresponds to the moisture equilibrium of approximately 75% RH where the pores up to a Kelvin Radii of 3.7 nm are filled with water while the much larger capillaries remain empty, apart from the adsorbed layer. Secondly, when the initial degree of saturation is above (ϕ_c) the capillary pores are partially saturated and the water has a tendency to move into smaller capillaries due to their higher suctions which will move the water into smaller pores (until equilibrium is reached). However, water uptake and water penetration depth will decrease, because the gel pores (smaller pores) filled with water does not contribute to capillary transport at the penetration front. Rucker-Gramm (2010) made the following conclusions:

- 1) The rate at which water can be absorbed by cementitious materials/concrete depends on the initials moisture content of the material.

- 2) If the gel pores are partially saturated it will affect the transport of water through the larger capillaries.
- 3) If water enters the gel pores of dry concrete, the water will no longer contribute to capillary transport. However, when the gel pores are partially saturated initially, there is more water available to fill the larger capillaries (uptake and penetration depth will increase).
- 4) If the original water content is above the critical degree of saturation, redistribution into gel pores will not take place. The uptake and penetration depth decreases due to the reduction in capillary pressure and there is a decrease in capillary pore space available for the transportation of water.
- 5) The amount of water which moves from the larger pores into the gel pores increase which cause the suctions to increase with time.

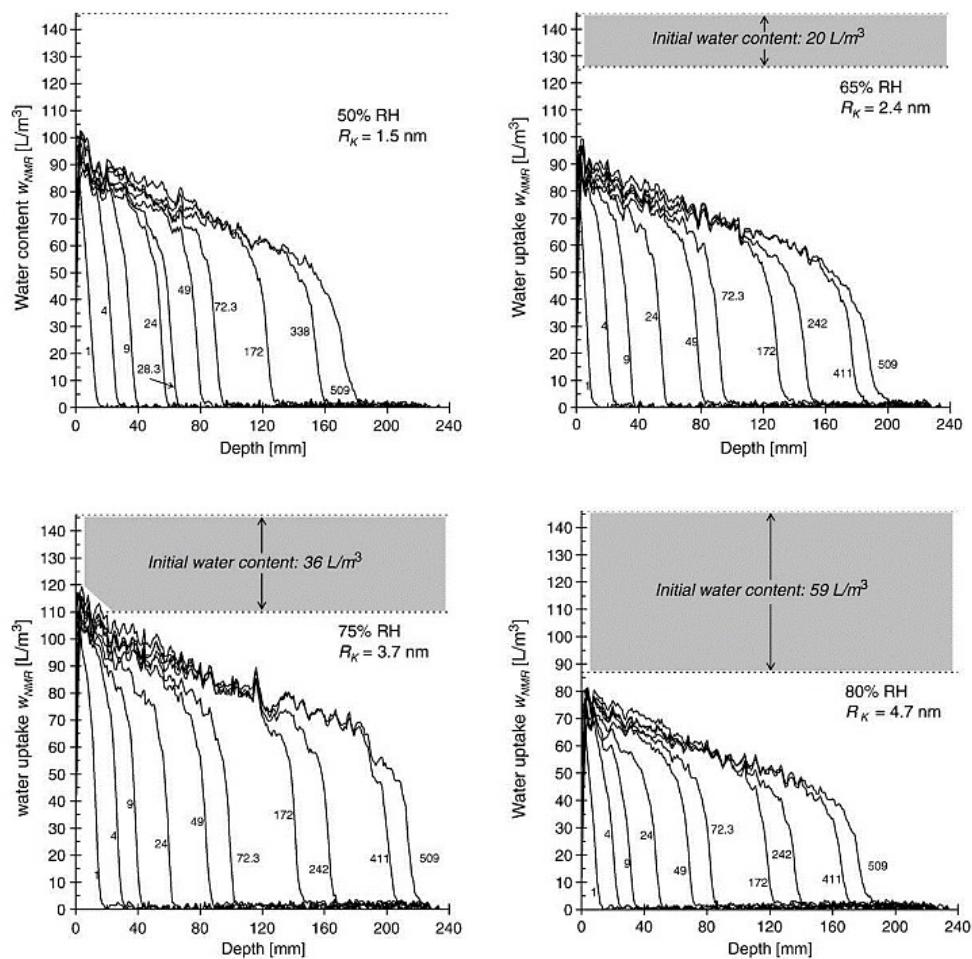


Figure 2-20: Penetration profiles for water, during capillary suction after storage at RH between 50 and 80% (Rucker-Gramm, 2010).

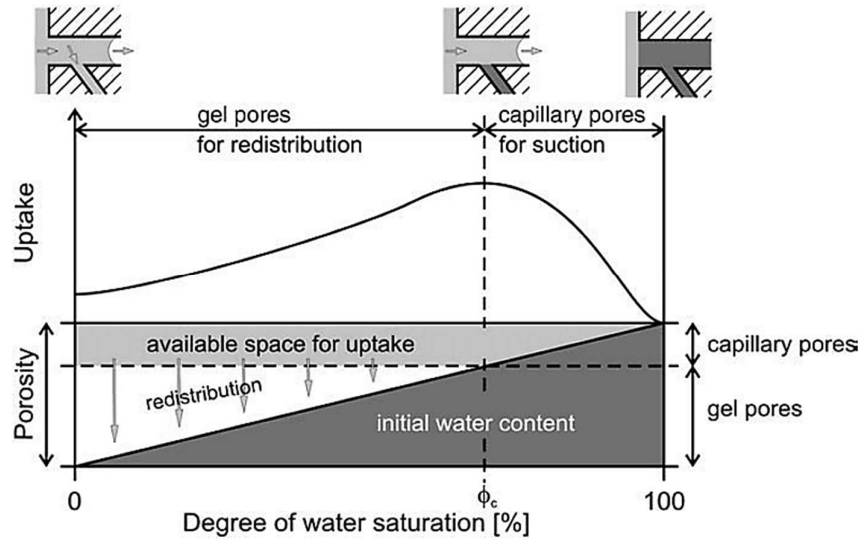


Figure 2-21: Effect of initial degree of saturation on water uptake of concrete (Rucker-Gramm, 2010).

Zeng and Xu (2015), present the schematic shown in Figure 2-22 illustrating the multilayer adsorption and capillary condensation in graded cylindrical pores. It was mentioned that Huang et al. (2015) considered an adsorbed liquid like layer (between the empty pores prior to capillary condensation and the pore walls) when determining the particle size distribution of concrete based on the water vapour sorption isotherm model (Xi et al., 1994). In Figure 2-22, t presents the water molecules that conceal the surface of all the open pores after the previous adsorption. The water can then condensate within the thin pores which satisfies the relationship as indicated in Equation 2-17 (Zeng and Xu, 2015):

$$r_p \leq r_{eq}(RH) + t(RH) \quad \text{Equation 2-17}$$

Where;

r_{eq} = kelvin radius (in equilibrium)

RH = relative humidity

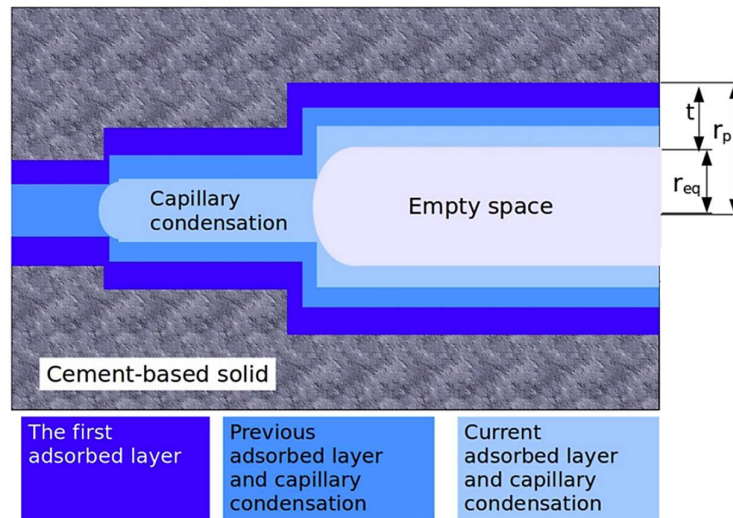


Figure 2-22: Multilayer adsorption and capillary condensation in graded cylindrical pores schematic illustration (Zeng and Xu, 2015).

2.5.1 SCANNING ELECTRON MICROSCOPY (SEM)

Hadley (1972), worked with secondary SEM techniques to study the films deposited on various layers of concrete paste. The layers were fractured and induced to drying shrinkage successively. It was noted that the hydration shell around individual cement grains were broken during the fracturing process which caused partly or occasionally completely hollow shells. Figure 2-23 is a reproduction of Figure 13 in the thesis written by Hadley (1972), showing the Hadley grain after 1 day of hydration, as presented by Diamond (1999). The early stage formation of a hollow shell is presented in Figure 2-24. The thin shell is separated by 1 to 2 mm gaps around the hydrated cement grains. Figure 2-25 shows a more advanced stage with a thicker shell generated at the early stage of hollow shell hydration. The reason for the difference could be because of the difficulty of visualising the grain. The grain will only be detected if it happened to be on the fractured plane being analysed.

SEM also have a backscatter mode that allows visualisation of the sample exposed by cutting and polished arbitrary plane surfaces. This mode provides a cross sectional view of all the structural components present (including the hydrated cement grains), allowing it to be a much more satisfactory procedure for most analysis purposes. However, the magnification that is usually obtained with the backscatter technique is limited to 2000X. Therefore, the finer details cannot always be seen in this SEM analysis mode (see Figure 2-25).

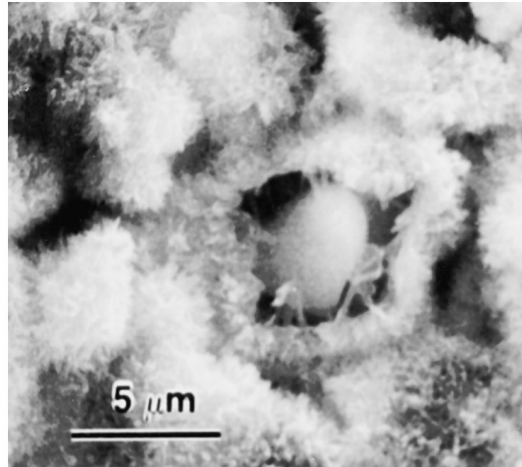


Figure 2-23: The original Haley grain (Diamond, 1999).

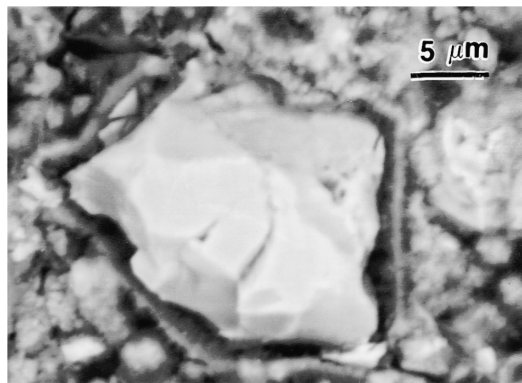


Figure 2-24: Secondary electron SEM analysis on a 1 day old, w/c ratio 0.5 cement paste (Diamond, 1999).

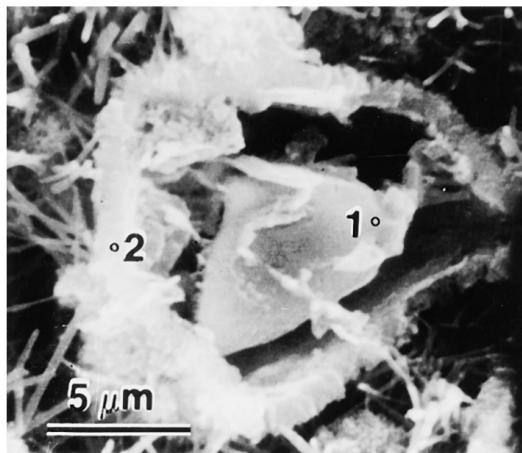


Figure 2-25: Secondary electron SEM analysis showing the early stage with a thicker shell generated of hollow shell hydration (Diamond, 1999).

Figure 2-26 illustrates the commonness of pores derived from hollow shell hydration of a 3 day old cement paste sample with a 0.5 w/c ratio (ASTM type I cement was used). In the upper left corner two fairly empty hollow shell grains with a bright floating core of un-hydrated material can be seen. Then, a large less hollowed out grain near the right corner is also present. Most of the groundmass structure consists of smaller (regular rimmed) pores which were also seen in the previous figures. These pores are derived from the small cement grain fragments that hydrate faster compared to the coarse grains. Therefore, a large portion of the pores that are determined using the SEM technique are not capillary pores, but consist of pores hollowed out by Hadley grain formation (Diamond, 1999).

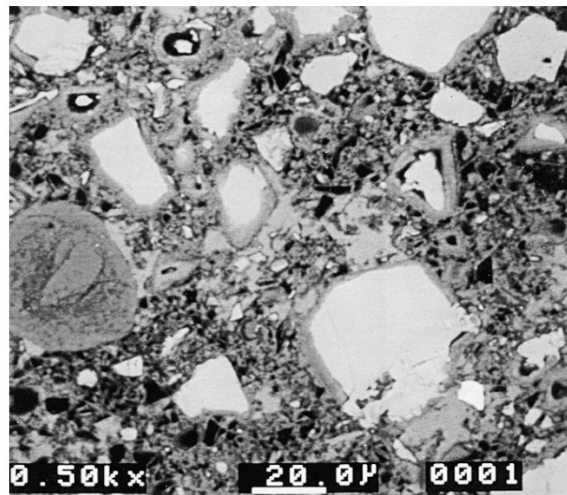


Figure 2-26: Backscatter SEM showing the pores derived from the hollow shell hydration after 3 days by Diamond (1999).

2.5.2 X-RAY MICROTOMOGRAPHY

The Micro-Focus X-ray Tomographic Facility (MIXRAD) at the South African Nuclear Energy Corporation (NECSA) is popular due to the non-invasive and non-destructive properties, therefore attracting researchers from various research fields. Including investigations such as geosciences which focuses on porosity measurements (De Gryze et al., 2006), quantification and distribution of minerals with 3D volume fraction is often analysed (Kuper et al., 2007), fracture or also known as cleat analysis (Vandersteen et al., 2003) and petrographic analysis (Long et al., 2009)). The X-Ray equipment was built in Europe and meets strict quality and safety standards (De_Beer, 2012). The system contains four separate functional units indicated in Figure 2-27 namely:

- 1) The lead-lined cabinet which surrounds the X-ray tube, the flat panel detector and the sample manipulator. This cabinet meets international radiation standards and is completely sealed.
- 2) An external chiller is implemented to cool down the X-Ray tubes as well as the internal cavity.

- 3) The external control module is used to control the facility which is not accessible inside the X-ray machine while testing.
- 4) PC's are connected to the machine with software to analyse and reconstruct the 3D virtual images as well as for visualisation of the sample being measured.



Figure 2-27: X-ray machine at the MIXRAD facility (De_Beer, 2012).

Figure 2-28 presents the tomographic process followed by the X-ray machine used at the MIXRAD facility. The MIXRAD facility is similar to the SANRAD facility (De_Beer, 2005). The only significant difference is the level of automation implemented during the tomographic acquisition process at the MIXRAD facility. The sample is fixed onto the sample manipulator in the cabinet to ensure no movement of the sample. Then, in order to obtain optimal spatial resolution during testing, the sample is horizontally adjusted for maximum enlargement. The adjustment also ensures that the sample is horizontal in each 2D radiograph for the correct normalisation during the tomography reconstruction process and at all angles of rotation. The density and energy settings are adjusted individually during operation allowing careful adjustment to reach at least 15% penetration through the sample. The virtual image reconstruction process can be time consuming, because data sets can be up to 30GB in size. Therefore, 64Bit computers with solid state hard drives are recommended (De_Beer, 2012).

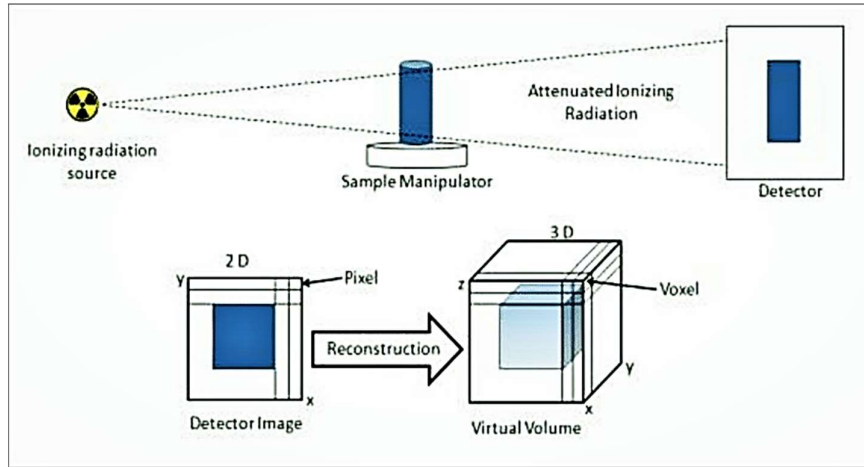


Figure 2-28: Tomographic process of the X-Ray machine at the MIXRAD facility (De_Beer, 2012).

Lu et al. (2006), states that concrete durability research mainly focuses on the transport properties of concrete. The long term performance and durability are influenced by the physical and chemical change in the microstructure of the material. This also affects the transport phenomena of water through the matrix. Figure 2-29 presents a 2D sliced image of a concrete microstructure and all the important features of hydrated cement paste. The white regions are the unhydrated cement grains and the dark spots are pore spaces. The variable darker grey shades are the density changing within the aggregate particles and the transition zone around the aggregates. The porous paste region can also be seen in Figure 2-29. Figure 2-30 shows how the tomographic data can be reconstructed into an arbitrary spatial orientation, giving a 3D image of the sample.

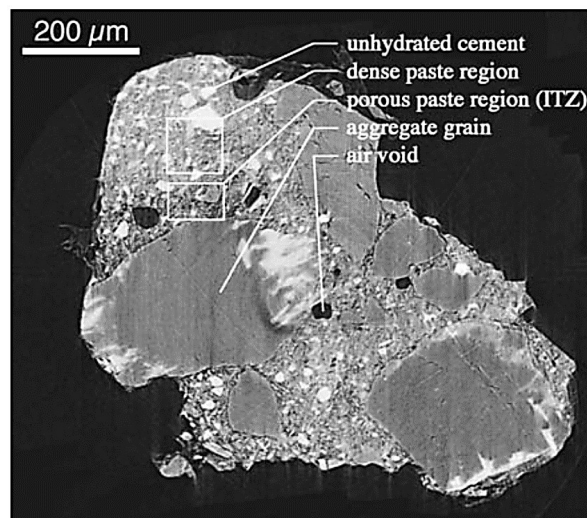


Figure 2-29: Tomographic slice of a small mortar sample (Lu et al., 2006).

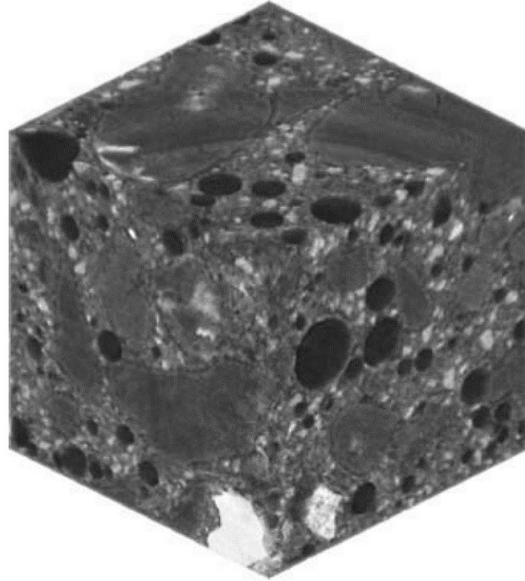


Figure 2-30: 3D Representation of tomographic data (Lu et al., 2006).

According to Lu et al. (2006), the voxel intensity of the images produced through the analysis is proportional to the density of the material at a specific point in space, where a voxel is a 3D pixel (volume element). Figure 2-31 presents the voxel count for the images (8-bit images), showing a voxel value of 0 representing black (matching the minimum density) and a voxel value of 255 representing white (matching the maximum density). The number of pores (left peak) and concrete paste or aggregates (right peak) present in the sample can be observed from the peaks in Figure 2-31. From the clear change in the intensity of grey values the images can be divided into the pore space and the solid materials (cement paste and aggregates) by choosing a threshold intensity at the minimum point between the peaks. This means that any pixel below the threshold is pore space and everything above the threshold are the solids. Figure 2-32 shows the change in grey values when the threshold is set. The left hand image presents the grey values before any threshold is applied, showing a wide range in different grey values. The right hand image (binary image of the left hand side image) presents the grey values after the threshold is set. A definite transformation between the two images can be seen. After the threshold is set one can easily distinguish the black pore space from the white solid materials.

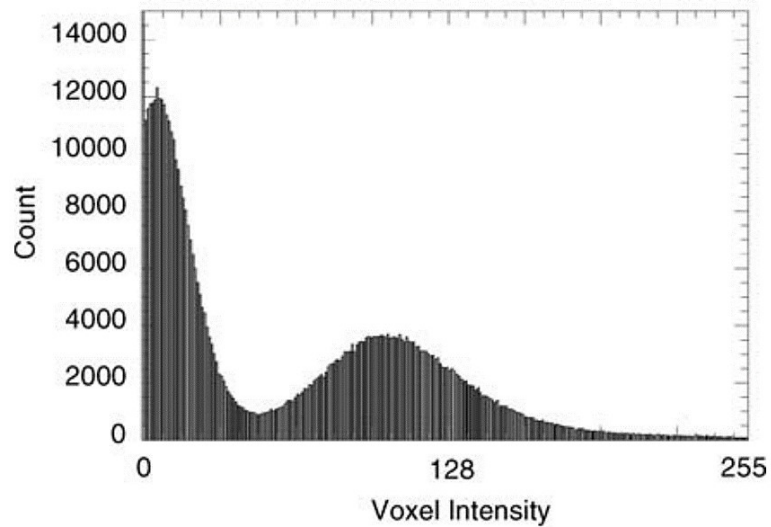


Figure 2-31: Pixel intensity of the images (Lu et al., 2006).

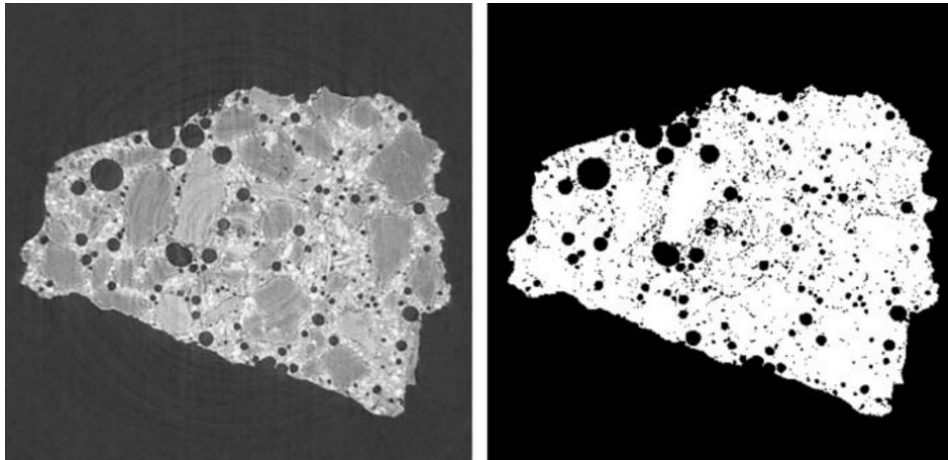


Figure 2-32: Greyscale images (Lu et al., 2006).

Du Plessis et al. (2016), studied the influence of high quality scans (slow scans) compared to low quality scans (fast scans). The slow scans take up to 1 hour compared to the fast scans with a scan duration of 5 minutes. It was observed that the fast scan measured a lower average porosity compared to the slow scan (see Figure 2-33). However, the size distribution of the two different scans are similar and with good data interpretation it is possible to determine a good correlation between the large pores and smaller pores, especially when large data sets are analysed. Figure 2-34 presented by Du Plessis et al. (2016) indicate that the larger pores are least spherical compared to the smaller pores.

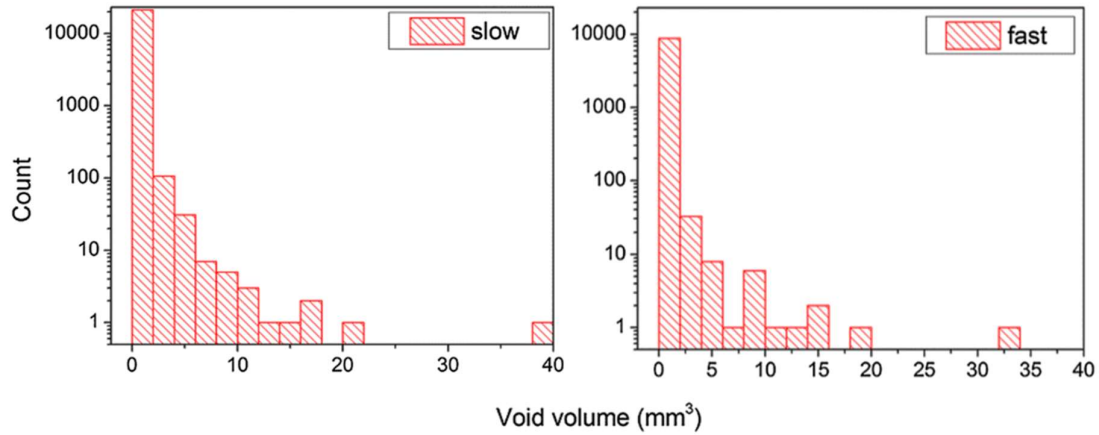


Figure 2-33: Comparison between a slow and fast scan on the void size of a concrete sample (Du Plessis et al., 2016).

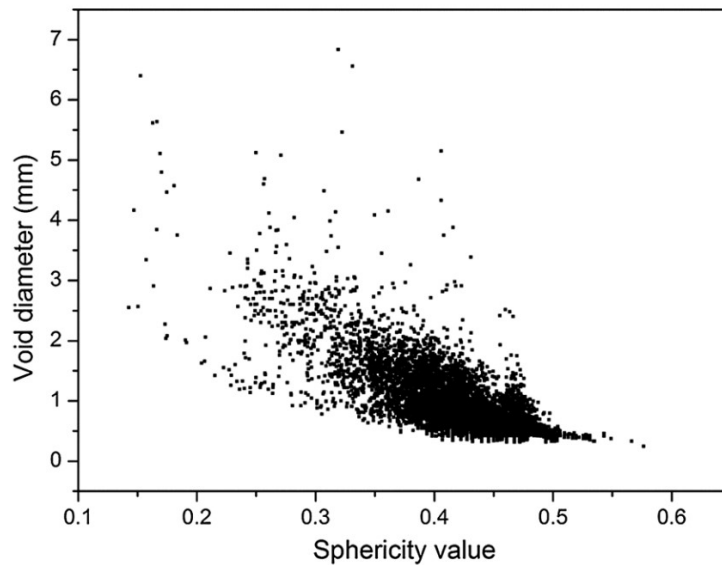


Figure 2-34: Void diameter as a function of sphericity (Du Plessis et al., 2016).

2.5.3 MERCURY INTRUSION POROSIMETRY (MIP)

The MIP testing technique is often used for the characterization of different pore sizes within a cementitious material. A heavy metal named mercury (Hg), in its liquid form, is forced into the capillaries of the material being tested by using high pressures. Equation 2-18 can be used to determine pore diameters (Washburn (1921); Abell et al. (1999)):

$$P = \frac{-2\gamma\cos\theta}{r}$$

Equation 2-18

Where;

P = pressure

r = capillary pore radius

γ = surface tension of the liquid

θ = angle of contact

The material being tested must be de-gassed (if necessary) by placing it into a steel pressure bomb vacuum until all gasses are removed. Mercury is forced into the pores with an incremental increase in pressure to determine the pore size distribution from the intruded volume at each pressure. The total porosity is determined through the total volume of pores intruded. Bhattacharjee (2003), stated that a large quantity of gel pores and closed pores remain non-intruded in the MIP test which limits the measurement of porosity. The “ink bottle” effect is a limitation pointed out specifically for this test regarding to measuring the entry sizes rather than the true pore size (Wild, 2001). When measuring the pore structure of cementitious materials it is usually assumed that each pore is directly connected to the mould surface or through larger pores. The pores which are not connected to this network is referred to as the “ink bottle” pores (Moro and Böhni, 2002).

A recent study conducted by Hou et al. (2019) confirmed that the “ink bottle” effect is not deceptive for the MIP test when measuring capillary pores, including the inter-hydrated pores. These pores are the smallest capillary pores and have a well-connected network. The gel pores were not taken into consideration, due to it rarely influencing the strength of cementitious materials. Figure 2-35 illustrates the porosity determined with the MIP technique for different w/c ratio cement pastes, as well as different cement grades (Hou et al., 2019). The porosity increased with an increase in the w/c ratio. As expected, with a higher water content, the interspaces between the cement particles expands leaving bigger capillary pores. The porosity decreased for the higher grade cement because it has finer particles which generates a denser pore structure compared to the lower grade cements.

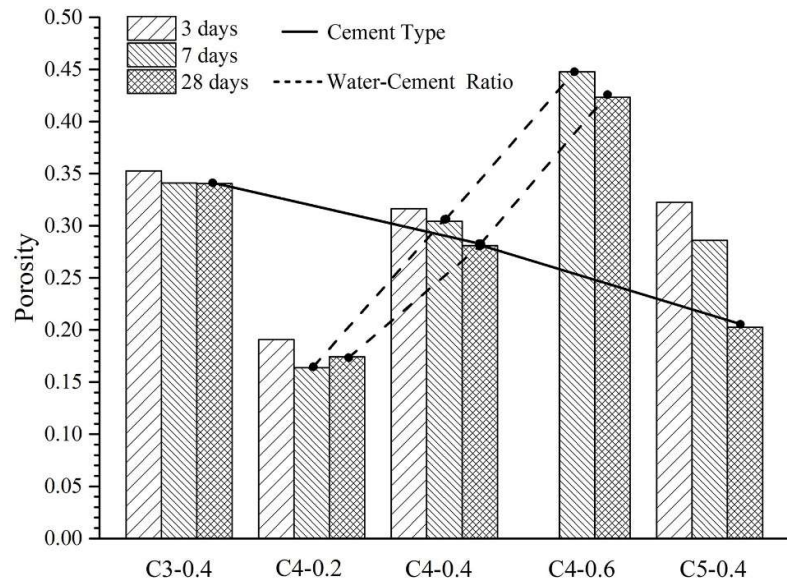


Figure 2-35: Porosity of different cement pastes determined with MIP (Hou et al., 2019).

Both the X-ray tomographic and MIP tests are limited by the sample size required for these testing procedures (small sample size required). The MIP test is a destructive test method and the sample needs to be demolished after testing. However, the X-ray testing procedure is a non-destructive test method which allows for re-using the sample after testing. Therefore, currently the X-ray test method is the preferable testing procedure (Kovarona et al., 2012).

2.5.4 GAS ADSORPTION TECHNIQUE FOR MEASURING POROSITY

Adsorption is a result of surface energy, similar to surface tension. Usually atoms that make up a solid are attached to other atoms (on all sides) in the bulk of the solid. Therefore, atoms that do not form part of the solid are incompletely bound and located on the surface of the solid. These surface atoms are more reactive compared to the bounded atoms. Due to van der Waals forces the surface atoms will attract gas, liquids and vapour until a balance in the atomic forces are reached. The gas adsorption technique can accurately measure the amount of gas adsorbed on the solid surface of a material, which directly links to the porous properties and structure of the material (Schmitt et al., 2013). Figure 2-36 illustrates four different stages during the gas adsorption testing technique, namely:

- Stage 1) At a low pressure the gas molecules are adsorbed through the sample surface and isolates only some areas.
- Stage 2) With an increase in the gas pressure the coverage of the adsorbed molecules increase until it forms a monolayer (thickness of one molecule) on the surface.
- Stage 3) Multilayer coverage will begin with a further increase in the gas pressure. The smaller pores in the sample will be filled first.

Stage 4) Increasing the gas pressure even more will result in complete coverage of all the pores within the sample.

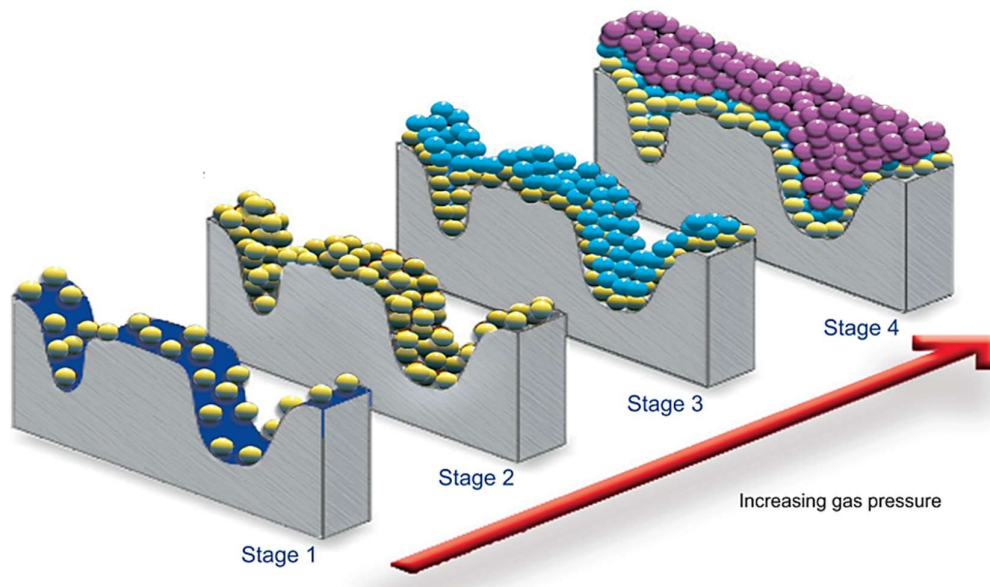


Figure 2-36: Illustration of the gas adsorption technique (Norcross, 1877).

According to Anovitz and Cole (2015) the N_2 gas adsorption technique is the most effective method for investigating the fine pores of a material when looking at the different gas adsorption techniques. Pores ranging from about 2 nm up to 300 nm in diameter can be measured using this technique. During stage 3 the BET method (named after Brunauer, Emmett and Teller) can be used to determine the specific surface area of the porous material from the adsorption data (Brunauer et al., 1938). The BJH method (named after Barrett, Joyner and Halenda) can be used during stage 4 to calculate the pore size distribution by using the Kelvin model of pore filling, but applies only for the meso-pores and the small macro-pore regions (Barrett et al., 1951).

The amount of adsorbed gas is measured at discrete pressures (P) which is incremented with the relative equilibrium pressure (P/P_0), ranging between 0.0075 and 0.995 (at a constant temperature). P_0 is the condensation pressure at a specific temperature and the pressure steadily increases up to the condensation pressure at the adsorbed area. This results in a reduction in the condensation pressure at the desorbed area. After pressure and temperature equilibrium is reached data is reported as the adsorption isotherm. Sing (1985), classified six different types of adsorption isotherms together with four hysteresis type shapes as shown in Figure 2-37. The most important adsorbed isotherm required to determine the porosity and pore size distribution is type IV. Materials with a large quantity of meso- and macro-pores (such as concrete) will have the same characteristics to the hysteresis loop shown for the type IV adsorbed isotherm.

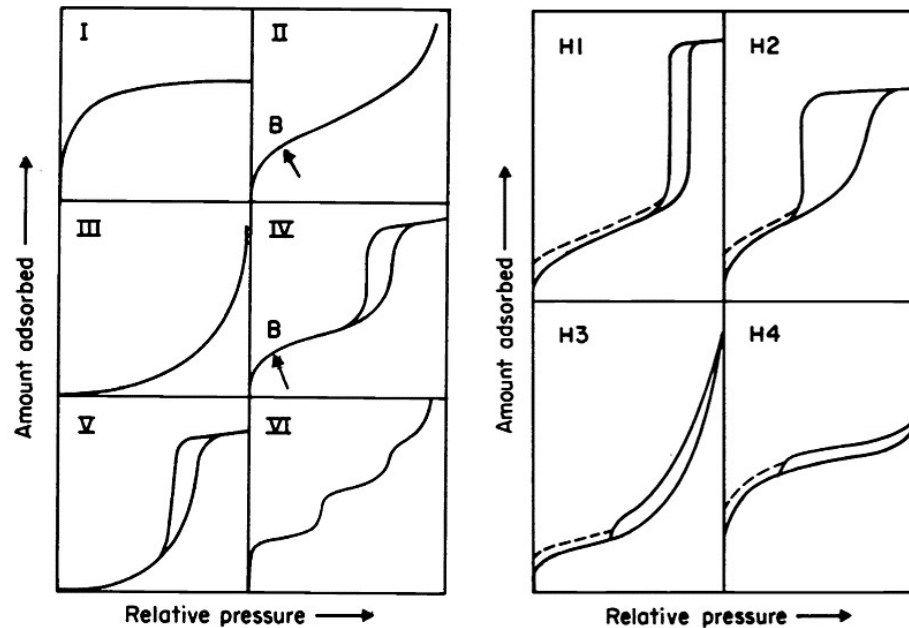


Figure 2-37: Types of isotherms (left graph) and hysteresis loops (right graph) by Sing (1985).

2.5.5 CONCRETE SORPTIVITY AND POROSITY TEST

The durability index testing procedure manual, assembled by University of Cape Town, University of the Witwatersrand and CoMSIRU (University of Cape Town et al., 2017) illustrates a simple method that can be used to determine the sorptivity and porosity of a concrete sample. The test must be conducted in a temperature controlled room with temperatures between 20 and 25 °C. All samples must be dried in the oven for 7 days at 50 °C before testing. The samples must be placed on filter paper with water up to a depth of 2 mm (illustrated in Figure 2-38). Then, the sample's weight must be measured after 3, 5, 7, 9, 12, 16, 20 and 25 minutes while sucking up water through the filter paper. Thereafter, the samples must be placed in a vacuum (-75 kPa) for about 18 hours as shown in Figure 2-39. After this period the samples should be saturated and weighed again for a final time. All the weight measurements must be taken with an accuracy of 0.01 g. The sample dimensions are also required for the final calculations. The manual suggests to download a free spreadsheet from <http://www.theconcreteinstitute.org.za/durability> to insert all data, which will then calculate the sorptivity as well as the porosity of the samples. The calculation details and equations used in this spreadsheet can be seen in the durability index testing procedure manual under Part 3 (Standard procedure for water sorptivity and porosity test).



Figure 2-38: Filter paper test setup (University of Cape Town et al., 2017).

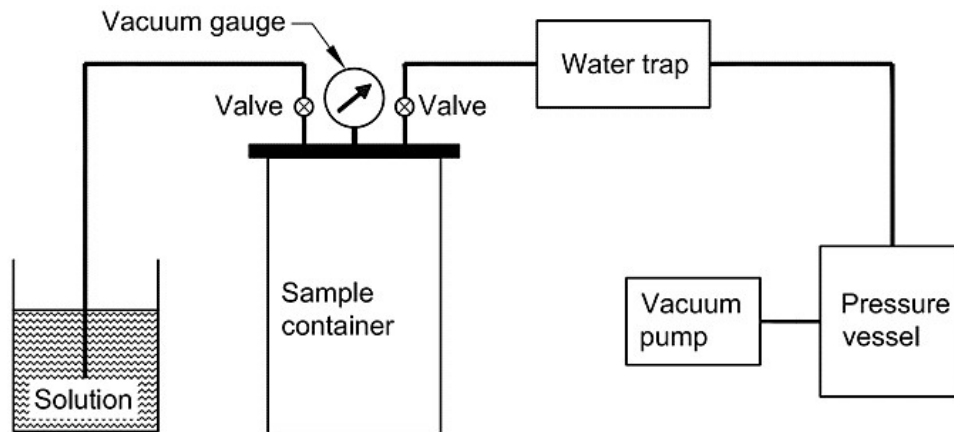


Figure 2-39: Vacuum saturation setup (University of Cape Town et al., 2017).

2.6 SHRINKAGE OF CONCRETE

The loss of water within cement grains causes shrinkage and is largely recoverable when regaining water. The schematic shown in Figure 2-40 illustrates the possible locations of water in a gel structure. The properties of the different water components are listed as follows (Domone and Illston, 2010):

- 1) Large pores will be filled partially with water while the remaining zones contain water vapour at a pressure that is in equilibrium with the surrounding environment, while taking the temperature and relative humidity of the environment into consideration.
- 2) Capillaries and large gel pores (larger than 5 nm in diameter) are filled with capillary water. If the water is found within a pore with a diameter larger than 50 nm, the water is considered as free water. Free water is not reachable by surface forces and when it is removed it will not

cause any shrinkage. However, the capillary water is subjected to capillary tension forces and the removal of this water can result in some shrinkage.

- 3) Water under the influence of surface attractive forces (close to the solid surface) is referred to as adsorbed water. The loss of this water can result in drying up to 30% relative humidity and is the main contributing factor to drying shrinkage.
- 4) Interlayer water can be found in the gel pores (smaller than 2.6 nm) and is under the influence of attractive forces from two surfaces. Therefore, this water is strongly held in its position and can only be removed by excessive drying, including relative humidities less than 10% and elevated temperatures. The loss in interlayer water can result in substantial shrinkage as the van der Waals forces pull the solid surfaces together.
- 5) The water that combines with the fresh cement in the hydration process is referred to as chemically combined water. This water does not contribute to shrinkage, because this water is depleted during the hydration process.

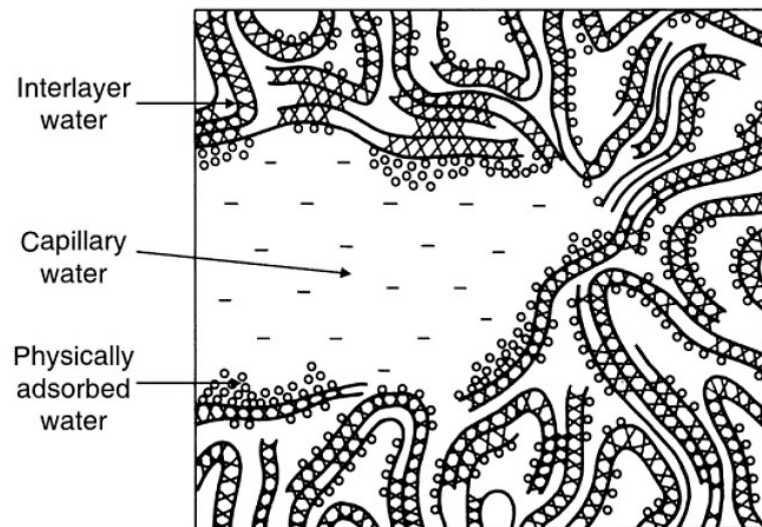


Figure 2-40: Schematic of types of water within calcium silica hydrate (Feldman and Sereda, 1970).

2.6.1 DRYING SHRINKAGE

Non uniform shrinkage establishes in concrete due to the progressive drying of concrete. This is a complex phenomenon which is affected by various factors, for example the composition of the concrete, the environment conditions, local temperatures, the sample size being measured and the humidity of the concrete at different points within the sample (Han and Lytton, 1995). In the past decade, some research has been focused on the shrinkage of concrete and unfortunately indistinct aspects of the shrinkage of concrete is still witnessed (Vinkler and Vitek, 2017).

Normal concrete usually shrinks between 5% and 20%. However, the aggregates stiffness in the concrete can influence the shrinkage of the sample. Lightweight aggregates will give less restraint compared to normal dense aggregates (stiffer). Therefore, lightweight aggregate concrete will result in bigger overall shrinkage compared to normal aggregate concrete, when the same volumetric mix proportions are used. The relationship between the aggregate content and the stiffness thereof is explained with Equation 2-19:

$$\frac{\varepsilon_c}{\varepsilon_p} = (1 - g)^n \quad \text{Equation 2-19}$$

Where;

ε_c = shrinkage strain of the concrete

ε_p = shrinkage strain of the paste

g = aggregate volumetric content

n = constant depending on the aggregate stiffness (between 1.2 and 1.7)

Bissonnette et al. (1999), stated that the w/c ratio (between 0.35 and 0.5) of a concrete mixture does not have a major influence on the drying shrinkage as presented in Figure 2-41. However, by incorporating fly ash, ground granulated blast furnace slag (GGBS) or microsilica into the concrete mixture, can change the mix proportions within the concrete which will greatly affect the overall shrinkage.

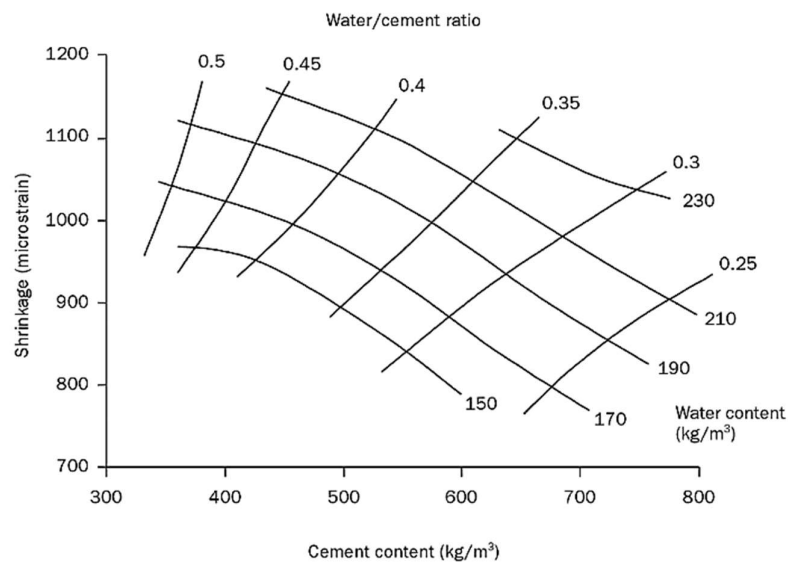


Figure 2-41: Effect of the cement, water content and w/c ratio on shrinkage of concrete – moist curing for 28 days followed by drying for 450 days (Shoya, 1979).

Li and Yao (2001) studied the drying shrinkage of high performance concrete. Table 2-2 presents the three different concrete mixtures that were analysed. Three different binding materials were used including silica fume (SF), portland cement and ultrafine Ground Granulated Blast-Furnace Slag (GGBS). Concrete mixtures A, B and C had a w/c ratio of 0.26, 0.37 and 0.43 respectively. All three mixtures had the same mix proportions except for the type of binding material used in each mixture. In concrete A, only portland cement was used as the binder and concrete B ultrafine GGBS replaced the cement by 30 % of the cement's weight. Furthermore, 40 % of the cement in concrete C was replaced by ultrafine GGBS (also by 30% of the cement's weight) and SF by the other 10 % of the cement's weight. The superplasticizer (SP) dosage was kept constant at 1.6 % of the total weight of binder for all the mixtures. The shrinkage of the samples were measured up to 180 days. It can be seen in Figure 2-42 that the GGBS and SF greatly influenced the strength of the concrete and reduced the amount of drying shrinkage.

Table 2-2: Concrete mix design (Li and Yao, 2001).

Mix proportioning (kg/m ³) and workability (cm) of HPC									
Concrete	Mix proportioning							Workability	
	C ^a	GGBS	SF	SP (%)	CA ^b	FA ^c	Water	Slump	Slump flow
A	600	–	–	1.6	1134	610	156	22.5	49.0
B	420	180	–	1.6	1134	610	156	24.5	67.0
C	360	180	60	1.6	1134	610	156	24.0	56.0

^a Cement.
^b Coarse aggregate.
^c Fine aggregate.

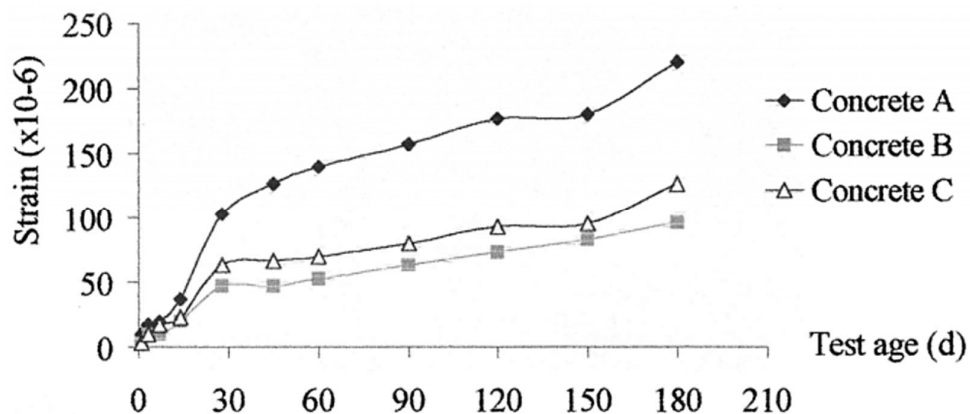


Figure 2-42: Drying shrinkage test results (Li and Yao, 2001).

2.7 STRENGTH OF CONCRETE

The strength of concrete increases significantly within the first 90 days. Individual products form during the hydration process of concrete which were briefly explained in Section 2.4. Figure 2-43 illustrates the different products forming after the concrete has been mixed. C-S-H products dominate after a day, plus the amount of calcium hydroxide increase, together with minor oxides, cause the HCP to be highly alkaline (pH between 12.5 and 13). Figure 2-44 shows the contribution of the different products to the strength development of the cement within 360 days. It also emphasises the long term strength gaining reactions of the calcium silicates and mostly the belite (C_2S).

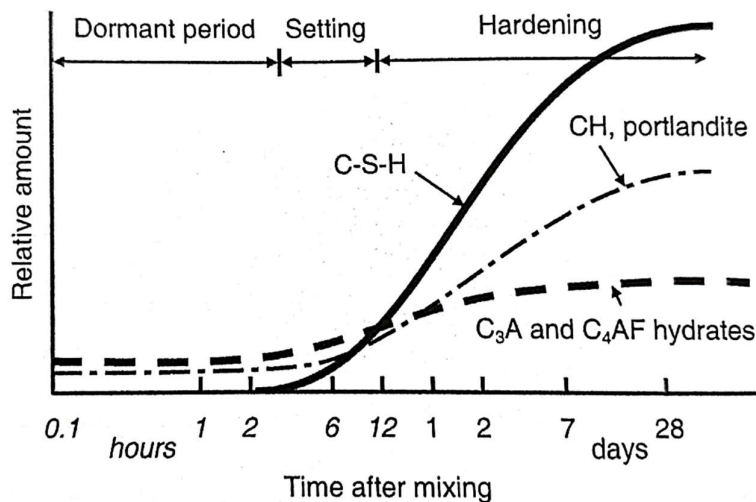


Figure 2-43: Development of the hydration products of Portland cement (Soroka, 1979b).

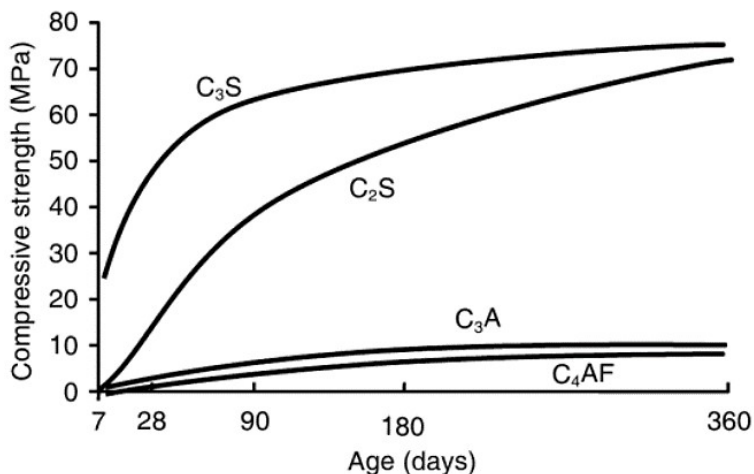


Figure 2-44: Development of strength of compounds in Portland cement on hydration (Bogue, 1955).

Sun et al. (2020) described the increase in dynamic strength of wet concrete as a result of free water in the concrete pores, named the Stefan effect (Cadoni et al., 2001, Wang and Li, 2007, Pedersen et al., 2008). The Stefan effect is explained by two circular plates parallel to one another with radii r , which is separated by an incompressible liquid with viscosity μ (measured in Pa·s) and with a thickness h , as shown in Figure 2-45. Equation 2-20 expresses the force (F) required to pull the circular plates apart with a velocity (v) perpendicular to the surface of the plates (Zheng et al., 2005).

$$F = \frac{3\pi\mu r^4 v}{2h^3} \quad \text{Equation 2-20}$$

The viscous tensile stress between the two plates can be expressed using Equation 2-21:

$$\sigma_v = \frac{3\mu r^2 v}{2h^3} \quad \text{Equation 2-21}$$

These equations illustrate that the viscous force is directly proportional to the magnitude of μ and v . It is assumed that the free water in the micro-pores, capillaries and micro-cracks of the hydrates is the source of viscosity when the solid frame is observed as a network of plates. This assumption is useful for the Stefan effect since it indicates why the loading rate effect is larger in wet concrete (Rossi et al., 1992).

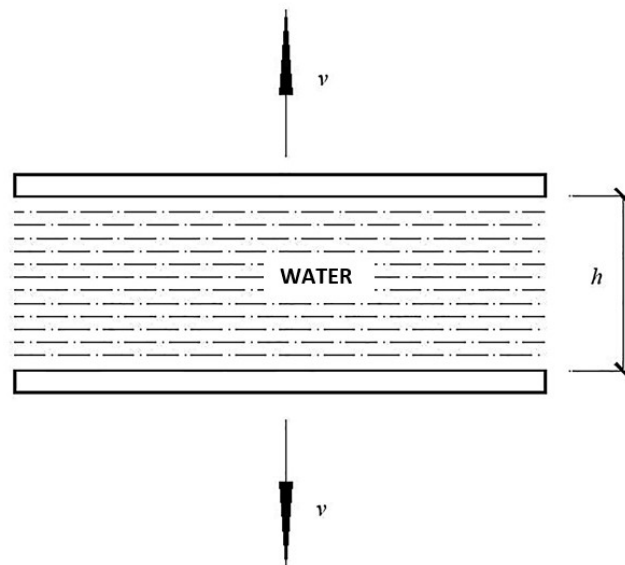


Figure 2-45: Demonstration of the Stefan effect (Wang et al., 2009).

Chen et al. (2013), presented a study on the effect porosity may have on the compressive and tensile strength of concrete. Several models were used to predict the comparison of compressive strength, flexural strength and splitting tensile strength in relationship to the porosity. Figures 2-46 to 2-48 illustrate that the total porosity decreases with an increase in the compressive strength, flexural strength and splitting tensile strength.

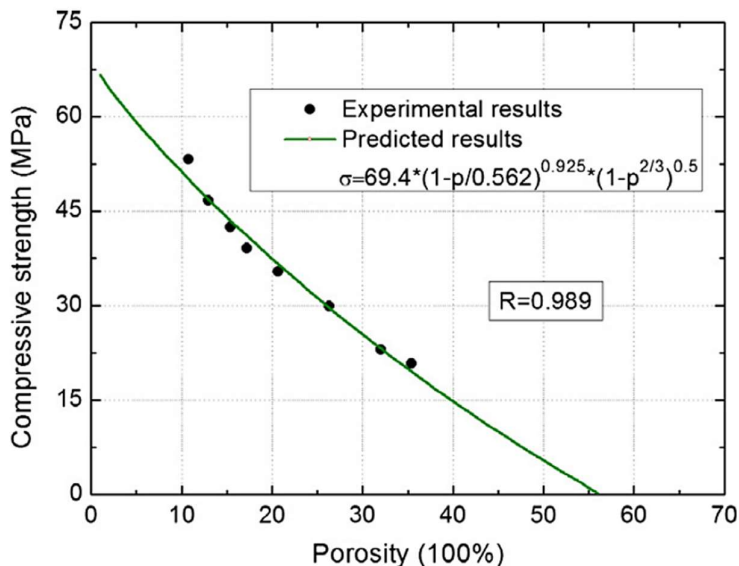


Figure 2-46: Compressive strength versus porosity (Chen et al., 2013).

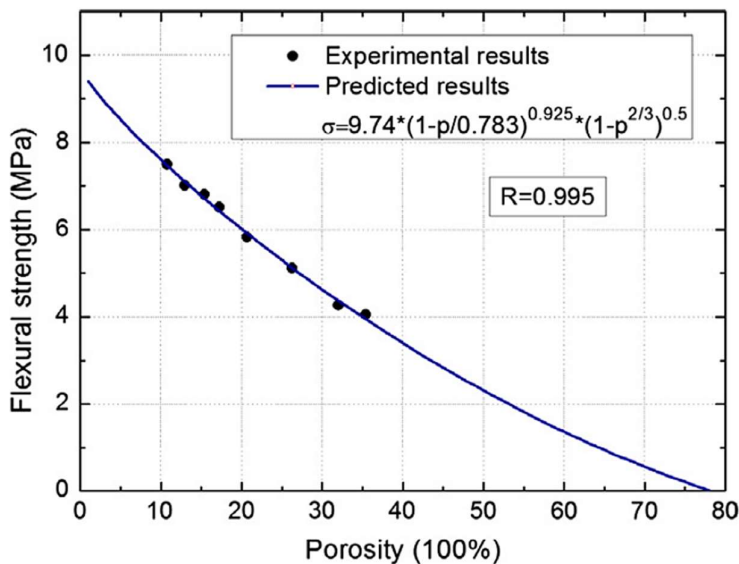


Figure 2-47: Flexural strength versus porosity (Chen et al., 2013).

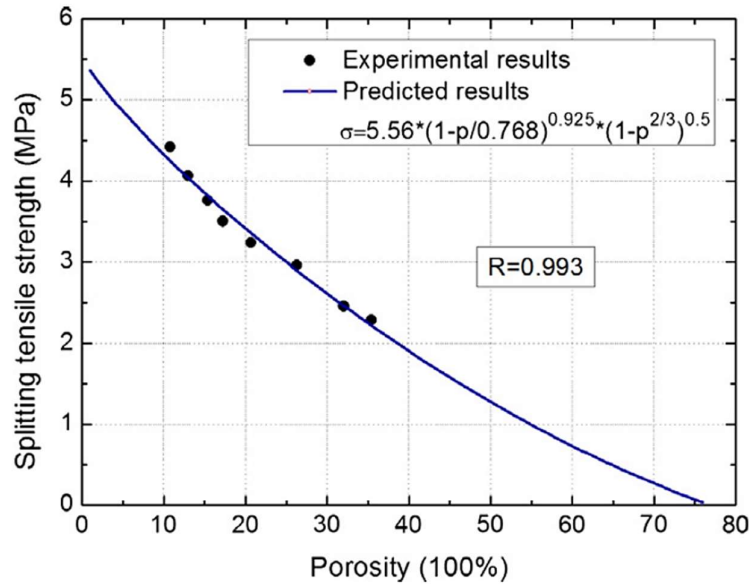


Figure 2-48: Splitting tensile strength versus porosity (Chen et al., 2013).

2.7.1 FLEXURAL TESTS

Two commonly used flexural test methods include the three point and four point bending tests. The main difference between these two tests are the positions where the load (P) is applied onto the beam (Bencardino, 2013). Figure 2-49 illustrates the four point bending test setup on the left hand side and the three point bending test on the right hand side.

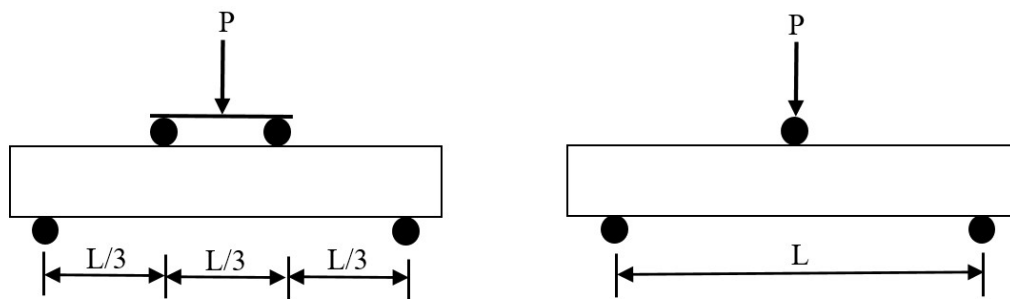


Figure 2-49: Three and four point bending tests.

Several standards adopted the three point bending test (TPBT) method including the European standard 14651 (EN, 2007) and RILEM technical committee guidelines document (Vandewalle et al., 2003). The European standard suggests that the sample length should be between 550 and 700 mm. However, the different codes have different requirements. The four point bending test (FPBT) has been adopted by the ASTM C1609 standards (Banthia and Islam, 2013) and similarly to the TPBT the different codes have different requirements for the geometry of the samples.

2.7.2 COMPRESSIVE TESTS

In South Africa, a concrete cube is typically used in the standard compressive strength test. In the USA, the cylinder compressive strength test is used. In Europe, both the concrete cube and cylinder strength tests are used (Domone and Illston, 2010). The compressive testing machine consist of two thick plates through which the load is applied onto the concrete cube. The bottom plate is fixed while the top plate has a ball seating which allows rotation of the plate to align with the bottom plate against the sample, just before starting the test. When the load is applied the top plate will slowly make contact with the concrete cube, covering the whole surface of the sample, preventing any local stress concentrations while testing.

After failure, a double pyramid shape crack pattern can be observed, indicating that the stress within the cube is not uniaxial. Lateral tensile strains are induced by the compressive load due to the Poisson effect. The concrete is in a triaxial stress state with a larger failure stress compared to the true (unstrained) strength, which is a big concern when using the cube compressive test. Alternatively, a cylindrical sample is used in the compressive test to overcome the triaxial stress problems (Raheem, 2019). The cylindrical sample should usually satisfy a height to diameter ratio of 2. The cylindrical sample typically has a height of 300 mm with a diameter of 150 mm and is tested vertically upright. The cylinder will fail near uniaxial cracking since the effect of the end restrains to the middle section of the cylindrical sample is significantly lower, see Figure 2-50. Therefore, indicating that the failure stress is close to the unconfined compressive strength. It is often assumed that the cylinder compressive strength is 20% lower compared to the cube compressive strength. To conform to the South African standards, the cube test was used for the compressive strength.

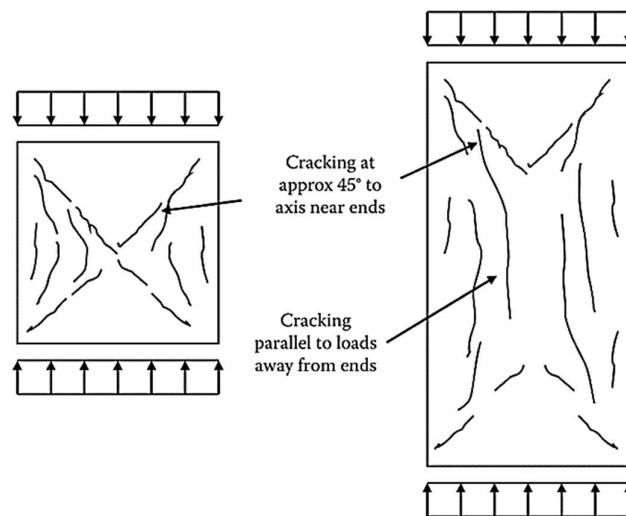


Figure 2-50: Cracking patterns during testing of concrete samples in compression (Soutsos and Domone, 2017).

2.7.3 SPLITTING TEST

The tensile strength of concrete is usually obtained through the standard split cylinder test method. The ASTM C496 Standard (2017) determines the tensile splitting strength of the sample from the peak load applied onto the sample during testing. The sample (concrete cylinder) is placed on its side in the compressive testing machine with two loads applied across its vertical width as demonstrated in Figure 2-51. The cylinder size is typically 200 mm or 300 mm in length and 100 mm in diameter (d). Hardboard is placed between the cylinder and the testing machine's top and bottom plates to ensure uniform loading across the cylinder's length. Failure occurs alongside the vertical crack plane, splitting the cylinder into two pieces. Horizontal stress develops on the crack plane, which is near uniform tension stress (f_s), and can be used to define the cylinder splitting strength. The cylinder splitting strength is given by the expression in Equation 2-22 where P is the failure load:

$$f_s = \frac{2P}{(\pi/d)} \quad \text{Equation 2-22}$$

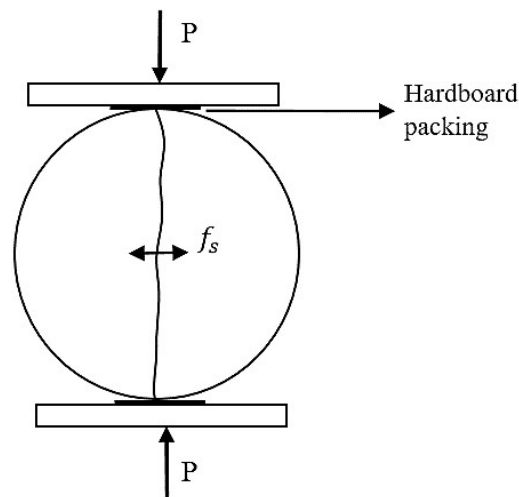


Figure 2-51: Cylinder splitting tensile strength test setup.

2.8 SUMMARY

The SWRC can be used to obtain multiple properties of soils. Therefore, the SWRC may also have the potential to describe the properties of concrete. The WP4C apparatus is used to measure the suctions within this research study, as well as to determine the water retention curves of cement paste and mortar samples with different w/c ratios.

It was also seen in the literature that the porosity of concrete is a difficult parameter to determine after concrete has set and that the concrete's porosity can change after some time. Therefore, different tests

were used to measure the porosity in an attempt to find representative results when comparing the porosity with the suction results obtained.

Different concrete strength parameters such as the flexural, compressive and splitting tests discussed in the literature review were measured to estimate whether there is a relationship between these properties and the suctions measured.

Lastly an overall comparison between all the different concrete properties measured and the suction results was investigated. The relationship between these parameters is described with visual and data interpretations.

3 EXPERIMENTAL WORK

3.1 INTRODUCTION

In this chapter the experimental procedures followed during the research project are discussed. A short study was conducted to determine whether the WP4C apparatus gives repeatable suction measurements. Cement paste with different w/c ratios were used in this study. The main objective of this research was to obtain a visual relationship between the water retention curves and different properties of the concrete such as the workability, porosity, shrinkage and strength.

3.2 DEW POINT POTENTIAMETER

The Dew Point PotentiaMeter (WP4C) is used to determine the suction measurements in this study (see Figure 3-1). Water potential or suction is defined as the potential energy per unit volume of water in a sample. The WP4C apparatus measures the total water potential which is equal to the sum of 4 components, namely:

- a) Gravitational potential which depends on the position of the water in the gravitational field.
- b) Matric potential which depends on the adsorptive forces binding the water to the matrix in a sample.
- c) Osmotic potential which depends on the concentration of dissolved substance in the water within the matrix.
- d) Pressure potential which depends on the hydrostatic pressure in the water.

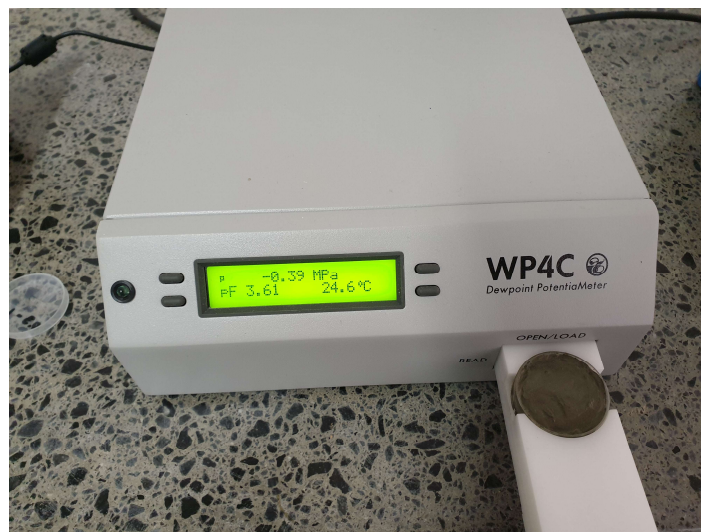


Figure 3-1: The WP4C apparatus measuring suction.

The relationship between the sample water potential (Ψ) and the vapour pressure of the air within the sample is used to calculate the suction of a solid or liquid matrix and is described by Equation 3-1:

$$\Psi = \frac{RT}{M} * \ln\left(\frac{p}{p_o}\right) \quad \text{Equation 3-1}$$

Where;

p = vapor pressure of the air

p_o = saturation vapor pressure at sample temperature

R = gas constant (8.31 J/mol K)

T = kelvin temperature of the sample

M = molecular mass of water

The WP4C uses the chilled mirror dew point technique to measure the water potential of a sample in mega pascal (Meter Group, June 2, 2017). Inside the chamber the sample cup is sealed against the sensor block which contains an internal fan, a dew-point sensor, temperature sensor and an infrared thermometer. The headspace of a sealed chamber containing a mirror is used in the apparatus to equilibrate the sample by detecting condensation on the mirror (see Figure 3-2). When the sample is at equilibrium, the water potential of the sample at that point will be the same as the water potential of the air inside the chamber. In the WP4C apparatus the temperature of the mirror is controlled by a thermoelectric cooler and the precise point at which condensation takes place on the mirror is detected by a photoelectric cell. A thermocouple is attached to the mirror to determine the temperature at which condensation takes place. The apparatus displays the final suction measurement together with the temperature of the sample. The WP4C also uses an internal fan which circulates the air in the chamber to reduce the overall time to equilibrate the sample. It measures both surface temperatures and the dew point simultaneously, which disregards the need for complete thermal equilibration. The sample size used in this apparatus is 24 x 23 x 9 mm or 15 ml. However, it is recommended that the container is filled up to 7 ml. The compatible standard used for this apparatus is the ASTM D6836-07.

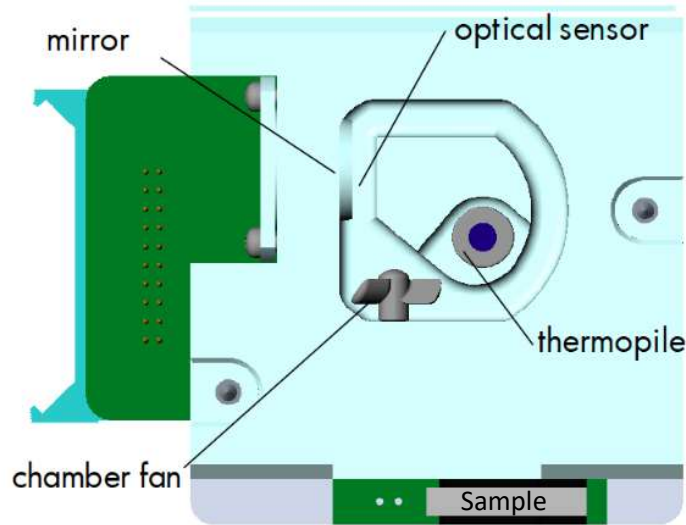


Figure 3-2: WP4C view of the inside block.

3.3 CEMENT PASTE TESTING

A study was conducted to ensure that this research project would deliver usable results when using the WP4C equipment for measuring the suctions in concrete. The relationship of the suction measurements for four different w/c ratio cement pastes, including 0.3, 0.35, 0.4 and 0.45 w/c ratios were investigated. Five samples of each cement paste were tested to predict whether the measuring technique yields repeatable results. The strength of the different w/c ratio pastes was also investigated and discussed.

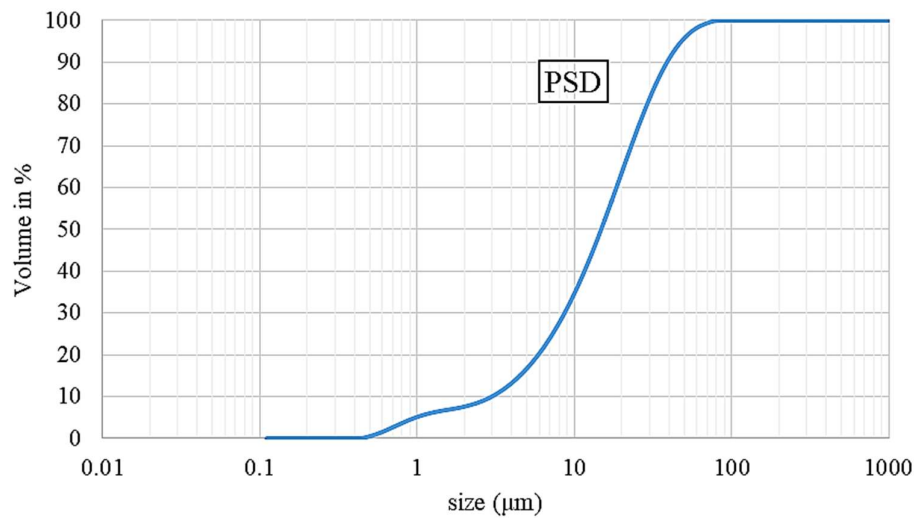
3.3.1 CEMENT PASTE TESTING METHODOLOGY

The methodology explains how the samples were prepared together with the suction measurements obtained. The flexural test (Indirect Modulus of Rupture testing (MOR)) that was utilized to obtain the strength of the concrete is also discussed. The mix design used for this study is tabulated in Table 3-1. Only the amount of cement varies in each concrete mixture and no aggregates or sand were added. The volume of all the mixtures varied. However, this would not have an impact on the relationship between the water and the cement together with the drying process during the suction measurements which were investigated.

Table 3-1: Mix design used in the cement paste testing.

Sample Type:	W/C Ratio	Water (l)	Cement (kg)	Volume (kg/l)
1	0.30	0.6	2.0	3.3
2	0.35	0.6	1.7	2.9
3	0.40	0.6	1.5	2.5
4	0.45	0.6	1.3	2.2

The particle size distribution (PSD) plot of the cement used in all the mixtures can be seen in Figure 3-3. The apparatus used to obtain the PSD was the Malvern Mastersizer 2000. The intensity of scattered light was measured after passing laser light through the cement in order to determine the PSD.

**Figure 3-3: PSD plot of the cement used in the cement paste study.**

3.3.2 SAMPLE PREPARATION AND SUCTION MEASUREMENTS

The steps followed for preparing the cement paste samples as well as the apparatus used are discussed in this section. Five samples for each w/c ratio (0.3, 0.35, 0.4 and 0.45) were prepared as already mentioned. The sample preparation steps can be listed as follows (also see Figure 3-4):



Figure 3-4: Sample preparation steps before suction measurements.

- 1) Portland Cement (PPC) with a specified strength of 52.5 N was used and the cement was sieved through a 300 μm sieve before casting to ensure no cement clots were included in the mixture.
- 2) For the cement paste study the mixtures were mixed by hand since only 0.0015 m^3 of cement paste was required for all the tests to be conducted and each mixture was prepared in a different container. Each mixture was mixed for 5 minutes.
- 3) Thereafter, three mortar prisms of each mixture were prepared for strength testing and also two to three suction measurement containers were filled. This procedure was repeated on a different day.
- 4) The suction measurements were taken directly after the suction containers were filled with the cement paste. The samples were kept in a temperature controlled room, at between 22 and 25 $^{\circ}\text{C}$. The suction for each sample was measured weekly for a minimum of 3 months. The apparatus on the left hand side of the WP4C machine (Figure 3-4) is a temperature equilibration plate which kept the sample temperature constant at 23 $^{\circ}\text{C}$ directly before obtaining the suction reading (using the WP4C).

Three mortar prisms of each mixture with a dimension of 150 mm x 40 mm x 40 mm were tested, with both flexural and compressive strength tests conducted. After the moulds were filled with cement paste it was placed on a vibrating table for one minute to ensure proper compaction. Thereafter, the samples were kept in a curing room, under a curing blanket for 1 day. The samples were then demoulded and placed in a water bath at 25 $^{\circ}\text{C}$ until tested.

The Modulus of rupture (MOR, f_b) of all sample was tested after 7 days of curing. According to Hall (1994), since the compressive strength of concrete is much higher than the flexural strength, when a load is applied at the middle of the beam the failure will occur when a flexural tensile crack propagates upwards through the beam. The maximum flexural stress in the concrete can be calculated by using Equation 3-2 (Hall, 1994):

$$f_b = \left(\frac{PL}{bd^2} \right) \quad \text{Equation 3-2}$$

After the MOR test was completed, the compressive strength was obtained for the two halves, from the MOR test. The samples were placed in a compressive testing machine with a maximum capacity of 300 kN (details on the machine setup is discussed in Section 2.7.2). The samples were loaded perpendicular to the direction of casting.

3.3.3 CEMENT PASTE RESULTS

The suction measurements for the sample types 1, 2, 3 and 4 as numbered in Table 3-1 are presented and discussed within this section. All the suction results and calculations of the cement paste study are tabulated in Appendix A. It can be seen that the samples for all the mixtures follow the same trend proving that the WP4C testing apparatus yields repeatable results. The suction measurements for the 0.3 w/c ratio cement paste (Figure 3-5) appear to be the highest over the 3 month testing period. The different sample types are discussed in detail in the following list:

- 1) Figure 3-5 presents the 0.3 w/c ratio suction measurements where it can be seen that the suction increased to a value of 20 MPa within the first 200 hours (8 days). Thereafter, the curve flattens out and the suction gradually increase to a value of 67 MPa after 2200 hours (3 months).
- 2) The 0.35 w/c ratio sample results can be seen in Figure 3-6. The suction measurements reach a suction value of 20 MPa after 400 hours (16 days) and a maximum suction value of 58 MPa is reached after 3 months.
- 3) The samples with a w/c ratio of 0.4 (Figure 3-7) reach a suction value of 20 MPa after 600 hours (25 days) and a maximum suction value of 54 MPa is reached after 3 months.
- 4) Figure 3-8 presents the suction measurements for a w/c ratio of 0.45, reaching a suction value of 20 MPa after 1000 hours (41 days) and a maximum suction value of 35 MPa is measured after 3 months.

For an increase in the w/c ratio there is a decrease in the total suction as well as a decrease in the slope at which the suction measurements increase. It can be concluded that the WP4C test results are repeatable when comparing the suction measurements of five samples (for the same w/c ratio) with one another. The time at which a specific suction value was reached increased with an increase in the w/c

ratio as seen at 20 MPa for the different mixtures. There is a clear trend in the data and it can be seen that the samples from the same batch of cement paste follow a similar path.

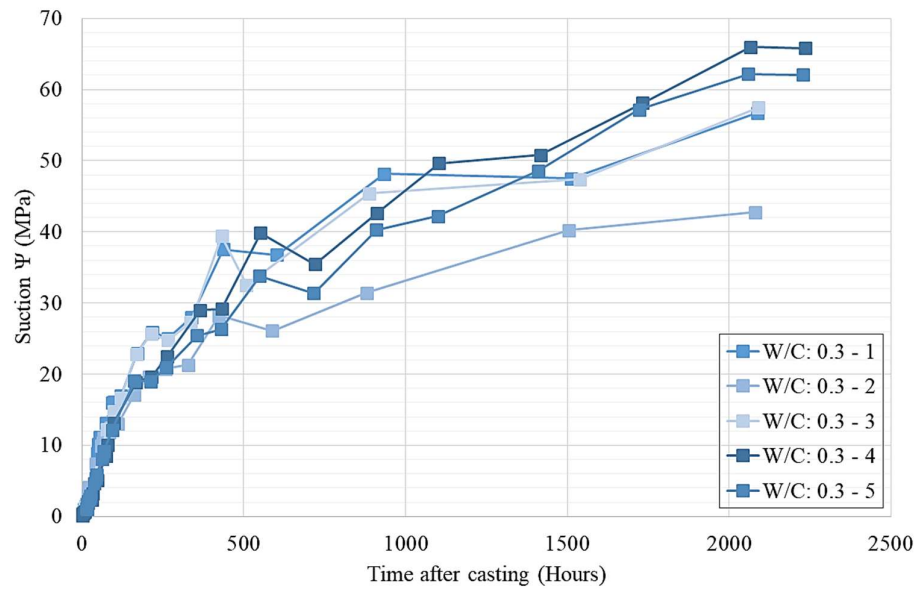


Figure 3-5: Suction measurements for w/c ratio 0.3 cement paste (1).

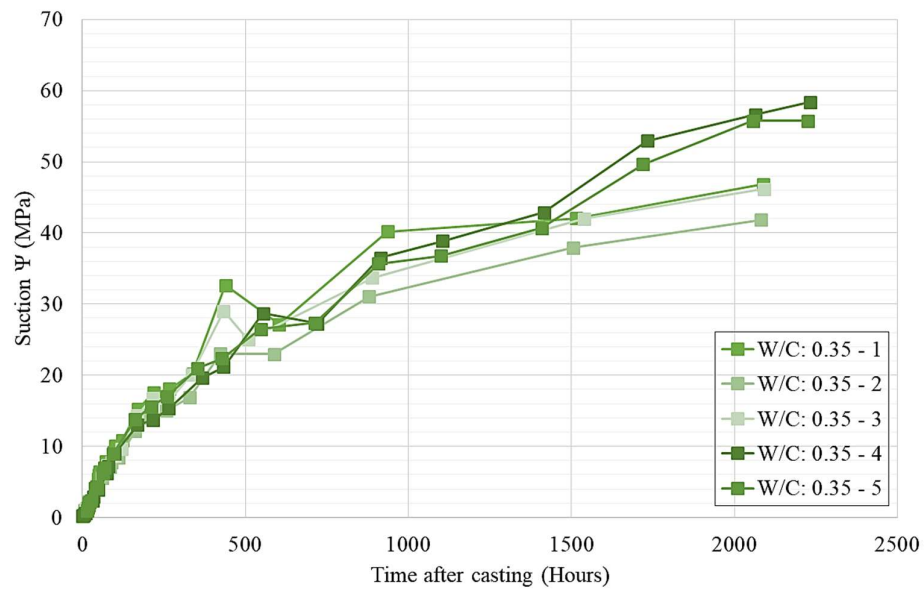


Figure 3-6: Suction measurements for w/c ratio 0.35 cement paste (2).

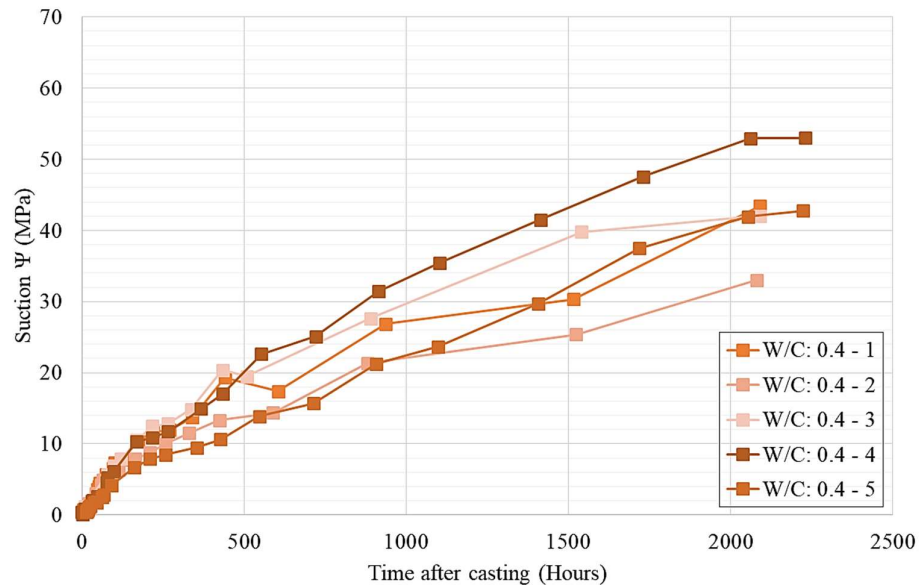


Figure 3-7: Suction measurements for w/c ratio 0.4 cement paste (3).

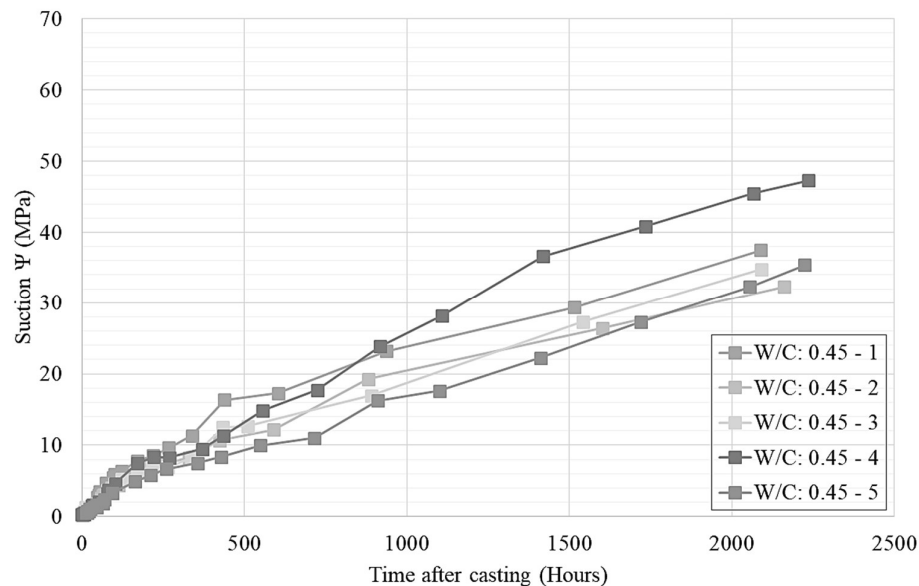


Figure 3-8: Suction measurements for w/c ratio 0.45 cement paste (4).

There was a sudden jump in the suctions at specific times. The reason for the jump in suction measurements were a results of water droplets forming on the container's lid due to condensation. Those water droplets then fell onto the sample when removing the lid from the container. This problem was avoided in the next study conducted on different mortar mixtures. The sample was turned upside down while removing the lid from the container, preventing the water on the lid to fall onto the sample. The lid were then wiped to ensure no water was left on the lid of the container.

The average suction measurements of the five different samples measured within the same day were calculated together with the 95% confidence interval of each data set for the different w/c ratio samples, presented in Figures 3-9 to 3-12. It is clear that the bandwidth of the 95% confidence interval increased from 400 hours (21 days). The upper and lower envelopes indicate that the suctions measured with the WP4C apparatus will lie within these bands, 95% of the time for any sample measured.

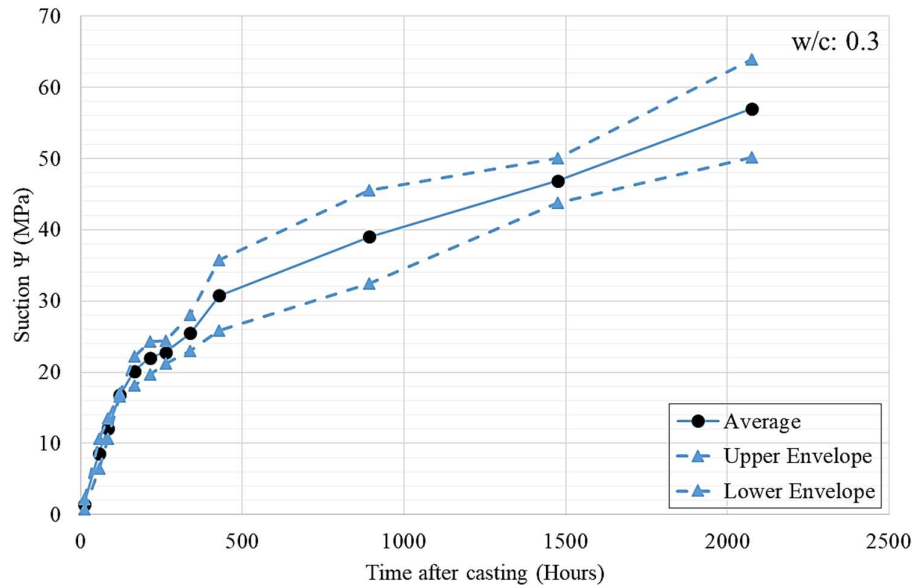


Figure 3-9: 95% Confidence interval for w/c ratio 0.3 cement paste (1).

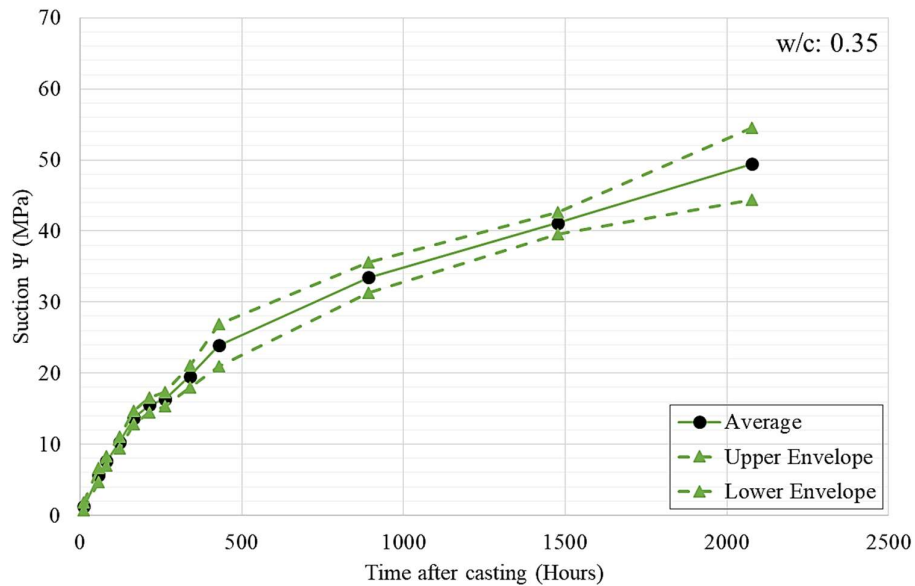


Figure 3-10: 95% Confidence interval for w/c ratio 0.35 cement paste (2).

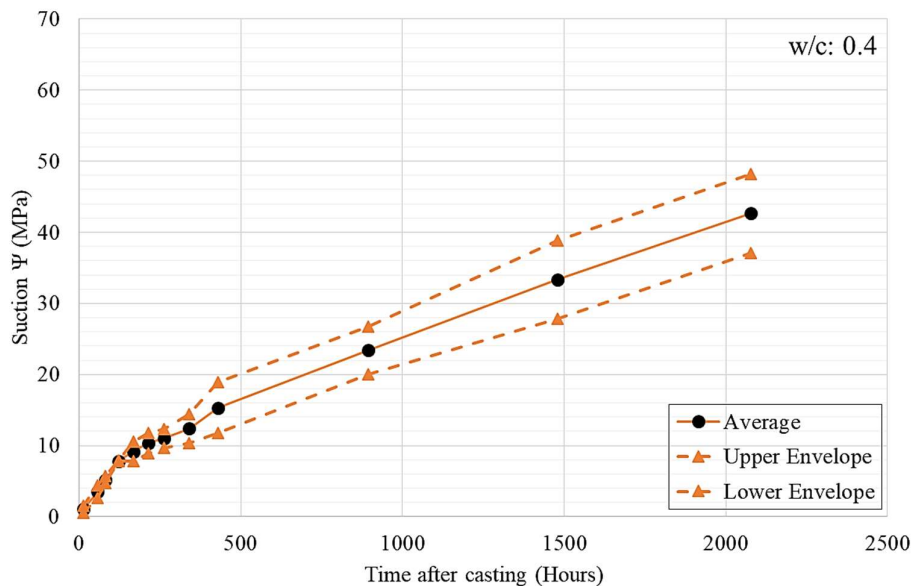


Figure 3-11: 95% Confidence interval for w/c ratio 0.4 cement paste (3).

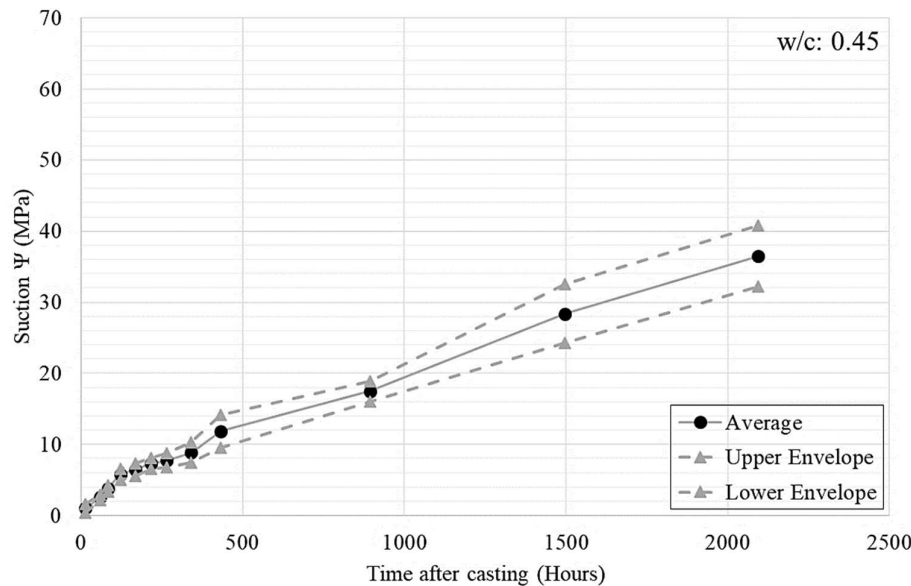


Figure 3-12: 95% Confidence interval for w/c ratio 0.45 cement paste (4).

Figure 3-13 shows the 95% confidence intervals (up to 700 hours or 28 days) for all the w/c ratio cement paste samples tested. It is clear that the different w/c ratio envelopes do not overlap significantly. Therefore, it can be stated that the different w/c ratio samples will give different results when measuring suctions with the WP4C apparatus.

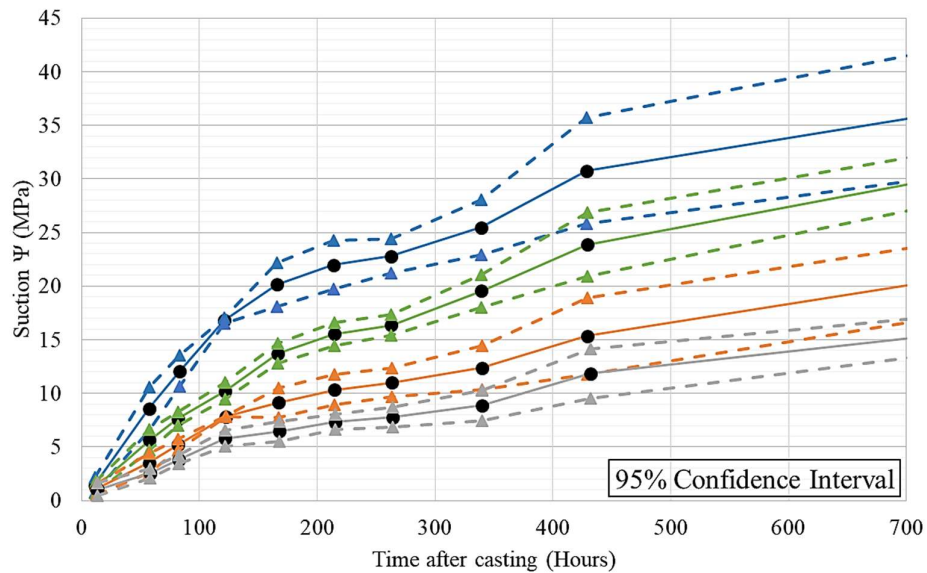


Figure 3-13: Combined 95% confidence intervals for the different w/c ratio cement paste samples.

The average suction measurements for all the w/c ratio cement paste samples tested are shown in Figure 3-14, for up to 87 days of testing. The average suction measurements developed after 28 days or 672 hours, relates well with literature (Kondraivendhan and Bhattacharjee, 2016), showing that with a decrease in the w/c ratio an increase in the suction measurements is achieved.

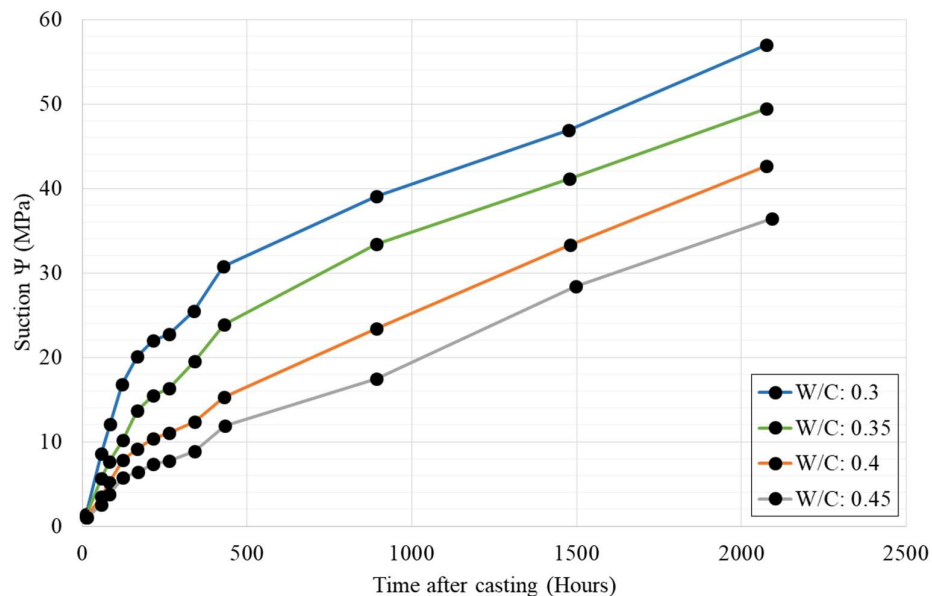


Figure 3-14: Average suction measurements for the different w/c ratio cement pastes.

The flexural and compressive strength developed over the 7 day curing period for the different w/c ratio cement paste samples are tabulated in Table 3-2. Four tests were carried out for each mixture and the average of the four results are presented. Both the compressive and flexural strength decreased with an increase in the w/c ratio, which was expected. Furthermore, a decrease in the suction measurements with an increase in both the compressive and flexural strength was obtained (presented in Figure 3-15).

Table 3-2: Average flexural and compressive strength after 7 Days.

W/C Ratio	Average 7th Day Compressive Strength (MPa)	Average 7th Day Flexural Strength (MPa)
0.30	80.2	11.1
0.35	74.4	10.3
0.40	57.0	8.87
0.45	46.9	8.02

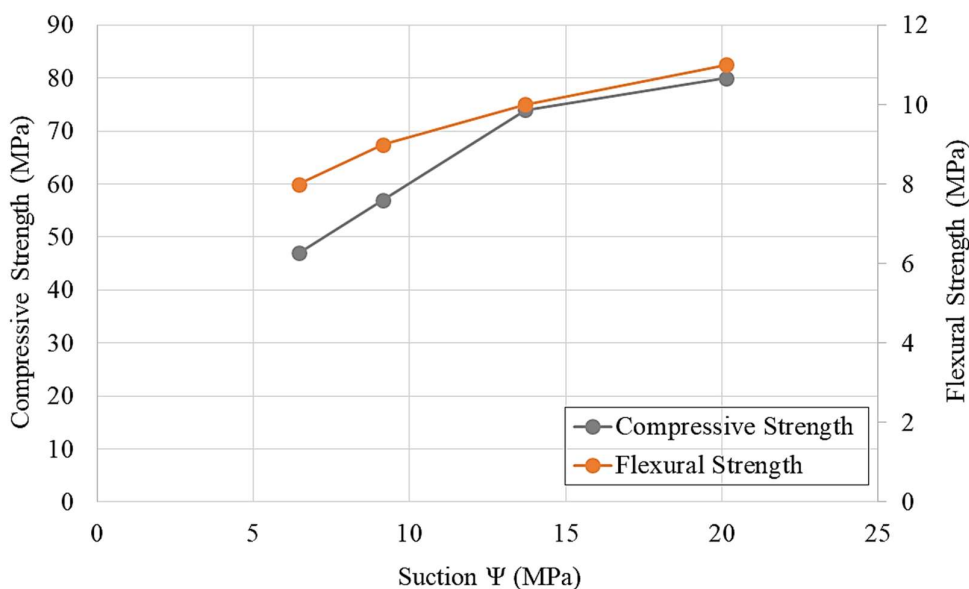


Figure 3-15: Strength developed after 7 days versus the suction.

3.3.4 CEMENT PASTE STUDY CONCLUSIONS

After analysing results of the cement paste tests it can be confirmed that the WP4C apparatus gives results that show clear and repeatable trends. Therefore, the WP4C apparatus was used to determine all the suction measurements in this research project. From the results it can also be concluded that with an increase in the w/c ratio a decrease in the suction measurements (over time) is obtained. Although

the smaller w/c ratio mixtures should yield the highest strength, when the w/c ratio is too small the workability and strength of the concrete will decrease, which needs to be taken into consideration for construction purposes. The suction measurements relate directly to the flexural and compressive strength as seen in literature (Bye et al., 2011). The cement paste with a higher suction coincides with a higher flexural and compressive strength. It can be concluded that with a decrease in the w/c ratio, an increase in the suctions is obtained, while an increase in the flexural and the compressive strength is also achieved.

3.4 MORTAR STUDY METHODOLOGY

For the main study the experimental work was expanded to include sand in the mixtures, as the properties of the concrete should be effected by the properties of the mortar between the inert and relatively impermeable coarse aggregates. The cement based mortar study includes the suction measurements of all the different mortar mixtures, the workability testing of the mortar, the porosity, strength and shrinkage measurements. The test procedures and analysis techniques used in the mortar study are discussed in this section. Table 3-3 presents the mortar mix designs used in the study which includes five different w/c ratios. The same cement as discussed in Section 3.3.1, with a relative density of 3.14, together with silica sand, with a relative density of 2.67 was used. The sand was sieved through a 1 mm sieve (shown in Figure 3-17) to ensure that a constant particle size grading was achieved, as determined for the PSD curve. The PSD of the cement and the silica sand used can be seen in Figure 3-16. More information regarding the cement and silica sand particle size distributions can be found in Appendix B.

Table 3-3: Mix design used for mortar mixtures.

w/c ratio:	0.30	0.40	0.50	0.60	0.70
Materials	kg/m³				
Silica Sand	1254	1437	1546	1620	1672
Cement (CEM 1 - 52.5 R)	859	644	515	430	368
Water	258	258	258	258	258

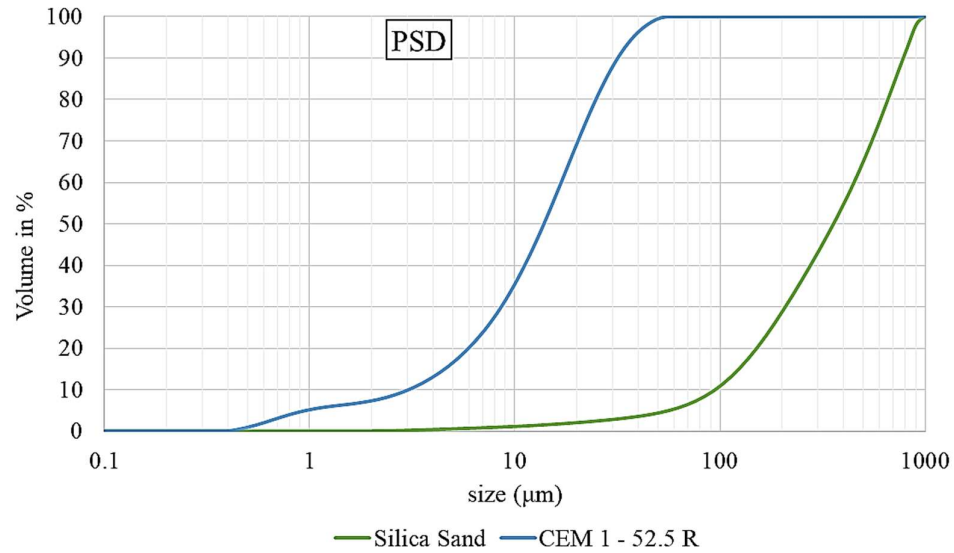


Figure 3-16: PSD for the silica sand and cement used in the mix design.



Figure 3-17: Size sieve used to sieve the cement before mixing.

The samples were placed on a vibrating table for one minute to ensure proper compaction. After the casting procedure all the samples were kept in a curing room, under a curing blanket for 24 hours. Thereafter, the samples were demoulded and some were placed in a water bath at 25°C (wet samples) until tested while the rest of the samples were placed in a room between 22 and 25°C (dry samples) until tested. Both wet and the dry samples were tested during this study.

The environmental conditions in the sample preparation room were monitored. A low-cost microcontroller solution was developed. The intended application required accurate measurements of both the ambient air temperature and the humidity over an extended period of time, with remote monitoring functionality. Based on the availability of commercial solutions, the SiPy microcontroller, developed by PyCom, was selected (Pycom_Go_Invent, 2018). The SiPy microcontroller was paired with a Pysense shield that features a wide selection of environmental sensors.

The electronics, battery and SigFox antenna were installed in a polycarbonate enclosure with a multiple air vents drilled into the sides of the enclosure to ensure adequate airflow. The transparent cover allows the user to observe the power and transmission status that is communicated to the user using the SiPy's RGB LED. The enclosure was positioned adjacent to the concrete samples to record representative environmental conditions over the entire duration of the study as shown in Figure 3-18. The Pysense shield features the following sensors that were logged for the duration of the study:

- Relative humidity and temperature sensor (SI7006-A20)(SiliconLabs, 2016)
- Barometric pressure sensor (MLP3115A2)(NXP_Semiconductors, 2018)
- Digital Ambient Light sensor (LTR-329ALS-01)(LiteOn_DCC, 2020)
- 3-Axis Accelerometer (LIS2HH12)(ST_life.augmented, 2015)

The relative humidity and temperature sensor datasheet provide the following information regarding the accuracy of the measurements:

- $\pm 5\%$ relative humidity over a range of 0-90% relative humidity
- $\pm 1\text{ C}^\circ$ temperature over a range of -10-85 C°

The barometric pressure sensor is indicative of the long-term weather effects, with the ambient light sensor providing a measure of cloud cover and differentiation between day-night cycles in the absence of a real time clock (RTC) reference. The Pysense was configured to turn on every 15 minutes to record, store and transmit sensor readings followed by a deep sleep cycle to conserve power. The short duration of data acquisition – 22 seconds in total - avoids systematic errors through self-heating effects. A 2000 mAh, 3.7V LiPo battery served as the primary energy source that was periodically recharged using the Pysense USB interface. Long-term testing provided a runtime of 70 consecutive days for the sensor platform solely on battery power. This equates to approximately 7000 power cycles in total, with each cycle consuming on average 1.05 mWh of energy.

The SiPy provides a suite of connectivity options in the form of SigFox, Wi-Fi and Bluetooth Low Energy (BLE). SigFox was used as the primary communication system owing to the lack of Wi-Fi availability in the control room, and the low power requirements associated with SigFox communications. SigFox allows a device to send up to 140 messages per day, with each message allocated a 12-byte payload to encode information. The narrowband modulation ensures high transmission reliability for the small messages. Even though the laboratory is situated below ground level, surrounded by taller buildings, adequate signal strength was achieved throughout the study. Only the temperature information was transmitted to the SigFox backend, with the complete set of sensor information stored on non-volatile storage in the form of a removable SD card. With SigFox supporting configurable call-backs, the received messages, in the form of hexadecimal encoded data, were in turn sent to AdafruitIO's IoT service for decoding, visualisation and remote monitoring of the sensor platform in the form of a dashboard (shown in Figure 3-19).

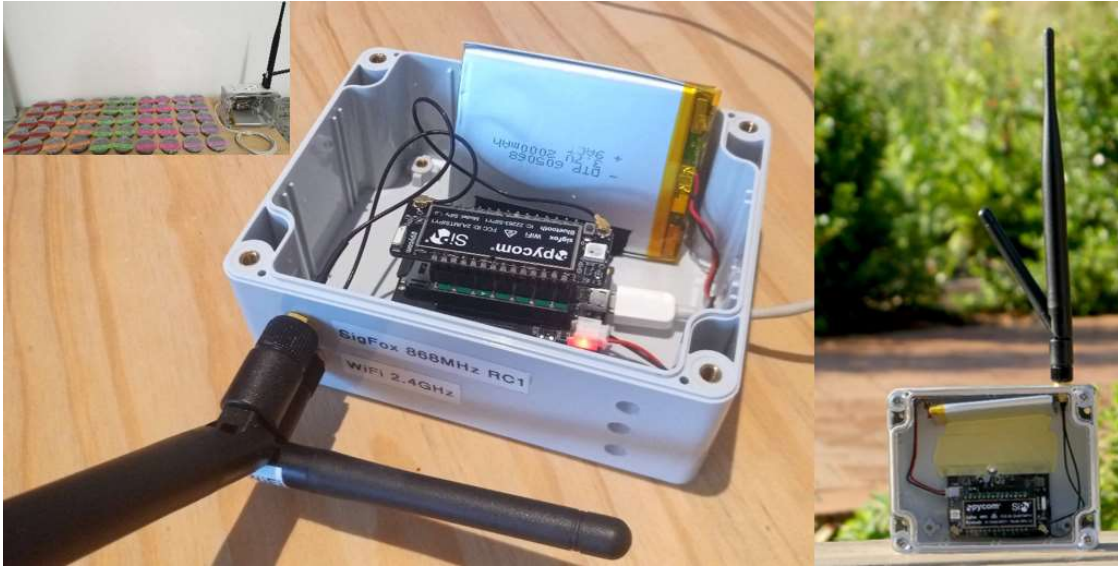


Figure 3-18: Humidity and temperature measuring apparatus.

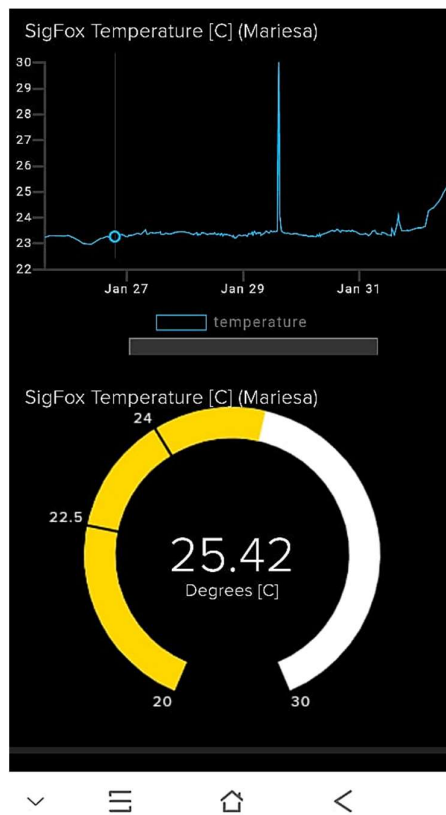


Figure 3-19: AdafruitIO dashboard accessed on a smartphone.

3.4.1 CONCRETE SLUMP FLOW

The procedure used for the slump flow test is similar for different standards such as the American Society for Testing and Materials Standards (ASTM, 2014) and the European Standards (EN, 1999 - 2004). The only minor difference between these two standards is the size of the cone used during the testing procedure.

The EN standard was used in this research with a cone height of 60 mm and cone diameter of 70 mm, together with the bigger cone diameter of 100 mm. Figure 3-20 shows the flow table test setup. The cone was placed in the middle of the flow table and the concrete was poured into the cone in two layers. Each layer was compacted with 10 turns of the tamper arm to ensure uniform filling of the cone. After filling the cone and compacting the concrete, the cone was carefully removed and the height of the concrete on the flow table was measured (called the slump). It is important that the flow table is clean before testing and that the cone is held in position while pouring the concrete into the cone as well as during compaction.



Figure 3-20: Flow table test setup.

After the height of the concrete cone was measured, the tamper arm was turned slowly at a constant rate of one turn per second for 15 turns. Thereafter, the diameter of the concrete spread on the flow table (illustrated in Figure 3-21) was measured in two directions. The average between these two diameters measured is called the slump flow of the concrete.



Figure 3-21: Measuring the slump flow.

3.4.2 SUCTION MEASUREMENTS

The cement paste study (Section 3.3.4) concludes that the WP4C apparatus gives repeatable suction results with clearly noticeable trends. Therefore, the WP4C testing apparatus was used to determine the suction measurements in the mortar study. Ten suction containers per mixture were prepared for different testing procedures (presented in Figure 3-22). These containers were only vibrated for 8 to 10 seconds on the vibrating table. The suction measurements of five containers per mixture were measured repeatedly, directly after casting. The suction readings were taken for three different cases namely dry, wet and partially wet. The dry samples were left open directly after casted and during testing, while the wet samples were placed in a curing bath at 25°C (after setting) for 28 days. The partially wet sample's lids were closed directly after casting and left on during the testing period. The suction measurement results are discussed in Chapter 4.



Figure 3-22: Suction samples and porosity analysis samples.

3.4.3 POROSITY ANALYSIS

Three different tests were performed to determine the porosity of the samples used to measure the suctions. The analysis procedure for each test is discussed in this section and the results are explained in detail in Chapter 4.

1) X-RAY MICROTOMOGRAPHY

This non-destructive testing technique has significantly developed over the last decade, in scanning time as well as spatial resolution (Leißner et al., 2020). The samples were tested at NECSA and more details regarding the X-ray scanning facility and procedure are explained in Section 2.5.2. The X-ray test was performed on all the dry and wet samples marked with a N. The porosity was measured within 7 and 28 days after casting the samples. The wet samples were transported to the facility in water together with the dry samples that were transported in a closed container. During the X-ray scanning procedure 2D images of the samples were taken and then these images were reconstructed using a computer program named CT Pro 3D to construct a 3D volume of all the images (Metris, 2008, Thostenson, 2013).

After all the images were reconstructed, they were analysed to determine the total porosity of each sample after 7 and 28 days. The analysis procedure was a tedious process. Therefore, two samples were scanned at the same time to complete 10 sample within one day. The samples were analysed separately which means that every sample was extracted from the double sample scan, as shown in Figure 3-23.

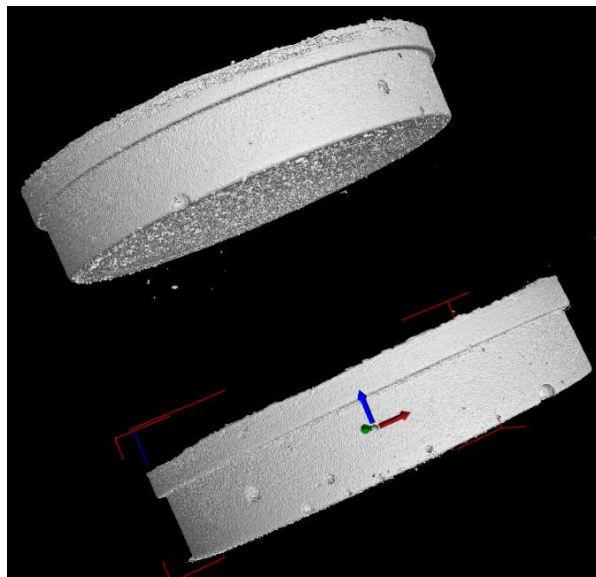


Figure 3-23: Two samples scanned at the same time.

The computer program, VGStudio Max 3.2 was used to analyse the images and to determine the porosity of each sample (Volume Graphics GmbH, 2018). All the scans in this research was set to a resolution/voxel size of 0.0263579 in the x, y and z directions. A detailed step by step procedure for analysing the samples can be seen in Appendix C.

2) MERCURY INTRUSION POROSIMETRY (MIP)

The MIP tests were performed at NECSA on three different samples to determine the quantity of pores below 100 μm in diameter. The 0.3, 0.5 and 0.7 w/c ratio samples (cured wet) were tested after 28 days in order to determine the amount of gel and capillary pores in each sample. The reason why the test was only performed on three samples is because of its destructive nature. It was not financially feasible to test all the samples. It was decided to perform the MIP test because the gel pores could not be detected in the X-ray test. Therefore, the influence of the smaller pores on the overall porosity of the samples was investigated through the performance of the MIP test. The sample preparation and test procedure performed is described in the next section.

MIP SAMPLE PREPERATION:

The suction samples used in the MIP test were sliced into four pieces allowing it to fit into the pipet of the testing machine. The samples were sliced with a diamond cutting machine (Brillant 220 made in Germany) as shown in Figure 3-24. The reason for using a diamond cutting machine was to prevent the pore structure of the concrete to be damaged while cutting. Figure 3-25 presents how neatly the samples were cut and a clean cutting surface was achieved. Dry samples were preferred for the MIP test since it decreases the running time of the machine during the test (explained in Section 2.5.3). After the cutting procedure the samples were placed in an oven at 50°C for 1 day before transported to NECSA for the MIP test.



Figure 3-24: Diamond cutting machine used to cut samples.



Figure 3-25: Samples sliced in four to be used in the MIP test.

MIP TEST PROCEDURE:

It was important to assemble the samples correctly before the MIP testing procedure could start. Figure 3-26 shows the tools required for the sample assembly, which includes a sample pipet (12 mm in height and a diameter of 24 mm), a tweezer, grease and a scale with a resolution up to 0.001g. The pipet was filled up to about three quarters of its capacity. Two quarters of the sample that was sliced into four pieces. Before placing the concrete pieces into the pipet, its weight was measured. Thereafter, the grease was carefully smeared onto the top lip surface as shown in Figure 3-27 (left hand side) and the pipet was sealed with the rubber lid, also shown in Figure 3-27 on the right hand side. It was important that the grease did not come into contact with the sample before or while testing. Therefore, only a small amount of the grease was smeared onto the surface and the grease close to the edge around the pipet was removed with a paper towel before sealing the lid.



Figure 3-26: Tools required for the sample assembly.

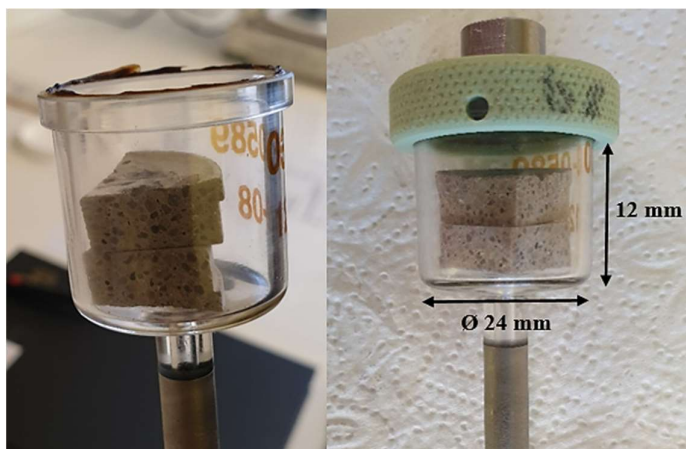


Figure 3-27: Sealing the pipet before placing it into the machine.

The weight of the pipet as well as the sample pieces placed inside the pipet was measured (Figure 3-28, left hand side) before placing it into the testing machine as shown in Figure 3-28, circled in red. Thereafter, the pipet was sealed with a cover, shielding the sample and preventing mercury from escaping from the system. When the machine started, a sucking pressure was applied to the sample to extract any water and air left within the sample. This process took up to 24 hours, with an increase in time for the wetter samples. The procedure continued by filling the pipet (sample) and the pipet's throat with mercury. The pressure of the filled penetrometer increased steadily, allowing the mercury to intrude into the pores of the sample (beginning with the largest pores first). As the pressure increased, the mercury intruded into all the pores (including the gel pores) and the amount of pores measured were exported to the computer. The high pressure analysis was selected and pressures up to 413685.44 kPa were achieved. This pressure was well below the actual safety limit of the machine (Micromeritics). Figure 3-29 shows the Micromeritics AutoPore IV Mercury Porosimeter (MIP) machine used at NECSA as well as the mercury used in the testing procedure, on the right hand side.

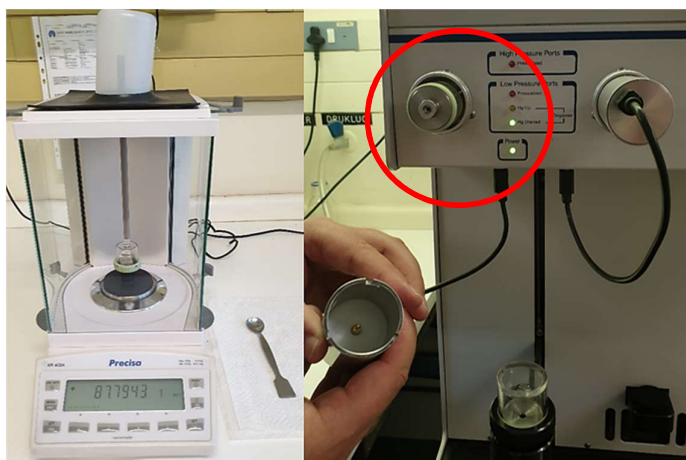


Figure 3-28: Inserting sample into the MIP testing machine.



Figure 3-29: MIP testing machine and mercury metal.

3) SORPTIVITY AND POROSITY TEST

A similar test procedure to the procedure discussed in Section 2.5.5 was used to determine the sorptivity and porosity of wet and dry mortar samples. Three mortar prisms (40 x 40 x 160 mm) of all five mixtures were prepared. The samples were placed in a 25°C curing room under a curing blanket for 24 hours after being casted. Thereafter, the samples were demoulded and sliced into four smaller samples to be tested at 7, 14 and 28 days. The dry samples (D1, D2 and D3) were kept in a room with a constant temperature between 22 and 25°C and the wet samples (W1, W2 and W3) were placed in a water bath at 25°C, until tested.

The testing procedure was started by placing all the samples (wet and dry) in an oven at 50°C for 7 days. Then the samples were placed in a vacuum saturated tank for about 4 hours to cool down (as shown in Figure 3-30). Thereafter, the dry sample weight was measured to a resolution of 0.01 g and placed on the filter paper in contact with water up to 2 mm (shown in Figure 3-31). The weight of each sample was then measured after 3, 5, 7, 9, 12, 16, 20 and 25 minutes, after wiping the wet piece of the sample using a cloth (only once). The samples were thus saturated surface dry (SSD) at the time the mass was being measured. It is important to carefully remove the sample from the filter paper, preventing water to drip onto the other samples during weight measurements. Each sample's surface area that was in contact with the water, as well as the height of the sample was measured for calculating the sorptivity and porosity. A vernier calliper was used to determine the size of each sample to a resolution of 0.02 mm.

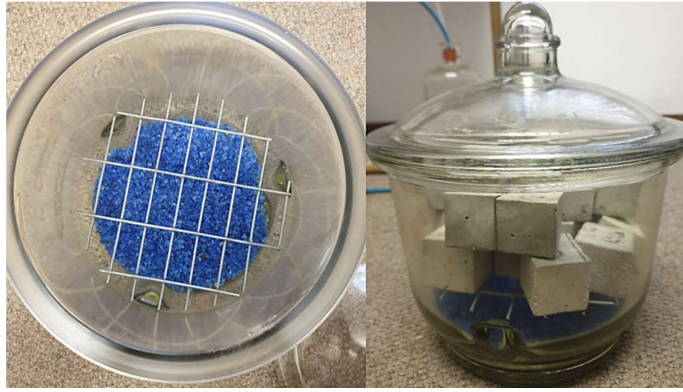


Figure 3-30: Vacuum saturated tank.



Figure 3-31: Test setup using filter paper.

The samples were placed in a sample container topped with water to measure the sample's final vacuum saturated mass. The vacuum saturation test setup used can be seen in Figure 3-32. The sample container was sealed with grease and a one-way valve was connected to the sample container, preventing air to travel backwards into the container. A water trap was placed between the sample container and vacuum pump to contain any water that was sucked towards the vacuum pump. A vacuum gauge was connected to investigate the pressure applied to the system. The vacuum pressure was kept between -75 and -80 kPa for 20 hours before the final vacuum saturated sample mass was measured. The spreadsheet recommended by the durability index testing procedure manual (University of Cape Town et al., 2017) was used to determine the final sorptivity and porosity values of each sample. The results are discussed in Chapter 4.

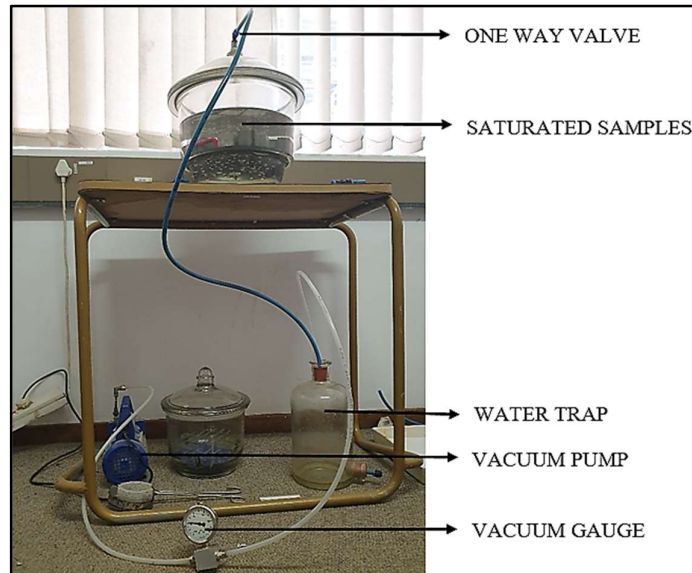


Figure 3-32: Vacuum saturated facility.

3.4.4 SHRINKAGE TEST

Drying shrinkage was investigated using three different samples of each mixture. The size of the samples were 50 x 50 x 300 mm and anvils were placed in the moulds and casted into the beams as illustrated in Figure 3-33 (circled in red). The samples were also placed under a curing blanket for 24 hours after being cast. Thereafter, the shrinkage beams were demoulded and the length of each beam was measured to an accuracy of 0.001 mm (initial beam length). It was decided to test two samples of each while curing in a room with a constant temperature between 22 and 25°C (dry). The other beam was placed in a curing bath at 25°C for the first 28 days (wet) while tested. The shrinkage beams were continuously measured for 60 days for both the dry and wet samples.



Figure 3-33: Shrinkage beams with anvils on each side.

Figure 3-34 illustrates the apparatus used to measure the shrinkage beams. The beams were carefully placed upright in the apparatus (arrow facing upwards) and the gauge was moved upwards to measure the change in length of the beam. It is important that the apparatus is set up on a flat surface and that nothing bumps into it. This type of measuring technique is sensitive and could give inaccurate results if the beams are not measured in exactly the same manner each time.



Figure 3-34: Shrinkage beams testing apparatus.

3.4.5 MECHANICAL PROPERTIES

Four different mechanical property tests were performed namely, flexural strength, compressive strength, modulus of elasticity test and the split cylinder strength. All the samples were cast on the same day and left in a curing room under a curing blanket for 24 hours, at 25°C, before being demoulded. Some of the samples were then placed in a curing bath at 25°C (wet) until testing, while the other samples were placed in a curing room between 22 and 25°C (dry) until testing. This section discusses all the test procedures followed for the different tests and the final results are presented in Chapter 4.

FLEXURAL TEST:

The TPBT discussed in Section 2.7.1 was used to determine the flexural strength of all five mixtures. Two wet and two dry mortar prism beams with dimensions 40 x 40 x 160 mm were tested at 7, 14 and 28 days. Therefore, in total 20 beams were tested on each day and the average of the two results were used. Figure 3-35 depicts the failure of one of the wet samples with a w/c ratio of 0.7 tested at 14 days.



Figure 3-35: Sample failure under TPBT.

COMPRESSIVE TEST:

The ends of the mortar prism beams that were broken into two halves during the flexural test were used to test the compressive strength. The crushing plate dimensions were 40 x 40 mm and a total of 40 samples were crushed at every testing age. The final compressive strength was calculated for a 40 x 40 x 40 mm cube and the average of all four test results was used at every age for each mixture. One of the two halves tested is shown in Figure 3-36. It was also decided to crush one cylinder of each mixture at 28 days. The cylinders (cured dry) had a diameter of 100 mm and a height of 200 mm.



Figure 3-36: Compressive testing machine.

MODULUS OF ELASTICITY:

The E-value test was performed on two cylinders (one wet and one dry) with a diameter of 100 mm and a height of 200 mm. The test was performed after 28 days and the maximum capacity of the machine used was 150 kN. The cylinder was placed in an instrumented steel collar to measure the deformation of the sample while testing. Three load cycles were repeated directly after each other and the slope of the load-deformation curve of the last cycle was used to calculate the modulus of elasticity or E-value. Figure 3-37 illustrates the E-value testing machine setup used in this research. The machine was connected to a computer which recorded all the results during the testing.



Figure 3-37: E-Value testing machine setup.

SPLIT CYLINDER TEST:

After the E-value testing procedure was completed, the samples were used to determine the split cylinder strength. The sample was carefully placed on its side between two strips of metal that were compressed together. The same machine used for the compressive test was used for the split cylinder test. Each sample's length and diameter was measured with a vernier to an accuracy of 0.02 mm. Figure 3-38 illustrates the fracture of one of the cylinders after being tested. The uniform tension stress (f_s) was calculated using Equation 3-3 (discussed in Section 2.7.3):

$$f_s = \frac{2P}{(\pi/d)} \quad \text{Equation 3-3}$$



Figure 3-38: Fracture of the split cylinder test sample.

4 RESULTS AND DATA ANALYSIS

4.1 INTRODUCTION

The aim of this chapter is to present all the results obtained during the mortar study of this project. The different test results are discussed separately. An overall comparison between all the results and the main objectives are presented at the end of this chapter.

4.1.1 CONCRETE SLUMP FLOW

The results recorded during the slump flow test are tabulated in Table 4-1. It can be seen that the slump (for the small cone) of the concrete increased with a decrease in the w/c ratio. However, the slump flow of the concrete increased with an increase in the w/c ratio. Figure 4-1 presents the slump flow versus the w/c ratio following a parabolic type curve, illustrating the increase in the slump flow with an increase in the w/c ratio of the concrete.

Table 4-1: Results of the slump flow test.

w/c ratio:	0.3	0.4	0.5	0.6	0.7
Slump of small cone	52	50	46	46	42
Diameter - 1 (mm)	103	156	189	210	220
Diameter - 2 (mm)	103	156	190	204	220
Slump flow (mm)	103	156	190	207	220

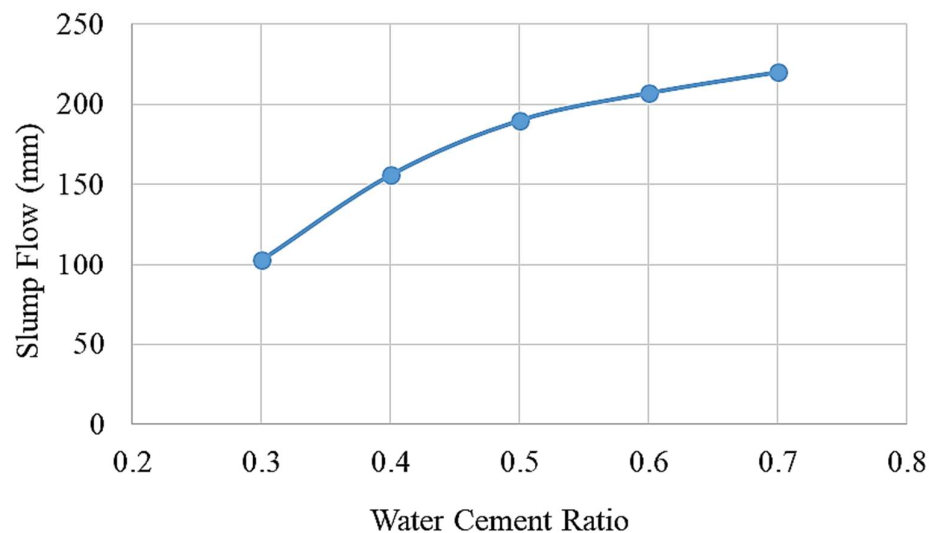


Figure 4-1: Slump flow for the different w/c ratio mortar mixtures.

4.2 WATER RETENTION CURVES (WRC) / SUCTION RESULTS

The water retention curves obtained during the mortar study are shown and discussed for the different w/c ratio samples within this section. Firstly, the suction measurements are presented against the time at which the results were recorded (after the mixtures were cast). Secondly, the suction measurements are presented against the volumetric water content, as done in Geotechnical studies (illustrated in Section 2.2). A description of each sample tested is shown in Table 4-2, named accordingly in all the graphs. All the suction results and calculations from the mortar study are tabulated in Appendix D.

Table 4-2: Sample names and description used in all the graphs.

Sample Number	Sample Name	Description
1	D - 1 (N)	Dry sample of which the porosity tests were conducted at NECSA
2	W - 1 (N)	Wet sample of which the porosity tests were conducted at NECSA
3	PD	Partially dry sample drying with a lid on after casted
4	D - 2	Additional dry sample for examining the repeatability of the test
5	W - 2	Additional wet sample for examining the repeatability of the test
6	W/D	Wet sample drying without a lid on from 28 days
7	W/PD	Wet sample drying with a lid on from 28 days

The suction measurements of the samples (numbers 1 to 7 as listed in Table 4-2) are discussed in terms of the time at which the suction reading was recorded, more specifically, in hours after the samples were cast. The wet samples were only measured up to 530 hours after casting, while the dry and partially dry sample measurements continued until 1500 hours after casting. Suction measurements for samples 6 and 7 started after 650 hours, while kept in water for the first 650 hours. Sample 6 was then left open during testing (without a lid on), similar to the curing procedure followed for samples 1 and 4. Samples 7's lid was kept on during the suction measurements, in the same manner as for samples 3's curing procedure.

Figures 4-2 to 4-6 present the suction versus time plots for each of the w/c ratios. It can be seen that the suction values rapidly increased (on the graph) up to a maximum value of about 85 MPa for the dry samples (1, 4 and 6), while the wet sample's (2 and 5) suction measurements remained stable between -5 and 5 MPa. Suctions in the partially dry samples (3 and 7) increased, on the graph, with a decrease in the w/c ratio. It can also be seen that suction measurements for sample 6 rapidly increased towards the 1st sample suction measurements (dry samples). However, sample 7's suction measurements did not rise as rapidly towards the 3rd sample suction measurements (partially dry samples), compared to the dry samples. It is interesting to note that there is no significant difference in the suction developed in the dry samples, regardless of the age where drying started. Figure 4-7 presents the suction readings used in the mortar study to compare all the different properties.

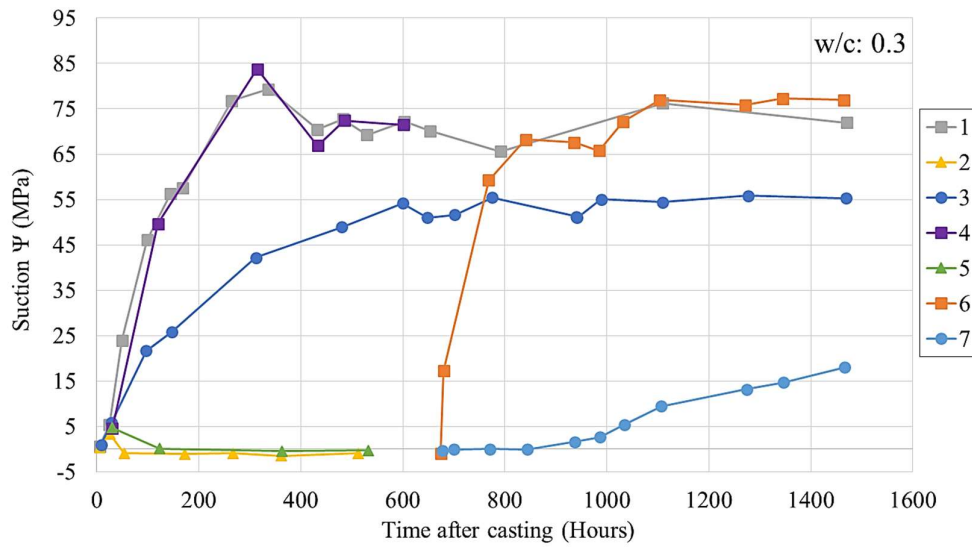


Figure 4-2: Suction versus time plot for the 0.3 w/c ratio mixture.

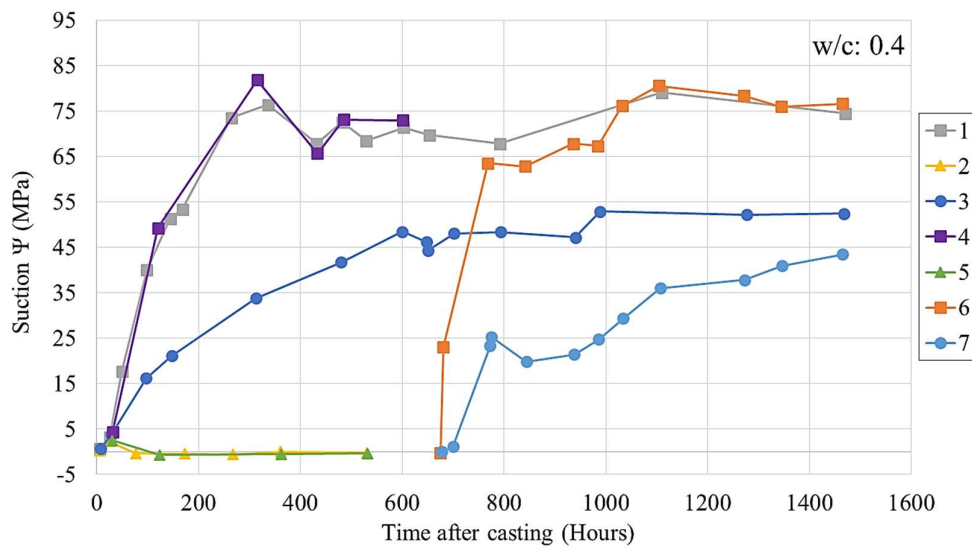


Figure 4-3: Suction versus time plot for the 0.4 w/c ratio mixture.

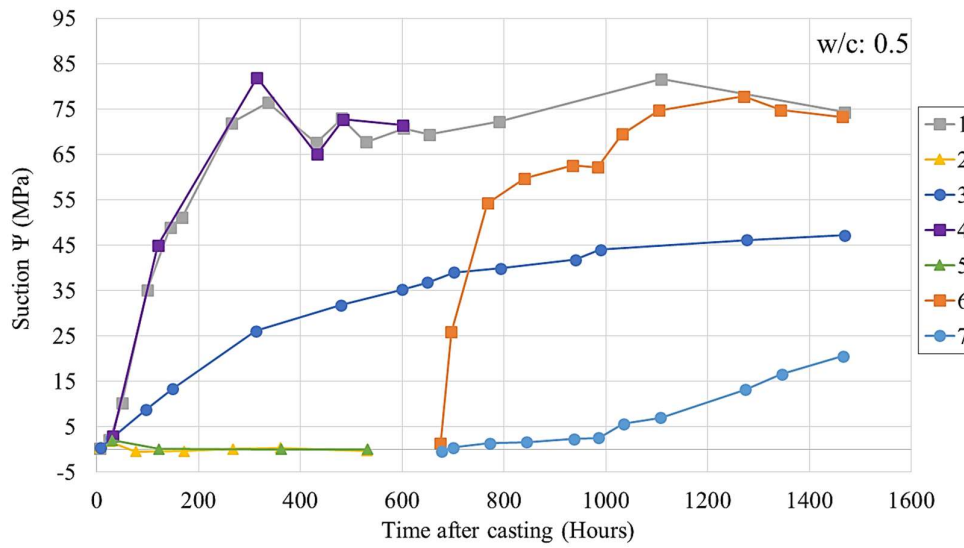


Figure 4-4: Suction versus time plot for the 0.5 w/c ratio mixture.

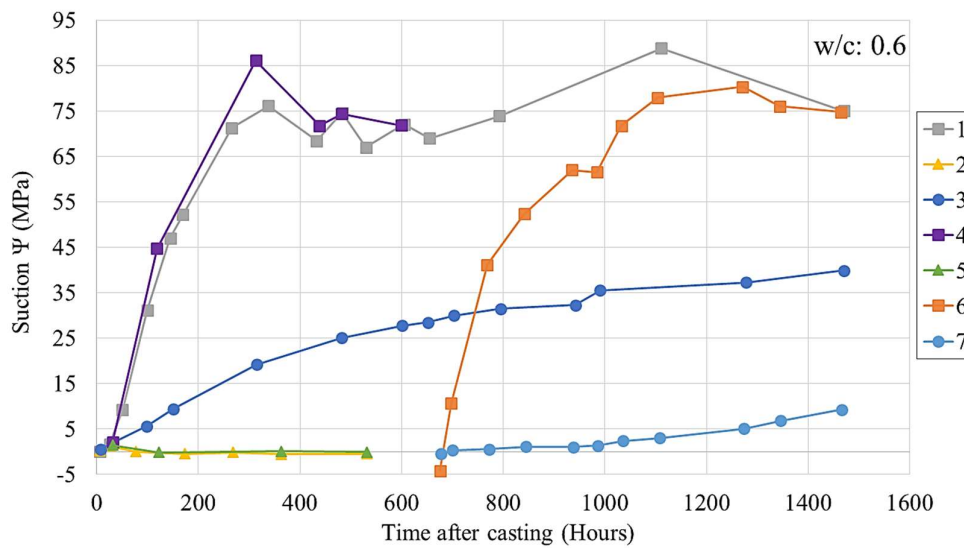


Figure 4-5: Suction versus time plot for the 0.6 w/c ratio mixture.

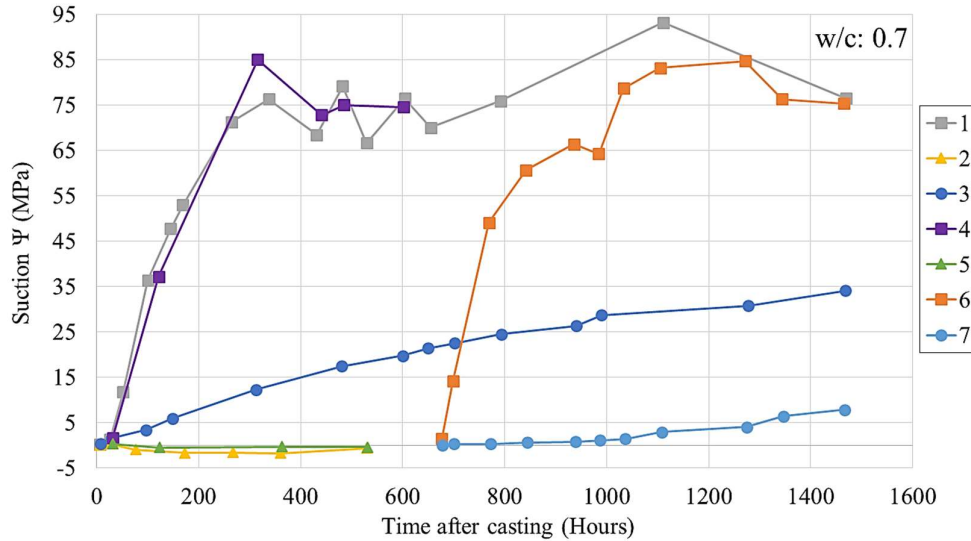


Figure 4-6: Suction versus time plot for the 0.7 w/c ratio mixture.

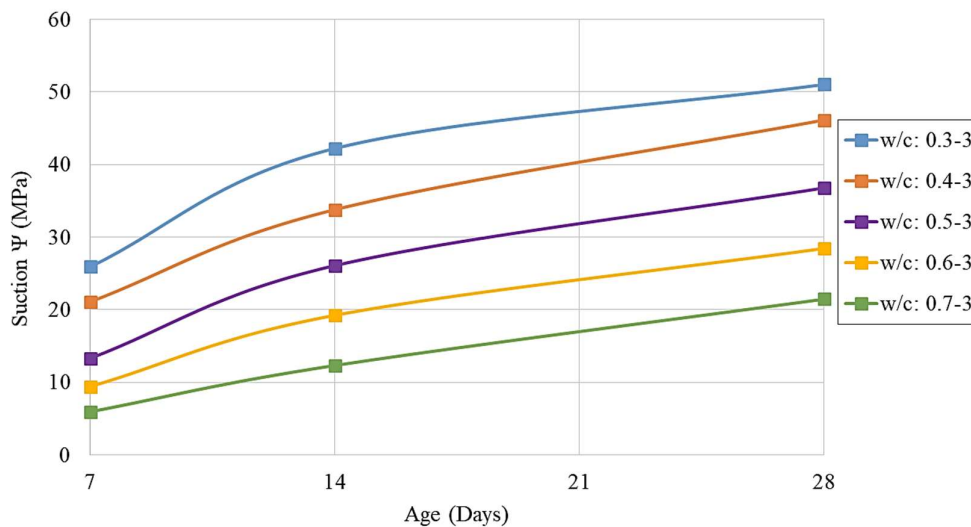


Figure 4-7: Suction versus the age of the samples number 3 (partially wet).

The environmental data recorded throughout the testing period (1600 hours or 67 days) are presented in Figure 4-8. It is clear how the light intensity changes from day to night time. The battery was charged only four times. This can be seen when the temperature rapidly increased during the charging phase, since the battery voltage spiked upwards, implying that the battery was being charged. Figure 4-9 shows the humidity and temperature readings recorded for the first 530 hours of testing. It can be seen that the humidity decreased for the first 300 hours and thereafter increased up to 450 hours (during a rainy week). The dry samples followed a similar trend, since the maximum suction readings were recorded at the lowest percentage humidity. Therefore, the dry samples were highly influenced by the humidity

and the temperature, allowing the concrete to dry out or to obtain water through condensation. The partially dry samples showed no sign of rapid change compared to the dry sample. Therefore, the partially dry samples were not influenced by the humidity and the temperature readings, due to the sealed container (lid on). It can be said that the dry samples represent the outer surface of a concrete block which is open to the surrounding environment. However, the partially dry samples represent the middle or the inside of a concrete block which is not open to the surrounding environment. The wet samples present saturated concrete and did not lose any water.

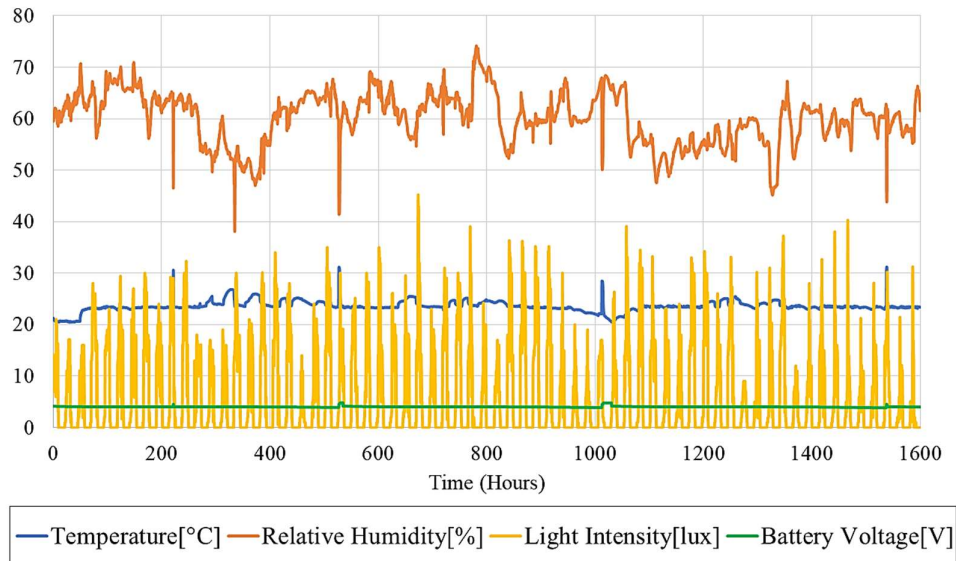


Figure 4-8: Environmental data logged throughout the duration of testing.

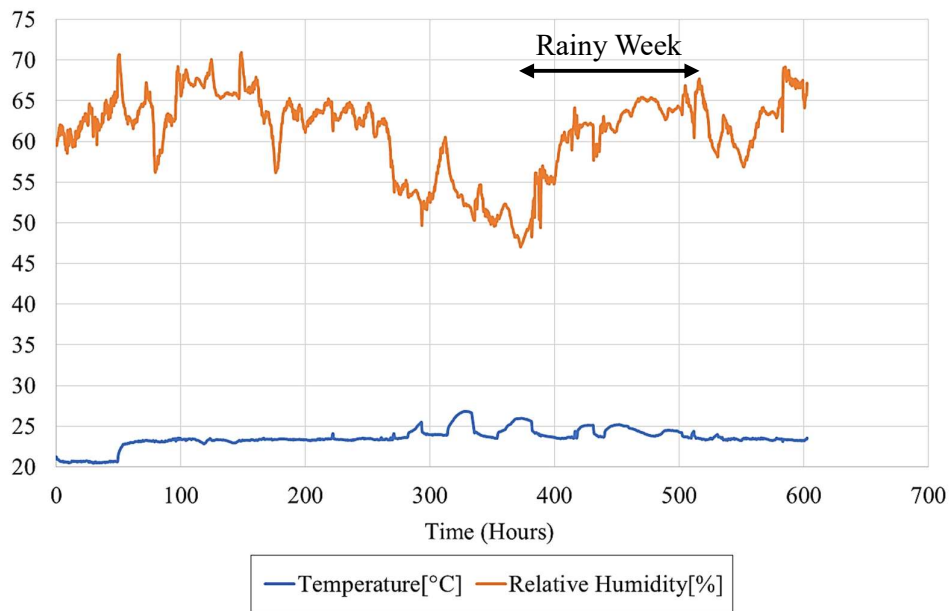


Figure 4-9: Humidity and temperature readings for the first 530 hours.

When looking at the soil water retention curves (Figure 2-3 and Figure 2-4) discussed in Section 2.2, the curves follow a bimodal water retention curve. The first curve (sub-curve 1) can be seen in the water retention curves determined in this study (as shown in Figure 4-10). The volumetric water content of the data was plotted against the total suction using a logarithmic scale. The weight of the samples were continuously measured during the suction readings and the volumetric water content was calculated by dividing the total water mass by the total mass of the solids (calculations shown in Appendix D). Figures 4-11 to 4-15 show the water retention curves for w/c ratios 0.4, 0.5, 0.6 and 0.7 respectively. It can be seen that the turning point (before the point where the volumetric water content decreased without a change in the total suction) suction values decreased with an increase in the w/c ratio of the mortar mixtures (illustrated in red on each graph). The turning points were estimated by hand and according to Geotechnical Engineers the turning point represents when air enters the pores (air-entry value).

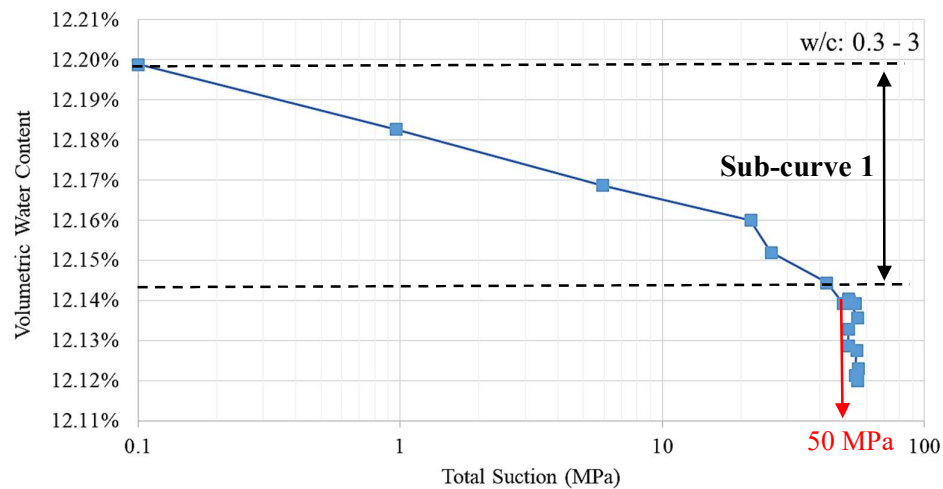


Figure 4-10: Water Retention Curve of the partially wet sample (3), 0.3 w/c ratio.

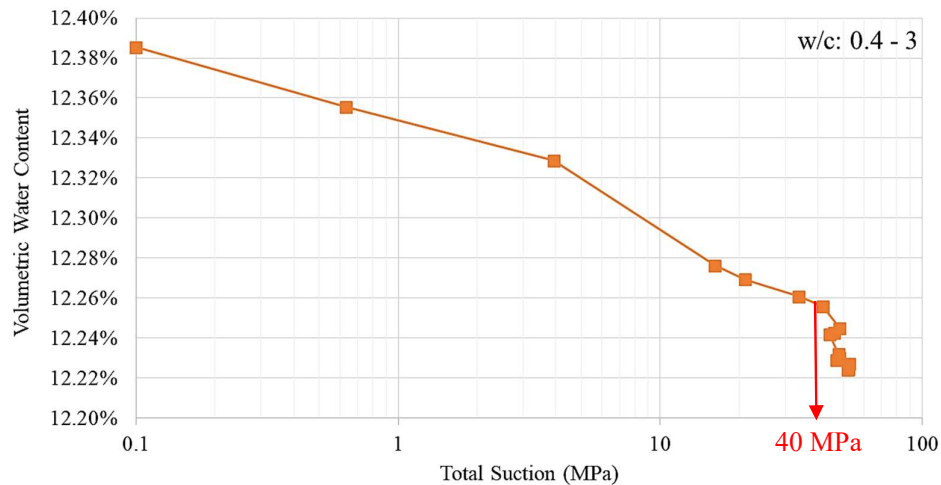


Figure 4-11: Water Retention Curve of the partially wet sample (3), 0.4 w/c ratio.

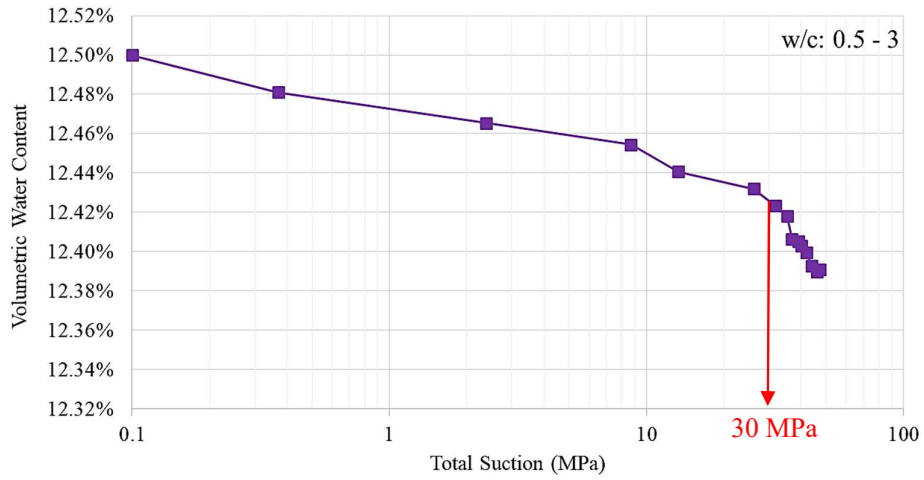


Figure 4-12: Water Retention Curve of the partially wet sample (3), 0.5 w/c ratio.

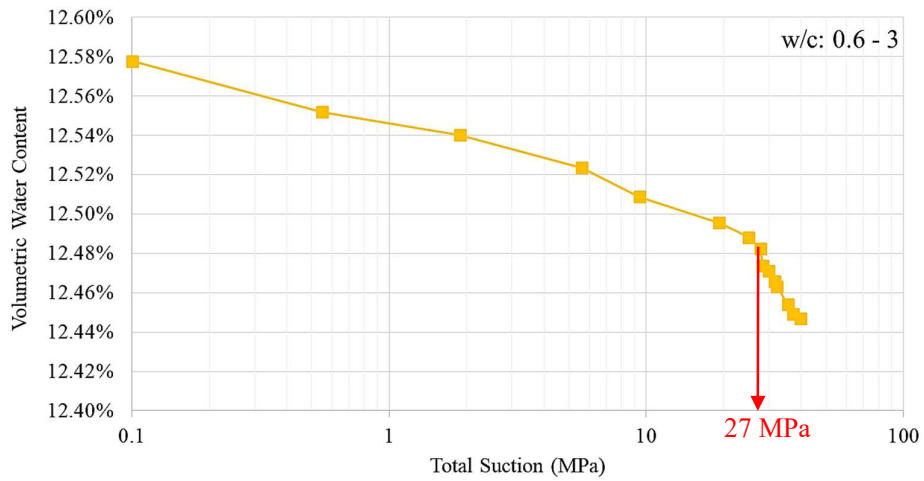


Figure 4-13: Water Retention Curve of the partially wet sample (3), 0.6 w/c ratio.

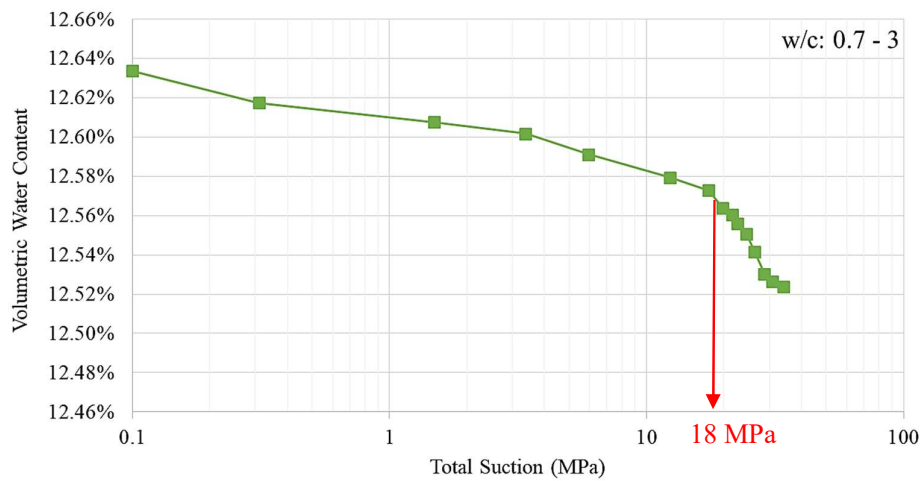


Figure 4-14: Water Retention Curve of the partially wet sample (3), 0.7 w/c ratio.

4.2.1 DISCUSSION OF THE WATER RETENTION CURVES

It was clear that the curing procedure of the samples (with or without the container's lid on) played a significant role during the suction measurements. The partially dry samples (recorded with the container's lid on for the entire duration of the test) were assumed to best represent the middle of a concrete block. Figure 4-15 presents the combined plots of all the w/c ratios of sample number 3, the partially dry samples measured up to 1450 hours (60 days). It can be seen that the total suction after 60 days increased with a decrease in the w/c ratio.

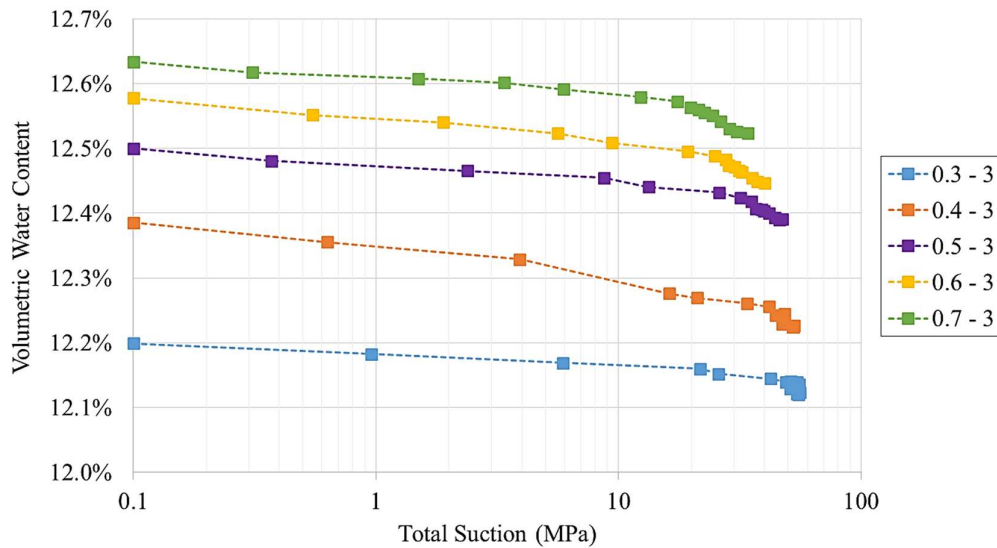


Figure 4-15: Combined water retention plot for all the w/c ratios.

Figure 4-16 shows the turning points of the suction measurements for the different w/c ratio samples. It can be seen that the turning point suction increased with a decrease in the w/c ratio. Therefore, the turning point of the suction measurements are dependent on the w/c ratio. The rate at which the turning point suction increased was fairly linear when looking at Figure 4-16. The R^2 value for a linear fit was 0.9752 which is a good fit through the data points.

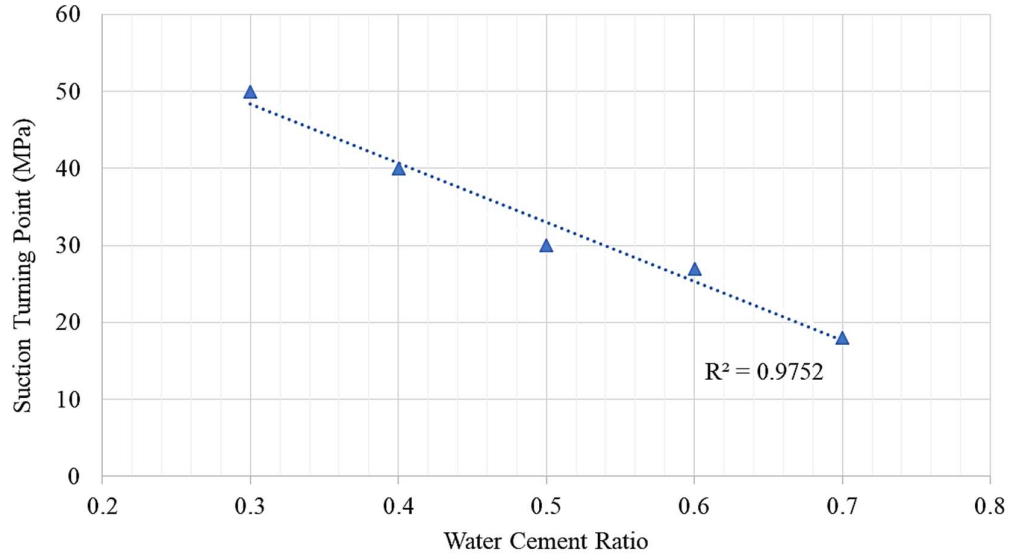


Figure 4-16: Turning points suction for the different w/c ratio samples.

4.3 POROSITY RESULTS

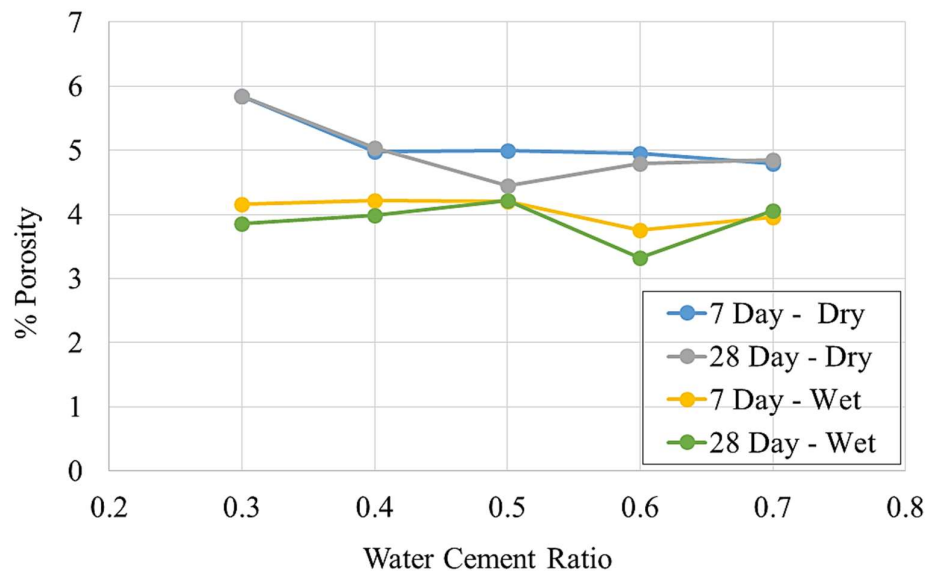
This section presents all the different porosity test results conducted throughout this study. Firstly, the X-ray micro-tomography results determined at NECSA are presented and discussed using a visual interpretation of the data obtained. Secondly, the MIP test results investigated for three different samples are discussed to examine whether the capillary or gel pores have a significant influence on the overall porosity of the concrete samples. Lastly, the standard sorptivity and porosity test performed during this study is discussed and an overall comparison of all the porosity tests executed is given at the end of this section.

4.3.1 X-RAY MICROTOMOGRAPHY RESULTS

The procedure and computer analysis steps explained in Section 3.4.3 under X-ray micro-tomography were used to determine the total porosity of the different samples as shown in Table 4-3. As mentioned before the same samples used for the suction measurements were tested at NECSA after 7 and 28 days (dry and wet samples). Figure 4-17 illustrates the percentage porosity versus the w/c ratio of the dry and wet samples, after 7 and 28 days. The dry samples had a higher porosity compared to the wet samples. The 7 day test results obtained also had a higher porosity compared to the 28 day test results.

Table 4-3: Porosity results from the X-Ray tests.

Sample Specification	w/c ratio	% Porosity	
		7 Days	28 Days
Dry	0.3	5.8	5.8
	0.4	5.0	5.0
	0.5	5.0	4.4
	0.6	4.9	4.8
	0.7	4.8	4.9
Wet	0.3	4.2	3.9
	0.4	4.2	4.0
	0.5	4.2	4.2
	0.6	3.8	3.3
	0.7	4.0	4.1

**Figure 4-17: Porosity versus w/c ratio after 7 and 28 days.**

The results discussed above are presented with a histogram plot, shown in Figure 4-18. It is clear that the 7 and 28 day dry samples had an overall higher porosity compared to the wet samples. A small decrease in the porosity was experienced in most cases, between the 7th and the 28th day tests for both the dry and the wet samples as seen in Figure 4-18. An overall decrease in the total porosity with an increase in the w/c ratio was seen, which does not correspond to literature. Therefore, extra porosity tests were performed to investigate and ensure that the porosity results obtained were representable.

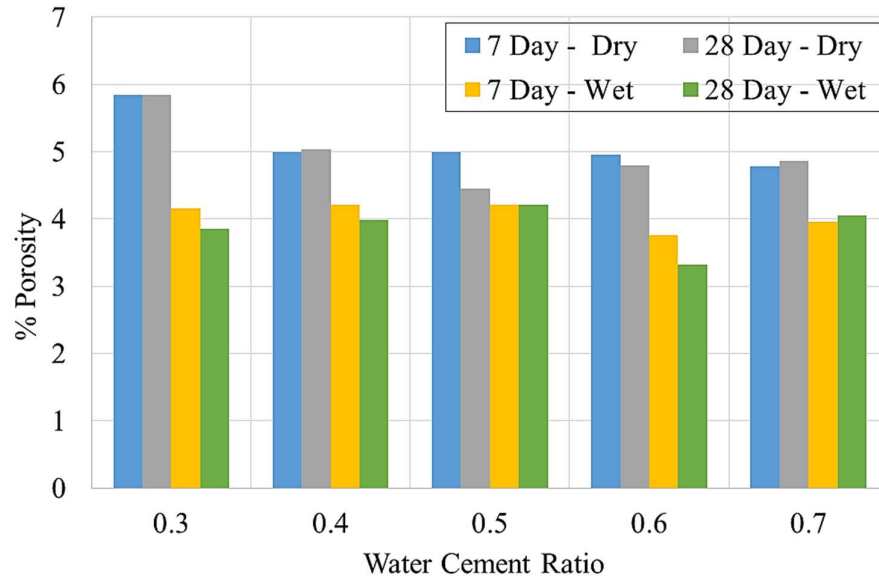


Figure 4-18: Histogram of the porosity for the different w/c ratio samples after 7 and 28 days.

It was possible to export image stacks of the sample analysed (sliced through the sample) to investigate the pores within the sample, as shown in Figure 4-19 (top view) and Figure 4-20 (side view). The pores are highlighted in different colours showing the pore volume of the different pore sizes within the concrete sample. As seen in Section 2.5.2, previous research showed that unhydrated cement can be seen in the X-ray scans. The samples analysed in this research study also showed the presence of unhydrated cement within the sample (see Figure 4-19, circled in red). The enlarged images of the top view for all the samples are presented in Appendix E.

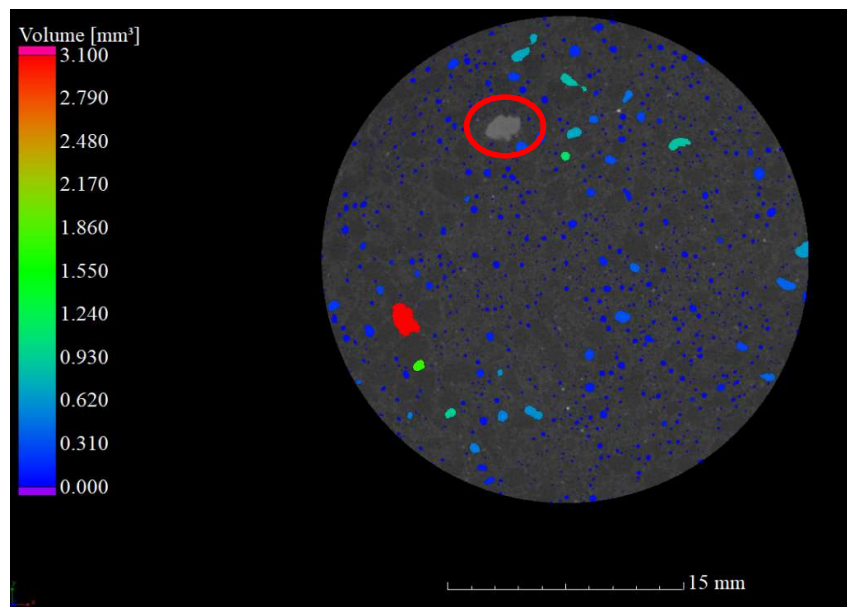


Figure 4-19: Enlarged top view image presenting the pore sizes of the sample.

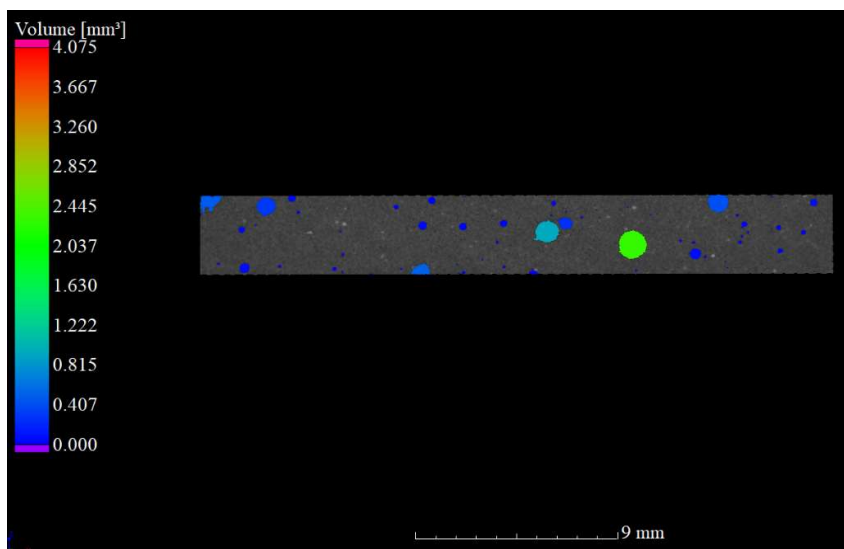


Figure 4-20: Enlarged side view image presenting the pore sizes of the sample.

The images of the pores within the samples are compared visually (sliced within the same ROI) to investigate the different pores in each sample. Figure 4-21 presents the dry samples with w/c ratios of 0.3, 0.4, 0.5, 0.6 and 0.7 and were scanned at 7 and 28 days. An increase in the amount of large pores (entrapped air) for the larger w/c ratio samples (w/c ratios 0.5 to 0.7), as well as a large amount of smaller pores for the smaller w/c ratio samples (w/c ratios 0.3 and 0.4) were examined. Through the visual investigation it was concluded that there was a small change in the quantity of pores from the 7th to the 28th day (especially when looking at the 0.5 w/c ratio samples). Figure 4-22 shows the wet samples scanned at 7 and 28 days. Again an increase in the amount of larger pores for the 0.6 and 0.7 w/c ratio samples were seen and a larger amount of smaller pores for the 0.3 and 0.4 w/c ratio samples.

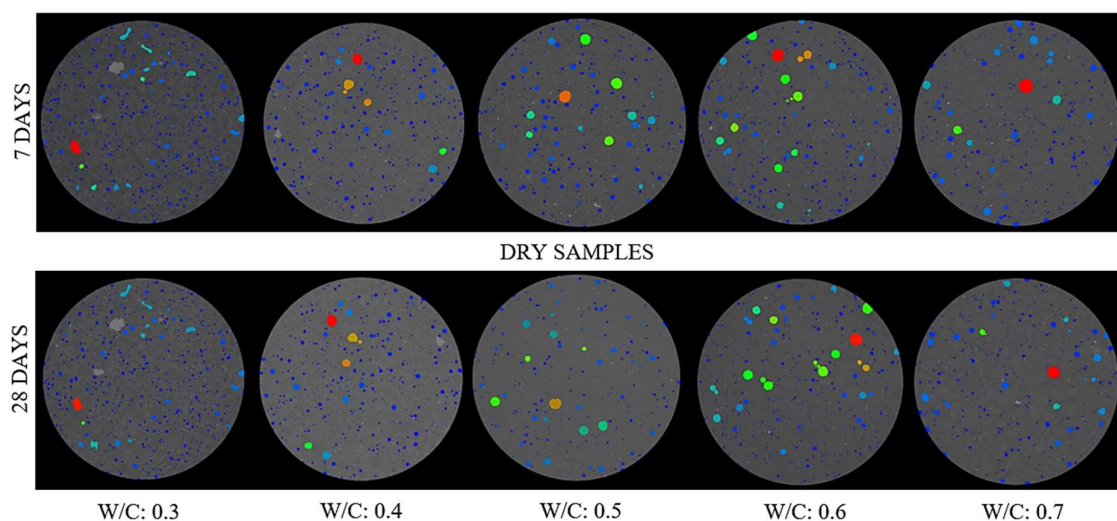


Figure 4-21: Visual representation of the pores for the dry samples after 7 and 28 days.

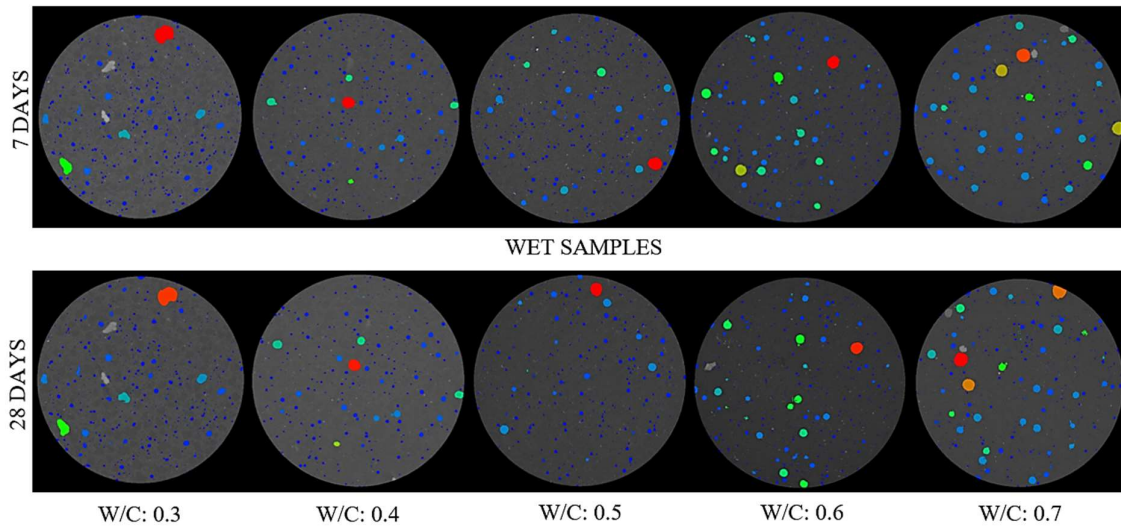


Figure 4-22: Visual representation of the pores for the wet samples after 7 and 28 days.

Figure 4-23 presents the void diameter versus the sphericity value of the pores for the dry (0.3 w/c ratio sample) after 7 days. It indicates that the larger pores are least spherical compared to the smaller pores as seen in Section 2.5.2 (Figure 2-34 presented by Du Plessis et al. (2016)). The void volume of the pores were counted and are shown in Figure 4-24, also for the dry 0.3 w/c ratio sample after 7 days. A slow scan was performed on all the samples during the X-ray scanning procedure, as discussed under Section 2.5.2, illustrated in Figure 2-33.

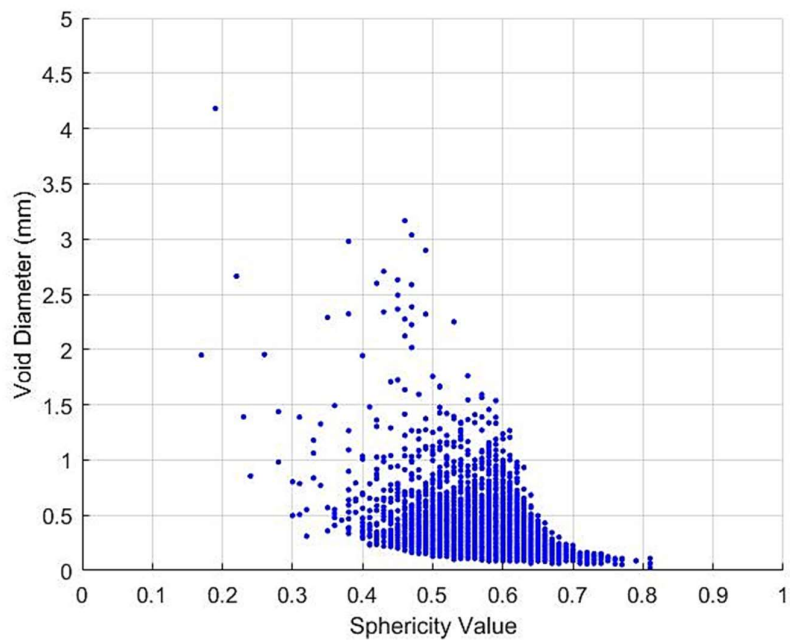


Figure 4-23: Void diameter versus the sphericity for the 0.3 dry w/c ratio sample after 7 days.

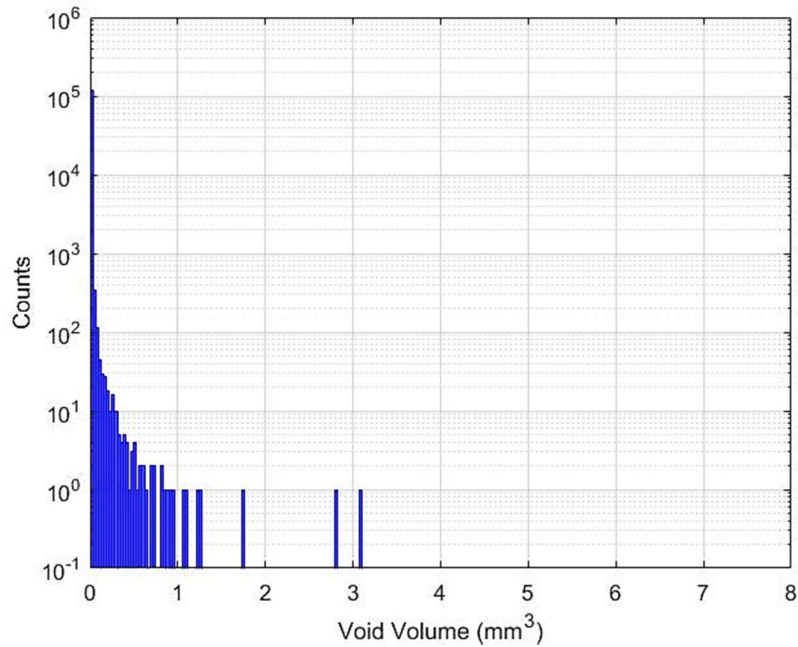


Figure 4-24: Void volume count for the 0.3 dry w/c ratio sample after 7 days.

When plotting the cumulative percentage distribution shown in Figure 4-25, the cumulative % over the size distribution of the pore's diameter was obtained, illustrated in Figure 4-26. Diameter measurements that fell within either the bottom or the top five percent of the diameter data were not considered for the exponential fitting of the given data, as seen in Figure 4-26. This was done to obtain a good fit of the data, due to the exclusion of the outliers.

The 50 percent oversize air void diameter (known as the D_{50} value) in mm was read from the exponential fit of the data as shown in Figure 4-26. The value obtained during this procedure gives an indication of the average void size of each mixture. The same procedure was followed to obtain the ten percent oversize air void diameter (D_{10}) in each mixture. However, the D_{10} value was read off from the 90 % on the graph (since the graph is usually plotted in the reverse order when determining the D_{50} and D_{10} values), it was decided to read the D_{10} value from the same graph, at 90%. The D_{10} value shows the difference in the number of larger voids in the mortar mixture.

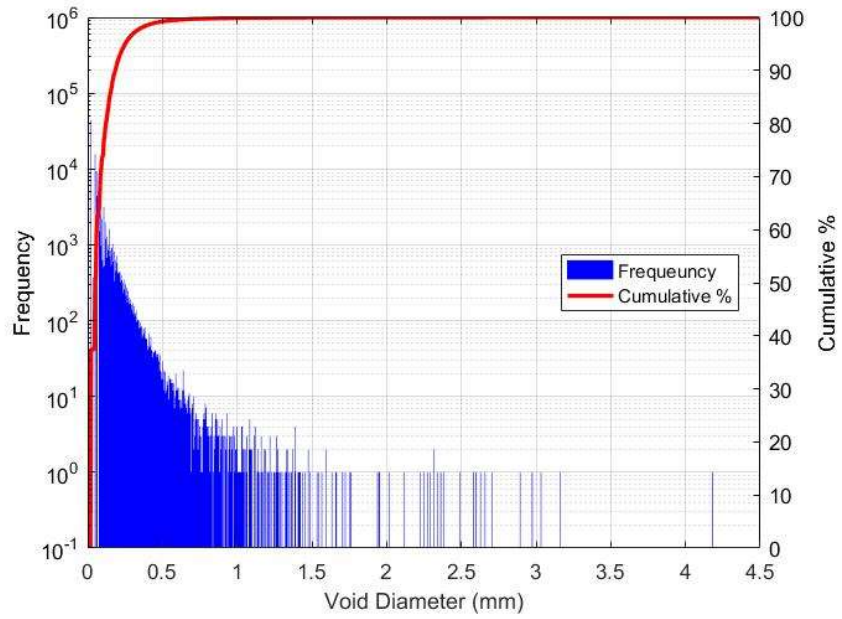


Figure 4-25: Pore diameter frequency and cumulative percentage for the 0.3 dry w/c ratio sample after 7 days.

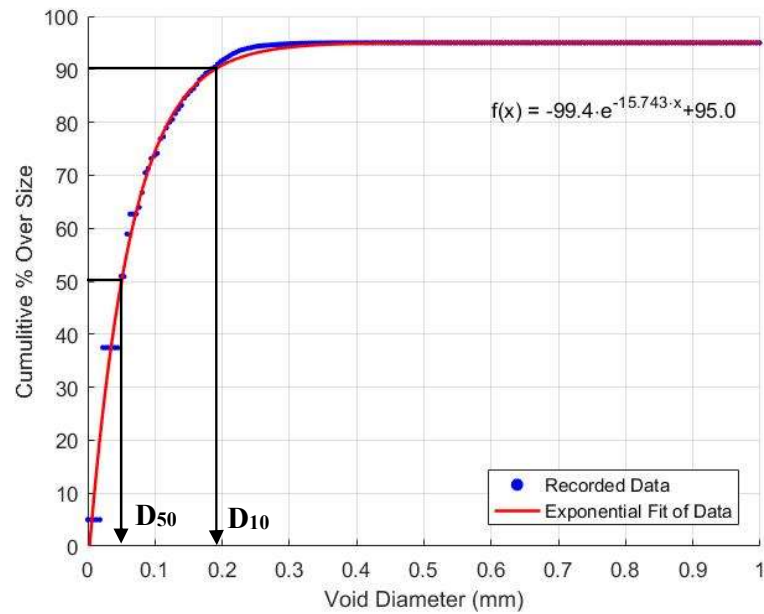


Figure 4-26: Pore diameter cumulative percentage exponential fit for the 0.3 dry w/c ratio sample after 7 days.

The four figures discussed above were plotted for each sample at 7 and 28 days and are presented in Appendix F. The plots were fairly similar for all the samples. A large amount of data was obtained for each sample. Therefore, it was decided to write a Matlab script to plot the figures for each excel data file obtained during the X-ray data analysis (discussed in Section 3.4.3). The Matlab script written to plot the data is shown in Appendix G.

Table 4-4 and Table 4-5 show the D_{50} and D_{10} parameters after 7 and 28 days which can be compared for the different mortar mixtures. It can be seen that these parameters increased for the dry samples after 28 days. However, the parameters decreased after 28 days for the first three w/c ratio mortar mixtures (wet samples), including w/c ratios of 0.3, 0.4 and 0.5. The average void size (D_{50} values) decreased for the wet samples compared to the dry samples, indicating that the average void size for the wet samples are smaller. The same can be said for the D_{10} values, showing that the dry samples had larger voids compared to the wet samples. The parameters (a, b and c) of the exponential function fitted through the data points are also shown in the tables. Parameter b indicates the slope of the function (of the wet samples) which decreased for w/c ratios 0.3, 0.4 and 0.5 and thereafter increased for w/c ratios 0.6 and 0.7.

Table 4-4: Fitted function and parameters of oversize air void diameter distribution at 7 days.

Sample Specification	W/C Ratio	Fitted Function: $y = ae^{bx} + c$			Oversize Air-Void Diameter Distribution Parameters	
		a	b	c	D_{50} (mm)	D_{10} (mm)
Dry	0.3	-99.4	-15.743	95.0	0.0503	0.1899
	0.4	-97.9	-18.227	95.0	0.0426	0.1632
	0.5	-103.6	-23.697	95.0	0.0352	0.1279
	0.6	-101.9	-20.374	95.0	0.0401	0.1480
	0.7	-102.7	-21.236	95.0	0.0389	0.1423
Wet	0.3	-103.0	-21.632	95.0	0.0383	0.1399
	0.4	-98.1	-19.945	94.9	0.0392	0.1503
	0.5	-93.1	-12.069	95.0	0.0602	0.2423
	0.6	-100.0	-16.303	95.0	0.0490	0.1838
	0.7	-101.5	-19.100	95.0	0.0426	0.1576

Table 4-5: Fitted function and parameters of oversize air void diameter distribution at 28 days.

Sample Specification	W/C Ratio	Fitted Function: $y = ae^{bx} + c$			Oversize Air-Void Diameter Distribution Parameters	
		a	b	c	D ₅₀ (mm)	D ₁₀ (mm)
Dry	0.3	-99.9	-14.502	95.0	0.0550	0.2065
	0.4	-96.9	-16.122	95.0	0.0476	0.1839
	0.5	-104.1	-9.969	99.7	0.0742	0.2391
	0.6	-100.8	-17.150	95.0	0.0470	0.1751
	0.7	-102.0	-20.680	95.0	0.0396	0.1458
Wet	0.3	-104.2	-23.762	95.0	0.0353	0.1278
	0.4	-102.5	-21.979	95.0	0.0375	0.1374
	0.5	-97.6	-17.540	95.0	0.0441	0.1694
	0.6	-99.9	-14.996	95.1	0.0530	0.1984
	0.7	-102.8	-19.024	95.1	0.0433	0.1579

4.3.2 MERCURY INTRUSION POROSIMETRY (MIP) RESULTS

The MIP test procedure as explained in Section 3.4.3 was used to determine the porosity of three sample's (w/c ratios 0.3, 0.5 and 0.7) after 28 days. The study discussed in Section 2.5.3 concluded that the porosity increased with an increase in the w/c ratio. The porosity results obtained from the MIP test are tabulated in Table 4-6. The porosity increased with an increase in the w/c ratio, which was expected from literature results. More details regarding each test are shown in Appendix H.

Table 4-6: Porosity results obtained for the MIP test.

W/C Ratio	Porosity (%)
0.3	11.84
0.5	14.54
0.7	18.66

The cumulative pore area in m²/g versus the diameter of the pores in μm for the three different samples are shown in Figure 4-27. The pore area increased for the different pore sizes with an increase in the w/c ratio. Therefore, the porosity increased with an increase in the w/c ratio. It can also be seen that the cumulative pore area for a 0.01 μm pore increased from 5.5 m²/g to 8 m²/g for the 0.3 to 0.7 w/c ratio samples respectively. It is clear that there was a large amount of capillary and gel pores which influenced the overall porosity of the samples. Therefore, the X-ray test porosity results are much smaller for not taking into account the quantity of capillary and gel pores within each sample. The size of the samples used in the X-ray porosity analysis limited the machine to not detect capillary and gel pores. Smaller samples will result in smaller pores detected when measuring the porosity of a mortar

sample. The sample size used for the X-ray analysis was too big which limited the size of the pores detected in each sample.

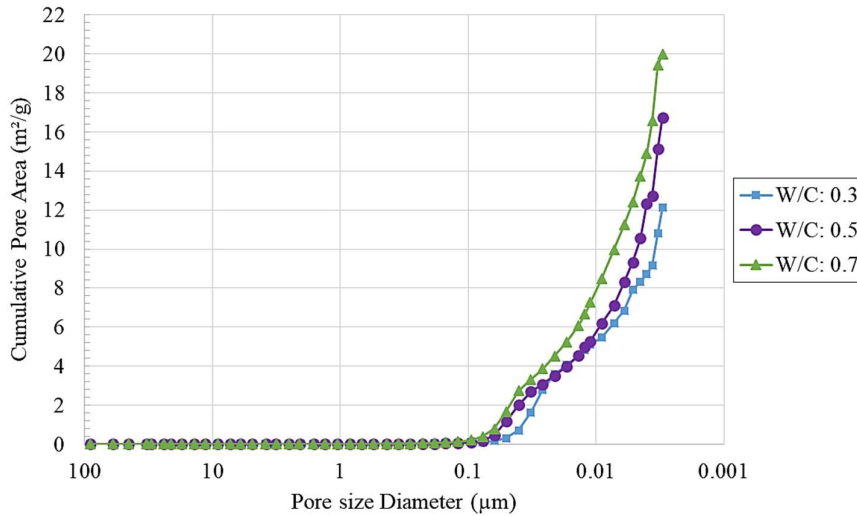


Figure 4-27: Cumulative pore area versus pore size for the different w/c ratio samples.

4.3.3 SIMPLE SORPTIVITY AND POROSITY TEST RESULTS

The procedure followed during the sorptivity and porosity tests are discussed in Section 3.4.3. As mentioned before two wet and two dry samples were tested for each w/c ratio. Tables 4-7 to 4-9 present the final results obtained during the testing procedures at 7, 14 and 28 days. The durability index testing procedure manual (University of Cape Town et al., 2017) referred to the correlation coefficient (R^2) to ensure that the results were usable. The coefficient should be equal to or above 0.98 for this purpose. Table 4-9 illustrates that all the results were accurate according to the manual's calculations.

Table 4-7: Dry and wet samples sorptivity results.

Average Sorptivity ($\text{mm/hr}^{0.5}$)			
Sample Name	7 Days	14 Days	28 Days
0.3 - Dry	8.5	9.0	12.1
0.4 - Dry	9.8	10.0	15.3
0.5 - Dry	10.8	9.7	15.3
0.6 - Dry	11.8	11.0	16.3
0.7 - Dry	13.3	12.2	18.5
0.3 - Wet	8.1	10.1	10.9
0.4 - Wet	11.2	10.5	15.3
0.5 - Wet	13.9	10.9	16.4
0.6 - Wet	15.6	12.8	16.4
0.7 - Wet	17.2	14.5	15.4

Table 4-8: Dry and wet samples porosity results.

Average Porosity (%)			
Sample Name	7 Days	14 Days	28 Days
0.3 - Dry	15.6	14.9	15.4
0.4 - Dry	16.5	16.0	16.1
0.5 - Dry	17.3	16.3	16.9
0.6 - Dry	17.4	16.6	17.1
0.7 - Dry	17.5	16.6	17.1
0.3 - Wet	11.4	10.1	10.0
0.4 - Wet	13.7	12.5	12.4
0.5 - Wet	15.8	14.8	14.2
0.6 - Wet	16.8	16.2	16.0
0.7 - Wet	16.9	16.7	17.0

Table 4-9: Correlation coefficient R^2 of the dry and wet samples.

Average R^2 (Must be > 0.98)			
Sample Name	7 Days	14 Days	28 Days
0.3 - Dry	0.994	0.997	0.999
0.4 - Dry	0.997	0.997	0.999
0.5 - Dry	0.995	0.999	0.999
0.6 - Dry	0.997	0.999	0.999
0.7 - Dry	0.999	0.999	0.999
0.3 - Wet	0.990	0.992	0.991
0.4 - Wet	0.998	0.999	0.999
0.5 - Wet	0.998	1.000	1.000
0.6 - Wet	0.998	0.999	1.000
0.7 - Wet	0.999	1.000	1.000

The sorptivity and porosity of w/c ratios 0.3, 0.4, 0.5, 0.6 and 0.7 determined at the 7th, 14th and 28th days are displayed in Figure 4-28 and Figure 4-29. The 7 and 14 day results of the dry samples had the smallest sorptivity. The 28th day sorptivity of the dry and wet samples was the highest. The 0.3 w/c ratio samples had the lowest porosity and the porosity increased with an increase in the w/c ratio. The porosity of the dry samples were higher compared to the wet samples, illustrated in Figure 4-29.

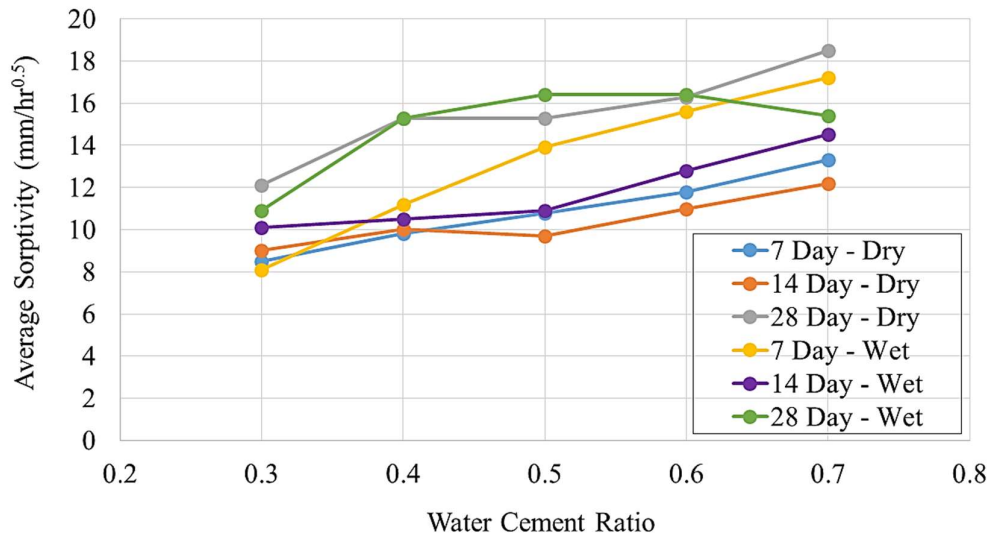


Figure 4-28: Sorptivity versus w/c ratio after 7, 14 and 28 days.

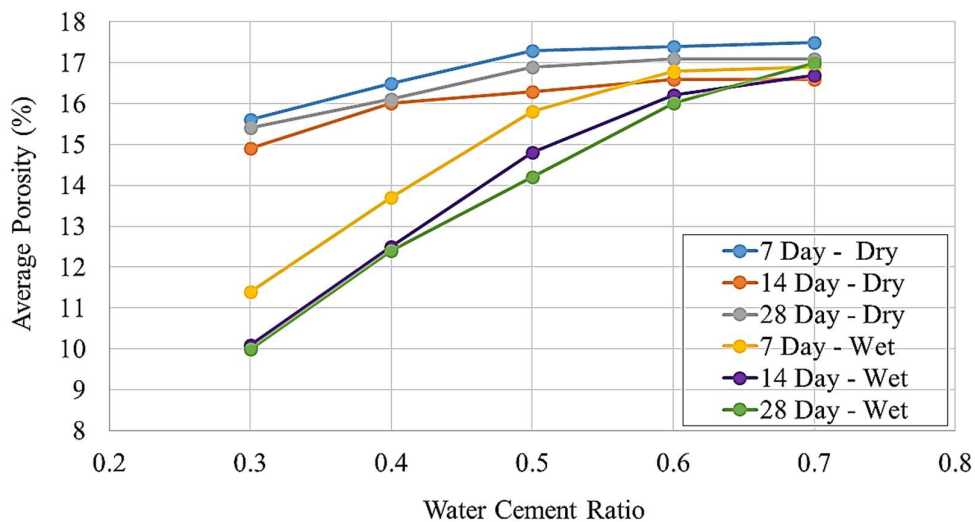


Figure 4-29: Porosity versus w/c ratio after 7, 14 and 28 days.

Figure 4-30 shows a histogram plot of the % porosity for the 0.3 up to 0.7 w/c ratio samples, from 7 to 28 days. Similarly to Figure 2-35 shown in Section 2.5.3 the porosity increased with an increase in the w/c ratio after the 7th, 14th and 28th day (dry and wet samples). It can also be seen that the porosity for the wet samples decreased from 7 to 28 days. The effect of water curing becomes more visible as the w/c ratio decreases.

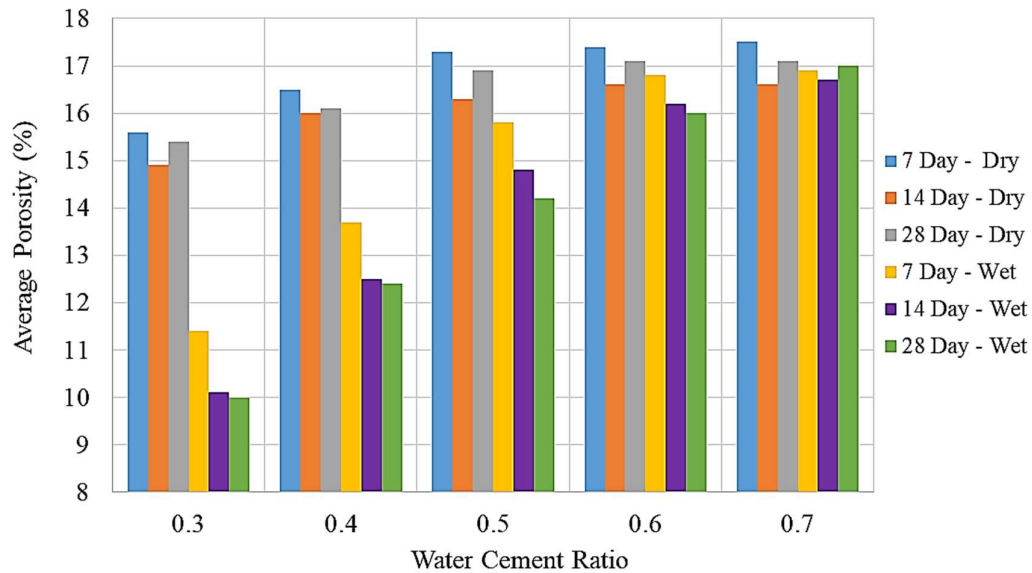


Figure 4-30: Histogram of the porosity for the different w/c ratio after 7, 14 and 28 days.

4.3.4 DISCUSSION OF THE POROSITY RESULTS

The porosity results of the different test methods utilized are displayed for three different samples in Table 4-10. Although general trends can be observed the X-ray results gave much lower porosities compared to the MIP test and the simple test method (described in the durability index testing procedure manual) results obtained. The reason for the significant difference could be that the X-ray test method did not detect the capillary and gel pores, but only the entrapped air within the concrete samples. It was seen in the MIP test results obtained that a large quantity of the pores were small (capillary and gel pores) which increased the total porosity of the samples. The MIP test results were much closer to the simple test method results compared to the X-ray results. The porosity of the MIP and simple test method results increased with an increase in the w/c ratio. However, no trend could be identified after investigating the X-ray results obtained.

Table 4-10: Porosity % results of three wet samples at 28 days.

W/C Ratio:	X-ray Test	MIP Test	Simple Test Method
0.3	3.9	11.8	10.0
0.5	4.2	14.5	14.2
0.7	4.1	18.7	17.0

4.4 SHRINKAGE RESULTS

The shrinkage and the swelling of the beams were measured. Equation 4-1 was used to determine the strain (ϵ) of each sample:

$$\epsilon = \frac{\Delta L}{L_0} \quad \text{Equation 4-1}$$

All the results obtained during the shrinkage tests are tabulated in Appendix I. It was decided to test two dry samples for each w/c ratio to investigate whether the two different samples gave consistent results. The shrinkage (in microstrain) versus the age of the samples (in days) were plotted for all the samples shown in Figures 4-31 to 4-35. The two dry shrinkage samples (blue and orange lines) gave fairly similar results for all the w/c ratios tested. Therefore, the wet sample results should also be consistent (green lines). The average of the two dry samples are also presented (dashed yellow lines) and were used to compare the different w/c ratio samples to one another.

The wet samples were kept in a water bath up to 28 days before the drying process started. Swelling was observed in the wet samples (while the samples were kept in the water bath). The swelling is presented with negative values in the graphs. The shrinkage of the samples are presented with positive values. It can be seen that the wet samples had an overall smaller shrinkage up to 60 days compared to the dry samples. The effect of water curing on the low w/c ratio samples can again be seen which means that less pores remained as the concrete completed its hydration process (Neville, 1981).

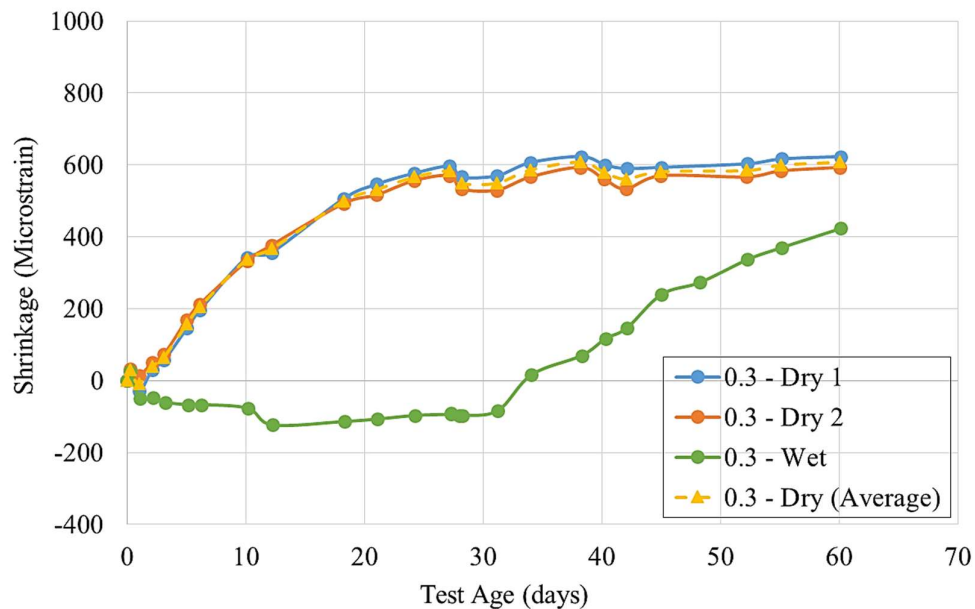


Figure 4-31: Shrinkage versus the test age in days of the 0.3 w/c ratio samples.

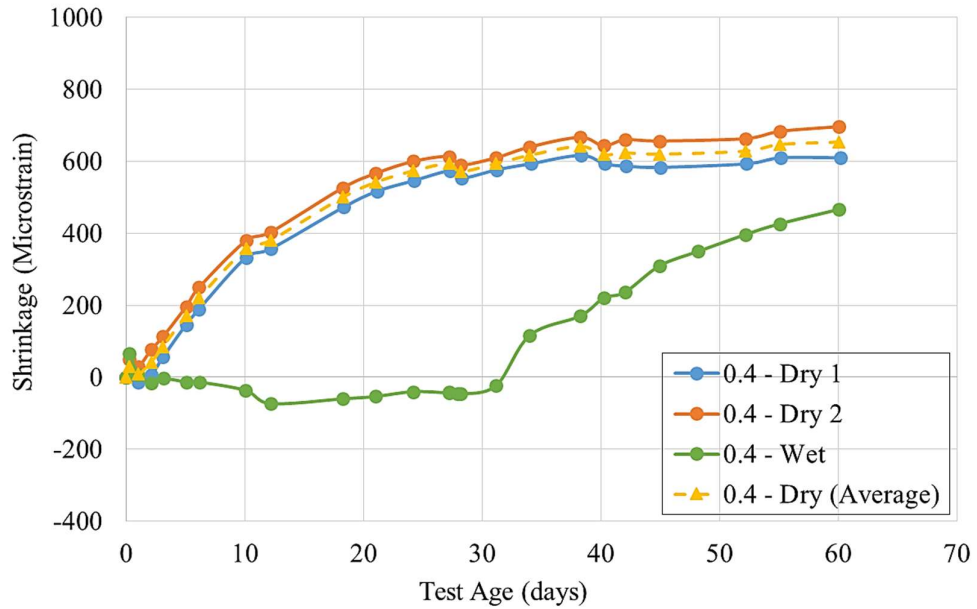


Figure 4-32: Shrinkage versus the test age in days of the 0.4 w/c ratio samples.

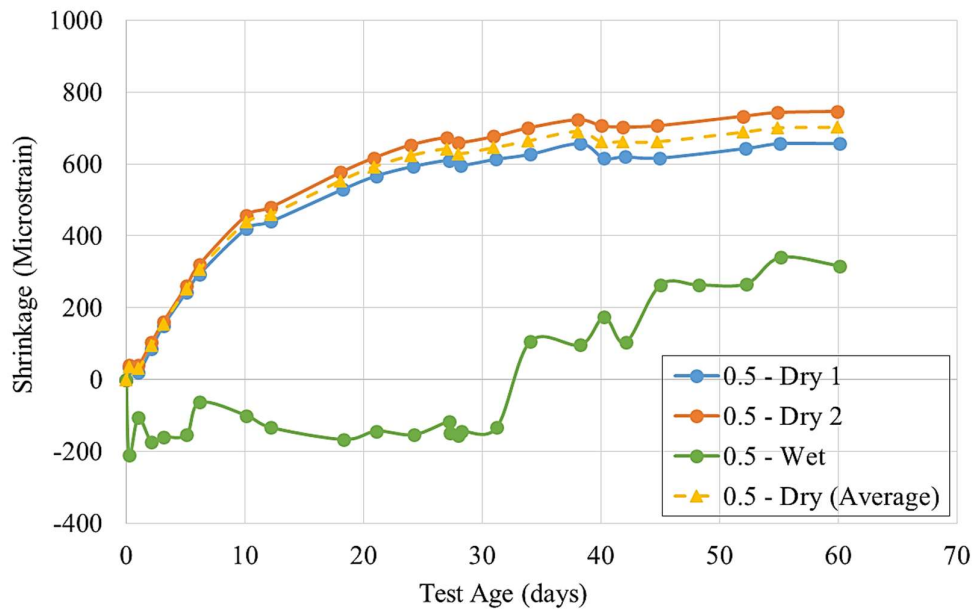


Figure 4-33: Shrinkage versus the test age in days of the 0.5 w/c ratio samples.

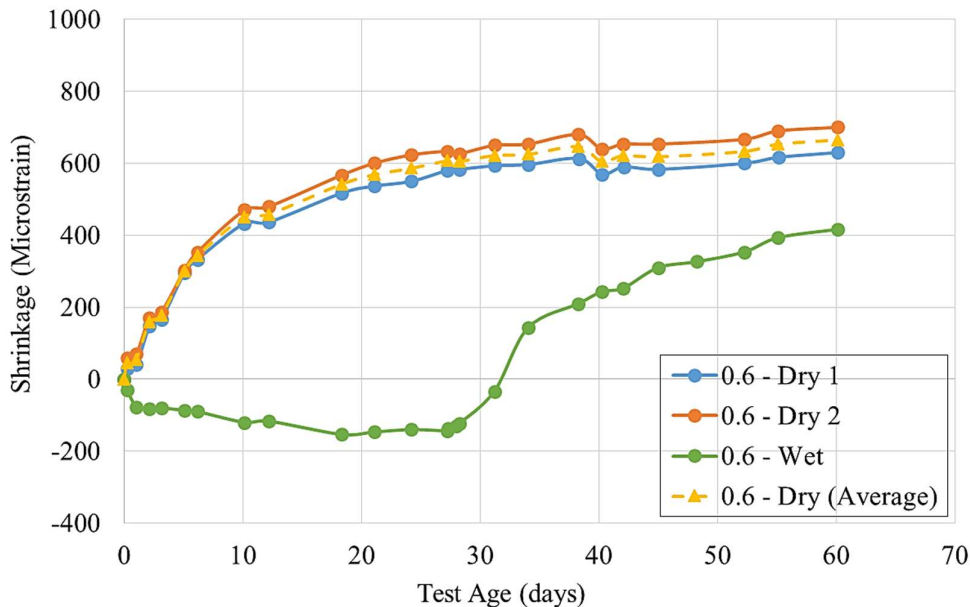


Figure 4-34: Shrinkage versus the test age in days of the 0.6 w/c ratio samples.

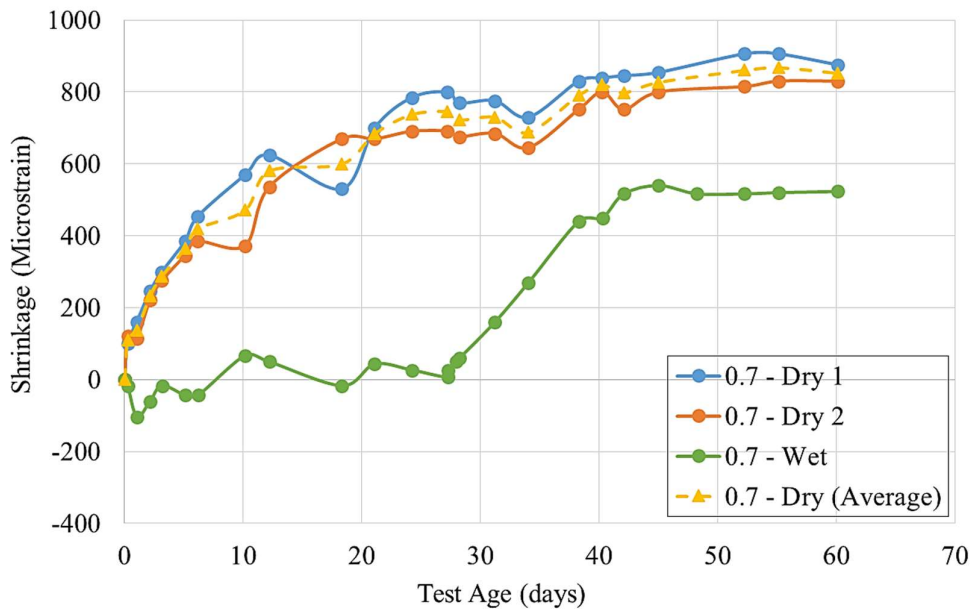


Figure 4-35: Shrinkage versus the test age in days of the 0.7 w/c ratio samples.

When comparing all the dry samples with different w/c ratios to one another it can be seen that the 0.3 w/c ratio (blue line) had the smallest shrinkage within the 60 day testing period (as shown in Figure 4-36). The 0.7 w/c ratio (green line) dry samples had the largest shrinkage within the 60 days. Figure 4-37 shows the shrinkage of all the wet samples for all the different w/c ratios tested. Again the 0.7 w/c ratio (green line) had the largest amount of shrinkage within the 60 day period. However, the 0.5 w/c ratio (purple line) had the smallest shrinkage within the 60 days.

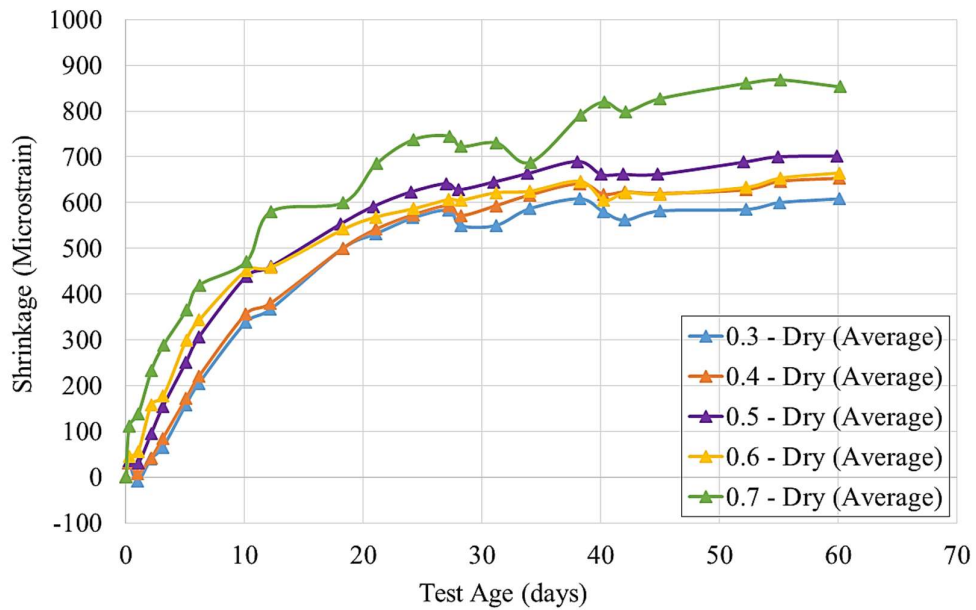


Figure 4-36: Shrinkage versus the test age in days of all the w/c ratio dry samples.

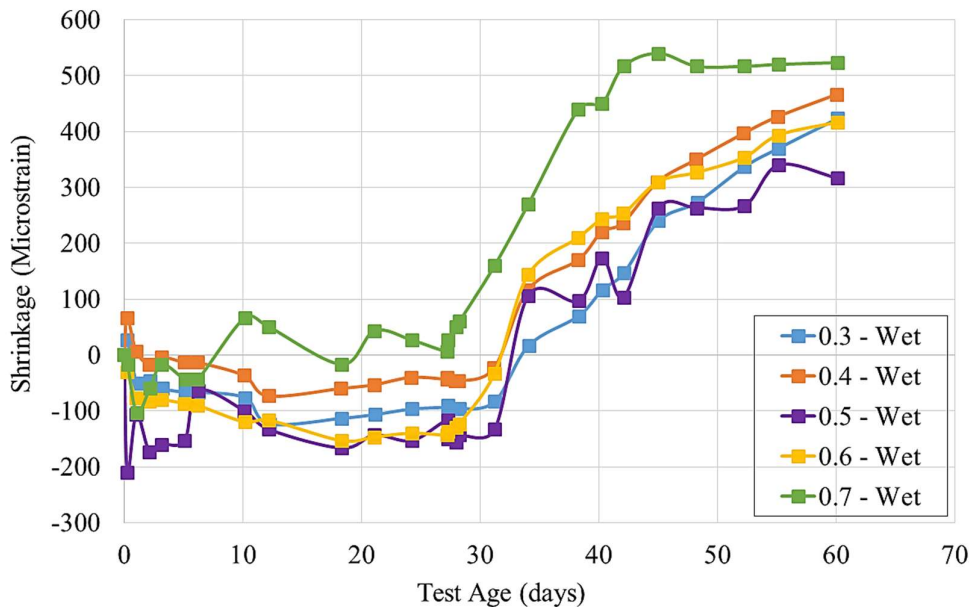


Figure 4-37: Shrinkage versus the test age in days of all the w/c ratio wet samples.

Figure 4-38 presents the dry shrinkage of the different w/c ratio samples (wet and dry samples) after 60 days of testing. It can be seen that the dry samples had an overall higher shrinkage after 60 days compared to the wet samples. It is clear that there is a turning point between w/c ratios 0.4 and 0.6 where the shrinkage changed. The same type of trends were observed in the porosity results (D_{50} and D_{10} values) showing that there was a turning point between w/c ratios 0.4 and 0.6. Overall it can be seen that the shrinkage increased with an increase in the w/c ratio which is similar to the porosity results.

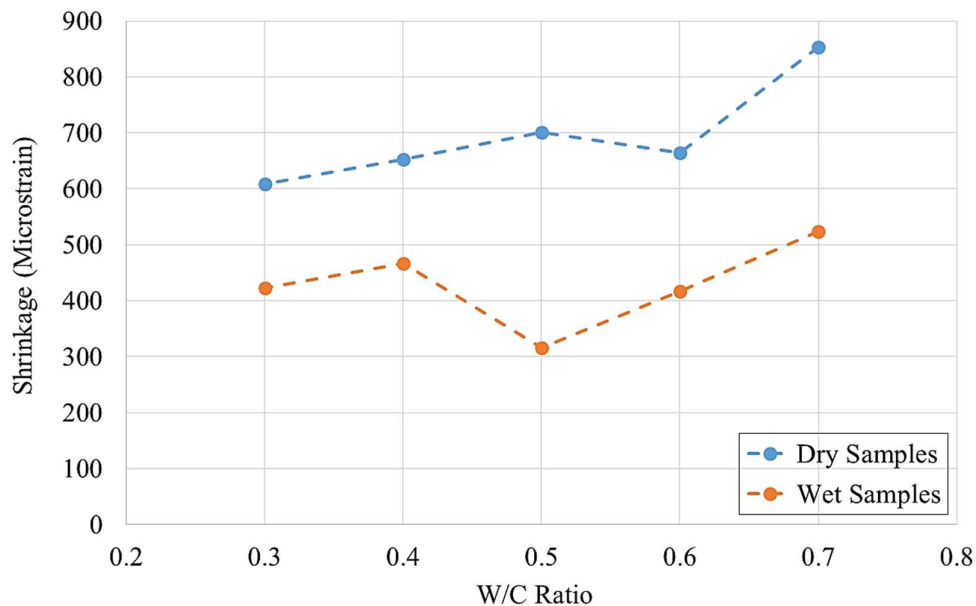


Figure 4-38: Dry shrinkage versus the w/c ratio of the dry and wet samples after 60 days.

4.5 MECHANICAL PROPERTIES

The results of all four test procedures, as explained in Section 3.4.5, are discussed in this section. These results are compared to the suction measurements discussed within Section 4.6. The strength and stiffness of the concrete are important aspects. The values shown are the average of three test results. The number of readings are insufficient to make any statement in terms of repeatability.

4.5.1 FLEXURAL TEST RESULTS

The TPBT results of the mortar prism beams tested are tabulated in Tables 4-11 to 4-13 after 7, 14 and 28 days respectively. Both the dry and wet sample results are presented and it can be seen that the strength increased with a decrease in the w/c ratio as expected.

Table 4-11: Mortar prism beams flexural strength after 7 days.

7 Day:	Flexural Strength (MPa)	
w/c ratio	Dry	Wet
0.3	8.4	8.5
0.4	7.6	8.5
0.5	5.2	6.9
0.6	4.5	5.5
0.7	4.0	4.9

Table 4-12: Mortar prism beams flexural strength after 14 days.

14 Day:	Flexural Strength (MPa)	
w/c ratio	Dry	Wet
0.3	8.8	10.5
0.4	8.6	8.7
0.5	7.7	8.2
0.6	6.6	6.6
0.7	5.2	6.6

Table 4-13: Mortar prism beams flexural strength after 28 days.

28 Day:	Flexural Strength (MPa)	
w/c ratio	Dry	Wet
0.3	9.0	10.9
0.4	8.9	9.7
0.5	8.1	8.3
0.6	7.1	7.2
0.7	6.0	6.8

Figure 4-39 shows the flexural strength of the five mixtures (w/c ratios 0.3 up to 0.7) and indicates that with an increase in the w/c ratio, the flexural strength decreases. The strength increased from the 7th day up to the 28th day, as expected from results shown in literature. It can also be seen that the dry samples' strength are lower compared to the wet samples' strength. The maximum strength reached was for the 0.3 w/c ratio (wet samples) after 28 days which was 10.9 MPa. The minimum strength reached was for the 0.7 w/c ratio (dry samples) after 7 days which was 4 MPa. It is clear that there is a turning point between w/c ratios 0.4 and 0.6 which was also seen in the shrinkage results for the different w/c ratio samples. Therefore, strength can also be linked to porosity as explained for the shrinkage results, showing that there was a turning point between w/c ratios 0.4 and 0.6 of the porosity (D_{50} and D_{10} values). This corresponds well with literature (Section 2.4) showing that the hydration process will stop

before completely finished at w/c ratios below 0.38 for the samples with no moisture movement (cured dry) (Hansen, 1970).

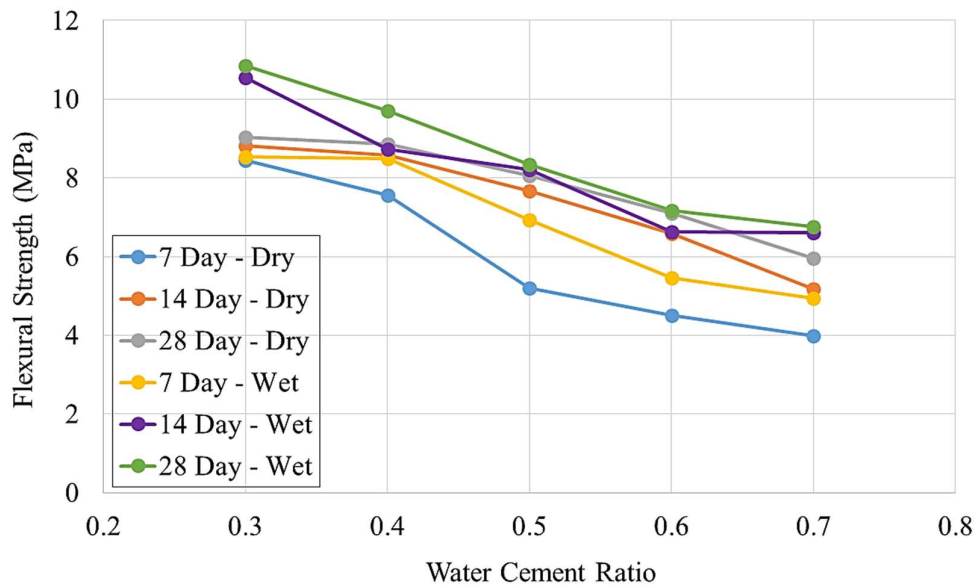


Figure 4-39: Flexural strength of all five mixtures at 7, 14 and 28 days.

4.5.2 COMPRESSIVE TEST RESULTS

The compressive test results are presented in Tables 4-14 to 4-16 for the 7th, 14th and 28th days respectively. From the dry and wet sample results presented, it can be seen that the compressive strength increased with a decrease in the w/c ratio. The wet samples had a higher compressive strength compared to the dry samples and this trend was also seen for the flexural strengths. Figure 4-40 shows the compressive strength versus the w/c ratio. It is clear that the strength increased with time. The compressive strength was higher compared to the flexural strength which was expected according to literature. The percentage difference between the dry and wet samples strength is also shown and it can be seen that the curing process (for the wet samples) has a bigger influence on the lower w/c ratio samples compared to the higher w/c ratio samples.

Table 4-14: Mortar prism beams compressive strength after 7 days.

<u>7 Day:</u>	Compressive Strength (MPa)		% Difference of dry and wet samples
w/c ratio	Dry	Wet	
0.3	53.4	74.7	40
0.4	44.7	65.1	46
0.5	35.9	47.2	32
0.6	27.6	33.1	20
0.7	22.9	26.7	17

Table 4-15: Mortar prism beams compressive strength after 14 days.

<u>14 Day:</u>	Compressive Strength (MPa)		% Difference of dry and wet samples
w/c ratio	Dry	Wet	
0.3	59.5	81.7	37
0.4	51.3	73.4	43
0.5	42.7	53.6	25
0.6	33.9	37.3	10
0.7	28.2	31.0	10

Table 4-16: Mortar prism beams compressive strength after 28 days.

<u>28 Day:</u>	Compressive Strength (MPa)		% Difference of dry and wet samples
w/c ratio	Dry	Wet	
0.3	61.3	82.1	34
0.4	51.7	75.4	46
0.5	43.4	54.5	26
0.6	34.4	41.1	20
0.7	29.5	32.7	11

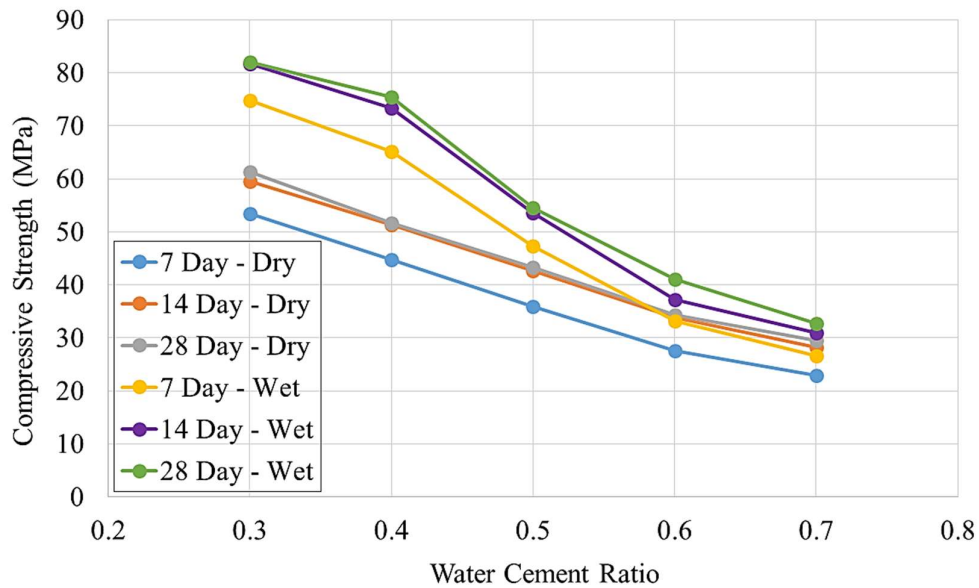


Figure 4-40: Compressive strength of all five mixtures at 7, 14 and 28 days.

The compressive strength test was also performed on cylindrical samples after 28 days and the results are tabulated in Table 4-17. These samples were cured dry (until tested) within a temperature controlled room with temperatures ranging between 20 and 25°C. Figure 4-41 shows the compressive strength versus the w/c ratio after 28 days. It can be seen that the cylinder's compressive strength also increased with a decrease in the w/c ratio when compared to the mortar prism beams tested. The compressive strength of the 28 day cylinders are similar compared to the 28 day compressive strength results of the mortar prism beams tested.

Table 4-17: Dry cylinders compressive strength after 28 days.

w/c ratio	28 Day Cylinder Compressive Strength (MPa)
0.3	65.6
0.4	55.4
0.5	43.8
0.6	32.0
0.7	25.7

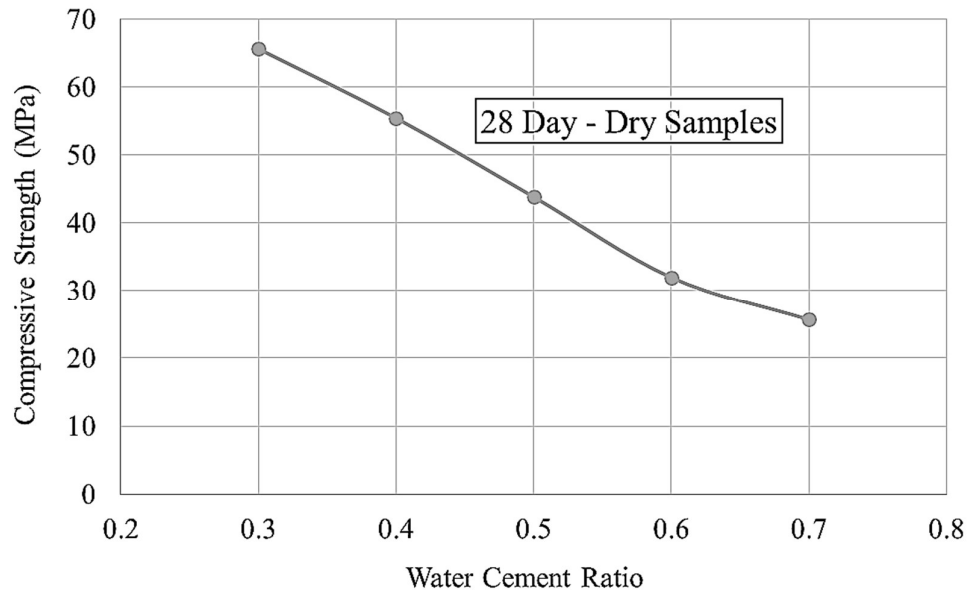


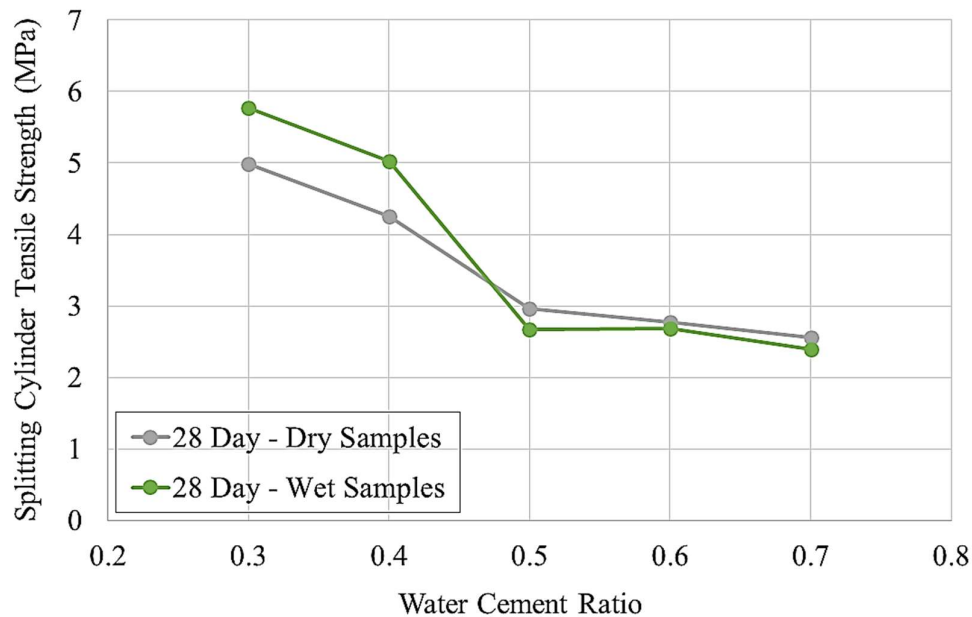
Figure 4-41: Compressive strength of cylindrical samples at 28 days.

4.5.3 SPLITTING CYLINDER TEST RESULTS

The results of the splitting cylinder test for both the dry and wet samples tested after 28 days are tabulated in Table 4-18. It can be seen that all the sample's lengths were close to 200 mm and the load (P) applied onto the samples (at failure) increased with a decrease in the w/c ratio. Figure 4-42 presents the difference in the tensile strength for the different w/c ratios (dry and wet samples). It can be seen that the 0.3 and 0.4 w/c ratios (of the wet samples) had a higher strength compared to the 0.5, 0.6 and 0.7 w/c ratio samples. The effect of curing on the splitting cylinder strength is negligible for w/c ratios larger than 0.5 and it can be said that curing had a more significant effect on strength development of samples with a low w/c ratio.

Table 4-18: Splitting cylinder tensile strength results at 28 days.

w/c ratio	Length (mm)	Force (kN)	Splitting Cylinder Tensile Strength, f_s (MPa)
0.3 - Dry	200.9	157.2	5.0
0.4 - Dry	201.3	134.4	4.3
0.5 - Dry	199.0	92.5	3.0
0.6 - Dry	201.2	87.7	2.8
0.7 - Dry	197.0	79.3	2.6
0.3 - Wet	201.0	182.3	5.8
0.4 - Wet	199.8	157.8	5.0
0.5 - Wet	199.9	83.9	2.7
0.6 - Wet	199.9	84.3	2.7
0.7 - Wet	199.1	74.8	2.4

**Figure 4-42: Splitting cylinder tensile strength for all the w/c ratios.**

4.5.4 E-VALUE TEST RESULTS

The E-value test was performed on cylindrical samples after 28 days (as mentioned in Section 3.4.5) for both dry and wet samples. Table 4-19 tabulates the E-value test results obtained for all the samples. It can be seen that the E-values increased with a decrease in the w/c ratio for both the dry and the wet samples. The graphs illustrating the E-values for each cylinder are shown in Appendix J. The results for the dry and wet samples of the same w/c ratios are similar to one another. The 0.3, 0.6 and 0.7 w/c ratios of the dry samples had higher E-values compared to the wet samples. However, the 0.4 and 0.5

w/c ratios of the wet samples had higher E-values compared to the dry samples as shown in Figure 4-43. Curing does not seem to have a significant effect on the stiffness of the mortars tested.

Table 4-19: Modulus of elasticity at 28 days for the cylindrical samples.

w/c ratio	E - value (GPa)
0.3 - Dry	34.8
0.4 - Dry	29.6
0.5 - Dry	26.8
0.6 - Dry	30.5
0.7 - Dry	28.2
0.3 - Wet	33.1
0.4 - Wet	31.9
0.5 - Wet	31.1
0.6 - Wet	26.8
0.7 - Wet	27.0

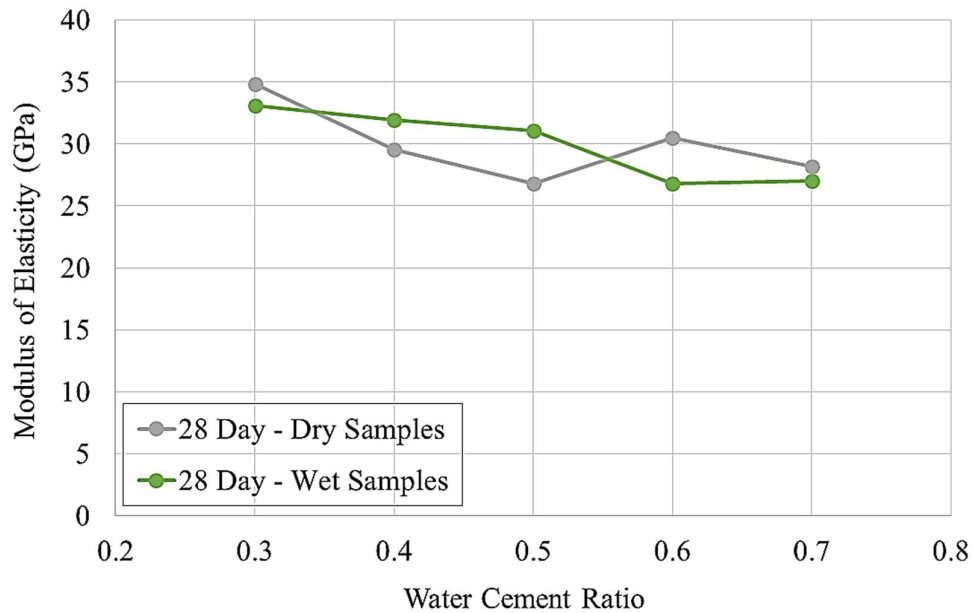


Figure 4-43: E-Value of cylindrical samples at 28 days.

4.5.5 DISCUSSION OF THE MECHANICAL PROPERTY RESULTS

From the results discussed above it can be concluded, as expected, that the wet samples had an overall higher strength compared to the dry samples. Both the flexural and compressive strength increased over time, together with a decrease in the w/c ratio. The splitting cylinder and the E-value tests were only performed on one sample for each w/c ratio (dry and wet samples) which could be the reason for the irregular results. However, more than one sample was tested during the flexural test (TPBT) and the compressive test (of the mortar prism beams) which showed reliable trends.

4.6 DISCUSSION OF THE OVERALL COMBINED RESULTS

This section gives an overall discussion of the relationship between the water retention curves and the other properties of the concrete tested in this research study, namely: the slump flow, the porosity, the shrinkage, the strength and the stiffness. A quick recap of the suction measurements determined in the mortar study for samples numbered 3 (partially wet samples) are shown in Figure 4-44, illustrated for a duration of 28 days. The same trend was followed compared to the cement paste study (shown in Figure 3-14). The suction increased with an increase in sample age, as well as a decrease in the w/c ratio. The suction results shown for sample number 3 of each w/c ratio set were used to discuss the relationship between the suctions and the slump flow, porosity, shrinkage, strength and stiffness of the mortar mixtures. Further investigation can be done to see whether these trends follow for different types of concrete with the same w/c ratios. This research is limited to the specific concrete and w/c ratios used in the mix design.

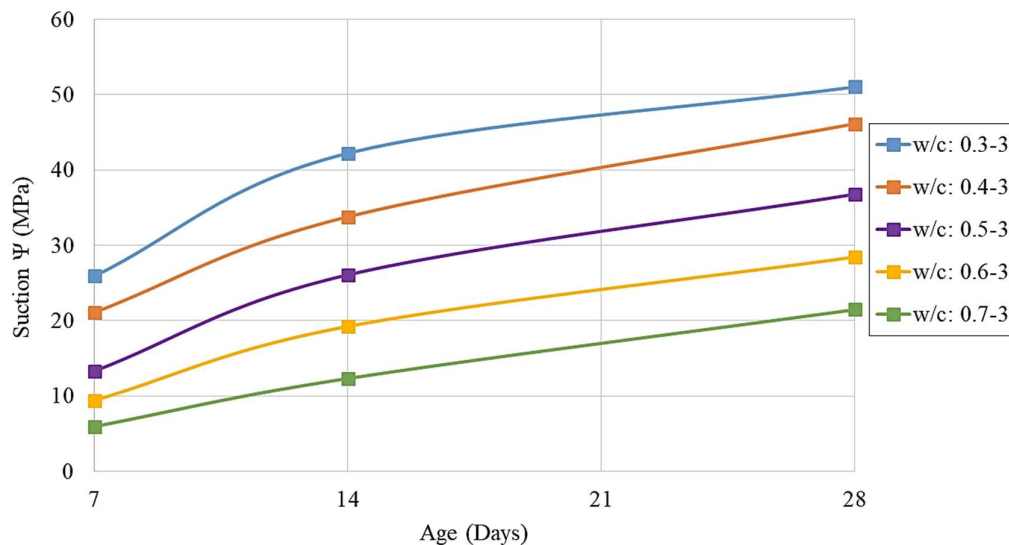


Figure 4-44: Suctions developed within 28 days for samples number 3.

4.6.1 RELATIONSHIP BETWEEN SUCTIONS & SLUMP FLOW

The slump flow of the different concrete mixtures discussed in Section 4.1.1 are compared to the suction measurements of the partially dry samples, tabulated in Table 4-20. It is clear that the suction measurements increased over time. The overall suction decreased with an increase in the w/c ratio. This trend held for all the days of testing (at 7, 14 and 28 days).

Figure 4-45 illustrates the relationship between the slump flow of the different w/c ratio samples tested compared to the suctions (only for the sample's numbered 3). Firstly, the suctions decreased with an increase in the slump flow. Secondly, the suctions decreased with an increase in the w/c ratio of the samples. Lastly, the suctions increased with an increase in the number of days of testing (from 7 to 28 days).

Table 4-20: Suction measurements of sample number 3 for all w/c ratios.

Total Suction (MPa) for Sample's Number 3			
W/C Ratio	7 Days	14 Days	28 Days
0.3	25.90	42.22	51.03
0.4	21.09	33.79	46.14
0.5	13.30	26.08	36.78
0.6	9.41	19.23	28.45
0.7	5.94	12.31	21.45

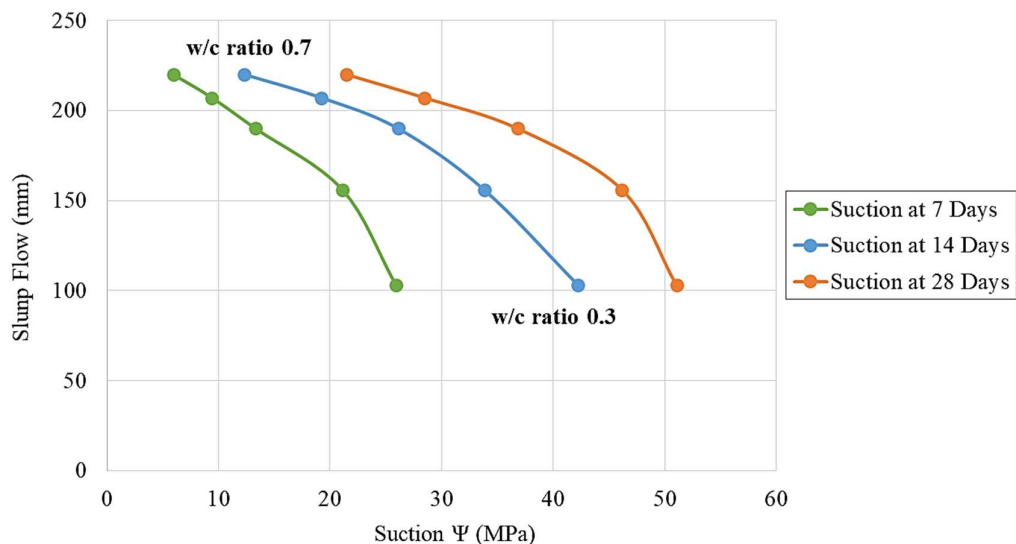


Figure 4-45: Slump flow versus suction from 7 to 28 days.

4.6.2 RELATIONSHIP BETWEEN SUCTIONS & POROSITY

Three different w/c ratio samples were compared for each of the three tests performed during this research study. These three porosity tests include the X-ray test, the MIP test and the simple test method described in the durability index testing procedure manual, results shown in Table 4-10 (in Section 4.3.4). These results were compared to the suction measurements obtained during the mortar study (presented in Figure 4-44, after 28 days). Both the suction and porosity measurements were obtained on the same day, 28 days after cast. The suction measurements increased with a decrease in the % porosity of the samples.

Figure 4-46 presents the % porosity of the different tests performed compared to the suction measurements after 28 days. It can be concluded that with an increase in the w/c ratio the % porosity also increased while the suctions decreased. The MIP test and the simple test method results were fairly similar to one another. However, the X-ray suction measurements did not show any significant change.

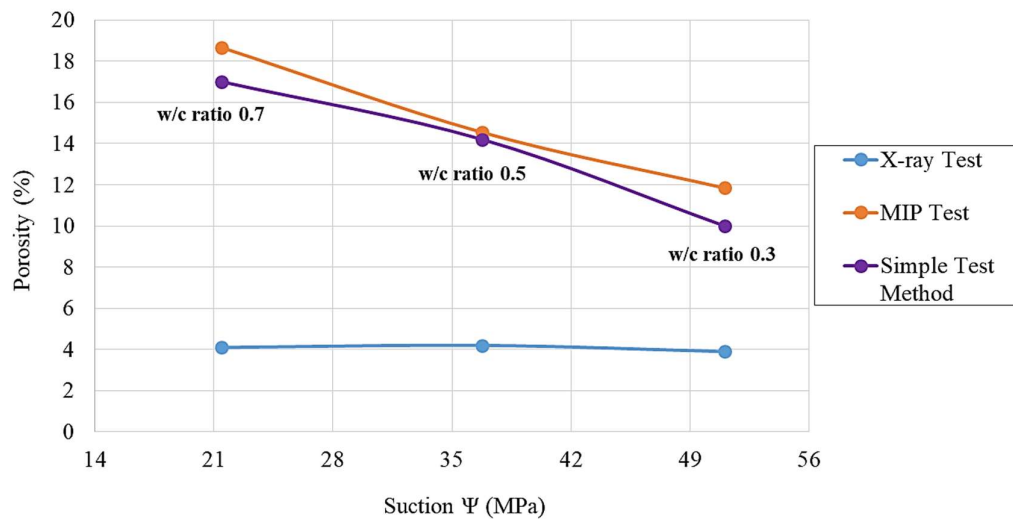


Figure 4-46: Porosity (%) versus suction of the different tests performed.

4.6.3 RELATIONSHIP BETWEEN SUCTIONS & SHRINKAGE

The drying shrinkage versus the suctions of the 5 different w/c ratios tested are shown in Figure 4-47. It is clear that there was an increase in the suction measurements as the drying shrinkage of the samples increased. The drying shrinkage also increased with an increase in the w/c ratio of the samples. It can be concluded that there is a definite trend between the suction measurements and the drying shrinkage of the concrete.

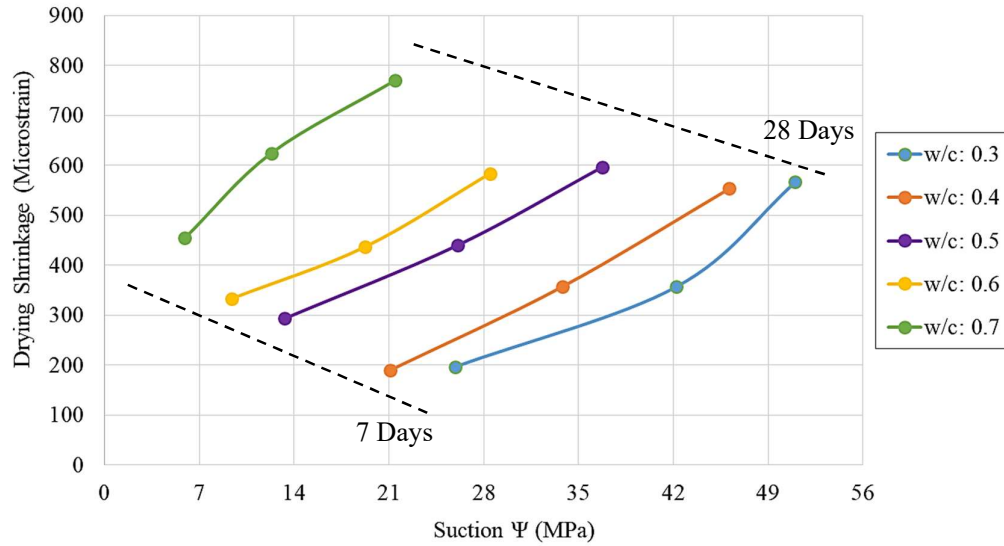


Figure 4-47: Drying shrinkage versus suctions from 7 to 28 days.

4.6.4 RELATIONSHIP BETWEEN SUCTIONS, STRENGTH AND STIFFNESS

In this section the four different strength tests conducted in the mortar study are compared to the suctions obtained. The four different tests include the flexural test, the compressive test, the splitting cylinder test and the E-value test (stiffness). The strength results discussed in Section 4.5 are compared to the suction measurements shown in Figure 4-44 (on page 4-35).

A definite trend between the suctions and the flexural strength (for the dry samples tested) of the different w/c ratio samples is shown in Figure 4-48. The flexural strength increased with a decrease in the w/c ratio of the samples. The suctions also increased with an increase in the flexural strength of the samples. For low strengths, there is a rapid increase in suction with an increase in strength, but for w/c ratios below 0.5 there is limited strength increase with significant increases in suction. The results indicate that there is a difference between the behaviour of low and high w/c ratio mixtures and more research should be conducted to determine the root cause of this trend.

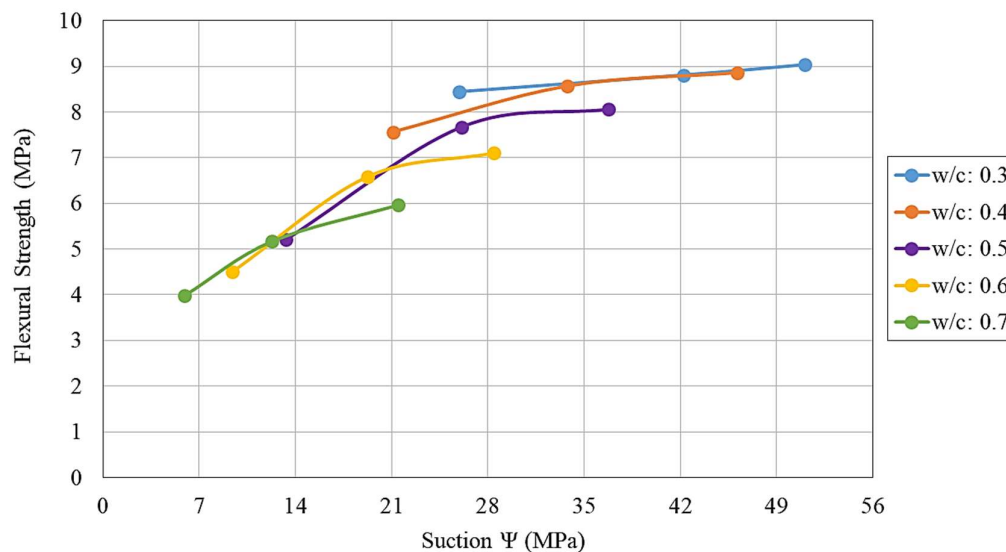


Figure 4-48: Flexural strength versus suctions from 7 to 28 days.

The suction versus the compressive strength results of the dry samples (for the 28th day results) are presented in Figure 4-49. Again a definite trend as seen for the flexural strength was seen for the compressive strength results. The compressive strength increased with a decrease in the w/c ratio. An increase in the suction with an increasing compressive strength was also seen. The wet samples show a similar trend compared to the dry samples tested. The only difference was that a higher strength was obtained for the wet samples (cured in water until tested) compared to the dry samples (cured outside in a temperature controlled room). Figure 4-50 shows the relationship between the suctions obtained

and the compressive strength of the wet samples. These results followed a similar trend compared to that of the dry sample results, as discussed above.

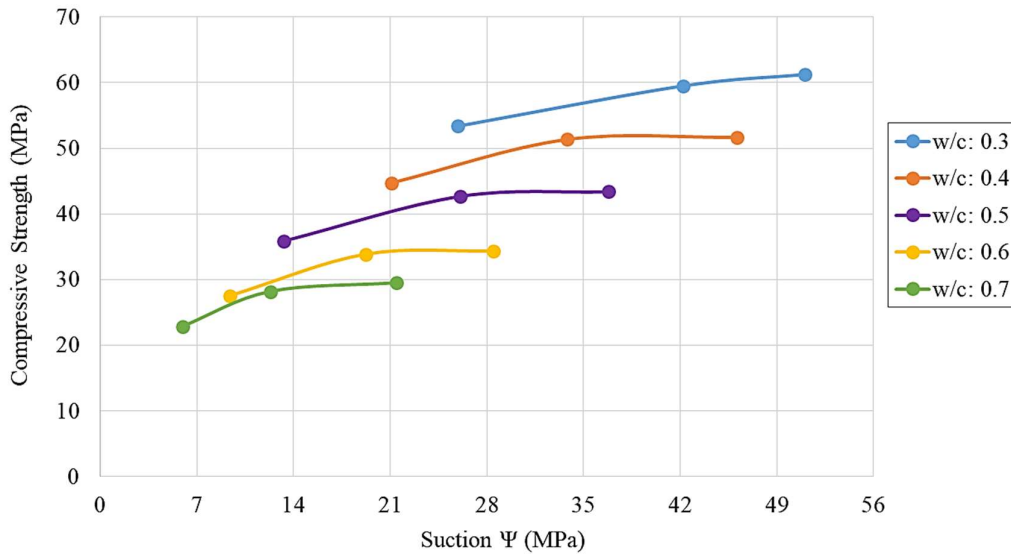


Figure 4-49: Compressive strength versus suctions of the dry samples from 7 to 28 days.

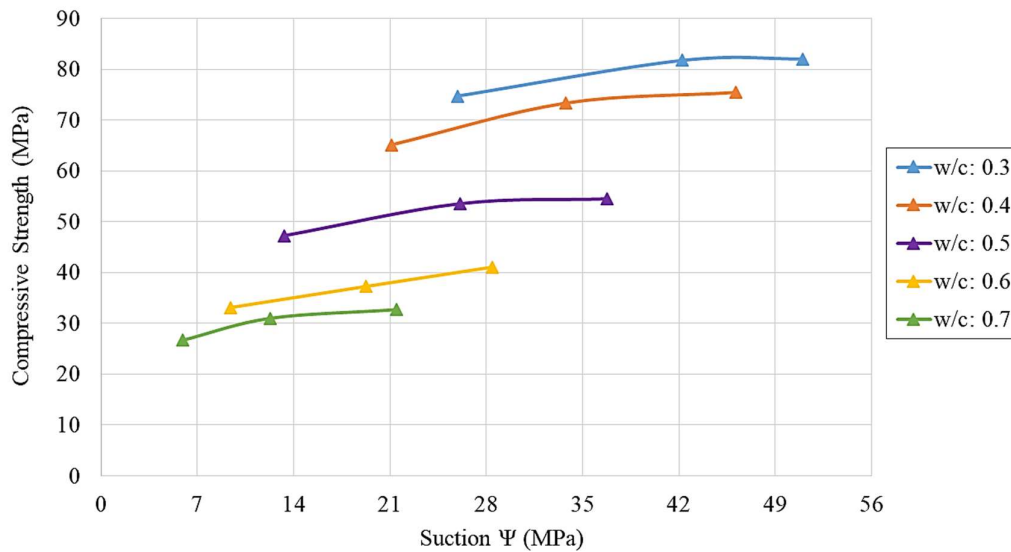


Figure 4-50: Compressive strength versus suctions of the wet samples from 7 to 28 days.

Figure 4-51 illustrates the relationship between the splitting cylinder strength and the suctions, from the 0.3 up to 0.7 w/c ratio samples (after 28 days). The dry and wet sample results (as shown in Section 4.5.3) are shown in the graph. The splitting cylinder tensile strength increased with a decrease in the w/c ratio. It is also clear that the suctions increased with an increase in the splitting cylinder tensile strength. Therefore, it can be concluded that the suctions increased with a decrease in the w/c ratio,

together with an increase in the splitting cylinder tensile strength. These results yet again indicate that there is a significant difference in the behaviour between the mixtures with w/c ratio below and above 0.5.

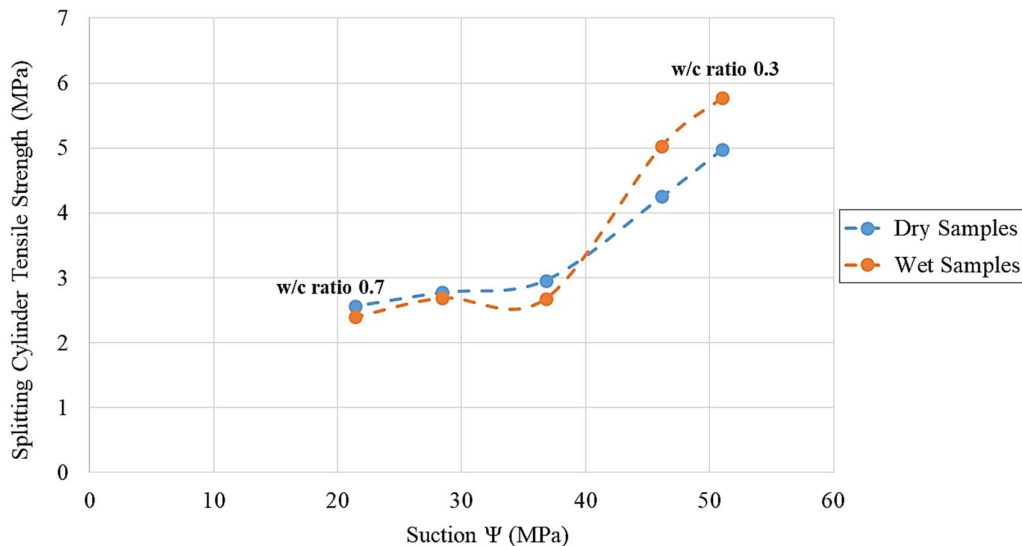


Figure 4-51: Splitting cylinder tensile strength versus suctions at 28 days.

The modulus of elasticity (E-value or stiffness) versus the suctions of the wet samples (cured in water) are shown in Figure 4-52. It can be seen that the E-values increased with a decrease in the w/c ratio (from 0.3 up to 0.7 w/c ratios were presented in the graph). It is also clear that the suctions increased with an increase in the stiffness of the concrete samples.

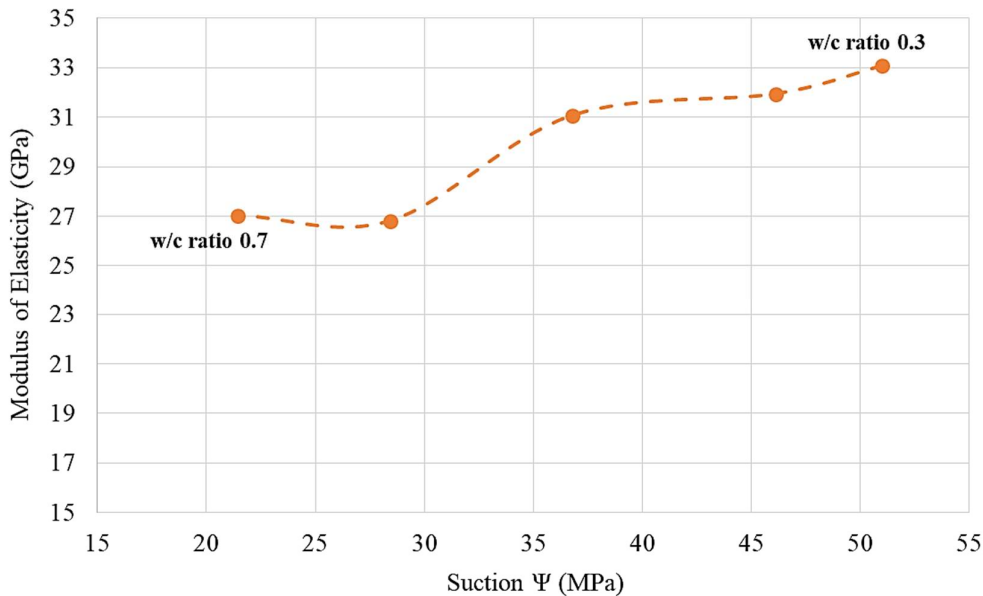


Figure 4-52: Modulus of elasticity versus suctions at 28 days.

4.7 SUMMARY OF OBSERVED TRENDS

The overall suction measurements increased with a decrease in the w/c ratio for the different mortar mixtures tested. The following trends were observed during this research study:

- The suctions increased with a decrease in the slump flow and the slump flow increased with an increase in the w/c ratio.
- The suctions increased with a decrease in the % porosity. The porosity increased with an increase in the w/c ratio.
- The suctions increased with an increase in the drying shrinkage of the samples tested, together with an increase in the w/c ratio.
- The suctions increased with an increase in the flexural strength, the compressive strength and the splitting cylinder tensile strength of the mortar samples. The strength increased with a decrease in the w/c ratio as expected. There was a rapid increase in suction with an increase in strength for the high w/c ratio mixtures (low strengths). However, w/c ratios below 0.5 had limited strength increase with significant increases in suction. These results indicate that there is a difference between the behaviour of low and high w/c ratio mixtures and further research should be conducted to determine the main cause of this trend.
- The suctions also increased with an increase in the stiffness (E-value) of the samples and the stiffness increased with a decrease in the w/c ratio.

5 CONCLUSIONS AND RECOMMENDATIONS

5.1 CONCLUSIONS

The following list of conclusions were obtained during this research study:

- 1) From the cement paste study it can be concluded that the WP4C apparatus generates representative results. Therefore, this testing procedure can be used to generate reliable water retention curves, as done within this study.
- 2) The X-ray test did not manage to measure the capillary and the gel pores within the samples. However, the MIP test which was designed to measure significantly small pores showed that the capillary and the gel pores could play a significant role when measuring the porosity of a sample.

The simple porosity test results are fairly similar to the MIP test results. Therefore, it can be concluded that the simple test method gives representative results and that the X-ray test cannot detect the capillary and gel pores for the sample size used in this study.
- 3) The environment had an impact on the dry samples (which cured without a lid on during the suction measurements). However, there was no impact on the partially dry samples (samples numbered 3) which were sealed with the container's lid until the suction measurements started. Therefore, the partially dry sample results can be used to determine the relationship between the suctions and the other concrete properties obtained during this research study.
- 4) The water retention curves obtained during this research study follow a similar trend to that of the SWRC obtained by Geotechnical Engineers in the past. The water retention curves of the mortar samples follow the bimodal SWRC's path (following sub-curve 1). Therefore, it can be concluded that the water retention curve for mortar is similar to the bimodal SWRC (discussed in Section 2.2).
- 5) The following relationships have been established between the suction measurements and the different mortar properties tested during this research:
 - a. The suctions increase with a decrease in the slump flow of the concrete.
 - b. The % porosity decreases with an increase in the suctions.
 - c. The suctions increase with an increase in the drying shrinkage of the samples tested.
 - d. The suctions increase with an increase in the flexural strength, the compressive strength and the splitting cylinder tensile strength of the mortar sample.
 - e. The suctions also increase with an increase in the stiffness (E-value) of the samples.
- 6) The total suction of the concrete samples increases with a decrease in the w/c ratio of the various mortar mixtures.

- 7) The suction measurements (or the soil water retention curves) of the concrete have the potential to replace tests currently used in the industry. It is clear that the properties of the concrete (mortar) discussed throughout this research have a clear relationship to the suction measurements. Further research to establish a mathematical relationship between these properties should be investigated.

5.2 RECOMMENDATIONS

During this research project some limitations arose which can be improved for future studies in this field, including:

The necessary equipment to perform the study could be placed within the same facility to prevent moving the samples to other facilities. This will ensure that there is no environmental impact on the samples being measured.

Specific sample moulds could be prepared to cast the correct sample sizes for each porosity test, to prevent cutting of the samples. The pore structure of the samples could be damaged during the cutting procedure if it is not done properly.

It could also be worthwhile to relate the water retention curve to the setting time of concrete, since this topic is not well researched. A mathematic relationship between the suctions and the properties of concrete will also have great potential (as seen in Geotechnical studies).

6 REFERENCES

- ABELL, A. B., WILLIS, K. L. & LANGE, D. A. 1999. Mercury Intrusion Porosimetry and Image Analysis of Cement-Based Materials. *Journal of Colloid And Interface Science*, 211, 39-44.
- ANOVITZ, L. M. & COLE, D. R. 2015. Characterization and Analysis of Porosity and Pore Structures. *Reviews in Mineralogy and Geochemistry*, 80, 61-164.
- ASTM 2014. Standard Specification for Flow Table for Use in Test of Hydraulic Cement. *C230 / C230M-14*. West Conshohocken, PA: ASTM International.
- ATAHAN, H. N., OKTAR, O. N. & TAŞDEMİR, M. A. 2009. Effects of water-cement ratio and curing time on the critical pore width of hardened cement paste. *Construction and Building Materials*, 23, 1196-1200.
- BANTHIA, N. & ISLAM, S. 2013. Loading Rate Concerns in ASTM C1609. *Journal of Testing and Evaluation*, 41, 1032-1036.
- BARRETT, E. P., JOYNER, L. G. & HALENDA, P. P. 1951. The Determination of Pore Volume and Area Distributions in Porous Substances. I. Computations from Nitrogen Isotherms. *Journal of the American Chemical Society*, 73, 373-380.
- BENCARDINO, F. 2013. Mechanical parameters and post-cracking behaviour of HPC according to three-point and four-point bending test. *Advances in Civil Engineering*, 2013.
- BHATTACHARJEE, B. 2003. Porosity, pore size distribution and in situ strength of concrete. *Cement and Concrete Research*, 33, 155-164.
- BISSONNETTE, B. T., PIERRE, P. & PIGEON, M. 1999. Influence of key parameters on drying shrinkage of cementitious materials. *Cement and Concrete Research*, 29, 1655-1662.
- BOGUE, R. 1955. Chemistry of Portland Cement.
- BROOKS, R. H. & COREY, A. T. 1964. Hydraulic properties of porous media. *Hydrology papers (Colorado State University); no. 3*.
- BRUNAUER, S., EMMETT, P. H. & TELLER, E. 1938. Adsorption of gases in multimolecular layers. *Journal of the American chemical society*, 60, 309-319.
- BU, J. & TIAN, Z. 2016. Relationship between pore structure and compressive strength of concrete: Experiments and statistical modeling. *Sādhanā : Published by the Indian Academy of Sciences*, 41, 337-344.
- BYE, G. C., LIVESEY, P. & STRUBLE, L. J. 2011. Portland cement. Third edition. ed. London: Institution of Civil Engineers Publishing.

- CADONI, E., LABIBES, K., ALBERTINI, C., BERRA, M. & GIANGRASSO, M. 2001. Strain-rate effect on the tensile behaviour of concrete at different relative humidity levels. *Materials and structures*, 34, 21.
- CAO, Y., YU, Q., BROUWERS, H. & CHEN, W. 2019. Predicting the rate effects on hooked-end fiber pullout performance from Ultra-High Performance Concrete (UHPC). *Cement and Concrete Research*, 120, 164-175.
- CHEN, X., WU, S. & ZHOU, J. 2013. Influence of porosity on compressive and tensile strength of cement mortar. *Construction and Building Materials*, 40, 869-874.
- DÄRR, G. & LUDWIG, U. 1973. Determination of permeable porosity. *Matériaux et Construction*, 6, 185-190.
- DE GRYZE, S., JASSOGNE, L., SIX, J., BOSSUYT, H., WEVER, M. & MERCKX, R. 2006. Pore structure changes during decomposition of fresh residue: X-ray tomography analyses. *Geoderma*, 134, 82-96.
- DE_BEER 2005. Characteristics of the neutron/X-ray tomography system at the SANRAD facility in South Africa. *Nuclear Instruments and Methods in Physics Research Section A: Accelerators, Spectrometers, Detectors and Associated Equipment*, 542, 1-8.
- DE_BEER 2012. Characteristics of the Micro-Focus X-ray Tomography Facility (MIXRAD) at Necsa in South Africa.
- DIAMOND, S. 1999. Aspects of concrete porosity revisited. *Cement and Concrete Research*, 29, 1181-1188.
- DOMONE, P. L. J. & ILLSTON, J. M. 2010. *Construction materials : their nature and behaviour*, Milton Park, Abingdon, Oxon ;, Spon Press.
- DU PLESSIS, A., OLAWUYI, B. J., BOSHOFF, W. P. & LE ROUX, S. G. 2016. Simple and fast porosity analysis of concrete using X-ray computed tomography. *Materials and Structures*, 49, 553-562.
- EN, B. 2007. 14651: 2005+ A1: 2007. Test method for metallic fibre concrete—Measuring the flexural tensile strength (limit of proportionality (LOP), residual). *British Standards Institution*.
- EN, C. F. S. 1999 - 2004. European Standard. *Method of test for mortar for masonry - Part 3: Determination of consistence of fresh mortar (by flow table)* B-1050 Brussels.
- FELDMAN, R. & SEREDA, P. 1970. A new model for hydrated Portland cement paste and its practical implications. *Eng J (Canada)*, 53, 53-59.
- FORESTER, J. 1970. A conduction calorimeter for the study of cement hydration. *Cement Technology* 1, 95-99.

- FREDLUND, D., VANAPALLI, S., XING, A. & PUFAHL, D. Predicting the shear strength function for unsaturated soils using the soil-water characteristic curve. First International Conference on Unsaturated Soils, Paris, France, 1995. 6-8.
- FREDLUND, D. G., RAHARDJO, H. & FREDLUND, M. D. 2012. Unsaturated soil mechanics in engineering practice. Hoboken, N.J.: John Wiley & Sons.
- FREDLUND, D. G., SHENG, D. & ZHAO, J. 2011. Estimation of soil suction from the soil-water characteristic curve. *Canadian Geotechnical Journal*, 48, 186-198.
- FREDLUND, D. G. & XING, A. 1994a. Equations for the soil-water characteristic curve. *Canadian geotechnical journal*, 31, 521-532.
- FREDLUND, D. G. & XING, A. 1994b. Equations for the soil-water characteristic curve. *CANADIAN GEOTECHNICAL JOURNAL*, 31, 521.
- GAO, Y., JIANG, J., DE SCHUTTER, G., YE, G. & SUN, W. 2014. Fractal and multifractal analysis on pore structure in cement paste. *Construction and Building Materials*, 69, 253-261.
- GIESCHE, H. 2006. Mercury Porosimetry: A General (Practical) Overview. *Particle & Particle Systems Characterization*, 23, 9-19.
- HADLEY, D. W. 1972. The Nature of the Past-Aggregate Interface: Interim Report.
- HALL, C. A. 1994. *Concrete Timber and Metals*, 2 Park Square, Milton Park, Abingdon, Oxon OX14 4RN, Spon Press.
- HAN, M. Y. & LYTTON, R. L. 1995. Theoretical Prediction of Drying Shrinkage of Concrete. *Journal of Materials in Civil Engineering* [Online], 7.
- HANSEN, T. 1970. Physical composition of hardened Portland cement paste. *Proceedings of the American Concrete Institute* 67, 404-407.
- HELLMICH, C., PICHLER, B. & KOLLEGGGER, J. 1.1 Introduction and Observations Requiring a New Comprehensive Mathematical Model. *Concreep 10 - Mechanics and Physics of Creep, Shrinkage, and Durability of Concrete and Concrete Structures - Proceedings of the 10th International Conference, September 21-23, 2015, Vienna, Austria*. American Society of Civil Engineers (ASCE).
- HELLMICH, C., PICHLER, B. & KOLLEGGGER, J. 2.1 Introduction. *Concreep 10 - Mechanics and Physics of Creep, Shrinkage, and Durability of Concrete and Concrete Structures - Proceedings of the 10th International Conference, September 21-23, 2015, Vienna, Austria*. American Society of Civil Engineers (ASCE).
- HELLMICH, C., PICHLER, B. & KOLLEGGGER, J. 3.1 Introduction. *Concreep 10 - Mechanics and Physics of Creep, Shrinkage, and Durability of Concrete and Concrete Structures -*

Proceedings of the 10th International Conference, September 21-23, 2015, Vienna, Austria.
American Society of Civil Engineers (ASCE).

- HELLMICH, C., PICHLER, B. & KOLLEGGGER, J. References. *Concreep 10 - Mechanics and Physics of Creep, Shrinkage, and Durability of Concrete and Concrete Structures - Proceedings of the 10th International Conference, September 21-23, 2015, Vienna, Austria.* American Society of Civil Engineers (ASCE).
- HEWLETT, P. C. 2004. *Lea's chemistry of cement and concrete.* 4th ed. ed. Oxford: Elsevier Butterworth-Heinmann.
- HOU, LI, D., HUA, P., JIANG, J. & ZHANG, G. 2019. Statistical modelling of compressive strength controlled by porosity and pore size distribution for cementitious materials. *Cement and Concrete Composites*, 96, 11-20.
- HUANG, Q., JIANG, Z., GU, X., ZHANG, W. & GUO, B. 2015. Numerical simulation of moisture transport in concrete based on a pore size distribution model. *Cement and Concrete Research*, 67, 31-43.
- HUANG, S., BARBOUR, S.L. & FREDLUND, D.G. 1998. Development and verification of a coefficient of permeability function for a dormable unsaturated soil. *Canadian Geotechnical Journal*, 35, 411.
- INTERNATIONAL, A. 2016a. Standard Guide for Examination of Hardened Concrete Using Scanning Electron Microscopy.
- INTERNATIONAL, A. 2016b. Standard Test Method for Microscopical Determination of Parameters of the Air-Void System in Hardened Concrete.
- JIRŮK, M., BARTOŠ, M., TOMÁŠEK, P., MALEČKOVÁ, A., KURAL, T. S., HORÁKOVÁ, J., LUKÁŠ, D., SUCHÝ, T. S., KOCHOVÁ, P., HUBÁLEK KALBÁČOVÁ, M., KRÁLÍČKOVÁ, M. & TONAR, Z. K. 2018. Generating standardized image data for testing and calibrating quantification of volumes, surfaces, lengths, and object counts in fibrous and porous materials using X-ray microtomography. *Microscopy Research and Technique*, 81, 551-568.
- JIVKOV, A. P., ENGELBERG, D. L., STEIN, R. & PETKOVSKI, M. 2013. Pore space and brittle damage evolution in concrete. *Engineering Fracture Mechanics*, 110, 378-395.
- KIM, Y. Y., BANG, J. W., LEE, K. M. & KWON, S. J. 2014. Effect of W/C ratio on durability and porosity in cement mortar with constant cement amount. *Advances in Materials Science and Engineering*, 2014.

- KONDRAIVENDHAN, B. & BHATTACHARJEE, B. 2016. Strength and w/c ratio relationship of cement based materials through pore features. *Materials Characterization*, 122, 124-129.
- KOVARONA, K., ŠEVČÍK, R. & WEISHAUPTOVA, Z. 2012. Comparison of mercury porosimetry and X-ray microtomography for porosity study of sandstones. *Acta Geodynamica et Geromaterialia*, 9, 541-550.
- KUPER, K., ZEDGENIZOV, D. A., RAGOZIN, A., SHATSKY, V., POROSEV, V., ZOLOTAREV, K. V., BABICHEV, E. & IVANOV, S. 2007. Three-dimensional distribution of minerals in diamondiferous eclogites, obtained by the method of high-resolution X-ray computed tomography. *Nuclear Instruments & Methods in Physics Research Section A-accelerators Spectrometers Detectors and Associated Equipment - NUCL INSTRUM METH PHYS RES A*, 575, 255-258.
- LEIBNER, T., DIENER, A., LÖWER, E., DITSCHERLEIN, R., KRÜGER, K., KWADE, A. & PEUKER, U. A. 2020. 3D ex-situ and in-situ X-ray CT process studies in particle technology – A perspective. *Advanced Powder Technology*, 31, 78-86.
- LI, J. & YAO, Y. 2001. A study on creep and drying shrinkage of high performance concrete. *Cement and Concrete Research*, 31, 1203-1206.
- LIKOS, W. J. & LU, N. 2003. Automated Humidity System for Measuring Total Suction Characteristics of Clay. *GEOTECHNICAL TESTING JOURNAL*, 26, 179-190.
- LITEON_DCC 2020. Optical Sensor Production Data Sheet *LTR-329ALS-01*.
- LIU, F., JIA, B., CHEN, B. & GENG, W. 2017. Moisture transfer in building envelope and influence on heat transfer. *Procedia Engineering*, 205, 3654-3661.
- LONG, H., RUDY, S., FOUBERT, A., DIERICK, M. & JACOBS, P. 2009. 3D quantification of mineral components and porosity distribution in Westphalian C sandstone by microfocus X-ray computed tomography. *Sedimentary Geology*, 220, 116–125.
- LU, N. & LIKOS, W. J. 2006. Suction Stress Characteristic Curve for Unsaturated Soil. *Journal of geotechnical and geoenvironmental engineering.*, 132, 131.
- LU, S., LANDIS, E. & KEANE, D. 2006. X-ray microtomographic studies of pore structure and permeability in Portland cement concrete. *Materials and Structures/Materiaux et Constructions*, 39, 611-620.
- MACPHEE, D. E. & LACHOWSKI, E. E. 1998. Cement Components and Their Phase Relations. *Lea's Chemistry of Cement and Concrete*. Elsevier.

- MARCHESE, B. 1979. A discussion of the paper “The contact zone between portland cement paste and glass ‘aggregate’ surfaces” by B.D. Barnes, S. Diamond and W.L. Dolch. *Cement and Concrete Research*, 9, 519-522.
- MARFISI, E., BURGOYNE, C., AMIN, M. & HALL, L. 2005. The use of MRI to observe the structure of concrete. *Magazine of concrete research*, 57, 101-109.
- MARTYS, N. S. & FERRARIS, C. F. 1997. Capillary transport in mortars and concrete. *Cement and Concrete Research*, 27, 747-760.
- MEHTA, P. K. 1986. Concrete. Structure, properties and materials.
- METER GROUP, I. June 2, 2017 *WP4C Dew Point Potential Meter*, 2365 NE Hopkins Court Pullman WA 99163, Meter Group, Inc.
- METRIS 2008. *CT-Pro User Manual*, Hertfordshire, HP23 4JX, UK, Metris, Reliable and Innovative Metrology Solutions.
- MICROMERITICS AutoPore IV Series Automated Mercury Porosimeter. www.micromeritics.com.
- MOORE, R. E. 1939. Water conduction from shallow water tables. *Hilgardia*, 12(6), 383-426.
- MORO, F. & BÖHNI, H. 2002. Ink-Bottle Effect in Mercury Intrusion Porosimetry of Cement-Based Materials. *Journal of Colloid and Interface Science*, 246, 135-149.
- NEVILLE, A. M. 1981. *Properties of concrete*, London ;, Pitman Pub.
- NEVILLE, A. M. & BROOKS, J. J. 1987. *Concrete technology*, Longman Scientific & Technical England.
- NORCROSS, D. 1877. Gas Adsorption Theory. *In: CORPORATION, M. I. (ed.)*. USA.
- NXP_SEMICONDUCTORS 2018. I²C Precision pressure sensor *MPL3115A2*.
- OKTAR, O. N., MORAL, H. & TAŞDEMİR, M. A. 1996. Sensitivity of concrete properties to the pore structure of hardened cement paste. *Cement and Concrete Research*, 26, 1619-1627.
- PAP ET AL., M., MAHLER, A. & NEHME, S. G. 2019. Estimation of permeability function for concrete *Proceedings of the XVII ECSMGE-2019*, Reykjavic, pp. 1-7. doi: 10.32075/17ECSMGE-2019-0844.
- PAP ET AL., M. M., ANDRAS & NEHME, SALEM 2018. Measurement of water retention curve for different concrete mixtures.
- PAP, M., MAHLER, A. & NEHME, S. G. 2015. A betonokban történő vízmozgás vizsgálata és modellezése. *VASBETONÉPÍTÉS XVII*, 3, 56-63.

- PARK, K. D. & FLEMING, I. R. 2006. Evaluation of a geosynthetic capillary barrier. *Geotextiles and Geomembranes*, 24, 64-71.
- PEDERSEN, R., SIMONE, A. & SLUYS, L. 2008. An analysis of dynamic fracture in concrete with a continuum visco-elastic visco-plastic damage model. *Engineering fracture mechanics*, 75, 3782-3805.
- PYCOM_GO_INVENT 2018. Sipy.
- RAHEEM, Z. 2019. *Standard Test Method for Compressive Strength of Cylindrical Concrete Samples 1*.
- RAYMENT, D. L. & MAJUMDAR, A. J. 1982. The composition of the C-S-H phases in portland cement pastes. *Cement and Concrete Research*, 12, 753-764.
- RIDLEY, A. Soil suction—what it is and how to successfully measure it. Proceedings of the Ninth Symposium on Field Measurements in Geomechanics, 2015. Australian Centre for Geomechanics, 27-46.
- ROSSI, P., VAN MIER, J., BOULAY, C. & LE MAOU, F. 1992. The dynamic behaviour of concrete: influence of free water. *Materials and Structures*, 25, 509-514.
- RUCKER-GRAMM, R. E. B. 2010. Effect of moisture content of concrete on water uptake. *Cement and Concrete Research*, 40, 102-108.
- SATYANAGA, A., RAHARDJO, H., LEONG, E. C. & WANG, J. Y. 2013. Water characteristic curve of soil with bimodal grain-size distribution. *Computers and Geotechnics*, 48, 51-61.
- SCHMITT, M., FERNANDES, C. P., DA CUNHA NETO, J. A. B., WOLF, F. G. & DOS SANTOS, V. S. S. 2013. Characterization of pore systems in seal rocks using Nitrogen Gas Adsorption combined with Mercury Injection Capillary Pressure techniques. *Marine and Petroleum Geology*, 39, 138-149.
- SHOYA, M. 1979. Drying shrinkage and moisture loss of superplasticizer admixed concrete of low water/cement ratio. *Transactions of the Japan Concrete Institute.*, 2, 103-110.
- SILICONLABS 2016. I²C Humidity and temperature sensor *Si7006-A20*.
- SING, K. S. 1985. Reporting physisorption data for gas/solid systems with special reference to the determination of surface area and porosity (Recommendations 1984). *Pure and applied chemistry*, 57, 603-619.
- SORET, M., BACHARACH, S. L. & BUVAT, I. 2007. Partial-volume effect in PET tumor imaging. *Journal of nuclear medicine : official publication, Society of Nuclear Medicine*, 48, 932-45.
- SOROKA, I. 1979a. *Portland cement paste and concrete*, London, Macmillan.

- SOROKA, I. 1979b. Structure of the hardened paste. In: SOROKA, I. (ed.) *Portland Cement Paste and Concrete*. London: Macmillan Education UK.
- SOUTSOS, M. & DOMONE, P. 2017. *Construction Materials : Their Nature and Behaviour*, Fifth Edition. 5th ed. ed. Milton: Chapman and Hall/CRC.
- ST_LIFE.AUGMENTED 2015. MEMS digital output motion sensor: Ultra-low-power high-performace 3-axis "pico" accelerometer *LIS2HH12*.
- STANDARD, A. 2017. C496/C496M-17 (2017) Standard test method for splitting tensile strength of cylindrical concrete samples. *ASTM International, West Conshohocken, PA*.
- SUN, X., WANG, H., CHENG, X. & SHENG, Y. 2020. Effect of pore liquid viscosity on the dynamic compressive properties of concrete. *Construction and Building Materials*, 231, 117143.
- THOSTENSON, J. 2013. *Operating Procedure for ROCO1 & RECO2* [Online]. SMif, Shared Materials Instrumentation Facility. Available: <https://smif.pratt.duke.edu/sites/smif.pratt.duke.edu/files/operating/RECO2%20Operating%20Procedure%20Rev3%20Website.pdf> [Accessed].
- UNIVERSITY OF CAPE TOWN, UNIVERSITY OF THE WITWATERSRAND JOHANNESBURG & COMSIRU 2017. *Durability Index Testing Procedure Manual*. 4.2.
- VAN GENUCHTEN, M. 1980. A Closed-form Equation for Predicting the Hydraulic Conductivity of Unsaturated Soils1. *Soil Science Society of America Journal*, 44.
- VANDERSTEEN, K., B, B., VAN DEN ABEELE, K. & CARMELIET, J. 2003. Quantitative characterization of fracture apertures using microfocus computed tomography. *Geological Society London Special Publications*, 215, 61-68.
- VANDEWALLE, L., NEMEGEER, D., BALAZS, L., BARR, B., BARROS, J., BARTOS, P., BANTHIA, N., CRISWELL, M., DENARIE, E. & DI PRISCO, M. 2003. RILEM TC 162-TDF: Test and design methods for steel fibre reinforced concrete'-sigma-epsilon-design method-Final Recommendation. *Materials and Structures*, 36, 560-567.
- VINKLER, M. & VÍTEK, J. L. 2017. Drying shrinkage of concrete elements. *Structural Concrete*, 18, 92-103.
- VOLUME GRAPHICS GMBH, V. 2018. *VGSTUDIO MAX, High-End Industrial CT Software*
- VYDRA, V., KAPIČKOVÁ, O., DEMO, P. & SEMERÁK, P. 2007. Influence of temperature on induction period and on ultimate porosity of hardening cement paste. *Construction and Building Materials*, 21, 1262-1266.
- WANG, H., JIN, W. & LI, Q. 2009. Saturation Effect on Dynamic Tensile and Compressive Strength of Concrete. *Advances in Structural Engineering*, 12, 279-286.

- WANG, H. & LI, Q. 2007. Experiments of the compressive properties of dry and saturated concrete under different loading rates. *J. Hydroelectr. Eng*, 26, 84-89.
- WASHBURN, E. W. 1921. Note on a Method of Determining the Distribution of Pore Sizes in a Porous Material. *Proceedings of the National Academy of Sciences*, 7, 115.
- WILD, S. 2001. A discussion of the paper “Mercury porosimetry—an inappropriate method for the measurement of pore size distributions in cement-based materials” by S. Diamond. *Cement and Concrete Research - CEM CONCR RES*, 31, 1653-1654.
- WINSLOW, D. & LIU, D. 1990. The pore structure of paste in concrete. *Cement and Concrete Research*, 20, 227-235.
- WYRZYKOWSKI, M., KIESEWETTER, R., KAUFMANN, J., BAUMANN, R. & LURA, P. 2014. Pore structure of mortars with cellulose ether additions – Mercury intrusion porosimetry study. *Cement and Concrete Composites*, 53, 25-34.
- XI, Y., BAŽANT, Z. P. & JENNINGS, H. M. 1994. Moisture diffusion in cementitious materials Adsorption isotherms. *Advanced Cement Based Materials*, 1, 248-257.
- YU, B., BRADLEY, R. S., SOUTIS, C. & WITHERS, P. J. 2016. A comparison of different approaches for imaging cracks in composites by X-ray microtomography. *Philosophical Transactions: Mathematical, Physical and Engineering Sciences*, 374, 1-15.
- ZENG, Q. & XU, S. 2015. Discussion of “Numerical simulation of moisture transport in concrete based on a pore size distribution model”. *Cement and Concrete Research*, 73, 63-66.
- ZHANG, S., CAO, K., WANG, C., WANG, X., DENG, G. & WEI, P. 2018. Influence of the porosity and pore size on the compressive and splitting strengths of cellular concrete with millimeter-size pores. *Construction and Building Materials*, 235, 117508.
- ZHANG, Y. & ZHANG, M. 2014. Transport properties in unsaturated cement-based materials - A review. *Construction and Building Materials*, 72, 367-379.
- ZHENG, D., LI, Q. & WANG, L. 2005. A microscopic approach to rate effect on compressive strength of concrete. *Engineering fracture mechanics*, 72, 2316-2327.

APPENDIX A

CEMENT PASTE STUDY

SUCTION RESULTS

Sample Name	Sample Age (hours)	Sample Mass (g)	Temperature (°C)	Water Potential (MPa)	Mass solids, Ms (g)	Mass Water, Mw (g)	Volumetric Water Content (%)
0.3 - 1	0.0	21.9265	/	/	16.8665	5.0600	30.00%
0.3 - 1	1.0	21.9055	24.60	-0.39	16.8665	5.0390	29.88%
0.3 - 1	4.0	21.8895	24.70	-0.50	16.8665	5.0230	29.78%
0.3 - 1	7.5	21.8793	25.00	-1.01	16.8665	5.0128	29.72%
0.3 - 1	48.2	21.8764	24.20	-8.89	16.8665	5.0099	29.70%
0.3 - 1	51.2	21.8736	24.10	-10.17	16.8665	5.0071	29.69%
0.3 - 1	54.0	21.8711	24.10	-11.10	16.8665	5.0046	29.67%
0.3 - 1	73.3	21.8688	24.10	-13.07	16.8665	5.0023	29.66%
0.3 - 1	94.3	21.8670	24.10	-16.00	16.8665	5.0005	29.65%
0.3 - 1	99.5	21.8650	24.10	-16.06	16.8665	4.9985	29.64%
0.3 - 1	121.3	21.8637	24.00	-16.98	16.8665	4.9972	29.63%
0.3 - 1	169.8	21.8611	24.10	-22.92	16.8665	4.9946	29.61%
0.3 - 1	216.9	21.8582	24.10	-25.93	16.8665	4.9917	29.60%
0.3 - 1	265.5	21.8565	23.90	-25.03	16.8665	4.9900	29.58%
0.3 - 1	337.5	21.8549	23.90	-27.93	16.8665	4.9884	29.58%
0.3 - 1	436.2	21.8527	23.70	-37.54	16.8665	4.9862	29.56%
0.3 - 1	602.2	21.8507	23.70	-36.75	16.8665	4.9842	29.55%
0.3 - 1	934.2	21.8423	23.60	-48.17	16.8665	4.9758	29.50%
0.3 - 1	1511.8	21.8398	23.20	-47.47	16.8665	4.9733	29.49%
0.3 - 1	2088.0	21.8393	24.30	-56.71	16.8665	4.9728	29.48%
0.3 - 2	0.0	22.4921	/	/	17.3016	5.1905	30.00%
0.3 - 2	11.5	22.4863	25.00	-1.41	17.3016	5.1847	29.97%
0.3 - 2	14.5	22.4849	25.10	-1.83	17.3016	5.1833	29.96%
0.3 - 2	17.5	22.4807	24.70	-3.04	17.3016	5.1791	29.93%
0.3 - 2	20.5	22.4740	24.60	-4.06	17.3016	5.1724	29.90%
0.3 - 2	43.0	22.4714	24.30	-7.40	17.3016	5.1698	29.88%
0.3 - 2	59.3	22.4692	24.40	-9.90	17.3016	5.1676	29.87%
0.3 - 2	63.7	22.4673	24.40	-10.37	17.3016	5.1657	29.86%
0.3 - 2	66.6	22.4656	24.40	-11.01	17.3016	5.1640	29.85%
0.3 - 2	85.1	22.4638	24.20	-11.79	17.3016	5.1622	29.84%
0.3 - 2	89.7	22.4629	24.40	-12.47	17.3016	5.1613	29.83%
0.3 - 2	111.4	22.4617	24.40	-13.03	17.3016	5.1601	29.82%
0.3 - 2	161.2	22.4590	24.10	-17.05	17.3016	5.1574	29.81%
0.3 - 2	208.2	22.4570	24.10	-19.65	17.3016	5.1554	29.80%
0.3 - 2	257.7	22.4556	23.90	-20.72	17.3016	5.1540	29.79%
0.3 - 2	328.0	22.4545	23.80	-21.27	17.3016	5.1529	29.78%
0.3 - 2	422.7	22.4515	23.90	-28.22	17.3016	5.1499	29.77%
0.3 - 2	587.7	22.4497	23.90	-26.07	17.3016	5.1481	29.75%
0.3 - 2	879.2	22.4473	24.00	-31.41	17.3016	5.1457	29.74%
0.3 - 2	1504.5	22.4441	24.20	-40.20	17.3016	5.1425	29.72%
0.3 - 2	2080.2	22.4433	24.40	-42.78	17.3016	5.1417	29.72%
0.3 - 3	0.0	21.8545	/	/	16.8112	5.0433	30.00%
0.3 - 3	1.2	21.8235	24.20	-0.03	16.8112	5.0123	29.82%
0.3 - 3	4.4	21.7935	24.70	-0.65	16.8112	4.9823	29.64%
0.3 - 3	7.8	21.7827	25.00	-1.19	16.8112	4.9715	29.57%
0.3 - 3	77.3	21.7795	24.50	-12.23	16.8112	4.9683	29.55%
0.3 - 3	98.5	21.7777	24.10	-14.76	16.8112	4.9665	29.54%
0.3 - 3	120.2	21.7764	24.00	-16.61	16.8112	4.9652	29.54%
0.3 - 3	168.3	21.7739	23.90	-22.82	16.8112	4.9627	29.52%
0.3 - 3	215.3	21.7721	23.70	-25.70	16.8112	4.9609	29.51%
0.3 - 3	264.2	21.7706	24.00	-24.74	16.8112	4.9594	29.50%
0.3 - 3	335.8	21.7689	23.50	-27.30	16.8112	4.9577	29.49%
0.3 - 3	431.6	21.7654	23.80	-39.40	16.8112	4.9542	29.47%
0.3 - 3	507.6	21.7643	23.90	-32.54	16.8112	4.9531	29.46%
0.3 - 3	887.8	21.7619	24.20	-45.39	16.8112	4.9507	29.45%
0.3 - 3	1537.8	21.7585	24.10	-47.38	16.8112	4.9473	29.43%
0.3 - 3	2088.8	21.7574	23.90	-57.47	16.8112	4.9462	29.42%
0.3 - 4	0.0	22.1476	/	/	17.0366	5.1110	30.00%
0.3 - 4	0.5	22.1402	24.20	-0.23	17.0366	5.1036	29.96%
0.3 - 4	1.2	22.1155	24.20	-0.16	17.0366	5.0789	29.81%
0.3 - 4	2.7	22.1004	24.50	-0.40	17.0366	5.0638	29.72%
0.3 - 4	4.6	22.0769	24.40	-0.48	17.0366	5.0403	29.59%
0.3 - 4	6.4	22.0699	24.40	-0.53	17.0366	5.0333	29.54%
0.3 - 4	7.7	22.0643	24.40	-0.68	17.0366	5.0277	29.51%
0.3 - 4	29.6	22.0593	24.10	-2.32	17.0366	5.0227	29.48%
0.3 - 4	32.3	22.0531	24.10	-3.23	17.0366	5.0165	29.45%
0.3 - 4	48.6	22.0493	24.10	-5.14	17.0366	5.0127	29.42%

0.3 - 4	73.4	22.0467	24.00	-8.55	17.0366	5.0101	29.41%
0.3 - 4	78.3	22.0433	24.10	-10.07	17.0366	5.0067	29.39%
0.3 - 4	98.4	22.0389	24.00	-13.08	17.0366	5.0023	29.36%
0.3 - 4	166.8	22.0349	24.10	-18.86	17.0366	4.9983	29.34%
0.3 - 4	215.3	22.0315	23.80	-19.66	17.0366	4.9949	29.32%
0.3 - 4	263.8	22.0281	23.90	-22.48	17.0366	4.9915	29.30%
0.3 - 4	365.7	22.0199	24.20	-29.00	17.0366	4.9833	29.25%
0.3 - 4	431.7	22.0174	24.00	-29.15	17.0366	4.9808	29.24%
0.3 - 4	551.9	22.0121	24.20	-39.85	17.0366	4.9755	29.20%
0.3 - 4	719.7	22.0093	24.20	-35.46	17.0366	4.9727	29.19%
0.3 - 4	912.1	22.0079	24.40	-42.66	17.0366	4.9713	29.18%
0.3 - 4	1103.3	22.0061	24.20	-49.63	17.0366	4.9695	29.17%
0.3 - 4	1416.3	22.0045	24.20	-50.77	17.0366	4.9679	29.16%
0.3 - 4	1732.2	22.0034	24.30	-58.12	17.0366	4.9668	29.15%
0.3 - 4	2065.5	21.9994	24.50	-65.99	17.0366	4.9628	29.13%
0.3 - 4	2233.7	21.9976	24.50	-65.79	17.0366	4.9610	29.12%
0.3 - 5	0.0	20.0014	/	/	15.3857	4.6157	30.00%
0.3 - 5	14.1	19.9917	24.70	-1.15	15.3857	4.6060	29.94%
0.3 - 5	15.1	19.9857	24.40	-0.98	15.3857	4.6000	29.90%
0.3 - 5	16.7	19.9797	24.50	-1.63	15.3857	4.5940	29.86%
0.3 - 5	18.3	19.9761	24.40	-1.89	15.3857	4.5904	29.84%
0.3 - 5	19.8	19.9723	24.30	-2.12	15.3857	4.5866	29.81%
0.3 - 5	22.9	19.9693	24.40	-2.46	15.3857	4.5836	29.79%
0.3 - 5	25.7	19.9659	24.00	-2.93	15.3857	4.5802	29.77%
0.3 - 5	38.7	19.9620	24.00	-4.70	15.3857	4.5763	29.74%
0.3 - 5	43.3	19.9578	24.00	-5.42	15.3857	4.5721	29.72%
0.3 - 5	45.2	19.9545	24.00	-5.83	15.3857	4.5688	29.70%
0.3 - 5	62.7	19.9514	23.80	-8.07	15.3857	4.5657	29.68%
0.3 - 5	68.2	19.9489	24.10	-9.21	15.3857	4.5632	29.66%
0.3 - 5	92.5	19.9445	23.90	-12.18	15.3857	4.5588	29.63%
0.3 - 5	161.9	19.9411	23.90	-19.04	15.3857	4.5554	29.61%
0.3 - 5	212.7	19.9397	23.70	-19.00	15.3857	4.5540	29.60%
0.3 - 5	260.7	19.9383	23.90	-20.95	15.3857	4.5526	29.59%
0.3 - 5	355.3	19.9356	24.20	-25.44	15.3857	4.5499	29.57%
0.3 - 5	429.3	19.9337	24.10	-26.32	15.3857	4.5480	29.56%
0.3 - 5	549.0	19.9315	24.00	-33.77	15.3857	4.5458	29.55%
0.3 - 5	715.8	19.9306	24.10	-31.37	15.3857	4.5449	29.54%
0.3 - 5	909.4	19.9282	24.00	-40.27	15.3857	4.5425	29.52%
0.3 - 5	1099.9	19.9273	24.10	-42.21	15.3857	4.5416	29.52%
0.3 - 5	1410.5	19.9260	24.00	-48.60	15.3857	4.5403	29.51%
0.3 - 5	1721.2	19.9244	24.50	-57.19	15.3857	4.5387	29.50%
0.3 - 5	2058.5	19.9228	24.50	-62.18	15.3857	4.5371	29.49%
0.3 - 5	2226.5	19.9227	24.50	-62.09	15.3857	4.5370	29.49%

Sample Name	Sample Age (hours)	Sample Mass (g)	Temperature (°C)	Water Potential (MPa)	Mass solids, Ms (g)	Mass Water, Mw (g)	Volumetric Water Content (%)
0.35 - 1	0.0	20.7545	/	/	15.3737	5.3808	35.00%
0.35 - 1	1.5	20.6885	24.70	-0.19	15.3737	5.3148	34.57%
0.35 - 1	4.5	20.6536	24.70	-0.62	15.3737	5.2799	34.34%
0.35 - 1	8.0	20.6402	25.00	-1.01	15.3737	5.2665	34.26%
0.35 - 1	48.3	20.6375	24.20	-5.39	15.3737	5.2638	34.24%
0.35 - 1	51.5	20.6349	24.20	-5.98	15.3737	5.2612	34.22%
0.35 - 1	54.1	20.6322	24.50	-6.43	15.3737	5.2585	34.20%
0.35 - 1	73.6	20.6299	24.20	-7.82	15.3737	5.2562	34.19%
0.35 - 1	96.2	20.6275	24.20	-9.17	15.3737	5.2538	34.17%
0.35 - 1	100.8	20.6256	24.10	-10.05	15.3737	5.2519	34.16%
0.35 - 1	122.8	20.6235	24.20	-10.82	15.3737	5.2498	34.15%
0.35 - 1	171.5	20.6188	24.20	-15.24	15.3737	5.2451	34.12%
0.35 - 1	218.5	20.6153	21.10	-17.51	15.3737	5.2416	34.09%
0.35 - 1	267.3	20.6119	23.90	-18.07	15.3737	5.2382	34.07%
0.35 - 1	338.8	20.6102	23.80	-20.24	15.3737	5.2365	34.06%
0.35 - 1	438.7	20.6029	23.80	-32.67	15.3737	5.2292	34.01%
0.35 - 1	603.7	20.6007	23.60	-27.15	15.3737	5.2270	34.00%
0.35 - 1	935.9	20.5979	24.00	-40.20	15.3737	5.2242	33.98%
0.35 - 1	1513.8	20.5942	24.20	-42.06	15.3737	5.2205	33.96%
0.35 - 1	2089.0	20.5932	24.10	-46.85	15.3737	5.2195	33.95%
0.35 - 2	0.0	20.7675	/	/	15.3833	5.3842	35.00%
0.35 - 2	12.2	20.7425	25.20	-1.21	15.3833	5.3592	34.84%
0.35 - 2	15.1	20.7364	25.00	-1.41	15.3833	5.3531	34.80%

0.35 - 5	63.8	20.0171	24.10	-6.20	14.8530	5.1641	34.77%
0.35 - 5	68.4	20.0134	24.10	-6.93	14.8530	5.1604	34.74%
0.35 - 5	92.9	20.0087	23.90	-8.92	14.8530	5.1557	34.71%
0.35 - 5	162.4	20.0051	23.70	-13.75	14.8530	5.1521	34.69%
0.35 - 5	211.4	20.0036	23.80	-15.57	14.8530	5.1506	34.68%
0.35 - 5	258.9	20.0014	23.80	-16.96	14.8530	5.1484	34.66%
0.35 - 5	354.1	19.9980	24.30	-20.98	14.8530	5.1450	34.64%
0.35 - 5	427.7	19.9951	24.20	-22.36	14.8530	5.1421	34.62%
0.35 - 5	547.5	19.9934	24.00	-26.49	14.8530	5.1404	34.61%
0.35 - 5	714.4	19.9913	24.10	-27.37	14.8530	5.1383	34.59%
0.35 - 5	908.5	19.9874	24.10	-35.65	14.8530	5.1344	34.57%
0.35 - 5	1098.7	19.9843	24.10	-36.77	14.8530	5.1313	34.55%
0.35 - 5	1408.7	19.9827	24.00	-40.71	14.8530	5.1297	34.54%
0.35 - 5	1719.3	19.9810	24.40	-49.65	14.8530	5.1280	34.52%
0.35 - 5	2056.5	19.9796	24.50	-55.74	14.8530	5.1266	34.52%
0.35 - 5	2224.6	19.9783	24.60	-55.74	14.8530	5.1253	34.51%

Sample Name	Sample Age (hours)	Sample Mass (g)	Temperature (°C)	Water Potential (MPa)	Mass solids, Ms (g)	Mass Water, Mw (g)	Volumetric Water Content (%)
0.4 - 1	0.0	21.5215	/	/	15.3725	6.1490	40.00%
0.4 - 1	2.2	21.4435	24.80	-0.35	15.3725	6.0710	39.49%
0.4 - 1	4.3	21.4145	24.80	-0.74	15.3725	6.0420	39.30%
0.4 - 1	8.5	21.3994	25.10	-0.98	15.3725	6.0269	39.21%
0.4 - 1	48.6	21.3950	24.30	-3.62	15.3725	6.0225	39.18%
0.4 - 1	51.7	21.3919	24.30	-4.03	15.3725	6.0194	39.16%
0.4 - 1	54.2	21.3887	24.30	-4.47	15.3725	6.0162	39.14%
0.4 - 1	73.7	21.3870	24.50	-5.72	15.3725	6.0145	39.13%
0.4 - 1	96.2	21.3849	24.40	-6.56	15.3725	6.0124	39.11%
0.4 - 1	101.0	21.3831	24.50	-7.36	15.3725	6.0106	39.10%
0.4 - 1	123.9	21.3818	24.40	-7.81	15.3725	6.0093	39.09%
0.4 - 1	173.0	21.3774	24.20	-10.36	15.3725	6.0049	39.06%
0.4 - 1	220.0	21.3732	24.20	-11.72	15.3725	6.0007	39.04%
0.4 - 1	269.0	21.3701	23.90	-11.94	15.3725	5.9976	39.02%
0.4 - 1	340.2	21.3684	23.80	-13.71	15.3725	5.9959	39.00%
0.4 - 1	440.2	21.3649	24.00	-19.31	15.3725	5.9924	38.98%
0.4 - 1	604.3	21.3635	23.70	-17.38	15.3725	5.9910	38.97%
0.4 - 1	937.0	21.3604	24.20	-26.88	15.3725	5.9879	38.95%
0.4 - 1	1514.8	21.3587	24.20	-30.33	15.3725	5.9862	38.94%
0.4 - 1	2089.4	21.3578	24.20	-43.43	15.3725	5.9853	38.94%
0.4 - 2	0.0	21.6875	/	/	15.4911	6.1964	40.00%
0.4 - 2	13.0	21.6747	25.20	-1.02	15.4911	6.1836	39.92%
0.4 - 2	16.0	21.6714	24.90	-1.13	15.4911	6.1803	39.90%
0.4 - 2	18.5	21.6646	24.70	-1.43	15.4911	6.1735	39.85%
0.4 - 2	21.5	21.6592	24.70	-1.66	15.4911	6.1681	39.82%
0.4 - 2	43.8	21.6563	24.30	-3.12	15.4911	6.1652	39.80%
0.4 - 2	60.2	21.6543	24.40	-4.28	15.4911	6.1632	39.79%
0.4 - 2	64.5	21.6516	24.40	-4.96	15.4911	6.1605	39.77%
0.4 - 2	67.3	21.6501	24.40	-4.94	15.4911	6.1590	39.76%
0.4 - 2	85.5	21.6488	24.50	-5.25	15.4911	6.1577	39.75%
0.4 - 2	90.3	21.6475	24.60	-5.64	15.4911	6.1564	39.74%
0.4 - 2	112.0	21.6456	24.40	-6.32	15.4911	6.1545	39.73%
0.4 - 2	162.2	21.6430	24.30	-7.87	15.4911	6.1519	39.71%
0.4 - 2	209.2	21.6409	24.20	-8.75	15.4911	6.1498	39.70%
0.4 - 2	258.7	21.6390	24.10	-10.04	15.4911	6.1479	39.69%
0.4 - 2	329.0	21.6366	24.00	-11.52	15.4911	6.1455	39.67%
0.4 - 2	423.7	21.6338	24.00	-13.35	15.4911	6.1427	39.65%
0.4 - 2	588.8	21.6318	23.90	-14.39	15.4911	6.1407	39.64%
0.4 - 2	880.7	21.6297	23.70	-21.35	15.4911	6.1386	39.63%
0.4 - 2	1523.5	21.6257	24.40	-25.39	15.4911	6.1346	39.60%
0.4 - 2	2081.4	21.6241	24.30	-33.03	15.4911	6.1330	39.59%
0.4 - 3	0.0	20.2675	/	/	14.4768	5.7907	40.00%
0.4 - 3	2.6	20.1695	24.70	-0.29	14.4768	5.6927	39.32%
0.4 - 3	5.7	20.1474	24.70	-0.57	14.4768	5.6706	39.17%
0.4 - 3	10.0	20.1373	25.10	-1.25	14.4768	5.6605	39.10%
0.4 - 3	78.0	20.1352	24.10	-5.74	14.4768	5.6584	39.09%
0.4 - 3	99.4	20.1328	24.10	-6.95	14.4768	5.6560	39.07%
0.4 - 3	121.0	20.1303	24.10	-7.88	14.4768	5.6535	39.05%
0.4 - 3	169.3	20.1268	24.00	-10.51	14.4768	5.6500	39.03%

0.45 - 4	436.5	20.8219	24.20	-11.37	14.6016	6.2203	42.60%
0.45 - 4	556.3	20.8180	24.20	-14.86	14.6016	6.2164	42.57%
0.45 - 4	723.4	20.8161	24.20	-17.71	14.6016	6.2145	42.56%
0.45 - 4	916.7	20.8127	24.20	-23.83	14.6016	6.2111	42.54%
0.45 - 4	1107.8	20.8092	24.20	-28.21	14.6016	6.2076	42.51%
0.45 - 4	1418.2	20.8050	24.30	-36.62	14.6016	6.2034	42.48%
0.45 - 4	1734.3	20.8008	24.50	-40.84	14.6016	6.1992	42.46%
0.45 - 4	2066.2	20.7991	24.30	-45.47	14.6016	6.1975	42.44%
0.45 - 4	2234.4	20.7981	24.50	-47.28	14.6016	6.1965	42.44%
0.45 - 5	0.0	19.9706	/	/	13.7728	6.1978	45.00%
0.45 - 5	14.1	19.9667	24.50	-0.59	13.7728	6.1939	44.97%
0.45 - 5	15.5	19.9626	24.60	-0.72	13.7728	6.1898	44.94%
0.45 - 5	17.2	19.9594	24.50	-0.59	13.7728	6.1866	44.92%
0.45 - 5	18.5	19.9563	24.40	-0.75	13.7728	6.1835	44.90%
0.45 - 5	19.9	19.9538	24.50	-0.75	13.7728	6.1810	44.88%
0.45 - 5	22.7	19.9490	24.30	-1.13	13.7728	6.1762	44.84%
0.45 - 5	25.9	19.9464	24.40	-1.11	13.7728	6.1736	44.82%
0.45 - 5	38.9	19.9442	24.20	-1.36	13.7728	6.1714	44.81%
0.45 - 5	43.8	19.9424	24.20	-1.35	13.7728	6.1696	44.80%
0.45 - 5	45.5	19.9386	24.10	-1.66	13.7728	6.1658	44.77%
0.45 - 5	63.8	19.9359	24.20	-1.84	13.7728	6.1631	44.75%
0.45 - 5	68.7	19.9316	24.10	-2.40	13.7728	6.1588	44.72%
0.45 - 5	93.2	19.9270	24.00	-3.32	13.7728	6.1542	44.68%
0.45 - 5	163.4	19.9225	24.00	-4.91	13.7728	6.1497	44.65%
0.45 - 5	211.3	19.9198	23.90	-5.84	13.7728	6.1470	44.63%
0.45 - 5	259.2	19.9183	24.10	-6.67	13.7728	6.1455	44.62%
0.45 - 5	354.8	19.9139	24.20	-7.50	13.7728	6.1411	44.59%
0.45 - 5	428.8	19.9111	24.10	-8.35	13.7728	6.1383	44.57%
0.45 - 5	547.9	19.9072	24.10	-9.95	13.7728	6.1344	44.54%
0.45 - 5	715.2	19.9055	24.20	-11.00	13.7728	6.1327	44.53%
0.45 - 5	909.2	19.9022	24.10	-16.26	13.7728	6.1294	44.50%
0.45 - 5	1099.5	19.8997	24.10	-17.62	13.7728	6.1269	44.49%
0.45 - 5	1410.4	19.8963	24.30	-22.22	13.7728	6.1235	44.46%
0.45 - 5	1719.8	19.8917	24.60	-27.28	13.7728	6.1189	44.43%
0.45 - 5	2055.7	19.8888	24.80	-32.29	13.7728	6.1160	44.41%
0.45 - 5	2224.0	19.8862	24.80	-35.42	13.7728	6.1134	44.39%

APPENDIX B

PARTICLE SIZE DISTRIBUTION

INFORMATION



MASTERSIZER



Result Analysis Report

Sample Name:
Test 1 Cement Paste -Laser +Ultra
Sample Source & type:
Lab
Sample bulk lot ref:

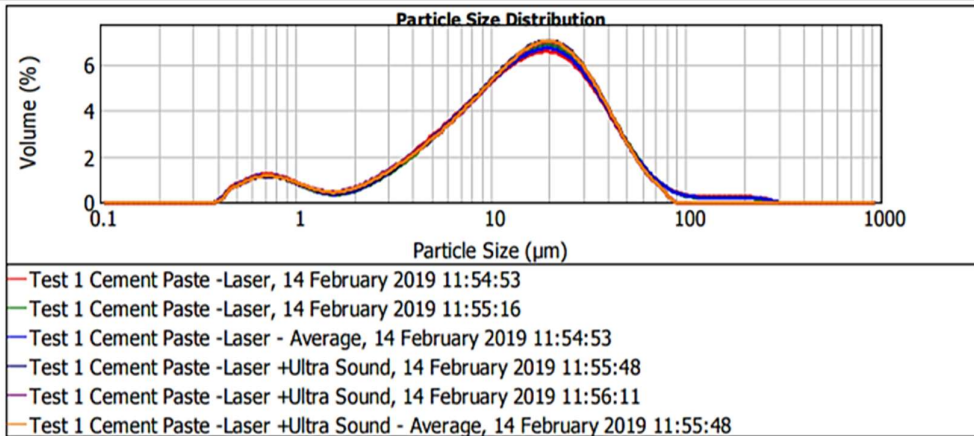
SOP Name:
Measured by:
User
Result Source:
Averaged

Measured:
14 February 2019 11:55:48
Analysed:
14 February 2019 11:55:49

Particle Name: Default	Accessory Name: Hydro 2000MU (A)	Analysis model: General purpose	Sensitivity: Normal
Particle RI: 1.520	Absorption: 0.1	Size range: 0.100 to 1000.000 um	Obscuration: 10.67 %
Dispersant Name: Water	Dispersant RI: 1.330	Weighted Residual: 0.682 %	Result Emulation: Off

Concentration: 0.0101 %Vol	Span : 2.421	Uniformity: 0.75	Result units: Volume
Specific Surface Area: 1.08 m ² /g	Surface Weighted Mean D[3,2]: 5.545 um	Vol. Weighted Mean D[4,3]: 18.375 um	

d(0.1): 2.971 um d(0.5): 14.804 um d(0.9): 38.820 um



Size (µm)	Volume In %	Size (µm)	Volume In %	Size (µm)	Volume In %	Size (µm)	Volume In %	Size (µm)	Volume In %	Size (µm)	Volume In %
0.100	0.00	0.538	0.60	2.900	0.89	15.614	4.44	84.081	0.00	452.768	0.00
0.110	0.00	0.595	0.70	3.202	1.05	17.240	4.53	92.835	0.00	499.903	0.00
0.122	0.00	0.656	0.74	3.535	1.22	19.005	4.56	102.499	0.00	551.945	0.00
0.135	0.00	0.725	0.74	3.903	1.40	21.016	4.51	113.170	0.00	609.406	0.00
0.149	0.00	0.800	0.70	4.309	1.58	23.204	4.38	124.952	0.00	672.848	0.00
0.164	0.00	0.884	0.63	4.758	1.78	25.620	4.17	137.960	0.00	742.894	0.00
0.181	0.00	0.976	0.54	5.253	1.98	28.287	3.88	152.322	0.00	820.233	0.00
0.200	0.00	1.077	0.45	5.800	2.19	31.232	3.53	168.179	0.00	905.623	0.00
0.221	0.00	1.189	0.36	6.404	2.42	34.483	3.12	185.688	0.00	999.903	0.00
0.244	0.00	1.313	0.30	7.070	2.65	38.073	2.68	205.019	0.00	1103.998	0.00
0.269	0.00	1.450	0.27	7.806	2.90	42.037	2.24	226.362	0.00	1218.929	0.00
0.297	0.00	1.601	0.28	8.619	3.15	46.413	1.80	249.927	0.00	1345.826	0.00
0.328	0.00	1.767	0.32	9.516	3.40	51.245	1.39	275.946	0.00	1485.933	0.00
0.362	0.00	1.951	0.40	10.507	3.65	56.580	1.02	304.673	0.00	1640.625	0.00
0.400	0.08	2.154	0.49	11.601	3.89	62.470	0.71	336.391	0.00	1811.422	0.00
0.442	0.35	2.379	0.61	12.809	4.10	68.973	0.51	371.411	0.00	2000.000	0.00
0.488	0.48	2.626	0.75	14.142	4.29	76.154	0.21	410.077	0.00		
0.538		2.900		15.614		84.081		452.768	0.00		



MASTERSIZER 2000

Result Analysis Report

Sample Name:
Centrifuge Sand +Ultra Sound -

Sample Source & type:
Lab

Sample bulk lot ref:

SOP Name:

Measured by:
User

Result Source:
Averaged

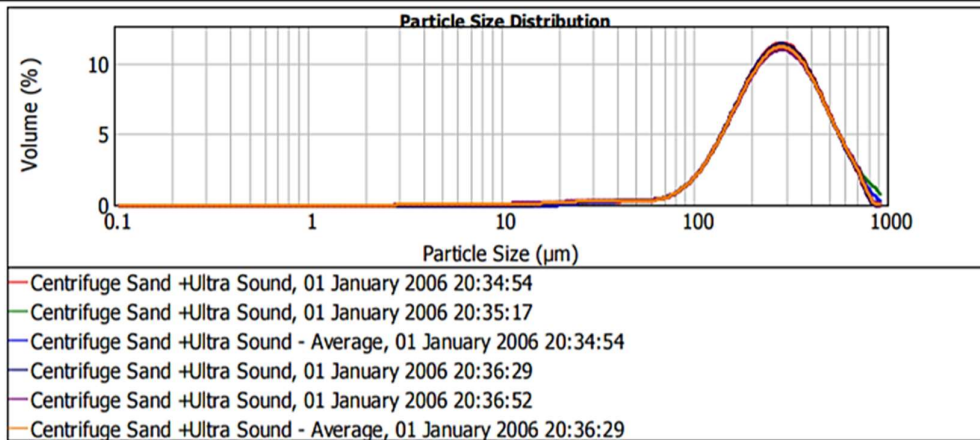
Measured:
01 January 2006 20:36:29

Analysed:
01 January 2006 20:36:30

Particle Name: Default	Accessory Name: Hydro 2000MU (A)	Analysis model: General purpose	Sensitivity: Normal
Particle RI: 1.520	Absorption: 0.1	Size range: 0.100 to 1000.000 um	Obscuration: 15.86 %
Dispersant Name: Water	Dispersant RI: 1.330	Weighted Residual: 0.615 %	Result Emulation: Off

Concentration: 0.4390 %Vol	Span : 1.438	Uniformity: 0.446	Result units: Volume
Specific Surface Area: 0.0333 m ² /g	Surface Weighted Mean D[3,2]: 179.932 um	Vol. Weighted Mean D[4,3]: 298.413 um	

d(0.1): 127.850 um d(0.5): 270.744 um d(0.9): 517.099 um



Size (µm)	Volume In %	Size (µm)	Volume In %	Size (µm)	Volume In %	Size (µm)	Volume In %	Size (µm)	Volume In %	Size (µm)	Volume In %
0.100	0.00	0.538	0.00	2.900	0.01	15.614	0.07	84.081	0.77	452.768	4.63
0.110	0.00	0.595	0.00	3.202	0.03	17.240	0.09	92.835	1.12	499.903	3.80
0.122	0.00	0.656	0.00	3.535	0.02	19.035	0.11	102.499	1.57	551.945	2.99
0.135	0.00	0.725	0.00	3.903	0.03	21.016	0.13	113.170	2.13	609.406	2.26
0.149	0.00	0.800	0.00	4.309	0.03	23.204	0.15	124.952	2.79	672.848	1.60
0.164	0.00	0.884	0.00	4.758	0.03	25.620	0.16	137.960	3.52	742.894	0.66
0.181	0.00	0.976	0.00	5.253	0.03	28.287	0.18	152.322	4.30	820.233	0.07
0.200	0.00	1.077	0.00	5.800	0.03	31.232	0.19	168.179	5.07	905.623	0.00
0.221	0.00	1.189	0.00	6.404	0.03	34.483	0.19	185.688	5.80	999.903	0.00
0.244	0.00	1.313	0.00	7.070	0.03	38.073	0.19	205.019	6.42	1103.998	0.00
0.269	0.00	1.450	0.00	7.806	0.03	42.037	0.19	226.362	6.90	1218.929	0.00
0.297	0.00	1.601	0.00	8.619	0.03	46.413	0.17	249.927	7.18	1345.826	0.00
0.328	0.00	1.767	0.00	9.516	0.03	51.245	0.18	275.946	7.24	1485.933	0.00
0.362	0.00	1.951	0.00	10.507	0.04	56.580	0.19	304.673	7.08	1640.625	0.00
0.400	0.00	2.154	0.00	11.601	0.04	62.470	0.25	336.391	6.14	1811.422	0.00
0.442	0.00	2.379	0.00	12.809	0.04	68.973	0.35	371.411	5.43	2000.000	0.00
0.488	0.00	2.626	0.00	14.142	0.05	76.154		410.077			
0.538	0.00	2.900	0.00	15.614		84.081		452.768			



MASTERSIZER



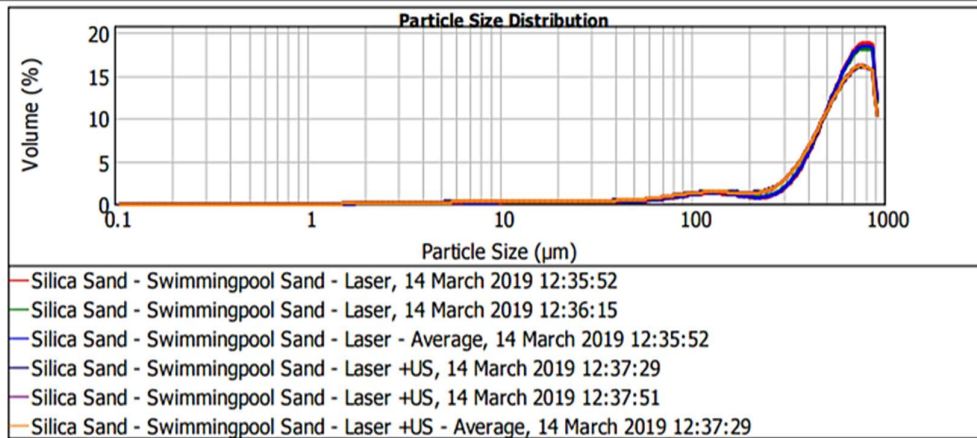
Result Analysis Report

Sample Name: Silica Sand - Swimmingpool Sand -	SOP Name:	Measured: 14 March 2019 12:37:29
Sample Source & type: Lab	Measured by: User	Analysed: 14 March 2019 12:37:30
Sample bulk lot ref:	Result Source: Averaged	

Particle Name: Default	Accessory Name: Hydro 2000MU (A)	Analysis model: General purpose	Sensitivity: Normal
Particle RI: 1.520	Absorption: 0.1	Size range: 0.100 to 1000.000 um	Obscuration: 21.31 %
Dispersant Name: Water	Dispersant RI: 1.330	Weighted Residual: 1.816 %	Result Emulation: Off

Concentration: 0.4555 %Vol	Span : 1.292	Uniformity: 0.364	Result units: Volume
Specific Surface Area: 0.0523 m ² /g	Surface Weighted Mean D[3,2]: 114.788 um	Vol. Weighted Mean D[4,3]: 533.359 um	

d(0.1): 113.827 um d(0.5): 570.204 um d(0.9): 850.544 um



Size (µm)	Volume In %	Size (µm)	Volume In %	Size (µm)	Volume In %	Size (µm)	Volume In %	Size (µm)	Volume In %	Size (µm)	Volume In %
0.100	0.00	0.538	0.00	2.900	0.09	15.614	0.19	84.081	0.69	452.768	6.26
0.110	0.00	0.595	0.00	3.202	0.10	17.240	0.20	92.835	0.77	499.903	7.52
0.122	0.00	0.656	0.00	3.535	0.11	19.035	0.21	102.499	0.83	551.945	8.67
0.135	0.00	0.725	0.00	3.903	0.11	21.016	0.22	113.170	0.87	609.406	9.62
0.149	0.00	0.800	0.00	4.309	0.11	23.204	0.22	124.952	0.89	672.848	10.28
0.164	0.00	0.884	0.00	4.758	0.12	25.620	0.22	137.960	0.87	742.894	10.42
0.181	0.00	0.976	0.00	5.253	0.12	28.287	0.23	152.322	0.84	820.233	10.16
0.200	0.00	1.077	0.00	5.800	0.12	31.232	0.23	168.179	0.81	905.623	3.59
0.221	0.00	1.189	0.00	6.404	0.13	34.483	0.23	185.688	0.79	999.903	0.00
0.244	0.00	1.313	0.00	7.070	0.13	38.073	0.24	205.019	0.82	1103.998	0.00
0.269	0.00	1.450	0.00	7.806	0.13	42.037	0.25	226.362	0.93	1218.929	0.00
0.297	0.00	1.601	0.04	8.619	0.14	46.413	0.29	249.927	1.17	1345.826	0.00
0.328	0.00	1.767	0.06	9.516	0.15	51.245	0.33	275.946	1.56	1485.933	0.00
0.362	0.00	1.951	0.06	10.507	0.15	56.580	0.38	304.673	2.14	1640.625	0.00
0.400	0.00	2.154	0.07	11.601	0.16	62.470	0.45	336.391	2.92	1811.422	0.00
0.442	0.00	2.379	0.08	12.809	0.17	68.973	0.52	371.411	3.90	2000.000	0.00
0.488	0.00	2.626	0.09	14.142	0.18	76.154	0.61	410.077	5.03		
0.538	0.00	2.900	0.09	15.614	0.18	84.081	0.61	452.768			

APPENDIX C

DETAILED PROCEDURE

OF THE X-RAY TEST

SAMPLE ANALYSIS

STEP 1 – IMPORT IMAGE STACK:

The images that were reconstructed using CT Pro 3D had to be imported into the program to begin with the analysis (Import Image Stack, Figure 1). Thereafter, the resolution of the x, y and z axes were defined which can be found within the scanning data details. All the scans in this research was set to a resolution/voxel size of 0.0263579 in the x, y and z directions (presented in Figure 2). Figure 3 depicts the 3D volume after the images were uploaded into the program. If the samples appear too dark the clarity was changed by moving the points on the graph (circled in red) in the right hand corner (at the bottom of the image). The 3D volumes of two different samples are shown in Figure 3, before they were separated to determine the porosity of each sample.

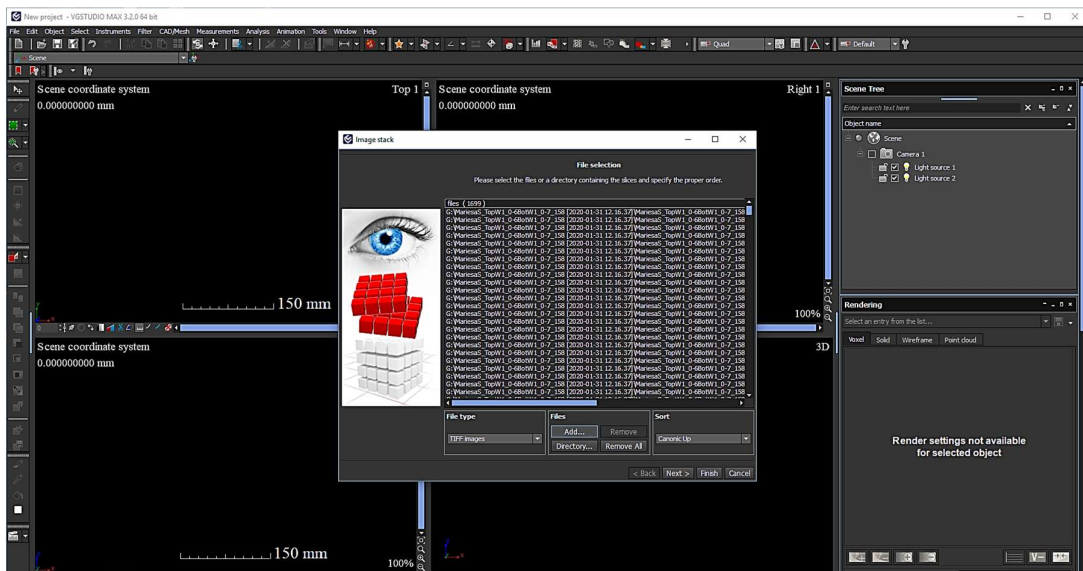


Figure 1: Import the reconstructed images created from CT Pro 3D.

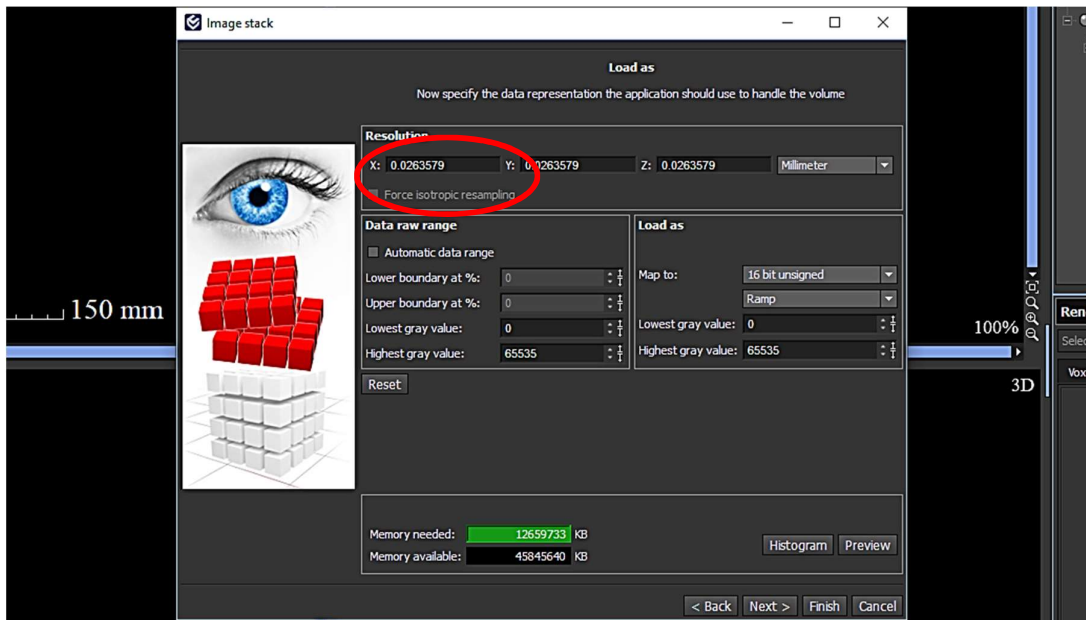


Figure 2: Specify the scanning resolution used.

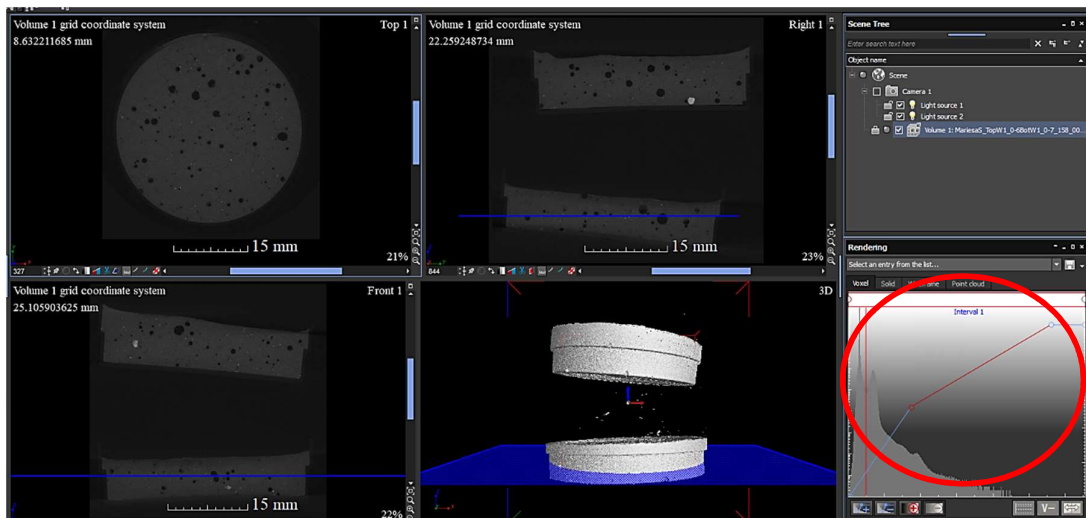


Figure 3: 3D Volumes imported into the analysis program.

STEP 2 – EXTRACT SAMPLE REGION OF INTEREST (ROI):

After the image stack was imported the volumes appeared as one item. Therefore, each sample needed to be extracted as a separate volume to be analysed. Next, a box was drawn around the sample being extracted using the draw command and then ‘extract ROI’ was selected (shown in Figure 4). This made a new volume with the single extracted sample available to work with. Thereafter, the surface determination was conducted for each sample separately. The surface of the different elements was then highlighted in yellow (it is important that the surfaces are clear).

All the samples analysed worked with the automatic surface determination command. However, the surface (highlighted in yellow) could also be changed manually by adjusting the histogram, as shown in Figure 5 (circled in red).

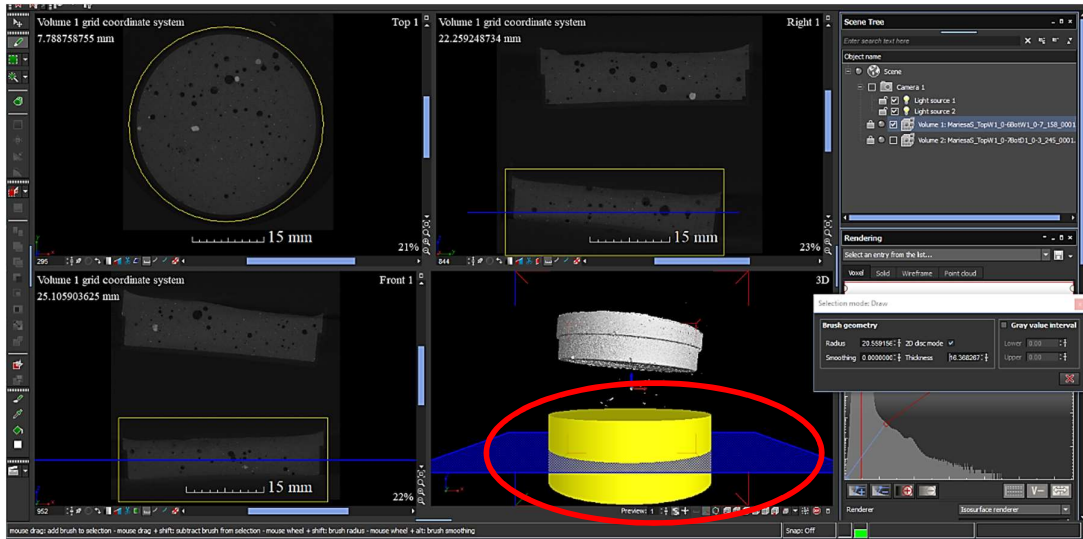


Figure 4: Extract each sample to be a separate volume.

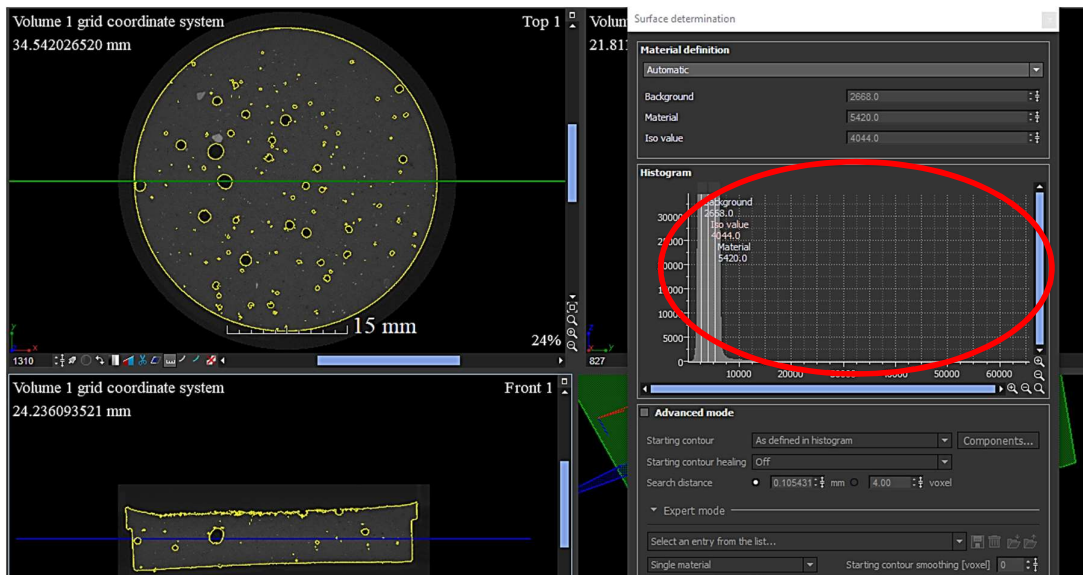


Figure 5: Object surface determination.

STEP 3 – EXTRACT THE POROSITY ROI:

The bottom surface of each sample had to be aligned (presented in Figure 6). After the bottom surface was aligned the same location for each sample was selected and used for the porosity analysis. The ROI (slice) selected for all the samples were 1.75 mm from the bottom of the

sample with a thickness of 3.5 mm and radius of 15.5 mm as presented in Figure 7 (the blue regions).

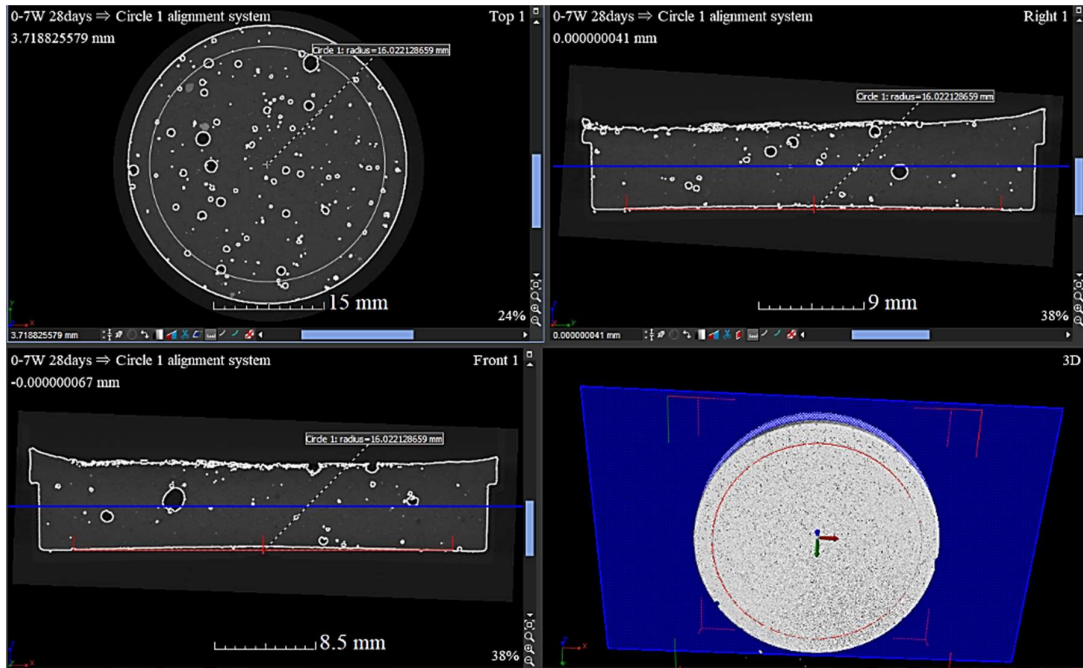


Figure 6: Align the object for further analysis.

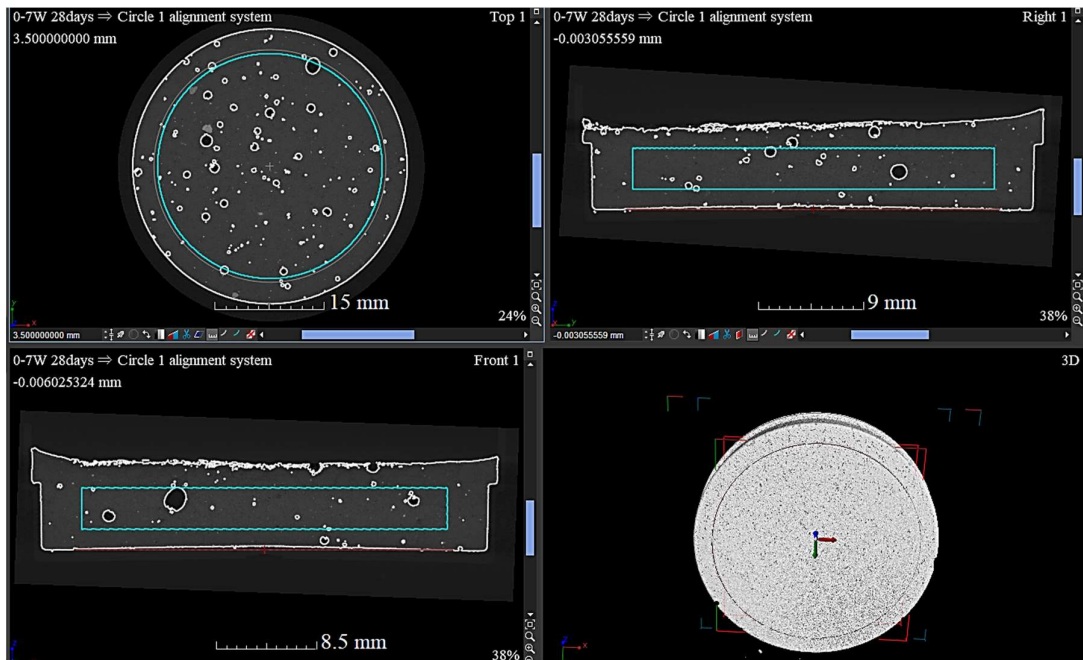


Figure 7: Determine the ROI for the porosity analysis.

STEP 4 – ALIGNMENT OF THE 7 AND 28 DAY SAMPLES:

After the ROI for the porosity analysis had been created, the 7 and 28 day samples were grouped together to analyse the porosity for both samples simultaneously (shown in Figure 8). The two ROIs were alligned using the simple registration command, as presented in Figure 9, before starting with the calibration procedure.

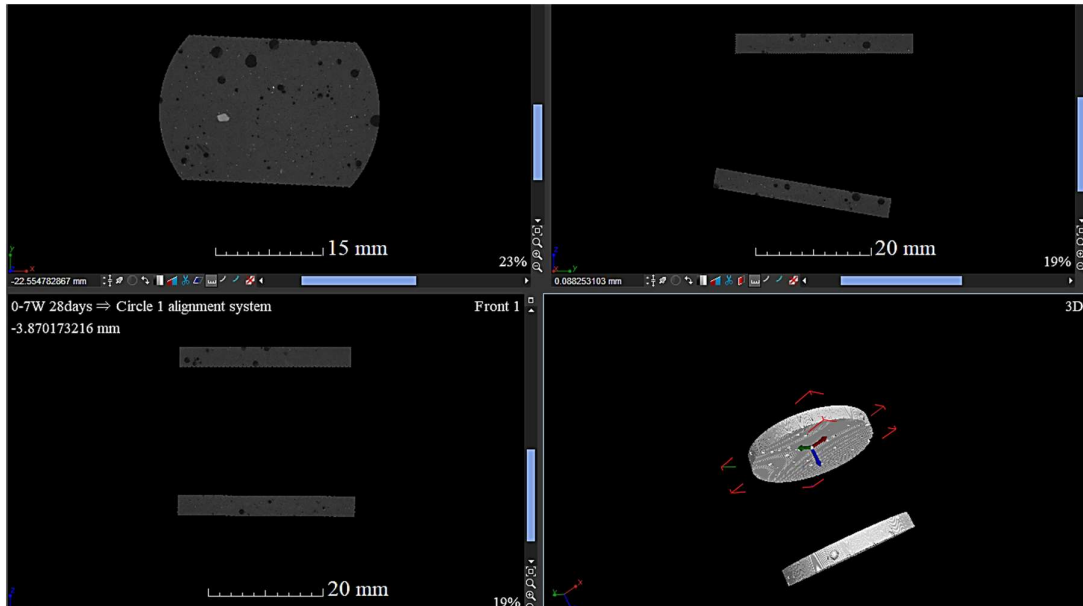


Figure 8: Import both the 7 and 28 day sample's ROIs to be analysed.

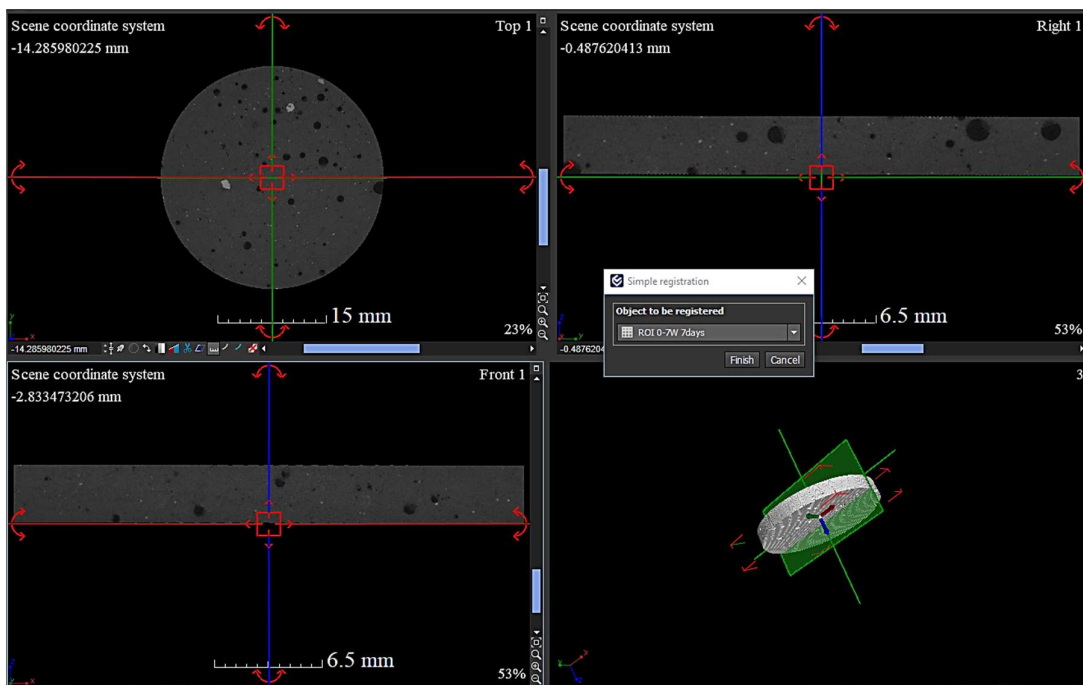


Figure 9: Align the samples by using the simple registration command.

STEP 5 – CALIBRATION PART 1:

The partial volume effect calibration method was used before determining the porosity of the samples (Soret et al., 2007, Yu et al., 2016). The calibration procedure was important because the grey values (pixels) for every sample tested could be different. The reason for the difference could be the light intensity in the room at the specific time the test was performed or even the temperature at which the sample was tested at.

Segmentation was used to identify the three different materials seen in the samples, namely the cement paste, the pores and the silica sand. Figure 10 illustrates the identification of a pore where all three axes can be investigated while determining the region which represents the specific material, or in this case the pore. The pore acknowledged in Figure 11 shows a 3D volume which was identified and extracted (ROI) for the calibration procedure. The three regions for each material in every sample was carefully assigned. Identifying the pores was easier compared to the silica sand and concrete paste (representation in Figure 12). The light grey areas are unhydrated cement also explained in Section 2.5.2. The main purpose of this analysis was to determine the pores within each sample and it was found that the pores were mainly surrounded by the cement paste and silica sand. Therefore, it was decided to not include the unhydrated cement in the calibration procedure (ROI), as it would not influence the determination of pores in the mortar.

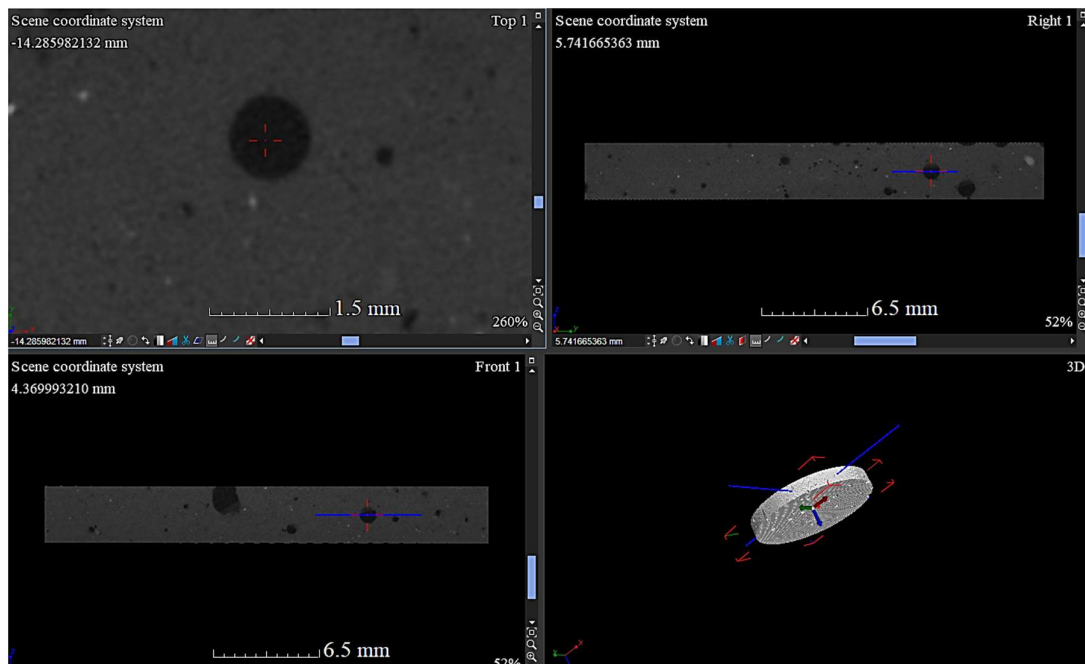


Figure 10: Select a clear open pore for analysing grey values.

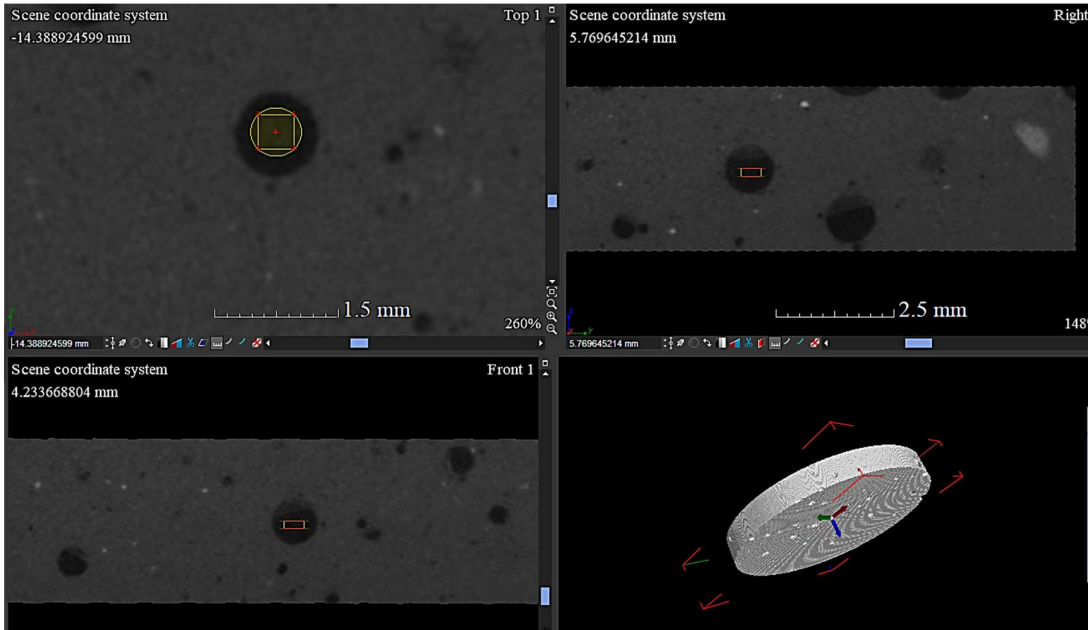


Figure 11: Create ROI for the different materials.



Figure 12: ROI for the pores, concrete and silica sand.

STEP 6 – CALIBRATION PART 2:

After each material's ROI was extracted the grey values were investigated (create grey value analysis command) and tabulated in Table 1 and Table 2. The mean grey values of all three material for the 7 and 28 day tests were recorded (presented in Figure 13). The average mean

grey values of the concrete paste, silica sand and the pores were used to calibrate the image stack and determine the porosity of the specified sample. The average mean grey value for the maximum void was inserted using the VGDEFX/only threshold command, shown in Figure 14.

Table 1: 7 Day test average mean grey values used for calibration.

Samples Tested at NECSA	7 DAY MEAN GREY VALUES			Average Mean Grey Value
	Pore region	Silica sand region	Concrete region	
0,3 Dry	4702	9510	10279	8164
0,4 Dry	4609	9226	10045	7960
0,5 Dry	2322	4702	5197	4073
0,6 Dry	2321	4601	4892	3938
0,7 Dry	4931	10016	10440	8462
0,3 Wet	5047	10086	11241	8791
0,4 Wet	2721	4694	4871	4095
0,5 Wet	2629	4617	4809	4018
0,6 Wet	3269	7448	7528	6081
0,7 Wet	3108	7177	7142	5809

Table 2: 28 Day test average mean grey values used for calibration.

Samples Tested at NECSA	28 DAY MEAN GREY VALUES			Average Mean Grey Values
	Pore region	Silica sand region	Concrete region	
0,3 Dry	2820	5857	5988	4888
0,4 Dry	3105	5980	6298	5128
0,5 Dry	3138	5433	5746	4772
0,6 Dry	4891	9106	9665	7887
0,7 Dry	4651	9476	9830	7986
0,3 Wet	3962	7937	8710	6870
0,4 Wet	3875	7656	8404	6645
0,5 Wet	7196	9362	9667	8742
0,6 Wet	7254	9280	9373	8636
0,7 Wet	2675	5667	5936	4759

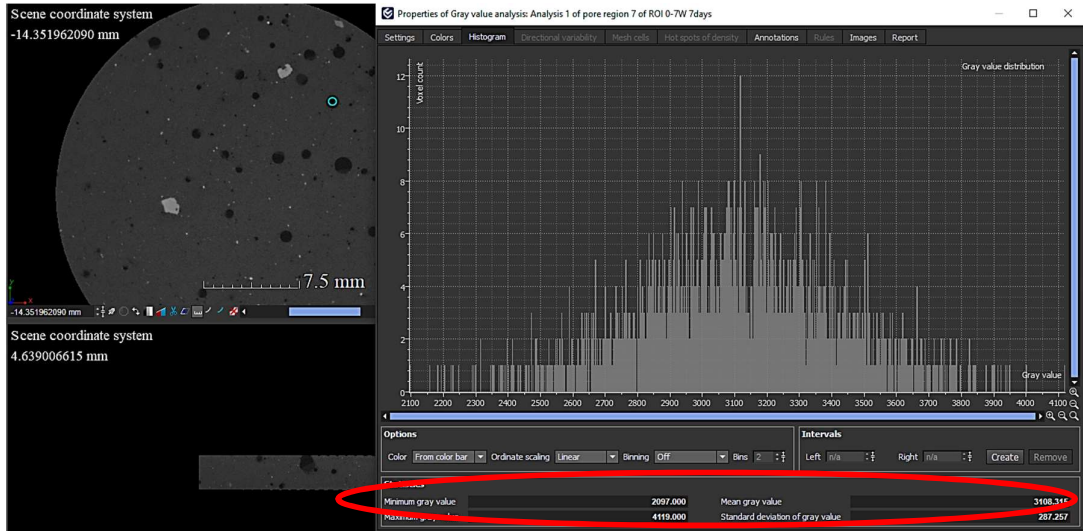


Figure 13: Determine all the regions mean grey values.

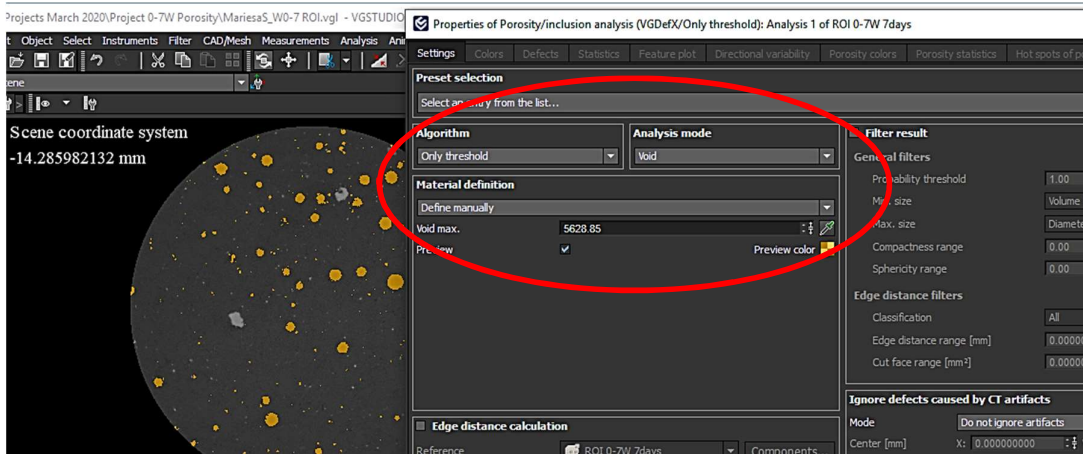


Figure 14: Calibrate the 28 day test sample.

STEP 7 – DETERMINE THE POROSITY:

After the image stack of each sample was calibrated, the porosity could be calculated. The porosity inclusion analysis was used with the threshold only algorithm while the void analysis mode was selected to calculate the percentage porosity of the sample. The computer program then presented the porosity results as shown in Figure 15. The pores were also highlighted in different colours showing the volume (mm³) of the different size pores within the mortar sample.

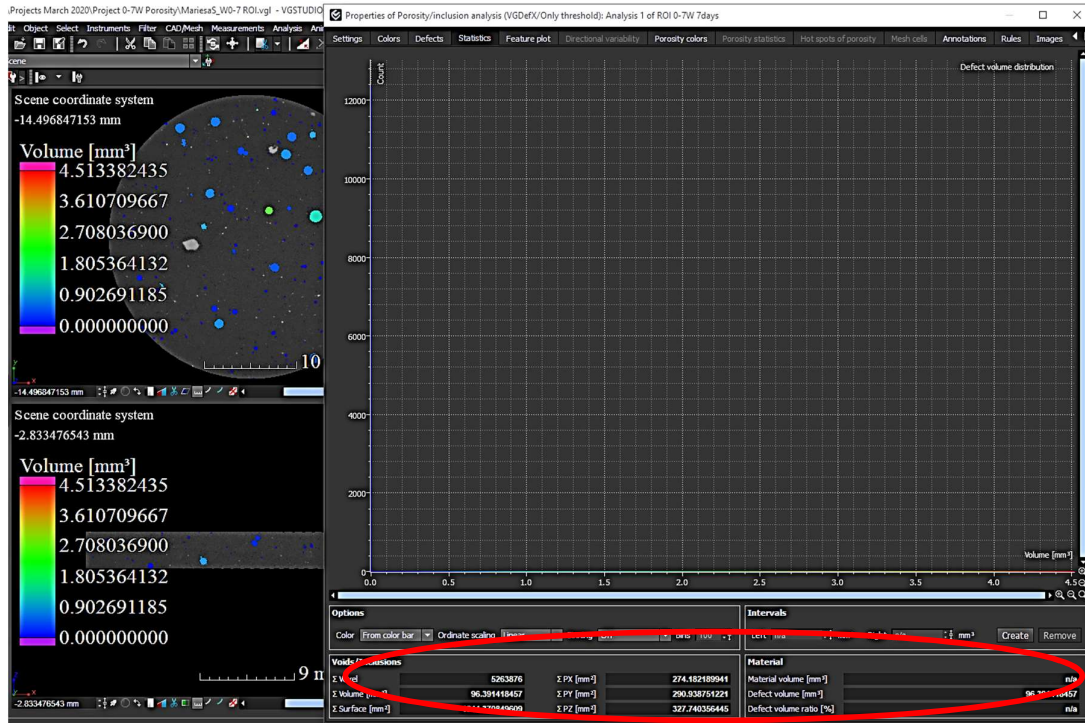


Figure 15: Determine the % porosity for every sample.

STEP 8 – SAVING THE DATA AND IMAGES:

After the porosity analysis was completed the results were exported (csv files) for further analysis. The results included the pore diameter, pore volume, surface, compactness, sphericity and the voxel values. The results were obtained after the porosity analysis was completed under defects as shown in Figure 16 (circled in red). The sample's image stack was also saved and exported to the computer in 2D format to be able to see the pore volume of the different samples (presented in Figure 17).

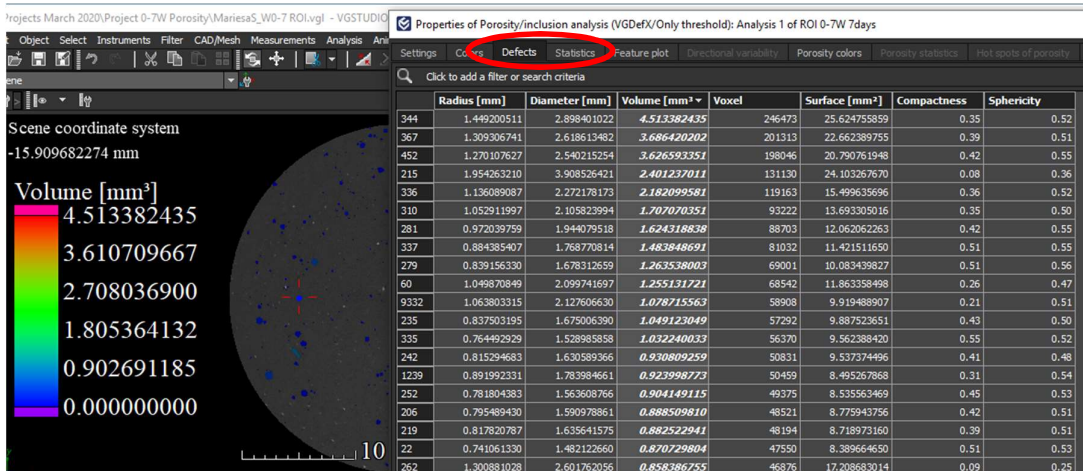


Figure 16: Export all the data required for analysis.

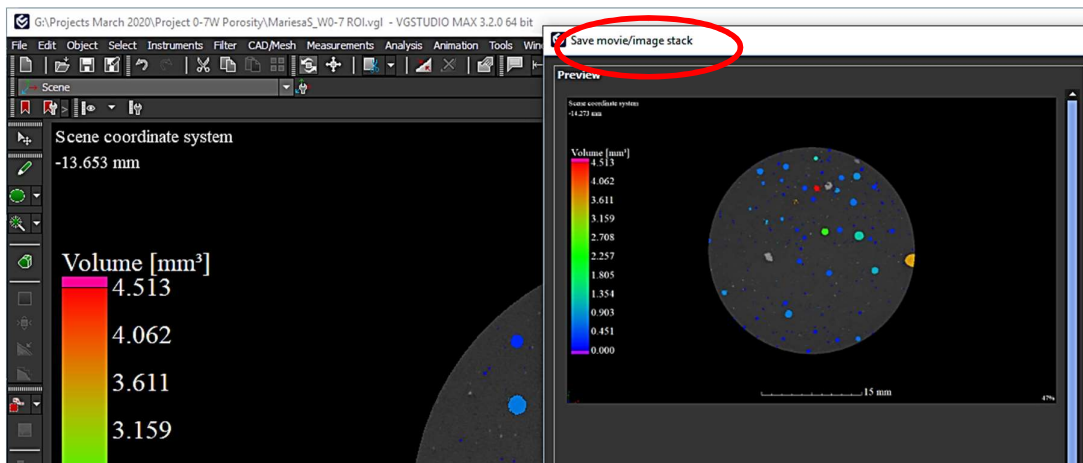


Figure 17: Export the image stack presenting the results.

APPENDIX D

MORTAR STUDY

SUCTION RESULTS

Sample Number	Sample Name	Description
1	D - 1 (N)	Dry sample of which the porosity tests were conducted at NECSA
2	W - 1 (N)	Wet sample of which the porosity tests were conducted at NECSA
3	PD	Partially dry sample drying with a lid on after casted
4	D - 2	Additional dry sample for examining the repeatability of the test
5	W - 2	Additional wet sample for examining the repeatability of the test
6	W/D	Wet sample drying without a lid on from 28 days
7	W/PD	Wet sample drying with a lid on from 28 days

W/C Ratio - Sample Number	Sample Age (hours)	Sample Mass (g)	Temperature (°C)	Water Potential (MPa)	pF	Mass solids, Ms (g)	Mass Water, Mw (g)	Mass Cement, Msc (g)	Volumetric Water Content (%)
0.3 - 1	0.0	19.2199	/	/	/	17.1302	2.0897	6.9656	12.20%
0.3 - 1	5.3	19.2175	23.00	-0.62	3.81	17.1302	2.0873	6.9656	12.18%
0.3 - 1	25.0	19.2157	24.20	-5.43	4.75	17.1302	2.0855	6.9656	12.17%
0.3 - 1	49.2	19.2140	23.40	-23.93	5.39	17.1302	2.0838	6.9656	12.16%
0.3 - 1	98.7	19.2138	22.90	-46.11	5.68	17.1302	2.0836	6.9656	12.16%
0.3 - 1	144.4	19.2132	23.80	-56.36	5.77	17.1302	2.0830	6.9656	12.16%
0.3 - 1	168.2	19.2130	23.70	-57.56	5.78	17.1302	2.0828	6.9656	12.16%
0.3 - 1	264.3	19.2111	23.00	-76.81	5.90	17.1302	2.0809	6.9656	12.15%
0.3 - 1	336.4	19.2113	23.20	-79.29	5.91	17.1302	2.0811	6.9656	12.15%
0.3 - 1	432.0	19.2113	24.40	-70.41	5.86	17.1302	2.0811	6.9656	12.15%
0.3 - 1	482.2	19.2112	23.70	-72.75	5.88	17.1302	2.0810	6.9656	12.15%
0.3 - 1	529.5	19.2106	23.20	-69.25	5.86	17.1302	2.0804	6.9656	12.14%
0.3 - 1	603.3	19.2106	23.80	-72.16	5.87	17.1302	2.0804	6.9656	12.14%
0.3 - 1	653.3	19.2108	23.20	-70.09	5.86	17.1302	2.0806	6.9656	12.15%
0.3 - 1	791.7	19.2107	24.30	-65.57	5.83	17.1302	2.0805	6.9656	12.15%
0.3 - 1	1109.8	19.2106	24.10	-76.23	5.90	17.1302	2.0804	6.9656	12.14%
0.3 - 1	1470.0	19.2102	23.10	-71.96	5.87	17.1302	2.0800	6.9656	12.14%
0.4 - 1	0.0	20.5486	/	/	/	18.2841	2.2645	5.6614	12.39%
0.4 - 1	5.3	20.5444	23.60	-0.68	3.85	18.2841	2.2603	5.6614	12.36%
0.4 - 1	25.0	20.5415	23.60	-3.21	4.52	18.2841	2.2574	5.6614	12.35%
0.4 - 1	49.2	20.5398	23.20	-17.72	5.26	18.2841	2.2557	5.6614	12.34%
0.4 - 1	98.7	20.5391	23.70	-40.06	5.62	18.2841	2.2550	5.6614	12.33%

0.4 - 1	144.4	20.5392	23.50	-51.32	5.70	18.2841	2.2551	5.6614	12.33%
0.4 - 1	168.2	20.5395	23.20	-53.37	5.74	18.2841	2.2554	5.6614	12.34%
0.4 - 1	264.3	20.5379	23.70	-73.54	5.88	18.2841	2.2538	5.6614	12.33%
0.4 - 1	336.4	20.5378	23.10	-76.40	5.90	18.2841	2.2537	5.6614	12.33%
0.4 - 1	432.0	20.5386	23.00	-67.80	5.85	18.2841	2.2545	5.6614	12.33%
0.4 - 1	482.2	20.5384	23.30	-72.57	5.88	18.2841	2.2543	5.6614	12.33%
0.4 - 1	529.5	20.5384	23.30	-68.40	5.86	18.2841	2.2543	5.6614	12.33%
0.4 - 1	603.3	20.5387	23.00	-71.33	5.87	18.2841	2.2546	5.6614	12.33%
0.4 - 1	653.3	20.5385	23.20	-69.67	5.86	18.2841	2.2544	5.6614	12.33%
0.4 - 1	791.7	20.5385	23.00	-67.79	5.85	18.2841	2.2544	5.6614	12.33%
0.4 - 1	1109.8	20.5379	23.80	-79.06	5.91	18.2841	2.2538	5.6614	12.33%
0.4 - 1	1470.0	20.5377	23.70	-74.50	5.89	18.2841	2.2536	5.6614	12.33%
0.5 - 1	0.0	22.6619	/	/	/	20.1439	2.5180	5.0360	12.50%
0.5 - 1	5.9	22.6497	23.70	-0.17	3.24	20.1439	2.5058	5.0360	12.44%
0.5 - 1	25.2	22.6477	23.70	-2.18	4.35	20.1439	2.5038	5.0360	12.43%
0.5 - 1	49.7	22.6458	23.40	-10.18	5.02	20.1439	2.5019	5.0360	12.42%
0.5 - 1	98.9	22.6442	23.30	-35.06	5.56	20.1439	2.5003	5.0360	12.41%
0.5 - 1	144.2	22.6434	23.60	-48.89	5.70	20.1439	2.4995	5.0360	12.41%
0.5 - 1	167.9	22.6420	23.60	-51.11	5.72	20.1439	2.4981	5.0360	12.40%
0.5 - 1	264.3	22.6414	22.80	-71.96	5.87	20.1439	2.4975	5.0360	12.40%
0.5 - 1	336.3	22.6415	23.80	-76.47	5.90	20.1439	2.4976	5.0360	12.40%
0.5 - 1	431.4	22.6409	23.40	-67.53	5.84	20.1439	2.4970	5.0360	12.40%
0.5 - 1	481.7	22.6404	23.70	-72.96	5.88	20.1439	2.4965	5.0360	12.39%
0.5 - 1	528.9	22.6401	23.30	-67.73	5.85	20.1439	2.4962	5.0360	12.39%
0.5 - 1	603.1	22.6401	24.00	-70.71	5.86	20.1439	2.4962	5.0360	12.39%
0.5 - 1	653.1	22.6398	23.40	-69.37	5.86	20.1439	2.4959	5.0360	12.39%
0.5 - 1	791.3	22.6398	24.00	-72.24	5.87	20.1439	2.4959	5.0360	12.39%
0.5 - 1	1109.3	22.6395	23.50	-81.63	5.93	20.1439	2.4956	5.0360	12.39%
0.5 - 1	1469.3	22.6392	23.30	-74.29	5.89	20.1439	2.4953	5.0360	12.39%
0.6 - 1	0.0	20.3366	/	/	/	18.0645	2.2721	3.7868	12.58%
0.6 - 1	6.2	20.3297	23.70	0.02	0.00	18.0645	2.2652	3.7868	12.54%
0.6 - 1	25.7	20.3259	23.50	-1.68	4.24	18.0645	2.2614	3.7868	12.52%
0.6 - 1	50.1	20.3237	23.00	-9.21	4.98	18.0645	2.2592	3.7868	12.51%

0.6 - 1	99.6	20.3216	23.10	-31.10	5.51	18.0645	2.2571	3.7868	12.49%
0.6 - 1	144.8	20.3211	23.20	-47.05	5.69	18.0645	2.2566	3.7868	12.49%
0.6 - 1	169.3	20.3203	23.50	-52.15	5.73	18.0645	2.2558	3.7868	12.49%
0.6 - 1	265.5	20.3198	23.30	-71.31	5.87	18.0645	2.2553	3.7868	12.48%
0.6 - 1	337.8	20.3193	23.60	-76.11	5.90	18.0645	2.2548	3.7868	12.48%
0.6 - 1	432.5	20.3197	23.70	-68.44	5.85	18.0645	2.2552	3.7868	12.48%
0.6 - 1	482.8	20.3193	23.10	-74.59	5.89	18.0645	2.2548	3.7868	12.48%
0.6 - 1	529.9	20.3191	23.30	-67.01	5.84	18.0645	2.2546	3.7868	12.48%
0.6 - 1	604.8	20.3191	23.80	-72.06	5.87	18.0645	2.2546	3.7868	12.48%
0.6 - 1	655.2	20.3190	23.90	-69.00	5.85	18.0645	2.2545	3.7868	12.48%
0.6 - 1	792.5	20.3187	23.60	-73.94	5.88	18.0645	2.2542	3.7868	12.48%
0.6 - 1	1111.3	20.3184	23.50	-88.81	5.96	18.0645	2.2539	3.7868	12.48%
0.6 - 1	1470.3	20.3180	23.10	-74.98	5.89	18.0645	2.2535	3.7868	12.47%
0.7 - 1	0.0	20.9167	/	/	/	18.5706	2.3461	3.3516	12.63%
0.7 - 1	6.4	20.9149	23.40	-0.22	3.36	18.5706	2.3443	3.3516	12.62%
0.7 - 1	26.6	20.9103	23.70	-1.38	4.15	18.5706	2.3397	3.3516	12.60%
0.7 - 1	51.6	20.9083	23.20	-11.72	5.08	18.5706	2.3377	3.3516	12.59%
0.7 - 1	100.6	20.9068	23.10	-36.40	23.10	18.5706	2.3362	3.3516	12.58%
0.7 - 1	145.1	20.9067	22.80	-47.70	5.69	18.5706	2.3361	3.3516	12.58%
0.7 - 1	168.8	20.9070	22.60	-53.01	5.74	18.5706	2.3364	3.3516	12.58%
0.7 - 1	264.7	20.9054	23.30	-71.31	5.87	18.5706	2.3348	3.3516	12.57%
0.7 - 1	337.7	20.9057	23.50	-76.32	5.90	18.5706	2.3351	3.3516	12.57%
0.7 - 1	431.5	20.9058	23.75	-68.47	5.85	18.5706	2.3352	3.3516	12.58%
0.7 - 1	482.0	20.9060	23.10	-79.17	5.91	18.5706	2.3354	3.3516	12.58%
0.7 - 1	529.0	20.9059	23.50	-66.62	5.84	18.5706	2.3353	3.3516	12.58%
0.7 - 1	604.0	20.9059	23.80	-76.45	5.90	18.5706	2.3353	3.3516	12.58%
0.7 - 1	654.6	20.9063	23.20	-70.04	5.86	18.5706	2.3357	3.3516	12.58%
0.7 - 1	791.8	20.9061	23.00	-75.86	5.90	18.5706	2.3355	3.3516	12.58%
0.7 - 1	1110.7	20.9061	23.60	-93.15	5.98	18.5706	2.3355	3.3516	12.58%
0.7 - 1	1469.3	20.9060	23.30	-76.48	5.90	18.5706	2.3354	3.3516	12.58%

W/C Ratio - Sample Number	Sample Age (hours)	Sample Mass (g)	Temperature (°C)	Water Potential (MPa)	pF	Mass solids, Ms (g)	Mass Water, Mw (g)	Mass Cement, Msc (g)	Volumetric Water Content (%)
0.3 - 2	0.0	18.6985	/	/	/	16.6655	2.0330	6.7767	12.20%
0.3 - 2	5.6	18.6963	23.90	-0.31	3.51	16.6655	2.0308	6.7767	12.19%
0.3 - 2	25.3	18.6943	23.20	-3.39	4.55	16.6655	2.0288	6.7767	12.17%
0.3 - 2	53.6	18.6845	23.20	0.91	0.00	16.6655	2.0190	6.7767	12.11%
0.3 - 2	172.2	18.6507	23.50	1.08	0.00	16.6655	1.9852	6.7767	11.91%
0.3 - 2	267.5	18.6416	23.40	0.96	0.00	16.6655	1.9761	6.7767	11.86%
0.3 - 2	361.6	18.6236	22.40	1.49	0.00	16.6655	1.9581	6.7767	11.75%
0.3 - 2	512.2	18.6093	23.50	0.95	0.00	16.6655	1.9438	6.7767	11.66%
0.4 - 2	0.0	19.5815	/	/	/	17.4235	2.1580	5.3949	12.39%
0.4 - 2	5.8	19.5791	23.70	-0.17	3.24	17.4235	2.1556	5.3949	12.37%
0.4 - 2	25.5	19.5779	23.50	-2.25	4.37	17.4235	2.1544	5.3949	12.36%
0.4 - 2	76.0	19.5683	23.10	0.42	0.00	17.4235	2.1448	5.3949	12.31%
0.4 - 2	172.3	19.5605	23.60	0.49	0.00	17.4235	2.1370	5.3949	12.26%
0.4 - 2	267.4	19.5549	23.00	0.67	0.00	17.4235	2.1314	5.3949	12.23%
0.4 - 2	361.2	19.5480	24.10	-0.02	2.29	17.4235	2.1245	5.3949	12.19%
0.4 - 2	530.0	19.5441	23.60	0.24	0.00	17.4235	2.1206	5.3949	12.17%
0.5 - 2	0.0	21.2019	/	/	/	18.8461	2.3558	4.7115	12.50%
0.5 - 2	6.2	22.1964	23.80	-0.31	3.50	18.8461	3.3503	4.7115	17.78%
0.5 - 2	25.6	22.1954	23.80	-1.71	4.25	18.8461	3.3493	4.7115	17.77%
0.5 - 2	76.2	22.1730	23.70	0.48	0.00	18.8461	3.3269	4.7115	17.65%
0.5 - 2	172.2	22.1511	23.90	0.39	0.00	18.8461	3.3050	4.7115	17.54%
0.5 - 2	267.3	22.1281	24.00	-0.06	2.80	18.8461	3.2820	4.7115	17.41%
0.5 - 2	361.0	22.1072	24.00	-0.35	3.56	18.8461	3.2611	4.7115	17.30%
0.5 - 2	530.1	22.0675	23.90	0.34	0.00	18.8461	3.2214	4.7115	17.09%
0.6 - 2	0.0	22.7392	/	/	/	20.1987	2.5405	4.2342	12.58%
0.6 - 2	6.4	22.7330	23.80	-0.21	3.34	20.1987	2.5343	4.2342	12.55%
0.6 - 2	27.3	22.7306	23.70	-1.30	4.13	20.1987	2.5319	4.2342	12.54%
0.6 - 2	77.3	22.7194	24.00	0.00	0.00	20.1987	2.5207	4.2342	12.48%
0.6 - 2	173.9	22.6856	24.20	0.50	0.00	20.1987	2.4869	4.2342	12.31%
0.6 - 2	268.6	22.6622	24.30	0.16	0.00	20.1987	2.4635	4.2342	12.20%
0.6 - 2	362.4	22.6250	24.30	0.55	0.00	20.1987	2.4263	4.2342	12.01%
0.6 - 2	531.4	22.6146	24.30	0.50	0.00	20.1987	2.4159	4.2342	11.96%

0.7 - 2	0.0	17.8387	/	/	/	15.8378	2.0009	2.8584	12.63%
0.7 - 2	6.7	17.8365	23.50	-0.08	2.90	15.8378	1.9987	2.8584	12.62%
0.7 - 2	26.9	17.8346	23.80	-0.31	3.50	15.8378	1.9968	2.8584	12.61%
0.7 - 2	76.5	17.8186	22.90	0.92	0.00	15.8378	1.9808	2.8584	12.51%
0.7 - 2	172.0	17.7794	23.90	1.66	0.00	15.8378	1.9416	2.8584	12.26%
0.7 - 2	266.7	17.7549	23.50	1.62	0.00	15.8378	1.9171	2.8584	12.10%
0.7 - 2	360.3	17.7444	23.70	1.74	0.00	15.8378	1.9066	2.8584	12.04%
0.7 - 2	529.5	17.7376	23.20	0.67	0.00	15.8378	1.8998	2.8584	12.00%

W/C Ratio - Sample Number	Sample Age (hours)	Sample Mass (g)	Temperature (°C)	Water Potential (MPa)	pF	Mass solids, Ms (g)	Mass Water, Mw (g)	Mass Cement, Msc (g)	Volumetric Water Content (%)
0.3 - 3	0.0	19.3690	/	/	/	17.2631	2.1059	7.0197	12.20%
0.3 - 3	8.3	19.3662	23.70	-0.96	4.00	17.2631	2.1031	7.0197	12.18%
0.3 - 3	28.9	19.3638	23.20	-5.90	4.79	17.2631	2.1007	7.0197	12.17%
0.3 - 3	96.5	19.3623	23.00	-21.67	5.35	17.2631	2.0992	7.0197	12.16%
0.3 - 3	147.1	19.3609	23.00	-25.90	5.43	17.2631	2.0978	7.0197	12.15%
0.3 - 3	312.0	19.3596	24.50	-42.22	5.64	17.2631	2.0965	7.0197	12.14%
0.3 - 3	480.0	19.3587	23.20	-48.92	5.70	17.2631	2.0956	7.0197	12.14%
0.3 - 3	599.8	19.3587	23.80	-54.22	5.75	17.2631	2.0956	7.0197	12.14%
0.3 - 3	648.1	19.3589	24.30	-51.03	5.75	17.2631	2.0958	7.0197	12.14%
0.3 - 3	701.9	19.3588	22.90	-51.63	5.73	17.2631	2.0957	7.0197	12.14%
0.3 - 3	775.4	19.3581	22.10	-55.43	5.76	17.2631	2.0950	7.0197	12.14%
0.3 - 3	940.3	19.3576	22.50	-51.27	5.72	17.2631	2.0945	7.0197	12.13%
0.3 - 3	941.6	19.3569	23.70	-51.02	5.72	17.2631	2.0938	7.0197	12.13%
0.3 - 3	988.8	19.3567	22.70	-55.02	5.76	17.2631	2.0936	7.0197	12.13%
0.3 - 3	1109.6	19.3556	24.10	-54.42	5.75	17.2631	2.0925	7.0197	12.12%
0.3 - 3	1276.9	19.3559	24.20	-55.87	5.76	17.2631	2.0928	7.0197	12.12%
0.3 - 3	1468.5	19.3554	23.70	-55.32	5.76	17.2631	2.0923	7.0197	12.12%
0.4 - 3	0.0	22.6403	/	/	/	20.1452	2.4951	6.2377	12.39%
0.4 - 3	8.1	22.6343	24.00	-0.63	3.82	20.1452	2.4891	6.2377	12.36%
0.4 - 3	28.7	22.6289	23.70	-3.92	4.61	20.1452	2.4837	6.2377	12.33%
0.4 - 3	96.6	22.6183	23.20	-16.19	5.22	20.1452	2.4731	6.2377	12.28%
0.4 - 3	147.2	22.6169	23.20	-21.09	5.34	20.1452	2.4717	6.2377	12.27%
0.4 - 3	312.2	22.6152	23.20	-33.79	5.54	20.1452	2.4700	6.2377	12.26%

0.4 - 3	479.8	22.6142	23.70	-41.69	5.64	20.1452	2.4690	6.2377	12.26%
0.4 - 3	599.7	22.6120	23.60	-48.42	5.70	20.1452	2.4668	6.2377	12.24%
0.4 - 3	647.9	22.6115	23.20	-46.14	5.68	20.1452	2.4663	6.2377	12.24%
0.4 - 3	651.1	22.6114	24.20	-44.33	5.66	20.1452	2.4662	6.2377	12.24%
0.4 - 3	701.8	22.6094	23.70	-48.02	5.70	20.1452	2.4642	6.2377	12.23%
0.4 - 3	793.1	22.6090	23.60	-48.34	5.70	20.1452	2.4638	6.2377	12.23%
0.4 - 3	940.1	22.6088	24.20	-47.22	5.69	20.1452	2.4636	6.2377	12.23%
0.4 - 3	988.8	22.6084	23.70	-52.86	5.74	20.1452	2.4632	6.2377	12.23%
0.4 - 3	1276.7	22.6078	23.80	-52.14	5.73	20.1452	2.4626	6.2377	12.22%
0.4 - 3	1468.2	22.6079	23.50	-52.43	5.73	20.1452	2.4627	6.2377	12.22%
0.5 - 3	0.0	19.4915	/	/	/	17.3258	2.1657	4.3314	12.50%
0.5 - 3	7.7	19.4882	23.70	-0.37	3.58	17.3258	2.1624	4.3314	12.48%
0.5 - 3	28.6	19.4855	23.70	-2.38	4.39	17.3258	2.1597	4.3314	12.47%
0.5 - 3	96.5	19.4836	23.10	-8.69	4.95	17.3258	2.1578	4.3314	12.45%
0.5 - 3	148.8	19.4812	22.60	-13.30	5.14	17.3258	2.1554	4.3314	12.44%
0.5 - 3	312.3	19.4797	22.80	-26.08	5.43	17.3258	2.1539	4.3314	12.43%
0.5 - 3	479.9	19.4782	22.80	-31.79	5.52	17.3258	2.1524	4.3314	12.42%
0.5 - 3	599.6	19.4773	23.10	-35.22	5.56	17.3258	2.1515	4.3314	12.42%
0.5 - 3	649.4	19.4753	22.90	-36.78	5.58	17.3258	2.1495	4.3314	12.41%
0.5 - 3	701.7	19.4751	22.90	-39.00	5.61	17.3258	2.1493	4.3314	12.41%
0.5 - 3	793.2	19.4747	22.60	-39.90	5.62	17.3258	2.1489	4.3314	12.40%
0.5 - 3	939.9	19.4741	23.50	-41.82	5.64	17.3258	2.1483	4.3314	12.40%
0.5 - 3	989.8	19.4729	23.20	-44.04	5.66	17.3258	2.1471	4.3314	12.39%
0.5 - 3	1277.3	19.4724	23.80	-46.13	5.68	17.3258	2.1466	4.3314	12.39%
0.5 - 3	1469.0	19.4726	23.10	-47.17	5.69	17.3258	2.1468	4.3314	12.39%
0.6 - 3	0.0	23.0374	/	/	/	20.4636	2.5738	4.2897	12.58%
0.6 - 3	7.8	23.0321	24.00	-0.55	3.76	20.4636	2.5685	4.2897	12.55%
0.6 - 3	29.7	23.0297	23.70	-1.89	4.29	20.4636	2.5661	4.2897	12.54%
0.6 - 3	98.6	23.0263	23.40	-5.63	4.77	20.4636	2.5627	4.2897	12.52%
0.6 - 3	150.9	23.0233	23.40	-9.41	4.99	20.4636	2.5597	4.2897	12.51%
0.6 - 3	314.5	23.0206	23.60	-19.23	5.30	20.4636	2.5570	4.2897	12.50%
0.6 - 3	482.0	23.0191	22.90	-25.02	5.41	20.4636	2.5555	4.2897	12.49%
0.6 - 3	601.6	23.0179	23.10	-27.73	5.46	20.4636	2.5543	4.2897	12.48%
0.6 - 3	651.6	23.0161	23.20	-28.45	5.47	20.4636	2.5525	4.2897	12.47%

0.6 - 3	703.6	23.0156	23.70	-30.00	5.49	20.4636	2.5520	4.2897	12.47%
0.6 - 3	795.5	23.0145	23.00	-31.47	5.51	20.4636	2.5509	4.2897	12.47%
0.6 - 3	941.6	23.0140	24.10	-32.28	5.52	20.4636	2.5504	4.2897	12.46%
0.6 - 3	990.9	23.0121	23.00	-35.53	5.57	20.4636	2.5485	4.2897	12.45%
0.6 - 3	1278.5	23.0111	22.80	-37.26	5.59	20.4636	2.5475	4.2897	12.45%
0.6 - 3	1469.9	23.0106	23.00	-39.92	5.62	20.4636	2.5470	4.2897	12.45%
0.7 - 3	0.0	17.2022	/	/	/	15.2727	1.9295	2.7564	12.63%
0.7 - 3	7.8	17.1997	23.60	-0.31	3.51	15.2727	1.9270	2.7564	12.62%
0.7 - 3	28.7	17.1982	23.60	-1.49	4.19	15.2727	1.9255	2.7564	12.61%
0.7 - 3	96.8	17.1973	23.40	-3.38	4.54	15.2727	1.9246	2.7564	12.60%
0.7 - 3	149.3	17.1957	23.30	-5.94	4.79	15.2727	1.9230	2.7564	12.59%
0.7 - 3	313.0	17.1939	23.30	-12.31	5.11	15.2727	1.9212	2.7564	12.58%
0.7 - 3	480.6	17.1929	22.40	-17.44	5.26	15.2727	1.9202	2.7564	12.57%
0.7 - 3	600.0	17.1915	23.20	-19.78	5.31	15.2727	1.9188	2.7564	12.56%
0.7 - 3	650.0	17.1910	23.60	-21.45	5.35	15.2727	1.9183	2.7564	12.56%
0.7 - 3	701.9	17.1903	23.90	-22.55	5.37	15.2727	1.9176	2.7564	12.56%
0.7 - 3	793.9	17.1895	23.30	-24.47	5.40	15.2727	1.9168	2.7564	12.55%
0.7 - 3	940.0	17.1881	23.70	-26.30	5.44	15.2727	1.9154	2.7564	12.54%
0.7 - 3	989.9	17.1864	22.80	-28.72	5.47	15.2727	1.9137	2.7564	12.53%
0.7 - 3	1276.9	17.1858	23.40	-30.73	5.50	15.2727	1.9131	2.7564	12.53%
0.7 - 3	1468.5	17.1854	22.50	-34.08	5.55	15.2727	1.9127	2.7564	12.52%

W/C Ratio - Sample Number	Sample Age (hours)	Sample Mass (g)	Temperature (°C)	Water Potential (MPa)	pF	Mass solids, Ms (g)	Mass Water, Mw (g)	Mass Cement, Msc (g)	Volumetric Water Content (%)
0.3 - 4	0.0	20.9826	/	/	/	18.7013	2.2813	7.6045	12.20%
0.3 - 4	30.6	20.9807	23.60	-4.64	4.68	18.7013	2.2794	7.6045	12.19%
0.3 - 4	120.2	20.9797	23.30	-49.69	5.71	18.7013	2.2784	7.6045	12.18%
0.3 - 4	314.8	20.9806	22.60	-83.77	5.94	18.7013	2.2793	7.6045	12.19%
0.3 - 4	433.3	20.9805	23.50	-66.83	5.84	18.7013	2.2792	7.6045	12.19%
0.3 - 4	485.0	20.9804	23.20	-72.43	5.87	18.7013	2.2791	7.6045	12.19%
0.3 - 4	601.6	20.9802	24.10	-71.49	5.87	18.7013	2.2789	7.6045	12.19%
0.4 - 4	0.0	22.6289	/	/	/	20.1351	2.4938	6.2345	12.39%
0.4 - 4	31.0	22.6261	23.60	-4.32	4.65	20.1351	2.4910	6.2345	12.37%
0.4 - 4	120.0	22.6258	23.60	-49.25	5.71	20.1351	2.4907	6.2345	12.37%

M.Schoeman

0.4 - 4	314.9	22.6260	22.80	-81.82	5.93	20.1351	2.4909	6.2345	12.37%
0.4 - 4	433.0	22.6262	23.50	-65.68	5.83	20.1351	2.4911	6.2345	12.37%
0.4 - 4	484.7	22.6260	23.70	-73.09	5.88	20.1351	2.4909	6.2345	12.37%
0.4 - 4	601.3	22.6259	23.80	-72.95	5.88	20.1351	2.4908	6.2345	12.37%
0.5 - 4	0.0	22.4093	/	/	/	19.9194	2.4899	4.9798	12.50%
0.5 - 4	31.1	22.4070	23.60	-2.83	4.47	19.9194	2.4876	4.9798	12.49%
0.5 - 4	120.1	22.4066	23.20	-44.98	5.67	19.9194	2.4872	4.9798	12.49%
0.5 - 4	315.0	22.4063	22.60	-81.88	5.93	19.9194	2.4869	4.9798	12.48%
0.5 - 4	432.7	22.4070	23.00	-64.99	5.83	19.9194	2.4876	4.9798	12.49%
0.5 - 4	484.4	22.4070	23.80	-72.69	5.88	19.9194	2.4876	4.9798	12.49%
0.5 - 4	601.2	22.4067	24.30	-71.46	5.87	19.9194	2.4873	4.9798	12.49%
0.6 - 4	0.0	19.2958	/	/	/	17.1400	2.1558	3.5930	12.58%
0.6 - 4	31.2	19.2942	23.70	-2.06	4.33	17.1400	2.1542	3.5930	12.57%
0.6 - 4	118.6	19.2939	22.90	-44.75	5.67	17.1400	2.1539	3.5930	12.57%
0.6 - 4	313.4	19.2939	23.60	-86.08	5.95	17.1400	2.1539	3.5930	12.57%
0.6 - 4	438.4	19.2936	24.10	-71.80	5.87	17.1400	2.1536	3.5930	12.56%
0.6 - 4	482.4	19.2935	23.50	-74.42	5.89	17.1400	2.1535	3.5930	12.56%
0.6 - 4	599.4	19.2933	23.50	-71.84	5.87	17.1400	2.1533	3.5930	12.56%
0.7 - 4	0.0	21.2984	/	/	/	18.9094	2.3890	3.4128	12.63%
0.7 - 4	31.6	21.2962	23.70	-1.56	4.21	18.9094	2.3868	3.4128	12.62%
0.7 - 4	121.5	21.2954	23.20	-37.19	5.59	18.9094	2.3860	3.4128	12.62%
0.7 - 4	315.8	21.2951	24.00	-85.00	5.94	18.9094	2.3857	3.4128	12.62%
0.7 - 4	440.8	21.2945	22.80	-72.78	5.88	18.9094	2.3851	3.4128	12.61%
0.7 - 4	484.5	21.2945	23.60	-75.03	5.89	18.9094	2.3851	3.4128	12.61%
0.7 - 4	601.6	21.2943	22.90	-74.55	5.89	18.9094	2.3849	3.4128	12.61%

W/C Ratio - Sample Number	Sample Age (hours)	Sample Mass (g)	Temperature (°C)	Water Potential (MPa)	pF	Mass solids, Ms (g)	Mass Water, Mw (g)	Mass Cement, Msc (g)	Volumetric Water Content (%)
0.3 - 5	0.0	19.4269	/	/	/	17.3147	2.1122	7.0407	12.20%
0.3 - 5	30.3	19.4253	23.60	-4.70	4.69	17.3147	2.1106	7.0407	12.19%
0.3 - 5	123.2	19.4099	24.50	-0.09	0.00	17.3147	2.0952	7.0407	12.10%
0.3 - 5	362.8	19.4035	24.20	0.48	0.00	17.3147	2.0888	7.0407	12.06%
0.3 - 5	532.0	19.3887	23.50	0.30	0.00	17.3147	2.0740	7.0407	11.98%

0.4 - 5	0.0	18.2996	/	/	/	16.2829	2.0167	5.0417	12.39%
0.4 - 5	30.6	18.2937	23.20	-2.47	4.41	16.2829	2.0108	5.0417	12.35%
0.4 - 5	123.0	18.2782	23.80	0.72	0.00	16.2829	1.9953	5.0417	12.25%
0.4 - 5	362.5	18.2694	23.90	0.59	0.00	16.2829	1.9865	5.0417	12.20%
0.4 - 5	531.8	18.2619	23.60	0.38	0.00	16.2829	1.9790	5.0417	12.15%
0.5 - 5	0.0	24.8904	/	/	/	22.1248	2.7656	5.5312	12.50%
0.5 - 5	30.9	24.8856	24.00	-1.98	4.31	22.1248	2.7608	5.5312	12.48%
0.5 - 5	122.8	24.8713	24.20	-0.11	3.04	22.1248	2.7465	5.5312	12.41%
0.5 - 5	362.7	24.8468	24.10	0.01	0.00	22.1248	2.7220	5.5312	12.30%
0.5 - 5	531.5	24.8368	23.30	-0.02	2.25	22.1248	2.7120	5.5312	12.26%
0.6 - 5	0.0	22.2844	/	/	/	19.7947	2.4897	4.1495	12.58%
0.6 - 5	31.1	24.8856	23.90	-1.45	4.18	19.7947	2.4875	4.1495	12.57%
0.6 - 5	123.0	24.8713	23.70	0.14	0.00	19.7947	2.4646	4.1495	12.45%
0.6 - 5	362.9	24.8468	23.90	-0.12	3.10	19.7947	2.4354	4.1495	12.30%
0.6 - 5	531.6	24.8368	24.00	0.09	0.00	19.7947	2.4172	4.1495	12.21%
0.7 - 5	0.0	19.7008	/	/	/	17.4910	2.2098	3.1568	12.63%
0.7 - 5	31.3	19.6992	23.70	-0.29	3.48	17.4910	2.2082	3.1568	12.62%
0.7 - 5	123.0	19.6886	23.90	0.49	0.00	17.4910	2.1976	3.1568	12.56%
0.7 - 5	363.4	19.6779	23.50	0.32	0.00	17.4910	2.1869	3.1568	12.50%
0.7 - 5	531.7	19.6728	23.50	0.41	0.00	17.4910	2.1818	3.1568	12.47%

W/C Ratio - Sample Number	Sample Age (hours)	Sample Mass (g)	Temperature (°C)	Water Potential (MPa)	pF	Mass solids, Ms (g)	Mass Water, Mw (g)	Mass Cement, Msc (g)	Volumetric Water Content (%)
0.3 - 6	0.0	18.2752	/	/	/	16.2882	1.9870	6.6233	12.20%
0.3 - 6	674.2	18.2544	23.40	1.00	0.00	16.2882	1.9662	6.6233	12.07%
0.3 - 6	680.2	18.2521	22.80	-17.19	5.25	16.2882	1.9639	6.6233	12.06%
0.3 - 6	767.9	18.2514	22.30	-59.22	5.79	16.2882	1.9632	6.6233	12.05%
0.3 - 6	840.8	18.2511	24.10	-68.18	5.85	16.2882	1.9629	6.6233	12.05%
0.3 - 6	935.7	18.2502	24.00	-67.58	5.84	16.2882	1.9620	6.6233	12.05%
0.3 - 6	984.3	18.2501	23.70	-65.74	5.83	16.2882	1.9619	6.6233	12.04%
0.3 - 6	1032.2	18.2498	21.80	-72.21	5.87	16.2882	1.9616	6.6233	12.04%
0.3 - 6	1104.1	18.2494	21.90	-76.90	5.90	16.2882	1.9612	6.6233	12.04%
0.3 - 6	1271.8	18.2499	21.60	-75.83	5.89	16.2882	1.9617	6.6233	12.04%

M.Schoeman

0.3 - 6	1344.5	18.2495	24.10	-77.29	5.90	16.2882	1.9613	6.6233	12.04%
0.3 - 6	1464.7	18.2492	24.10	-76.91	5.90	16.2882	1.9610	6.6233	12.04%
0.4 - 6	0.0	19.2429	/	/	/	17.1222	2.1207	5.3016	12.39%
0.4 - 6	674.8	19.2238	23.50	0.22	0.00	17.1222	2.1016	5.3016	12.27%
0.4 - 6	680.6	19.2178	23.00	-23.06	5.38	17.1222	2.0956	5.3016	12.24%
0.4 - 6	768.0	19.2168	22.50	-63.49	5.82	17.1222	2.0946	5.3016	12.23%
0.4 - 6	841.1	19.2162	22.50	-62.80	5.81	17.1222	2.0940	5.3016	12.23%
0.4 - 6	935.6	19.2148	23.50	-67.83	5.85	17.1222	2.0926	5.3016	12.22%
0.4 - 6	984.3	19.2140	23.50	-67.33	5.84	17.1222	2.0918	5.3016	12.22%
0.4 - 6	1031.8	19.2137	23.50	-76.11	5.90	17.1222	2.0915	5.3016	12.21%
0.4 - 6	1103.9	19.2134	23.70	-80.56	5.92	17.1222	2.0912	5.3016	12.21%
0.4 - 6	1271.5	19.2133	23.50	-78.38	5.91	17.1222	2.0911	5.3016	12.21%
0.4 - 6	1344.2	19.2120	23.20	-75.98	5.90	17.1222	2.0898	5.3016	12.20%
0.4 - 6	1464.6	19.2087	23.30	-76.58	5.90	17.1222	2.0865	5.3016	12.19%
0.5 - 6	0.0	21.2651	/	/	/	18.9023	2.3628	4.7256	12.50%
0.5 - 6	675.0	21.2610	22.80	-1.26	4.11	18.9023	2.3587	4.7256	12.48%
0.5 - 6	696.3	21.2569	23.00	-25.87	5.43	18.9023	2.3546	4.7256	12.46%
0.5 - 6	767.7	21.2558	23.60	-54.28	5.75	18.9023	2.3535	4.7256	12.45%
0.5 - 6	840.7	21.2555	23.60	-59.74	5.79	18.9023	2.3532	4.7256	12.45%
0.5 - 6	935.4	21.2538	23.80	-62.53	5.81	18.9023	2.3515	4.7256	12.44%
0.5 - 6	984.2	21.2530	23.80	-62.20	5.81	18.9023	2.3507	4.7256	12.44%
0.5 - 6	1031.8	21.2529	22.20	-69.46	5.86	18.9023	2.3506	4.7256	12.44%
0.5 - 6	1103.9	21.2526	22.50	-74.66	5.89	18.9023	2.3503	4.7256	12.43%
0.5 - 6	1271.2	21.2524	23.40	-77.79	5.91	18.9023	2.3501	4.7256	12.43%
0.5 - 6	1343.8	21.2521	23.40	-74.80	5.89	18.9023	2.3498	4.7256	12.43%
0.5 - 6	1464.3	21.2517	22.80	-73.25	5.88	18.9023	2.3494	4.7256	12.43%
0.6 - 6	0.0	20.9188	/	/	/	18.5817	2.3371	3.8952	12.58%
0.6 - 6	675.7	20.9167	23.10	4.23	-1.65	18.5817	2.3350	3.8952	12.57%
0.6 - 6	697.5	20.9141	23.00	-10.67	5.04	18.5817	2.3324	3.8952	12.55%
0.6 - 6	768.2	20.9134	22.70	-41.14	5.63	18.5817	2.3317	3.8952	12.55%
0.6 - 6	841.2	20.9134	22.60	-52.36	5.73	18.5817	2.3317	3.8952	12.55%
0.6 - 6	935.4	20.9133	23.50	-61.99	5.81	18.5817	2.3316	3.8952	12.55%

0.6 - 6	984.3	20.9128	23.80	-61.51	5.80	18.5817	2.3311	3.8952	12.55%
0.6 - 6	1032.2	20.9124	22.20	-71.74	5.87	18.5817	2.3307	3.8952	12.54%
0.6 - 6	1104.3	20.9127	22.30	-77.93	5.91	18.5817	2.3310	3.8952	12.54%
0.6 - 6	1271.4	20.9127	22.90	-80.31	5.92	18.5817	2.3310	3.8952	12.54%
0.6 - 6	1343.9	20.9127	23.20	-76.06	5.90	18.5817	2.3310	3.8952	12.54%
0.6 - 6	1464.3	20.9124	23.50	-74.78	5.89	18.5817	2.3307	3.8952	12.54%
0.7 - 6	0.0	16.5802	/	/	/	14.7205	1.8597	2.6568	12.63%
0.7 - 6	676.5	16.5776	23.00	-1.47	4.18	14.7205	1.8571	2.6568	12.62%
0.7 - 6	698.6	16.5749	22.80	-14.11	5.16	14.7205	1.8544	2.6568	12.60%
0.7 - 6	768.8	16.5740	22.30	-49.12	5.71	14.7205	1.8535	2.6568	12.59%
0.7 - 6	841.5	16.5734	21.90	-60.64	5.80	14.7205	1.8529	2.6568	12.59%
0.7 - 6	935.5	16.5725	23.70	-66.41	5.84	14.7205	1.8520	2.6568	12.58%
0.7 - 6	984.3	16.5725	23.60	-64.27	5.82	14.7205	1.8520	2.6568	12.58%
0.7 - 6	1032.6	16.5729	21.80	-78.69	5.91	14.7205	1.8524	2.6568	12.58%
0.7 - 6	1104.7	16.5730	21.90	-83.21	5.94	14.7205	1.8525	2.6568	12.58%
0.7 - 6	1271.5	16.5731	23.20	-84.66	5.94	14.7205	1.8526	2.6568	12.59%
0.7 - 6	1344.0	16.5729	23.30	-76.26	23.30	14.7205	1.8524	2.6568	12.58%
0.7 - 6	1464.4	16.5736	23.10	-75.36	5.89	14.7205	1.8531	2.6568	12.59%

W/C Ratio - Sample Number	Sample Age (hours)	Sample Mass (g)	Temperature (°C)	Water Potential (MPa)	pF	Mass solids, Ms (g)	Mass Water, Mw (g)	Mass Cement, Msc (g)	Volumetric Water Content (%)
0.3 - 7	0.0	20.3628	/	/	/	18.1488	2.2140	7.3799	12.20%
0.3 - 7	678.0	20.3563	23.70	0.30	0.00	18.1488	2.2075	7.3799	12.16%
0.3 - 7	700.1	20.3504	23.60	0.02	0.00	18.1488	2.2016	7.3799	12.13%
0.3 - 7	770.7	20.3437	23.40	-0.02	2.34	18.1488	2.1949	7.3799	12.09%
0.3 - 7	843.5	20.3376	22.50	0.05	0.00	18.1488	2.1888	7.3799	12.06%
0.3 - 7	937.3	20.3350	23.20	-1.64	4.23	18.1488	2.1862	7.3799	12.05%
0.3 - 7	986.3	20.3323	23.30	-2.66	4.44	18.1488	2.1835	7.3799	12.03%
0.3 - 7	1034.5	20.3291	22.60	-5.44	4.75	18.1488	2.1803	7.3799	12.01%
0.3 - 7	1107.0	20.3265	23.20	-9.45	4.99	18.1488	2.1777	7.3799	12.00%
0.3 - 7	1273.6	20.3244	23.00	-13.19	5.14	18.1488	2.1756	7.3799	11.99%
0.3 - 7	1346.2	20.3226	22.70	-14.70	5.18	18.1488	2.1738	7.3799	11.98%
0.3 - 7	1466.1	20.3215	23.50	-17.99	5.27	18.1488	2.1727	7.3799	11.97%

0.4 - 7	0.0	22.6145	/	/	/	20.1223	2.4922	6.2305	12.39%
0.4 - 7	677.7	22.6085	24.20	0.00	0.00	20.1223	2.4862	6.2305	12.36%
0.4 - 7	700.0	22.6030	23.70	-1.10	4.06	20.1223	2.4807	6.2305	12.33%
0.4 - 7	772.5	22.5908	23.20	-23.35	5.38	20.1223	2.4685	6.2305	12.27%
0.4 - 7	774.3	22.5871	23.20	-25.26	5.42	20.1223	2.4648	6.2305	12.25%
0.4 - 7	844.2	22.5830	23.00	-19.80	5.31	20.1223	2.4607	6.2305	12.23%
0.4 - 7	937.8	22.5779	23.70	-21.44	5.35	20.1223	2.4556	6.2305	12.20%
0.4 - 7	986.2	22.5764	23.70	-24.76	5.41	20.1223	2.4541	6.2305	12.20%
0.4 - 7	1033.8	22.5752	23.20	-29.37	5.48	20.1223	2.4529	6.2305	12.19%
0.4 - 7	1106.5	22.5676	23.10	-36.00	5.57	20.1223	2.4453	6.2305	12.15%
0.4 - 7	1273.0	22.5664	23.10	-37.85	5.59	20.1223	2.4441	6.2305	12.15%
0.4 - 7	1345.8	22.5660	23.60	-40.95	5.63	20.1223	2.4437	6.2305	12.14%
0.4 - 7	1464.7	22.5657	23.50	-43.49	5.65	20.1223	2.4434	6.2305	12.14%
0.5 - 7	0.0	18.3925	/	/	/	16.3489	2.0436	4.0872	12.50%
0.5 - 7	677.4	18.3887	23.90	0.36	0.00	16.3489	2.0398	4.0872	12.48%
0.5 - 7	700.1	18.3855	22.90	-0.37	3.58	16.3489	2.0366	4.0872	12.46%
0.5 - 7	772.3	18.3825	23.50	-1.34	4.14	16.3489	2.0336	4.0872	12.44%
0.5 - 7	844.3	18.3798	23.20	-1.59	4.22	16.3489	2.0309	4.0872	12.42%
0.5 - 7	937.9	18.3774	23.10	-2.31	4.38	16.3489	2.0285	4.0872	12.41%
0.5 - 7	986.2	18.3745	23.20	-2.53	4.42	16.3489	2.0256	4.0872	12.39%
0.5 - 7	1034.8	18.3709	23.60	-5.63	4.77	16.3489	2.0220	4.0872	12.37%
0.5 - 7	1107.3	18.3686	23.40	-7.01	4.86	16.3489	2.0197	4.0872	12.35%
0.5 - 7	1273.9	18.3673	22.40	-13.16	5.13	16.3489	2.0184	4.0872	12.35%
0.5 - 7	1346.1	18.3655	23.00	-16.56	5.23	16.3489	2.0166	4.0872	12.33%
0.5 - 7	1466.1	18.3641	23.00	-20.53	5.33	16.3489	2.0152	4.0872	12.33%
0.6 - 7	0.0	20.6209	/	/	/	18.3171	2.3038	3.8397	12.58%
0.6 - 7	677.7	20.6153	23.50	0.46	0.00	18.3171	2.2982	3.8397	12.55%
0.6 - 7	700.2	20.6125	23.90	-0.32	3.52	18.3171	2.2954	3.8397	12.53%
0.6 - 7	772.3	20.6097	23.70	-0.56	3.76	18.3171	2.2926	3.8397	12.52%
0.6 - 7	844.6	20.6069	23.50	-1.09	4.05	18.3171	2.2898	3.8397	12.50%
0.6 - 7	938.1	20.6049	23.90	-1.03	4.03	18.3171	2.2878	3.8397	12.49%
0.6 - 7	986.8	20.6017	23.70	-1.32	4.10	18.3171	2.2846	3.8397	12.47%

0.6 - 7	1036.3	20.5980	22.70	-2.41	4.40	18.3171	2.2809	3.8397	12.45%
0.6 - 7	1107.7	20.5952	23.30	-3.03	4.50	18.3171	2.2781	3.8397	12.44%
0.6 - 7	1274.2	20.5919	23.60	-5.08	4.72	18.3171	2.2748	3.8397	12.42%
0.6 - 7	1346.4	20.5897	23.40	-6.79	4.85	18.3171	2.2726	3.8397	12.41%
0.6 - 7	1466.6	18.9221	22.70	-9.28	4.98	18.3171	0.6050	3.8397	3.30%
0.7 - 7	0.0	23.3595	/	/	/	20.7394	2.6201	3.7431	12.63%
0.7 - 7	677.8	23.3491	24.10	0.02	0.00	20.7394	2.6097	3.7431	12.58%
0.7 - 7	700.1	23.3458	24.10	-0.29	3.47	20.7394	2.6064	3.7431	12.57%
0.7 - 7	772.6	23.3396	23.80	-0.32	3.51	20.7394	2.6002	3.7431	12.54%
0.7 - 7	844.6	23.3362	23.70	-0.60	3.80	20.7394	2.5968	3.7431	12.52%
0.7 - 7	938.5	23.3320	24.00	-0.82	3.93	20.7394	2.5926	3.7431	12.50%
0.7 - 7	986.9	23.3278	24.10	-1.09	4.05	20.7394	2.5884	3.7431	12.48%
0.7 - 7	1036.3	23.3243	23.90	-1.40	4.16	20.7394	2.5849	3.7431	12.46%
0.7 - 7	1108.1	23.3197	23.10	-2.95	4.49	20.7394	2.5803	3.7431	12.44%
0.7 - 7	1274.3	23.3165	23.70	-4.08	4.63	20.7394	2.5771	3.7431	12.43%
0.7 - 7	1346.7	23.3129	23.30	-6.44	4.82	20.7394	2.5735	3.7431	12.41%
0.7 - 7	1467.0	23.3101	23.20	-7.84	4.91	20.7394	2.5707	3.7431	12.40%

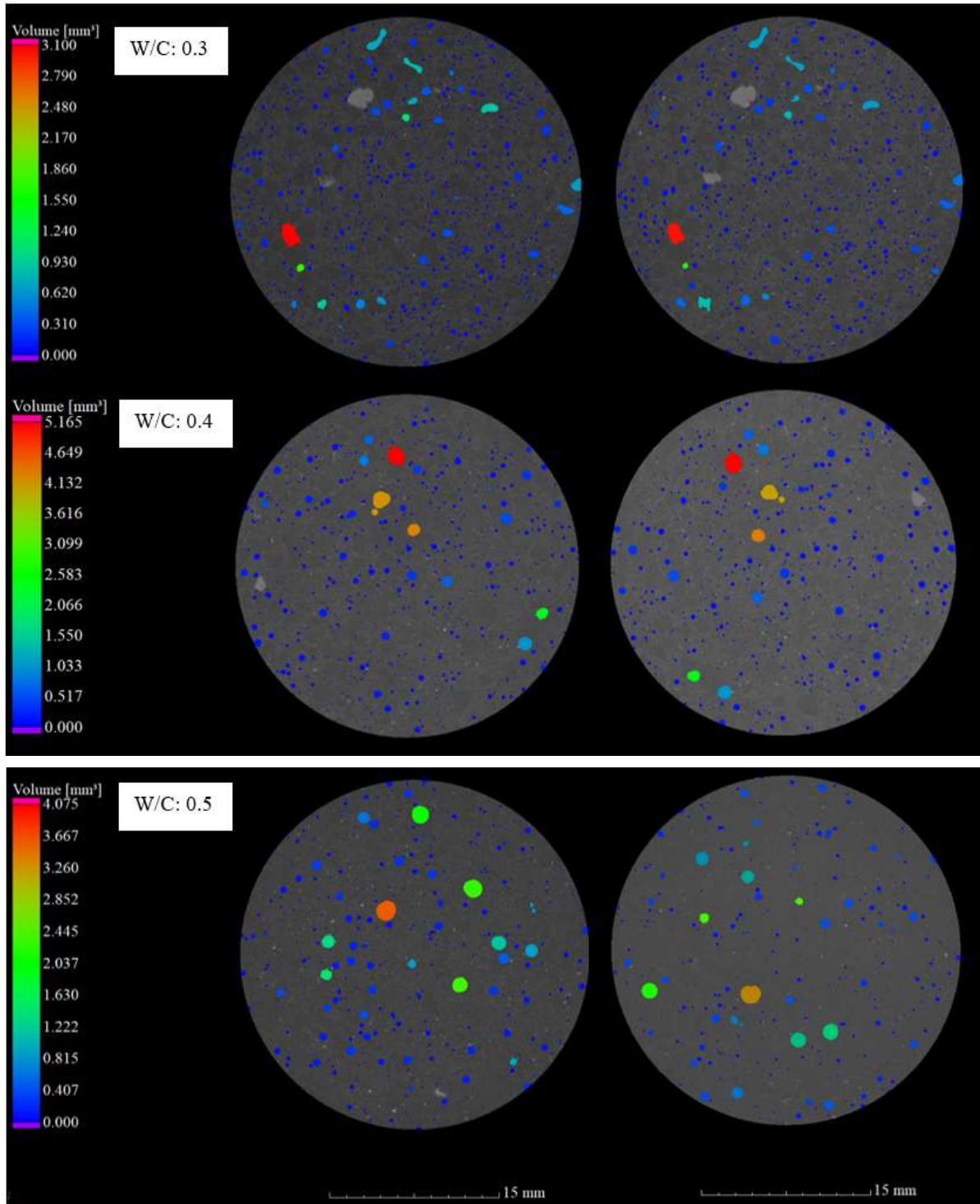
APPENDIX E

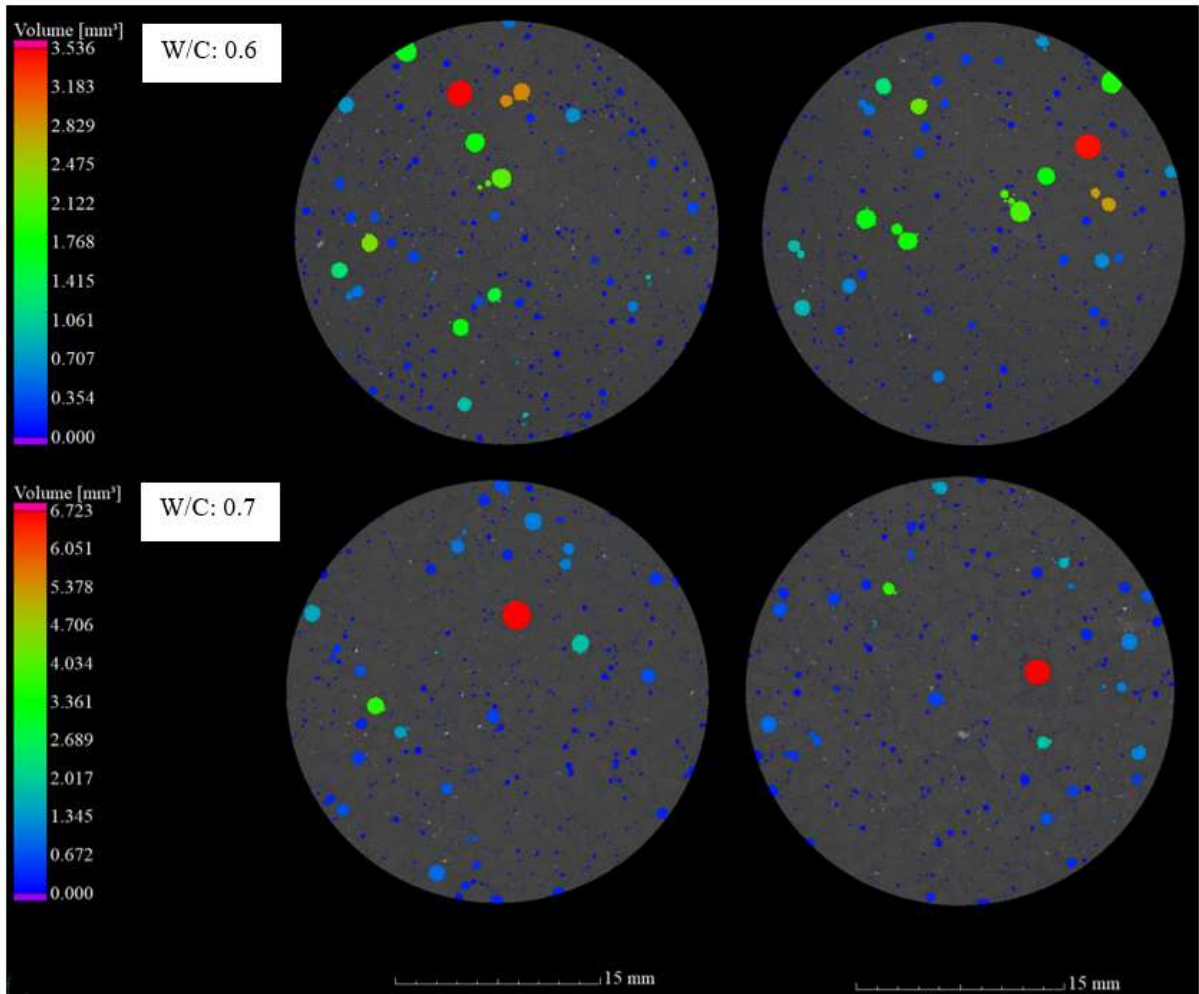
X-RAY RESULTS (IMAGES)

DRY SAMPLES:

7 DAYS

28 DAYS

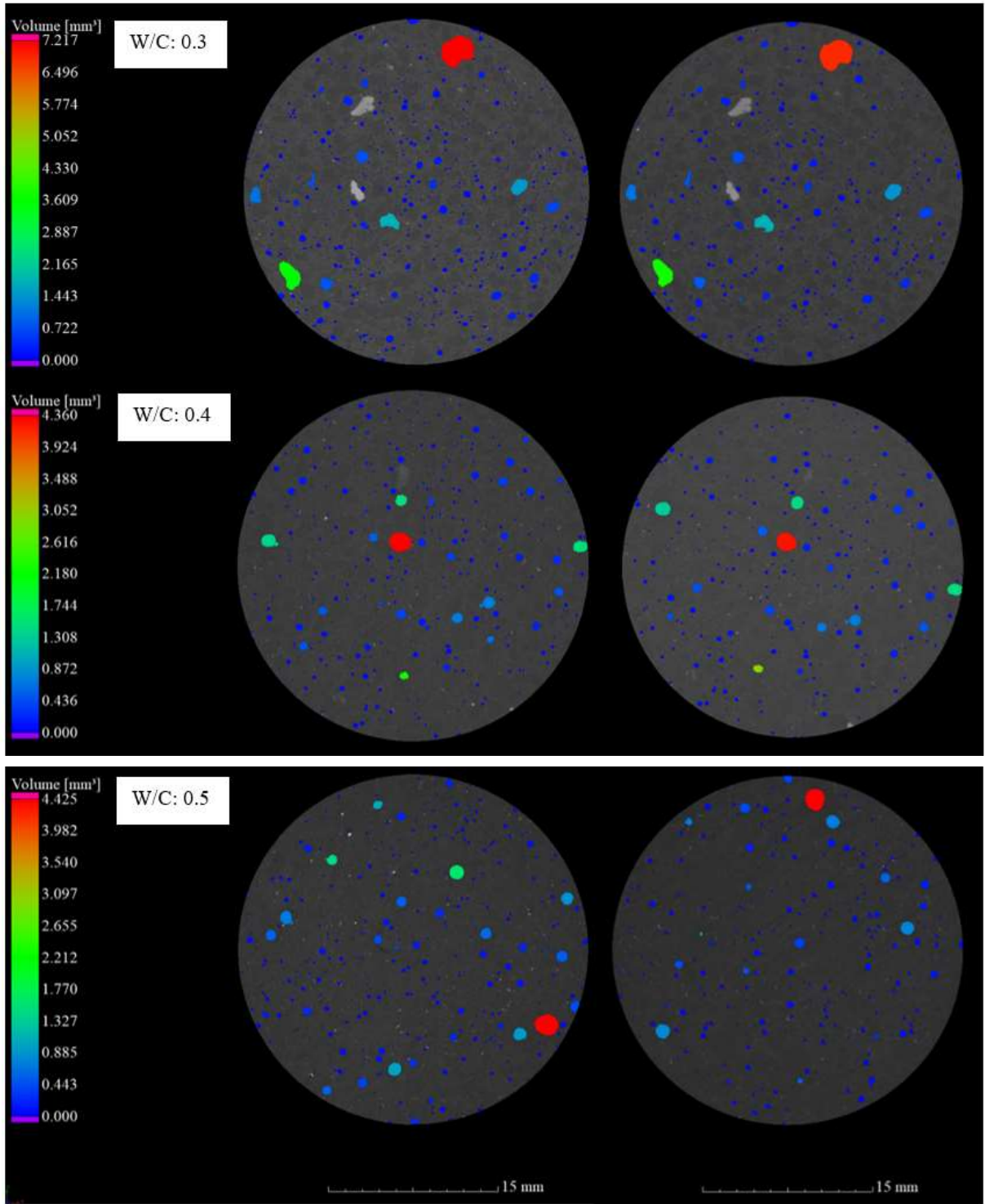


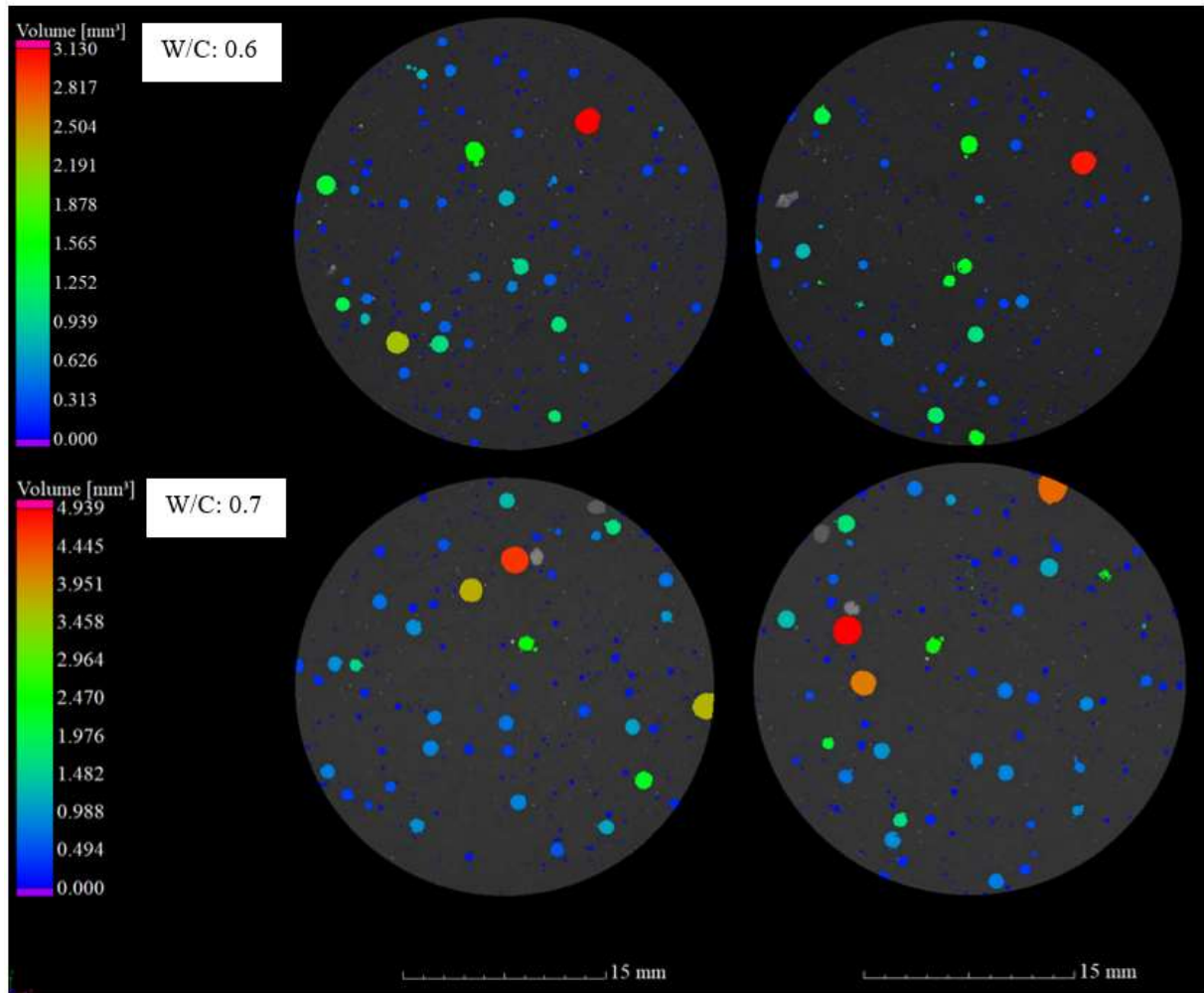


WET SAMPLES:

7 DAYS

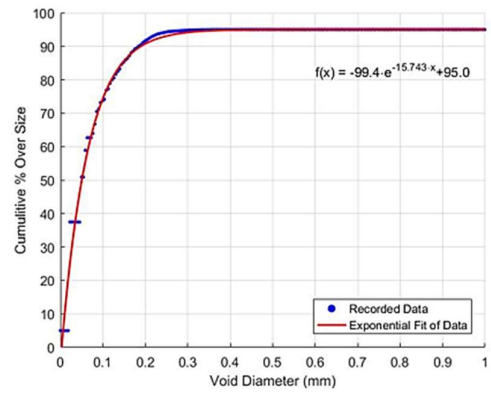
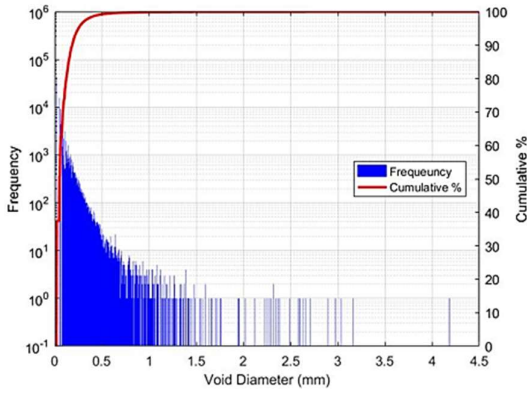
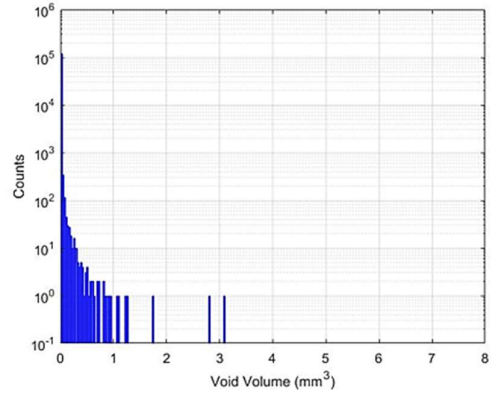
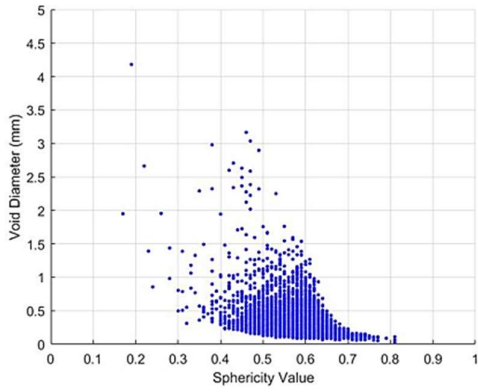
28 DAYS



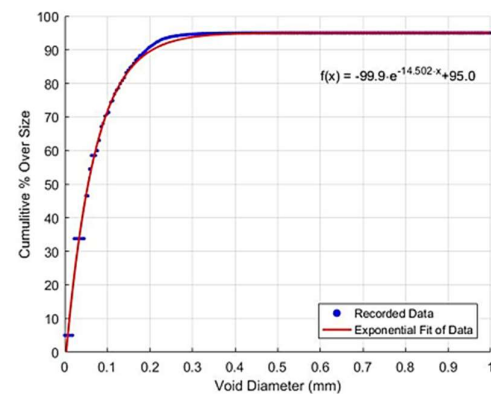
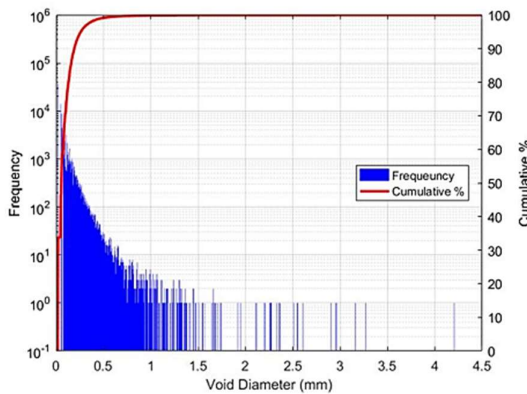
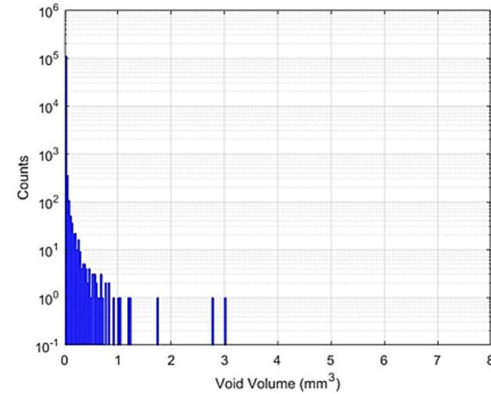
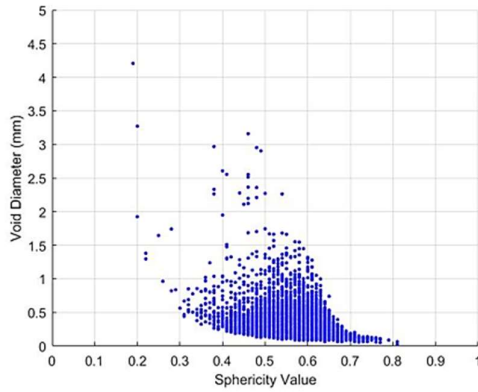


APPENDIX F

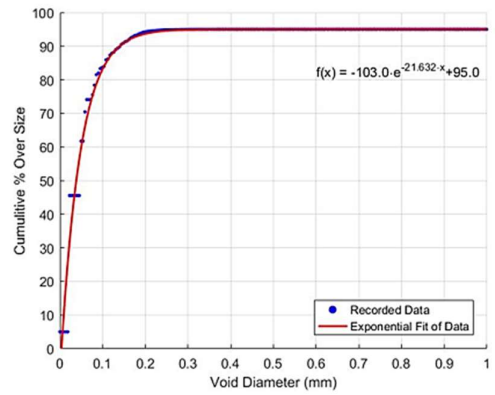
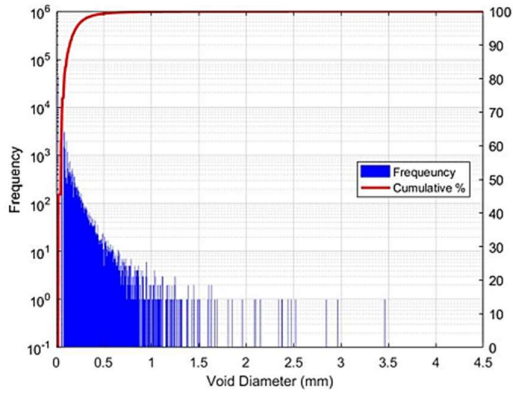
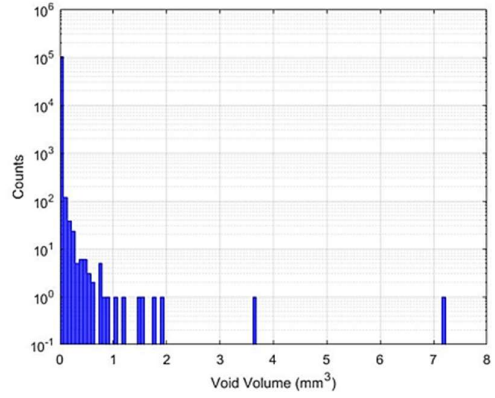
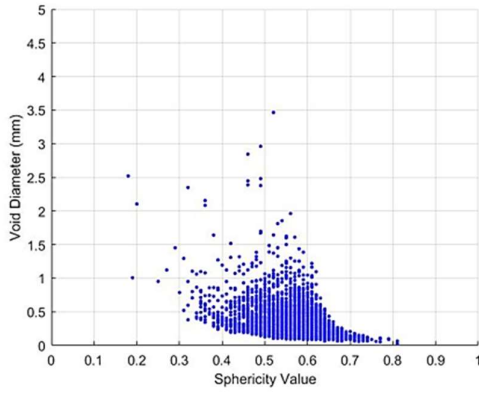
X-RAY RESULTS (GRAPHS)



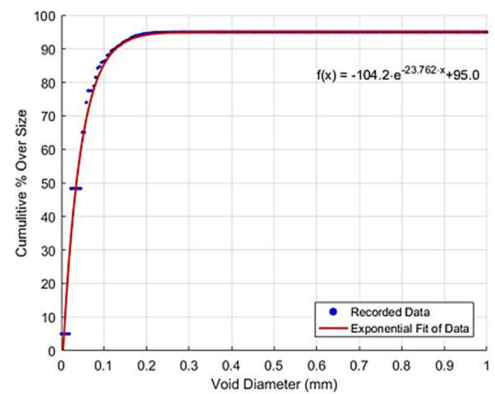
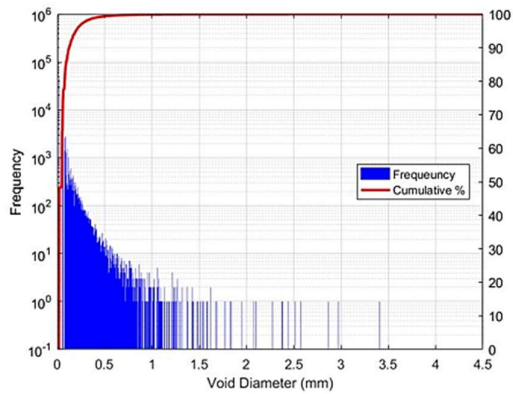
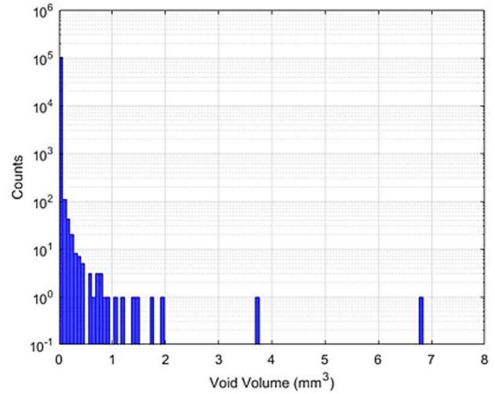
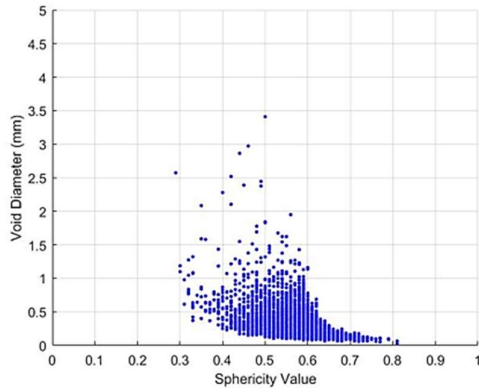
Dry 0.3 W/C Ratio Sample Results after 7 Days.



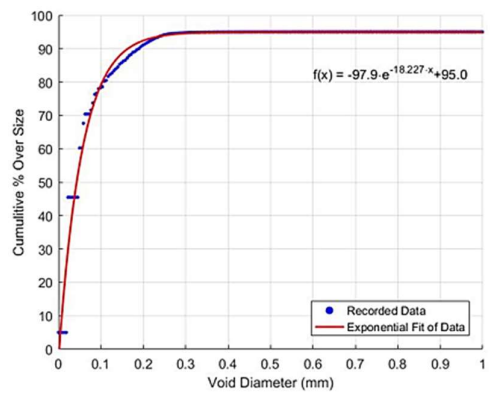
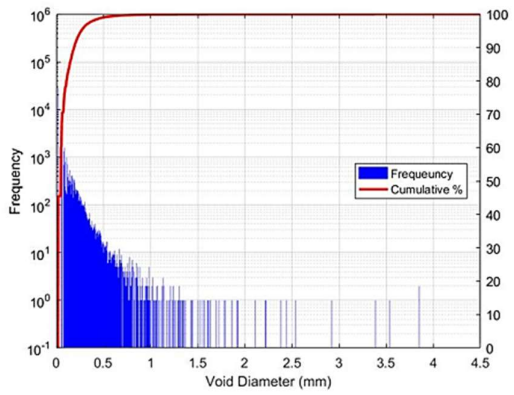
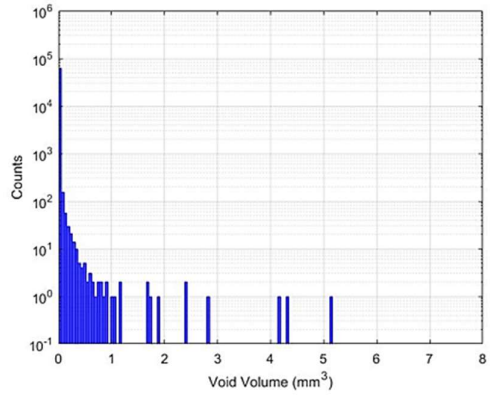
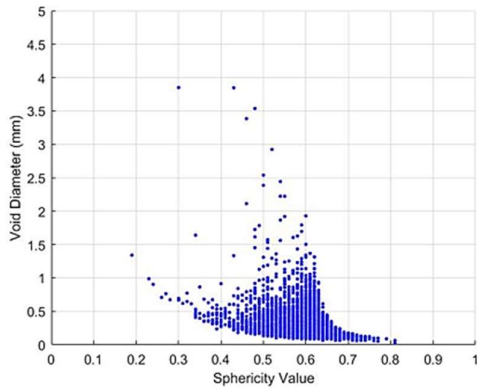
Dry 0.3 W/C Ratio Sample Results after 28 Days.



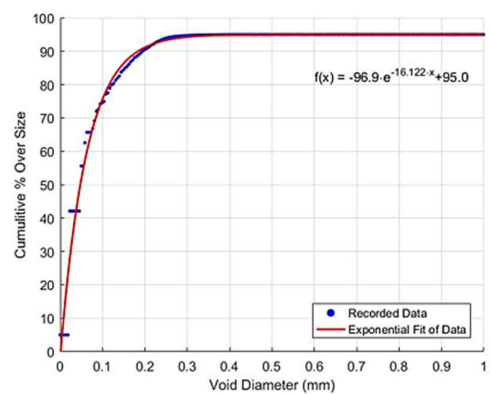
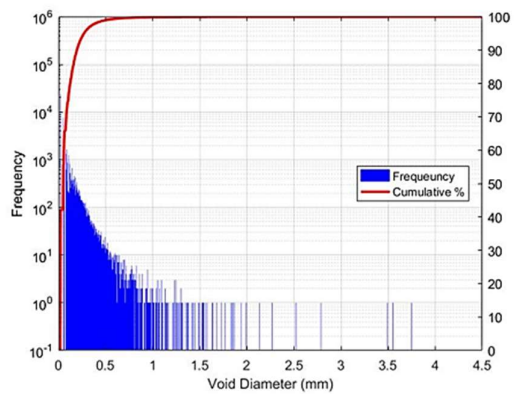
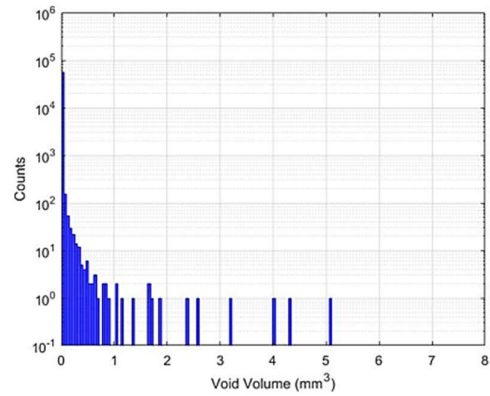
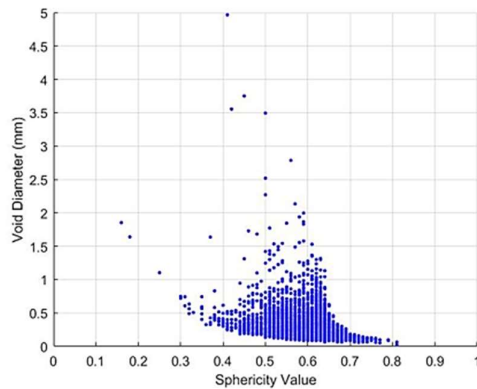
Wet 0.3 W/C Ratio Sample Results after 7 Days.



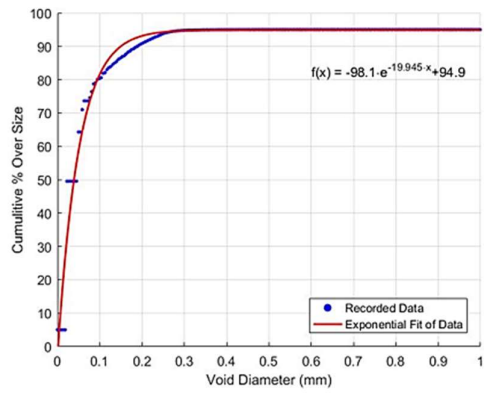
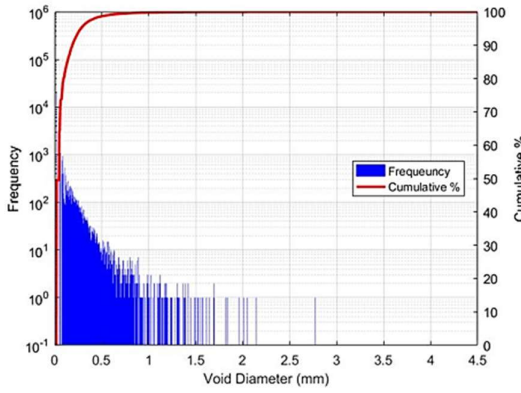
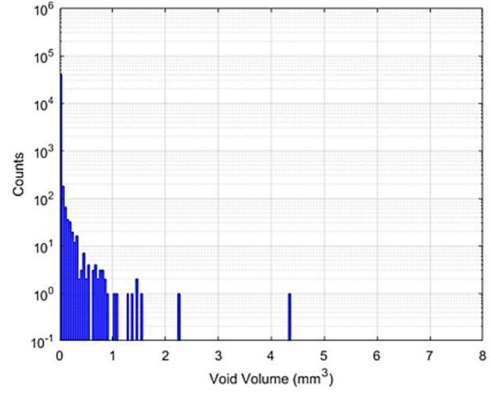
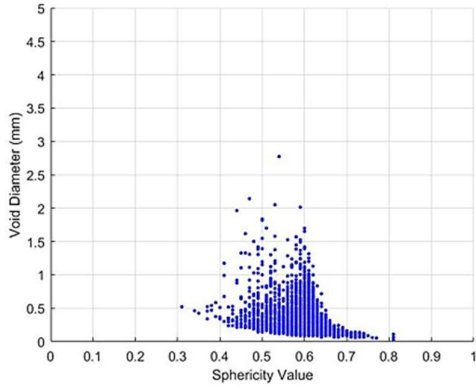
Wet 0.3 W/C Ratio Sample Results after 28 Days.



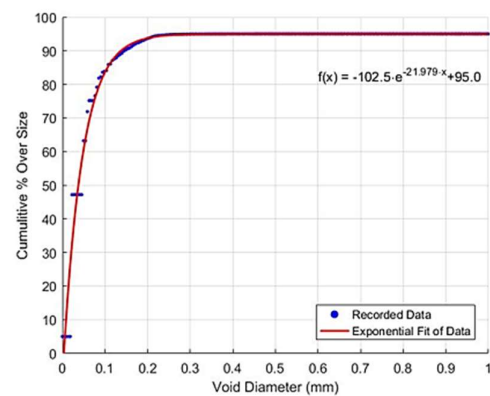
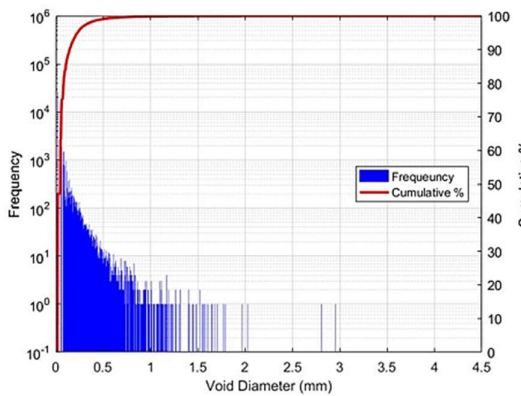
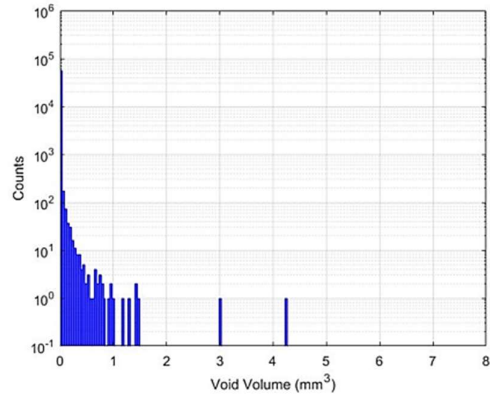
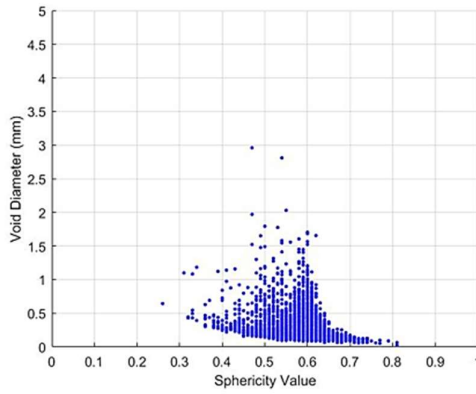
Dry 0.4 W/C Ratio Sample Results after 7 Days.



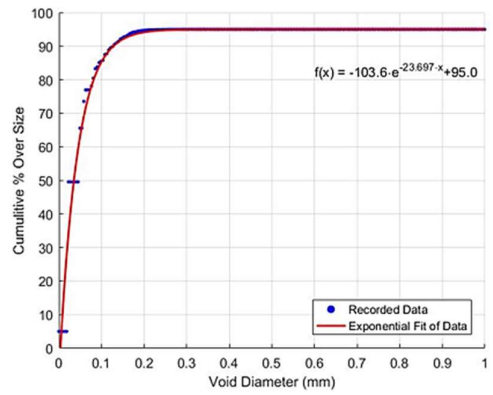
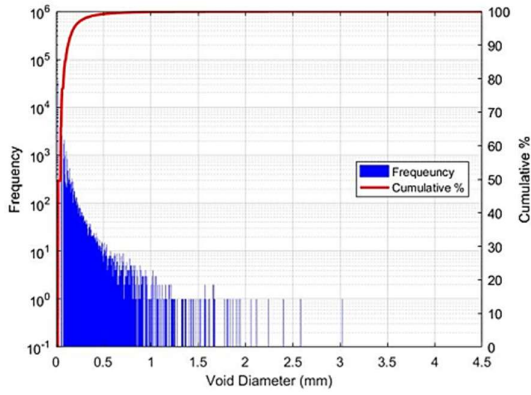
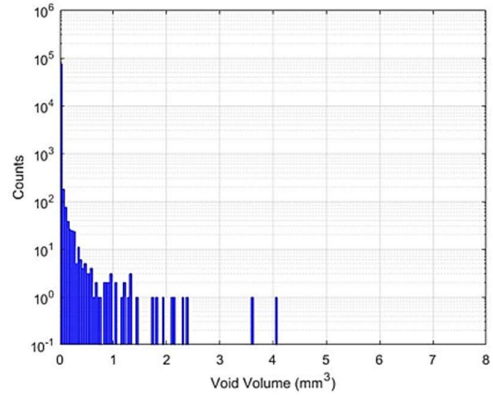
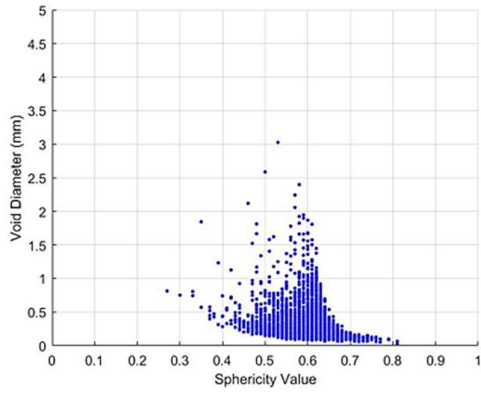
Dry 0.4 W/C Ratio Sample Results after 28 Days.



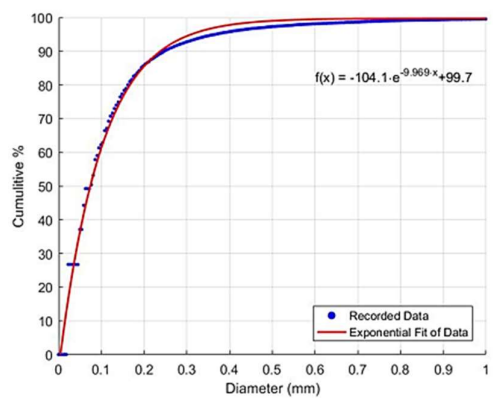
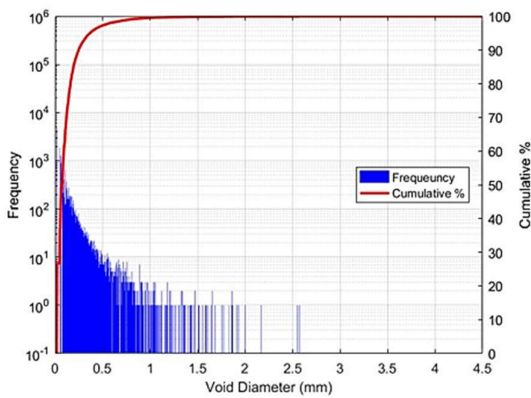
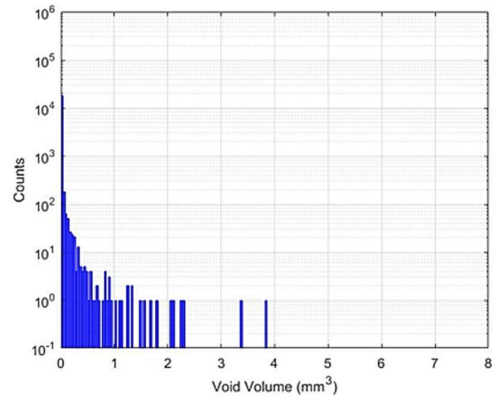
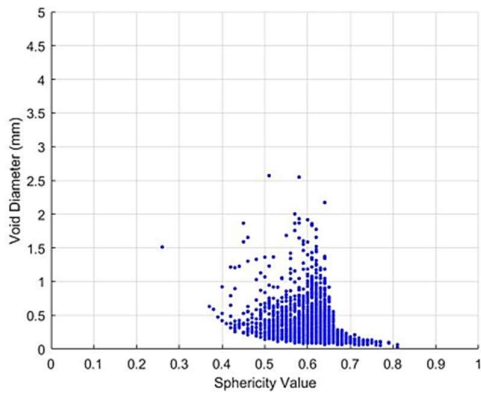
Wet 0.4 W/C Ratio Sample Results after 7 Days.



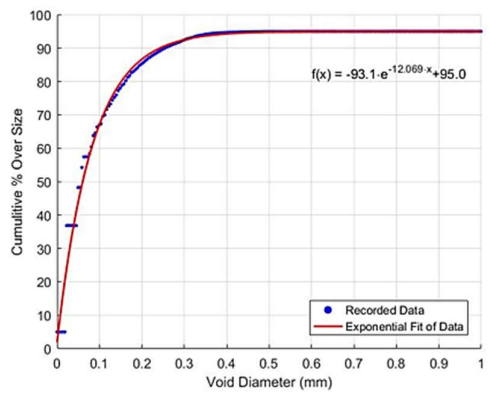
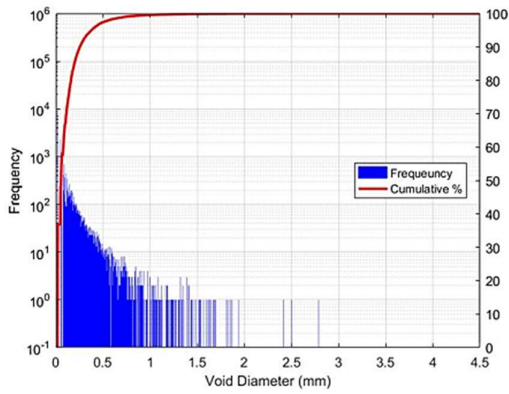
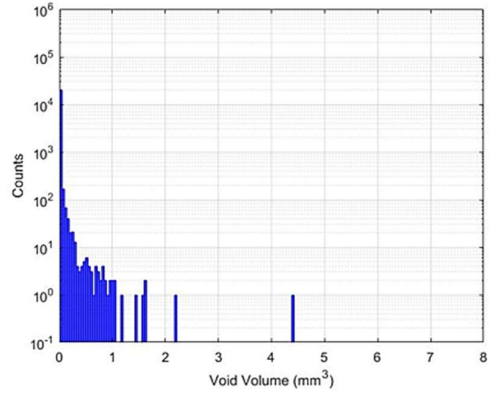
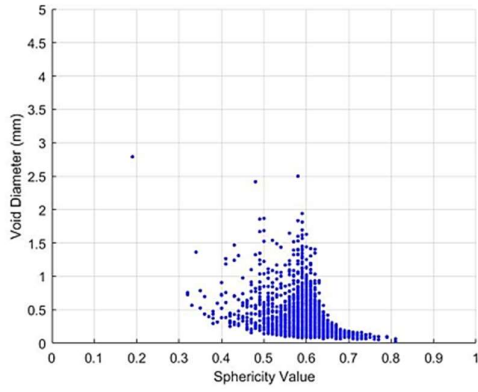
Wet 0.4 W/C Ratio Sample Results after 28 Days.



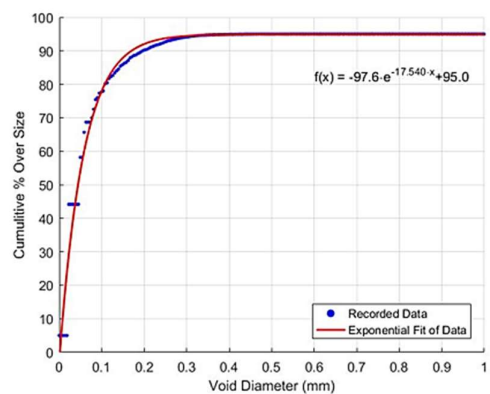
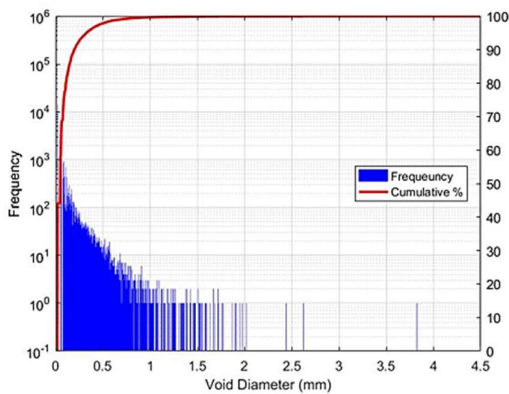
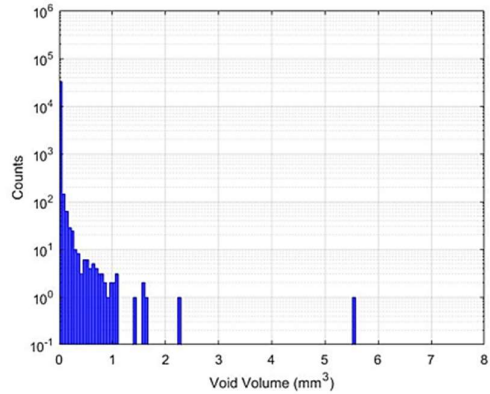
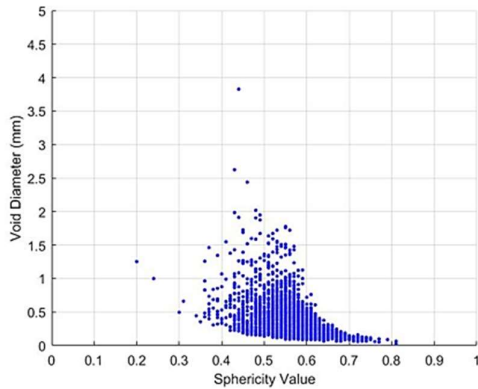
Dry 0.5 W/C Ratio Sample Results after 7 Days.



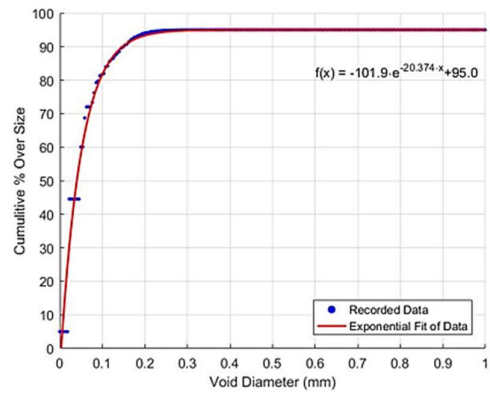
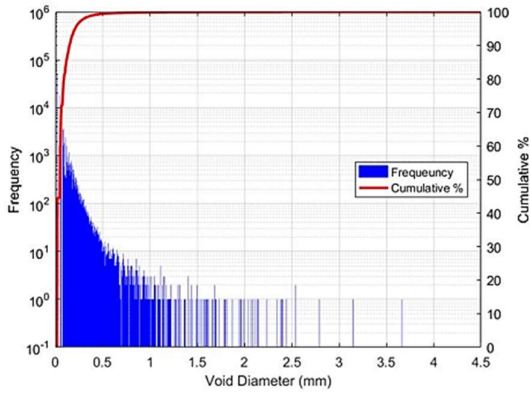
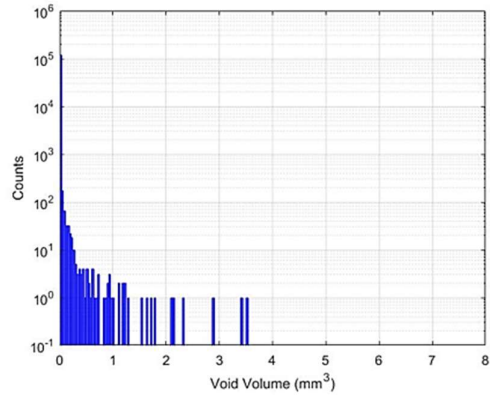
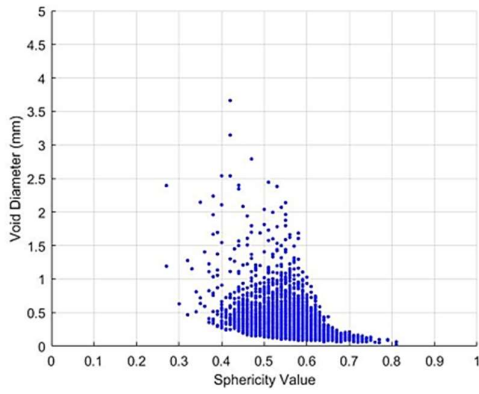
Dry 0.5 W/C Ratio Sample Results after 28 Days.



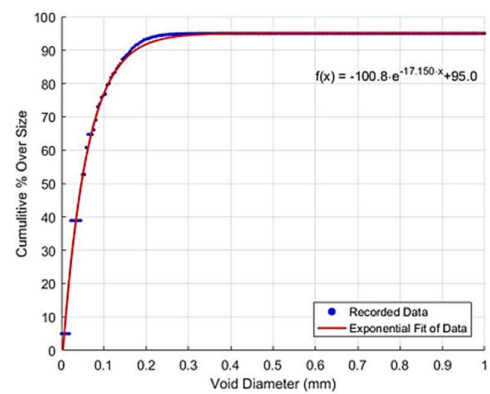
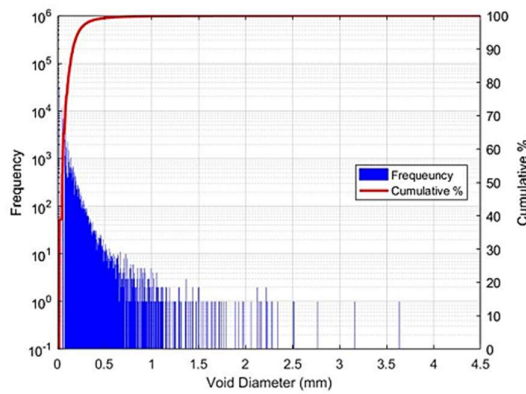
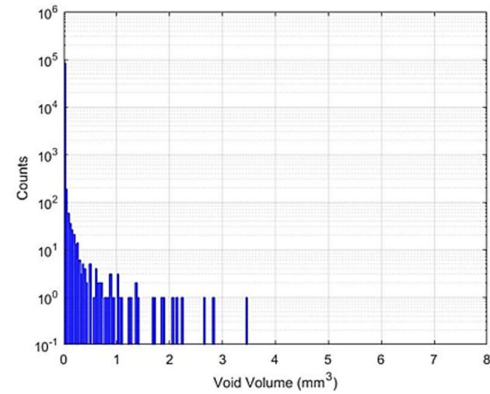
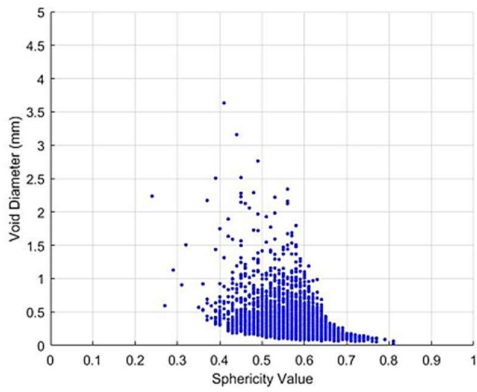
Wet 0.5 W/C Ratio Sample Results after 7 Days.



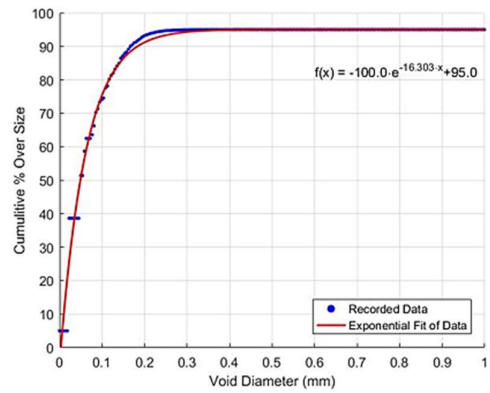
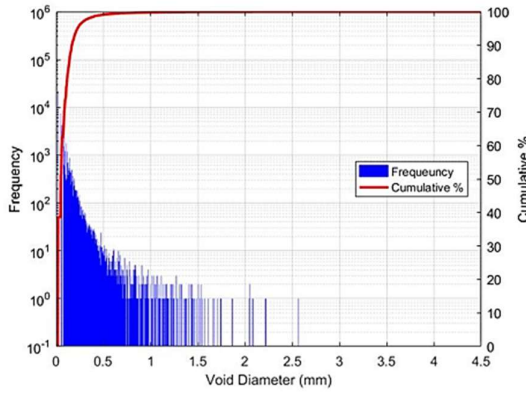
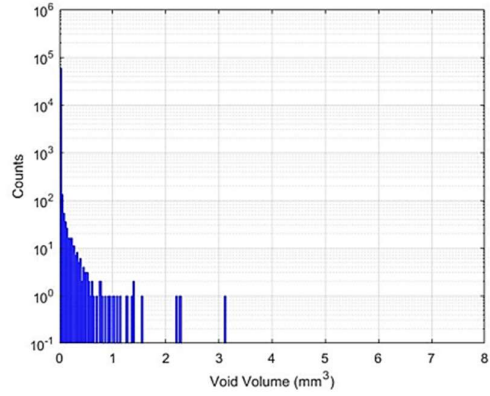
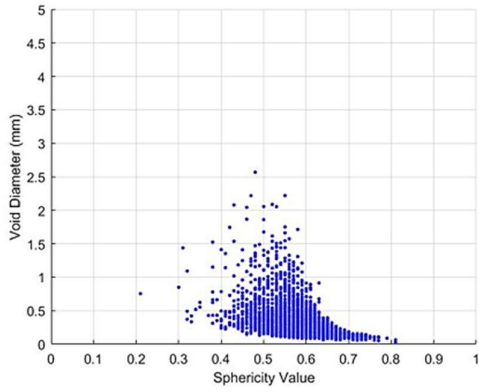
Wet 0.5 W/C Ratio Sample Results after 28 Days.



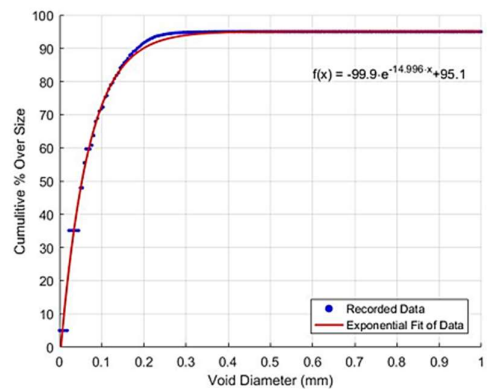
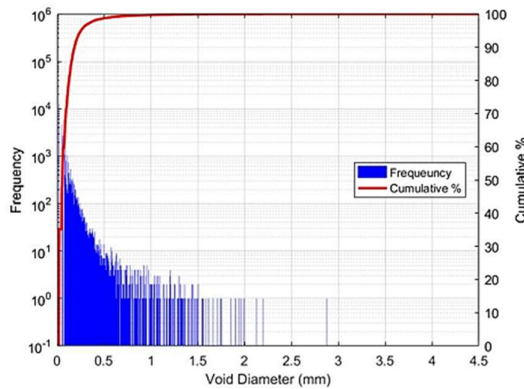
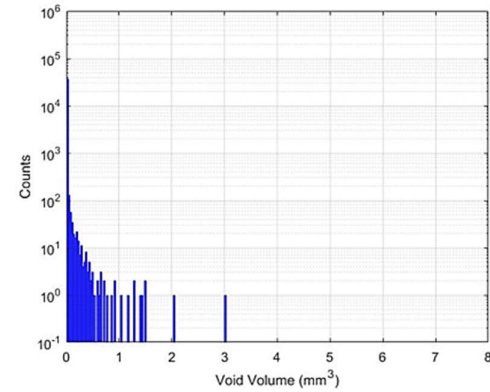
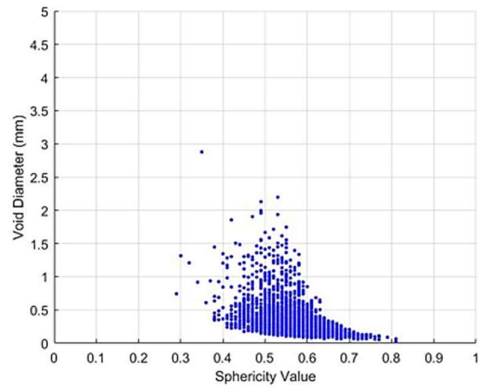
Dry 0.6 W/C Ratio Sample Results after 7 Days.



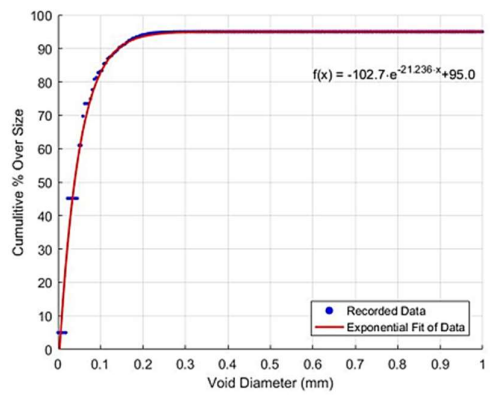
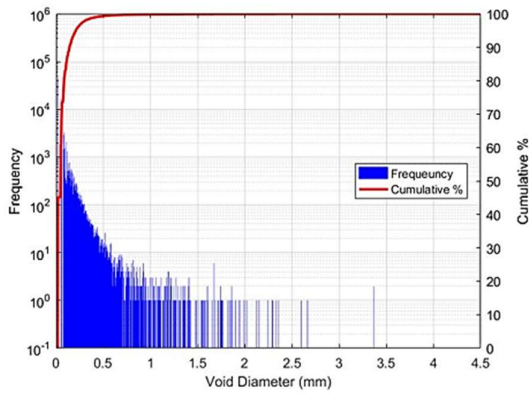
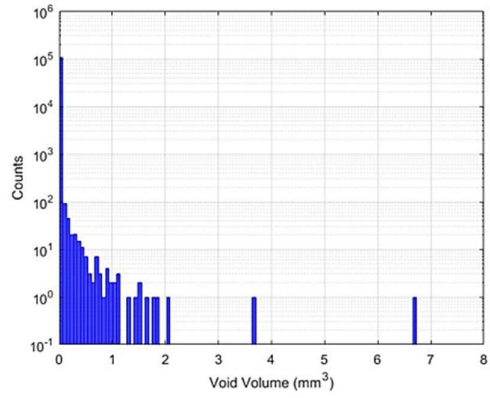
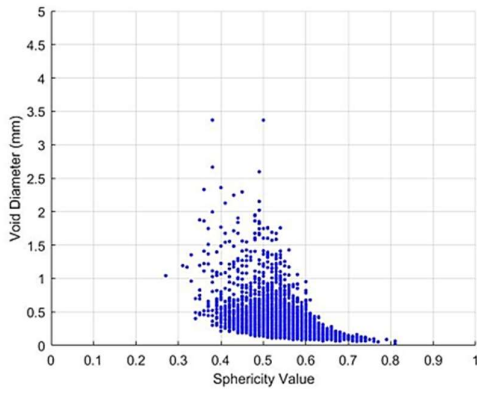
Dry 0.6 W/C Ratio Sample Results after 28 Days.



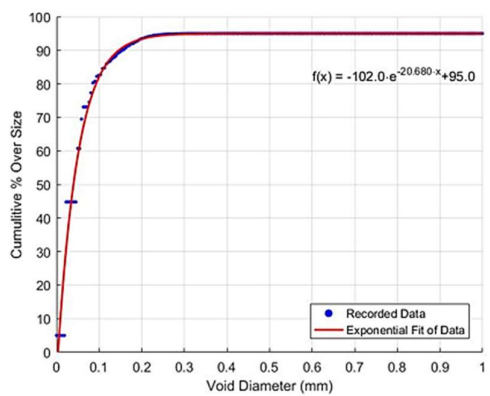
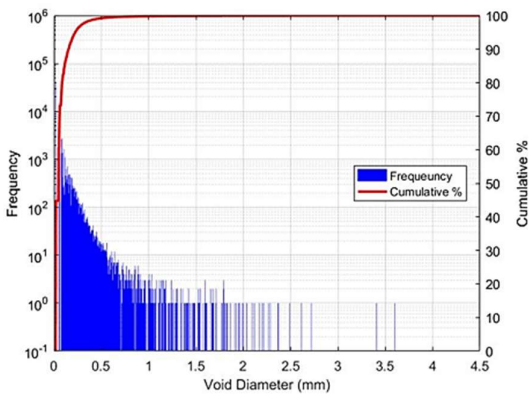
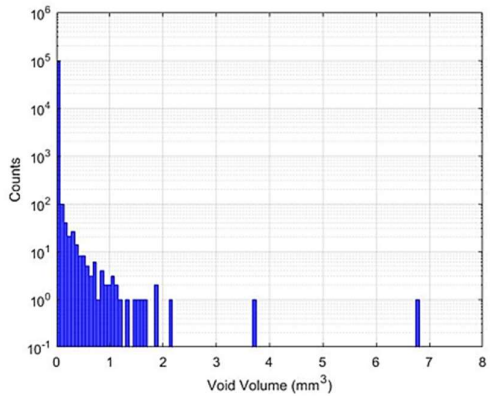
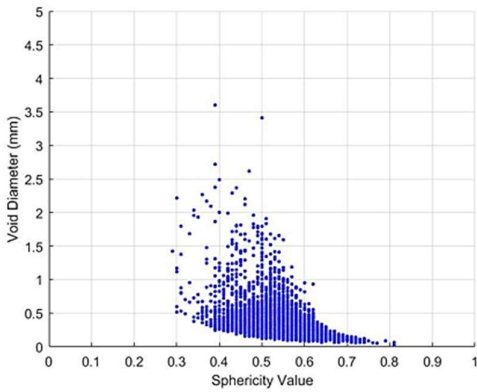
Wet 0.6 W/C Ratio Sample Results after 7 Days.



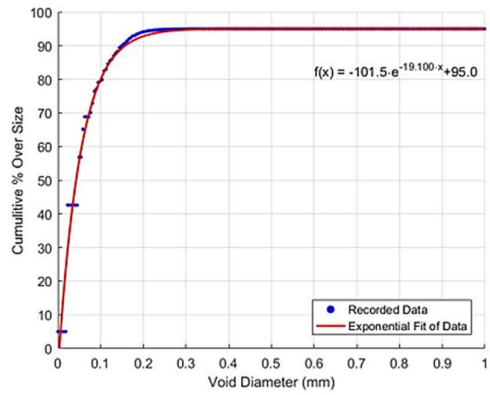
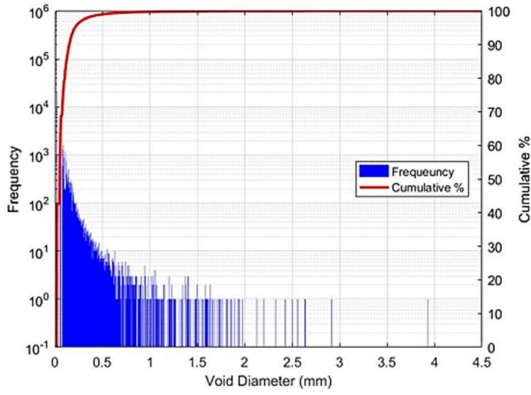
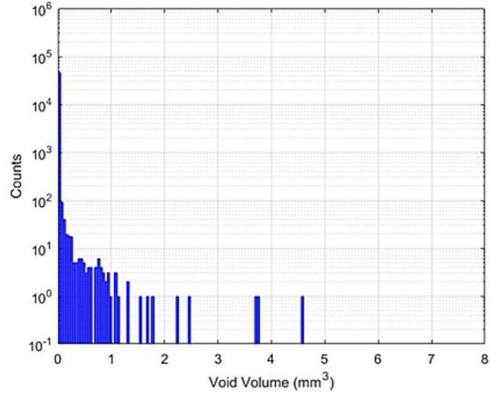
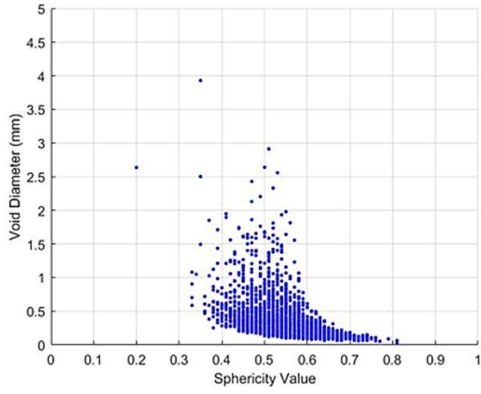
Wet 0.6 W/C Ratio Sample Results after 28 Days.



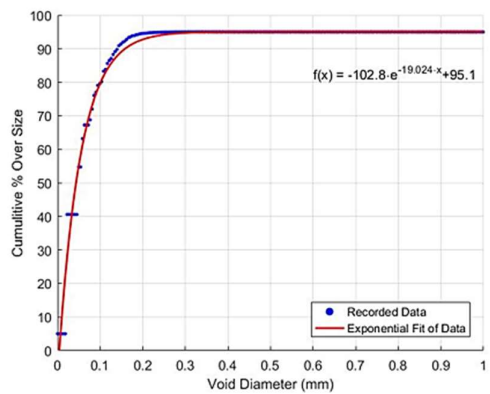
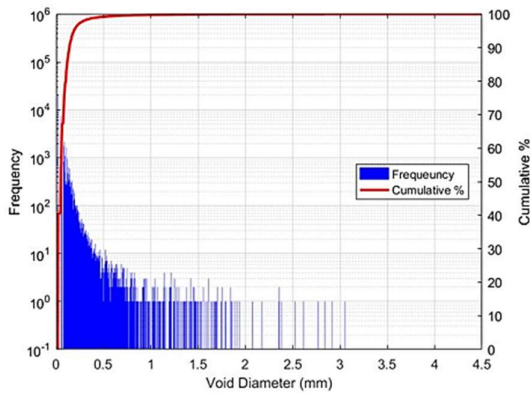
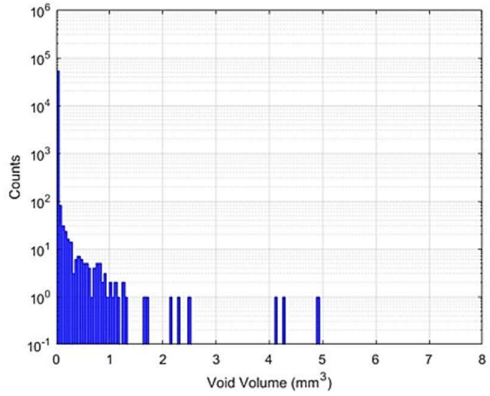
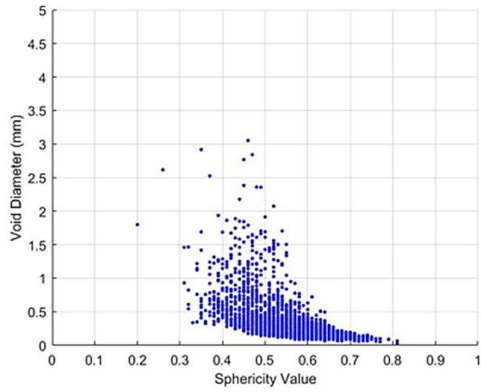
Dry 0.7 W/C Ratio Sample Results after 7 Days.



Dry 0.7 W/C Ratio Sample Results after 28 Days.



Wet 0.7 W/C Ratio Sample Results after 7 Days.



Wet 0.7 W/C Ratio Sample Results after 28 Days.

APPENDIX G

X-RAY RESULTS (MATLAB SCRIPT)

```

1 clc
2 clear all
3
4 %%%%%%%%%%%%%%%%%%%%%%%%%%%%%%%%%%%%%%%%%%%%%%%%%%%%%%%%%%%%%%%%%%%%%%%%%
5 %%%%%%%%%%%%%%%%%%%%%%%%%%%%%%%%%%%%%%%%%%%%%%%%%%%%%%%%%%%%%%%%%%%%%%%%% Import File Working With %%%%%%%%%%%%%%%%%%%%%%%%%%%%%%%%%%%%%%%%%%%%%%%%%%%%%%%%%%%%%%%%%%%%%%%%%
6 %%%%%%%%%%%%%%%%%%%%%%%%%%%%%%%%%%%%%%%%%%%%%%%%%%%%%%%%%%%%%%%%%%%%%%%%%
7
8 Table = readtable('D 7Days0_3.csv');
9
10 Radius = str2double(Table.Radius_mm_);
11 Diameter = str2double(Table.Diameter_mm_)/10^9;
12 Volume = str2double(Table.Volume_mm_)/10^9;
13 Sphericity = str2double(Table.Sphericity)/100;
14 Voxel      = Table.Voxel;
15 Surface    = str2double(Table.Surface_mm_);
16 Compactness = str2double(Table.Compactness);
17
18
19 %%%%%%%%%%%%%%%%%%%%%%%%%%%%%%%%%%%%%%%%%%%%%%%%%%%%%%%%%%%%%%%%%%%%%%%%%
20 %%%%%%%%%%%%%%%%%%%%%%%%%%%%%%%%%%%%%%%%%%%%%%%%%%%%%%%%%%%%%%%%%%%%%%%%% Start Plotting Figures %%%%%%%%%%%%%%%%%%%%%%%%%%%%%%%%%%%%%%%%%%%%%%%%%%%%%%%%%%%%%%%%%%%%%%%%%
21 %%%%%%%%%%%%%%%%%%%%%%%%%%%%%%%%%%%%%%%%%%%%%%%%%%%%%%%%%%%%%%%%%%%%%%%%%
22
23 nbins = 100; %Changing Thickness of bins
24
25
26 figure(1); %Plot Void Diameter vs Sphericity
27
28 scatter(Sphericity,Diameter, 7, 'b','filled' );
29
30 ylabel('Void Diameter (mm)');
31 xlabel('Sphericity Value');
32 xlim([0 1]);
33 ylim([0 5]);
34 grid('on');
35
36
37 figure(2); %Plot Amount of Voids with Specific Volume
38
39 %Count number of vals in ranges
40
41 histogram(Volume, nbins, 'DisplayStyle','bar', 'FaceColor', 'b', 'EdgeColor','b'
, 'FaceAlpha',0.75);
42 set(gca,'yscale','log');
43
44 ylabel('Counts');
45 xlabel('Void Volume (mm^3)');
46 xlim([0 8]);
47 ylim([0.1 10^6]);
48 grid('on');
49
50 figure(3); %Plot Cumulative Percentage of Diameter and Frequency
51
52 nbins = 1000;
53 diameter_max = 4.5;
54 diameter_min = 0;
55 range = diameter_max/nbins;
56 a = length(Diameter);
57 counter = zeros(1,nbins);
58 counter_2 = zeros(1,nbins);
59 range_array = zeros(1,nbins);

```

```

60
61 for i = 1 : nbins
62
63     for j = 1 : length(Diameter)
64         if (i-1)*range < Diameter(j)
65             if Diameter(j) < i*range
66                 counter(i) = counter(i) + 1;
67             end
68         end
69     end
70
71     if i > 1
72         counter_2(i) = 100*counter(i)/a + counter_2(i-1);
73     else
74         counter_2(i) = 100*counter(i)/a;
75     end
76
77     range_array(i) = (i-1)*range;
78 end
79
80 bar(range_array,counter, 1, 'b');
81 set(gca,'yscale','log');
82 ylim([0.1 10^6]);
83 xlim([0 diameter_max]);
84 grid();
85 ylabel('Frequency');
86 xlabel('Void Diameter (mm)');
87
88 hold on;
89
90 yyaxis right
91 ylabel('Cumulative %','Color','k');
92 ax = gca;
93 ax.YColor = 'k';
94 plot(range_array,counter_2, 'r', 'LineWidth',2);
95 ylim([0 100]);
96 xlim([0 diameter_max]);
97 legend('Frequency','Cumulative %');
98 set(legend,'Location','east');
99
100 hold off;
101
102
103 %***** Figure 4 *****
104 %Plot Cumulative Percentage of Diameter with Exponential Fit of Data
105
106 nbins2 = 1000;
107 diameter_max2 = 4.5;
108 diameter_min2 = 0;

```



```

120 range2 = diameter_max2/nbins2;
121 a2 = length(Diameter);
122 counter2 = zeros(1,nbins2);
123 counter_22 = zeros(1,nbins2);
124 range_array2 = zeros(1,nbins2);
125
126
127 %Better Fit of Data Excluding First 5% and Last 5% of Data if needed
128 dia_min2 = round(0.05*length(Diameter));
129 dia_max2 = round(0.95*length(Diameter));
130 Diameter_New2 = zeros(1,dia_max2-dia_min2);
131
132 for i = 1 : round(0.9*length(Diameter))
133
134     Diameter_New2(i) = Diameter(i + dia_min2); % Creates diameter array with
values from 5% to 95% of original array
135
136 end
137
138 for i = 1 : nbins2
139
140
141     for j = 1 : length(Diameter_New2)
142
143         if (i-1)*range2 < Diameter_New2(j)
144
145             if Diameter_New2(j) < i*range2
146
147                 counter2(i) = counter2(i) + 1;
148
149             end
150
151         end
152     end
153
154
155     if i > 1
156         counter_22(i) = 100*(counter2(i)/a2) + counter_22(i-1);
157
158     else
159
160         counter_22(i) = 100*(counter2(i)/a2) + 5;
161
162     end
163
164     range_array2(i) = (i-1)*range2;
165
166
167 end
168
169 %%%%%%%%%%%%%%%%%%%%%%%%%%%%%%%%%%%%%%%%%%%%%%%%%%%%%%%%%%%%%%%%%%%%%%%%%
170 %%%%%%%%%%%%%%%%%%%%%%%%%%%%%%%%%%%%%%%%%%%%%%%%%%%%%%%%%%%%%%%%%%%%%%%%% Scalped Range (5 - 95%) %%%%%%%%%%%%%%%%%%%%%%%%%%%%%%%%%%%%%%%%%%%%%%%%%%%%%%%%%%%%%%%%%%%%%%%%%
171 %%%%%%%%%%%%%%%%%%%%%%%%%%%%%%%%%%%%%%%%%%%%%%%%%%%%%%%%%%%%%%%%%%%%%%%%%
172
173
174 figure(4); %Plot Cumulative Percentage of Diameter with Exponential Fit of Data

```

```

175
176 ylabel('Cumulative % Over Size');
177 scatter(range_array2,counter_22, 7, 'b','filled' );
178 ylim([0 100]);
179 xlim([0 1]);
180 hold on
181 curve_array = zeros(nbins);
182
183 f = @(b,range_array2) b(1).*exp(b(2).*range_array2)+b(3);
184 B = fminsearch(@(b) norm(counter_22 - f(b,range_array2)) , [0; 0; 0]);
185
186 plot(range_array2, f(B,range_array2), 'r','linewidth', 1.5);
187
188 text(0.6, 83, sprintf('f(x) = %.1f\cdote^{%.3f\cdotx}%.1f', B));
189
190 ylabel('Cumulitive % Over Size');
191 xlabel('Void Diameter (mm)');
192 legend('Recorded Data','Exponential Fit of Data');
193 set(legend,'Location','southeast');
194
195 hold off;
196 grid();

```

APPENDIX H

MIP RESULTS



MICROMERITICS INSTRUMENT CORPORATION

AutoPore IV 9500 V1.09

Serial: 833

Port: 1/1

Page 1

Sample ID: 0.3 W_C
Operator: Ryno van der Merwe
Submitter: Mariesa Schoeman
File: C:\9500\DATA\000-370.SMP

LP Analysis Time: 2020/03/19 6:59:58PM
HP Analysis Time: 2020/03/23 10:27:50AM
Report Time: 2020/03/23 2:46:36PM
Sample Weight: 8.6817 g
Correction Type: Formula
Show Neg. Int: No

Summary Report

Penetrometer parameters

Penetrometer: #s/n - (03) 15 Bulb, 1.131 Stem, Solid
Pen. Constant: 22.508 µL/pF
Stem Volume: 1.1310 mL
Pen. Volume: 16.0019 mL
Pen. Weight: 80.2485 g
Max. Head Pressure: 4.4500 psia
Assembly Weight: 250.5856 g

Hg Parameters

Adv. Contact Angle: 130.000 degrees
Hg Surface Tension: 485.000 dynes/cm
Rec. Contact Angle: 130.000 degrees
Hg Density: 13.5335 g/mL

User Parameters

Param 1: 0.000 Param 2: 0.000 Param 3: 0.000

Low Pressure:

Evacuation Pressure: 50 µmHg
Evacuation Time: 30 mins
Mercury Filling Pressure: 0.52 psia
Equilibration Time: 10 secs

High Pressure:

Equilibration Time: 10 secs

Blank Correction by Formula

(From Pressure 7.54 to 60000.00 psia)

Intrusion Data Summary

Total Intrusion Volume = 0.0553 mL/g
Total Pore Area = 12.120 m²/g
Median Pore Diameter (Volume) = 0.0323 µm
Median Pore Diameter (Area) = 0.0076 µm
Average Pore Diameter (4V/A) = 0.0183 µm
Apparent (skeletal) Density = 2.4272 g/mL
Porosity = 11.8357 %
Stem Volume Used = 50 %

Pore Structure Summary

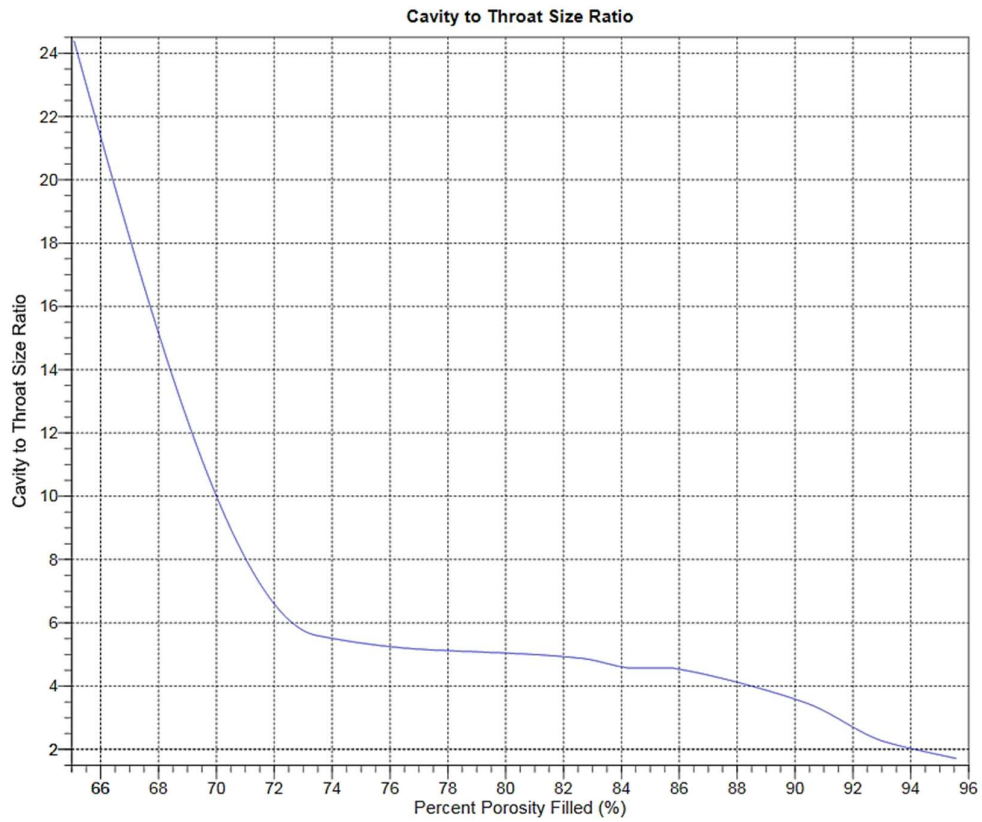
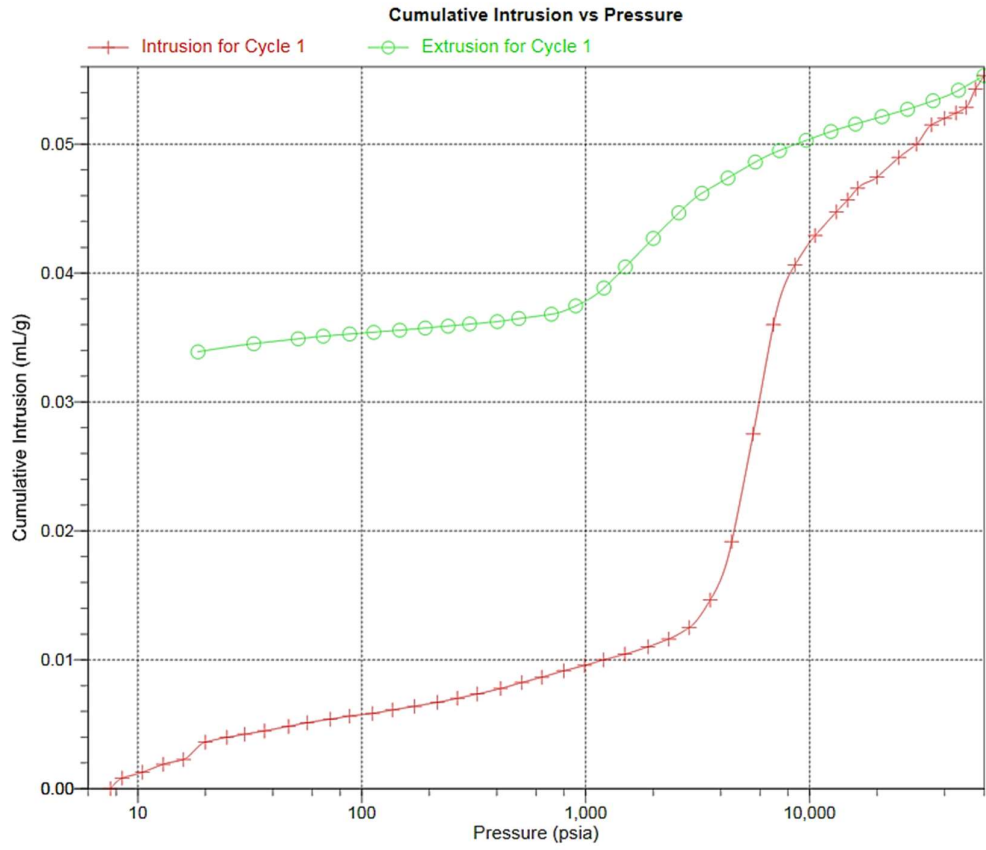
Threshold Pressure: 105.94 psia (Calculated)
Characteristic length = 1.7073 µm
Conductivity formation factor = 0.004
Permeability constant = 0.00442
Permeability = 0.0459 mDarcy
BET Surface Area = 230.0000 m²/g
Pore shape exponent = 1.00
Tortuosity factor = 0.006
Tortuosity = 37.2982
Percolation Fractal dimension = 1.822
Backbone Fractal dimension = 2.792

Mayer Stowe Summary

Interstitial porosity = 47.6300 %
Breakthrough pressure ratio = 3.3512

Material Compressibility

Linear Coefficient = N/A 1/psia
Quadratic Coefficient = N/A 1/psia²





MICROMERITICS INSTRUMENT CORPORATION

AutoPore IV 9500 V1.09

Serial: 833

Port: 1/1

Page 1

Sample ID: 0.5 W_C
Operator: Ryno van der Merwe
Submitter: Mariesa Schoeman
File: C:\9500\DATA\000-368.SMP

LP Analysis Time: 2020/03/17 3:09:44AM
HP Analysis Time: 2020/03/17 10:32:10AM
Report Time: 2020/03/23 2:50:03PM

Sample Weight: 10.8496 g
Correction Type: Formula
Show Neg. Int: No

Summary Report

Penetrometer parameters

Penetrometer: #s/n - (03) 15 Bulb, 1.131 Stem, Solid
Pen. Constant: 22.508 uL/pF
Stem Volume: 1.1310 mL
Pen. Volume: 16.0019 mL
Pen. Weight: 80.2464 g
Max. Head Pressure: 4.4500 psia
Assembly Weight: 239.7875 g

Hg Parameters

Adv. Contact Angle: 130.000 degrees
Hg Surface Tension: 485.000 dynes/cm
Rec. Contact Angle: 130.000 degrees
Hg Density: 13.5335 g/mL

User Parameters

Param 1: 0.000 Param 2: 0.000 Param 3: 0.000

Low Pressure:

Evacuation Pressure: 50 umHg
Evacuation Time: 30 mins
Mercury Filling Pressure: 0.52 psia
Equilibration Time: 10 secs

High Pressure:

Equilibration Time: 10 secs

Blank Correction by Formula

(From Pressure 5.96 to 60000.00 psia)

Intrusion Data Summary

Total Intrusion Volume = 0.0672 mL/g
Total Pore Area = 16.752 m^2/g
Median Pore Diameter (Volume) = 0.0410 um
Median Pore Diameter (Area) = 0.0060 um
Average Pore Diameter (4V/A) = 0.0160 um
Apparent (skeletal) Density = 2.5316 g/mL
Porosity = 14.5413 %
Stem Volume Used = 61 %

Pore Structure Summary

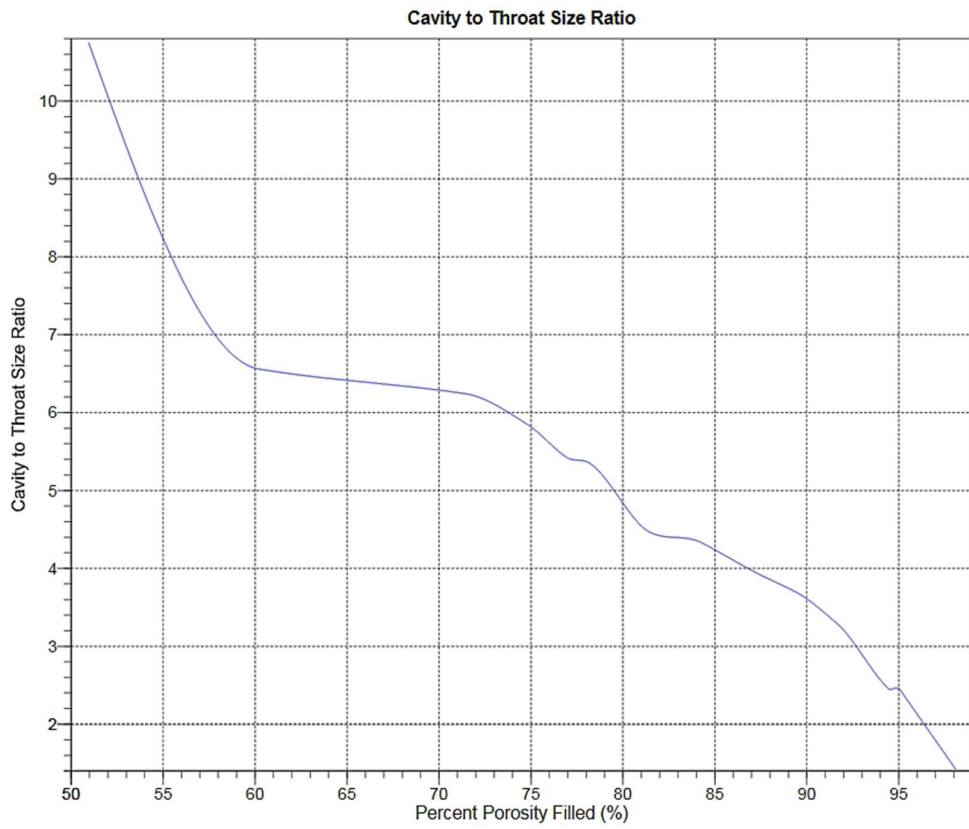
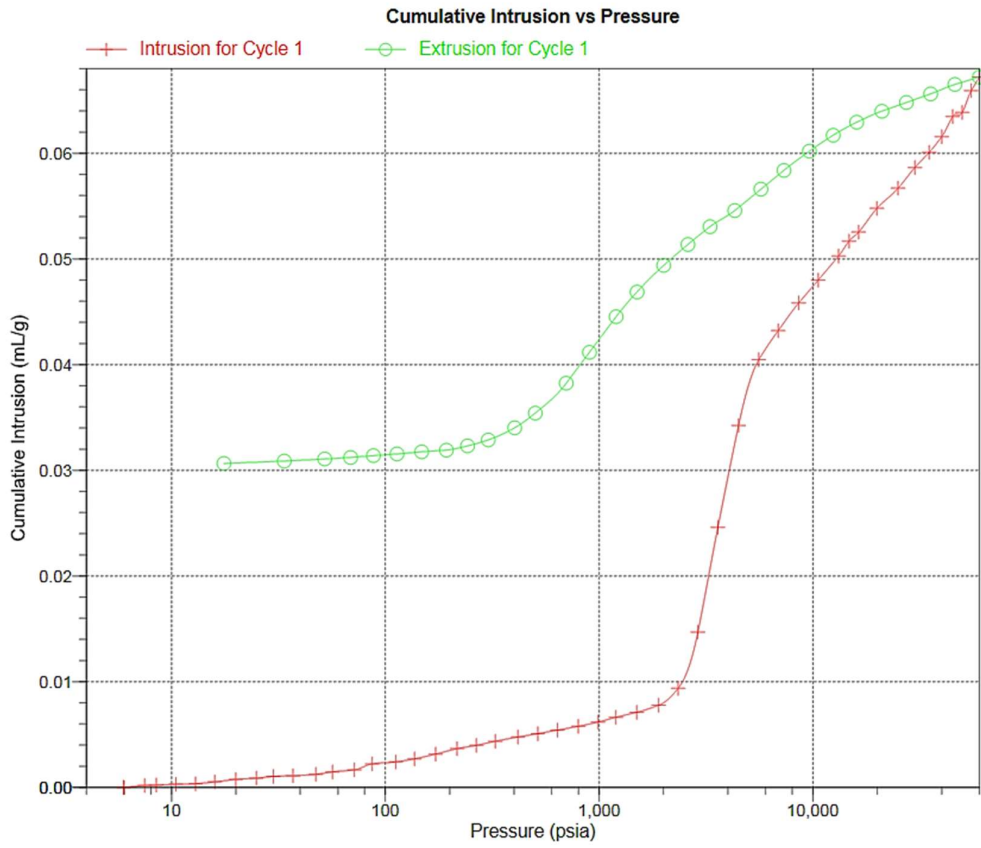
Threshold Pressure: 5.99 psia (Calculated)
Characteristic length = 30.1738 um
Conductivity formation factor = 0.000
Permeability constant = 0.00442
Permeability = 0.5888 mdarcy
BET Surface Area = 230.0000 m^2/g
Pore shape exponent = 1.00
Tortuosity factor = 0.011
Tortuosity = 5.4053
Percolation Fractal dimension = 2.005
Backbone Fractal dimension = 2.223

Mayer Stowe Summary

Interstitial porosity = 47.6300 %
Breakthrough pressure ratio = 3.3512

Material Compressibility

Linear Coefficient = N/A 1/psia
Quadratic Coefficient = N/A 1/psia^2





MICROMERITICS INSTRUMENT CORPORATION

AutoPore IV 9500 V1.09

Serial: 833

Port: 1/1

Page 1

Sample ID: 0.7 W_C
Operator: Ryno van der Merwe
Submitter: Mariesa Schoeman
File: C:\9500\DATA\000-366.SMP

LP Analysis Time: 2020/03/11 4:46:39PM
HP Analysis Time: 2020/03/12 9:26:23AM
Report Time: 2020/03/23 2:52:46PM
Sample Weight: 7.5562 g
Correction Type: Formula
Show Neg. Int: No

Summary Report

Penetrometer parameters

Penetrometer: #s/n - (03) 15 Bulb, 1.131 Stem, Solid
Pen. Constant: 22.508 uL/pF
Stem Volume: 1.1310 mL
Pen. Volume: 16.0019 mL
Pen. Weight: 80.2381 g
Max. Head Pressure: 4.4500 psia
Assembly Weight: 254.8595 g

Hg Parameters

Adv. Contact Angle: 130.000 degrees
Hg Surface Tension: 485.000 dynes/cm
Rec. Contact Angle: 130.000 degrees
Hg Density: 13.5335 g/mL

User Parameters

Param 1: 0.000 Param 2: 0.000 Param 3: 0.000

Low Pressure:

Evacuation Pressure: 50 uHg
Evacuation Time: 30 mins
Mercury Filling Pressure: 0.52 psia
Equilibration Time: 10 secs

High Pressure:

Equilibration Time: 10 secs

Blank Correction by Formula

(From Pressure 13.00 to 60000.00 psia)

Intrusion Data Summary

Total Intrusion Volume = 0.0903 mL/g
Total Pore Area = 19.997 m^2/g
Median Pore Diameter (Volume) = 0.0443 um
Median Pore Diameter (Area) = 0.0072 um
Average Pore Diameter (4V/A) = 0.0181 um
Apparent (skeletal) Density = 2.5400 g/mL
Porosity = 18.6594 %
Stem Volume Used = 59 %

Pore Structure Summary

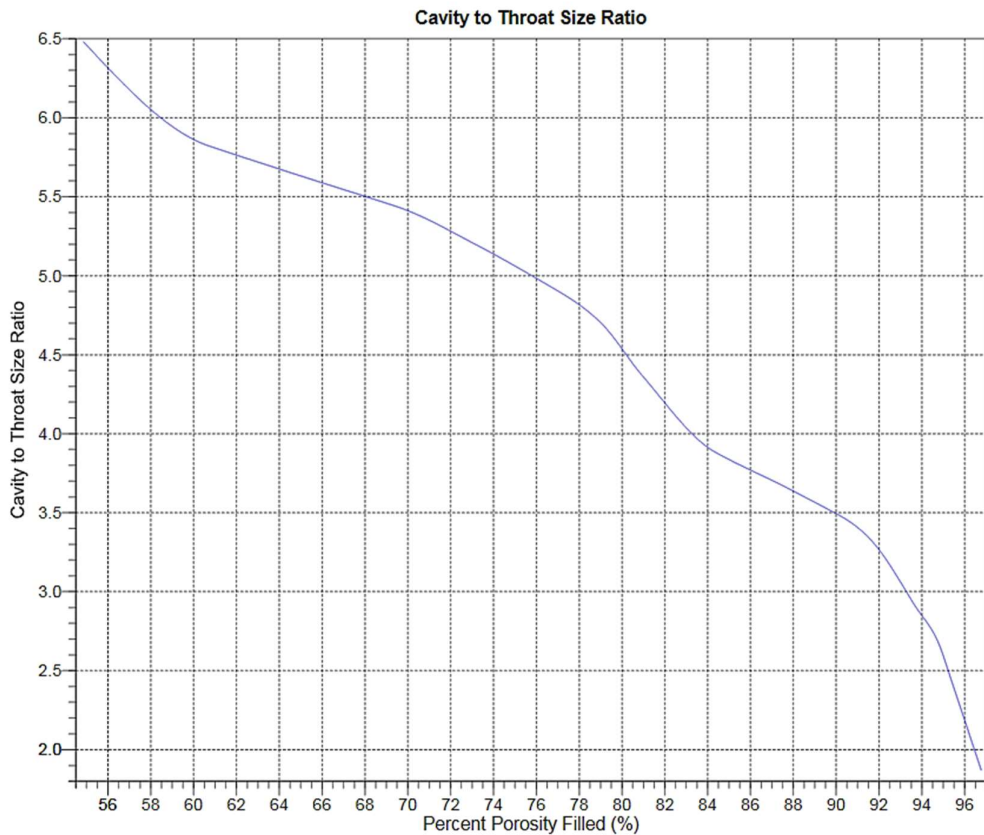
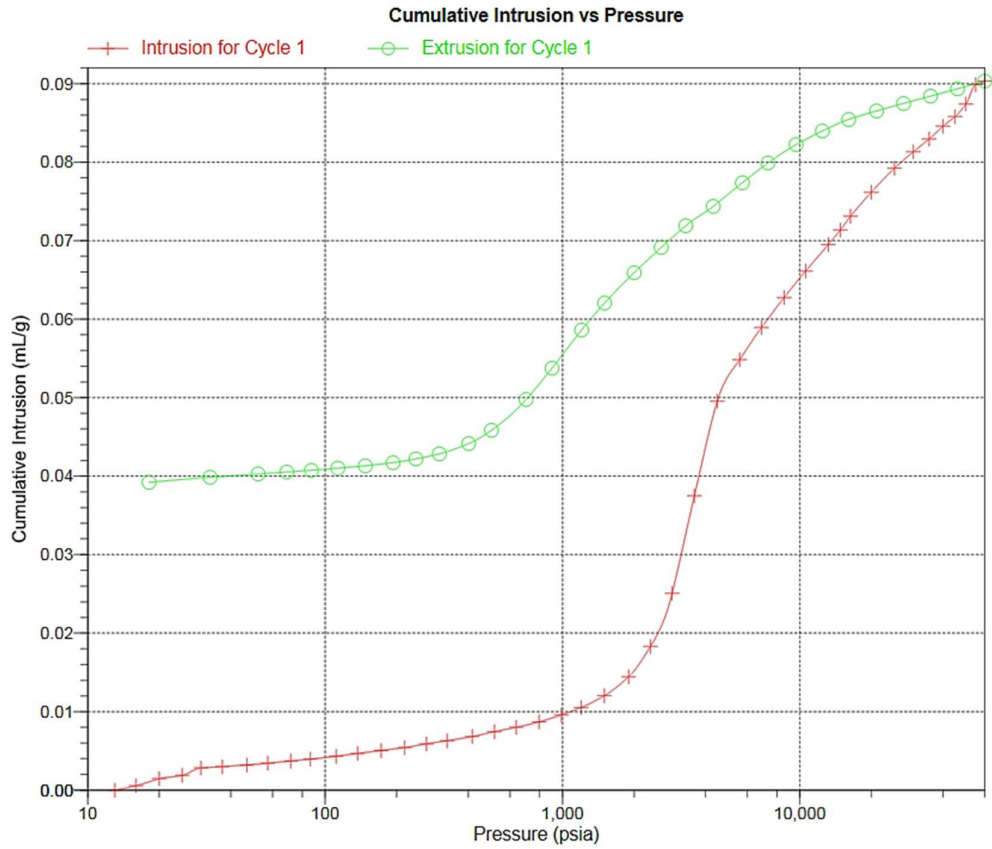
Threshold Pressure: 17.51 psia (Calculated)
Characteristic length = 10.3297 um
Conductivity formation factor = 0.001
Permeability constant = 0.00442
Permeability = 0.4733 mdarcy
BET Surface Area = 230.0000 m^2/g
Pore shape exponent = 1.00
Tortuosity factor = 2.163
Tortuosity = 5.6848
Percolation Fractal dimension = 2.204
Backbone Fractal dimension = 2.542

Mayer Stowe Summary

Interstitial porosity = 47.6300 %
Breakthrough pressure ratio = 3.3512

Material Compressibility

Linear Coefficient = N/A 1/psia
Quadratic Coefficient = N/A 1/psia^2



APPENDIX I

SHRINKAGE RESULTS

Sample Name	ΔL (mm)	Test Age (days)	Shrinkage (Microstrain, ϵ)	Sample Name	ΔL (mm)	Test Age (days)	Shrinkage (Microstrain, ϵ)	Average Shrinkage (Microstrain, ϵ)
0.3 - Dry 1	0.00	0.0	0.0	0.3 - Dry 2	0.00	0.0	0.0	0.0
0.3 - Dry 1	0.01	0.2	26.7	0.3 - Dry 2	0.01	0.2	33.3	30.0
0.3 - Dry 1	-0.01	1.0	-30.0	0.3 - Dry 2	0.00	1.0	13.3	-8.3
0.3 - Dry 1	0.01	2.1	30.0	0.3 - Dry 2	0.02	2.1	50.0	40.0
0.3 - Dry 1	0.02	3.1	56.7	0.3 - Dry 2	0.02	3.1	73.3	65.0
0.3 - Dry 1	0.04	5.0	146.7	0.3 - Dry 2	0.05	5.0	170.0	158.3
0.3 - Dry 1	0.06	6.1	196.7	0.3 - Dry 2	0.06	6.1	213.3	205.0
0.3 - Dry 1	0.10	10.1	343.3	0.3 - Dry 2	0.10	10.1	333.3	338.3
0.3 - Dry 1	0.11	12.2	356.7	0.3 - Dry 2	0.11	12.2	376.7	366.7
0.3 - Dry 1	0.15	18.3	506.7	0.3 - Dry 2	0.15	18.3	493.3	500.0
0.3 - Dry 1	0.16	21.0	546.7	0.3 - Dry 2	0.16	21.0	516.7	531.7
0.3 - Dry 1	0.17	24.2	576.7	0.3 - Dry 2	0.17	24.2	556.7	566.7
0.3 - Dry 1	0.18	27.2	596.7	0.3 - Dry 2	0.17	27.2	570.0	583.3
0.3 - Dry 1	0.17	28.2	566.7	0.3 - Dry 2	0.16	28.2	533.3	550.0
0.3 - Dry 1	0.17	31.2	570.0	0.3 - Dry 2	0.16	31.2	530.0	550.0
0.3 - Dry 1	0.18	34.0	606.7	0.3 - Dry 2	0.17	34.0	566.7	586.7
0.3 - Dry 1	0.19	38.3	623.3	0.3 - Dry 2	0.18	38.2	593.3	608.3
0.3 - Dry 1	0.18	40.3	600.0	0.3 - Dry 2	0.17	40.2	560.0	580.0
0.3 - Dry 1	0.18	42.1	590.0	0.3 - Dry 2	0.16	42.0	533.3	561.7
0.3 - Dry 1	0.18	45.0	593.3	0.3 - Dry 2	0.17	45.0	570.0	581.7
0.3 - Dry 1	0.18	52.3	603.3	0.3 - Dry 2	0.17	52.2	566.7	585.0
0.3 - Dry 1	0.19	55.1	616.7	0.3 - Dry 2	0.18	55.1	583.3	600.0
0.3 - Dry 1	0.19	60.2	623.3	0.3 - Dry 2	0.18	60.1	593.3	608.3

Sample Name	ΔL (mm)	Test Age (days)	Shrinkage (Microstrain, ϵ)
0.3 - Wet	0.00	0.0	0.0
0.3 - Wet	0.01	0.2	26.7
0.3 - Wet	-0.02	1.1	-50.0
0.3 - Wet	-0.01	2.2	-46.7
0.3 - Wet	-0.02	3.2	-60.0
0.3 - Wet	-0.02	5.1	-66.7
0.3 - Wet	-0.02	6.2	-66.7
0.3 - Wet	-0.02	10.2	-76.7
0.3 - Wet	-0.04	12.2	-123.3
0.3 - Wet	-0.03	18.3	-113.3
0.3 - Wet	-0.03	21.1	-106.7
0.3 - Wet	-0.03	24.3	-96.7
0.3 - Wet	-0.03	27.3	-93.3
0.3 - Wet	-0.03	27.3	-90.0
0.3 - Wet	-0.03	28.0	-96.7
0.3 - Wet	-0.03	28.3	-96.7
0.3 - Wet	-0.03	31.2	-83.3
0.3 - Wet	0.01	34.1	16.7
0.3 - Wet	0.02	38.3	70.0
0.3 - Wet	0.03	40.3	116.7
0.3 - Wet	0.04	42.1	146.7
0.3 - Wet	0.07	45.0	240.0
0.3 - Wet	0.08	48.3	273.3
0.3 - Wet	0.10	52.3	336.7
0.3 - Wet	0.11	55.2	370.0
0.3 - Wet	0.13	60.2	423.3

Sample Name	ΔL (mm)	Test Age (days)	Shrinkage (Microstrain, ϵ)	Sample Name	ΔL (mm)	Test Age (days)	Shrinkage (Microstrain, ϵ)	Average Shrinkage (Microstrain, ϵ)
0.4 - Dry 1	0.00	0.0	0.0	0.4 - Dry 2	0.00	0.0	0.0	0.0
0.4 - Dry 1	0.00	0.2	10.0	0.4 - Dry 2	0.01	0.2	50.0	30.0
0.4 - Dry 1	0.00	1.0	-13.3	0.4 - Dry 2	0.01	1.0	30.0	8.3
0.4 - Dry 1	0.00	2.1	6.7	0.4 - Dry 2	0.02	2.1	76.7	41.7
0.4 - Dry 1	0.02	3.1	56.7	0.4 - Dry 2	0.03	3.1	113.3	85.0
0.4 - Dry 1	0.04	5.1	146.7	0.4 - Dry 2	0.06	5.1	196.7	171.7
0.4 - Dry 1	0.06	6.1	190.0	0.4 - Dry 2	0.07	6.1	250.0	220.0
0.4 - Dry 1	0.10	10.1	333.3	0.4 - Dry 2	0.11	10.1	380.0	356.7
0.4 - Dry 1	0.11	12.2	356.7	0.4 - Dry 2	0.12	12.2	403.3	380.0
0.4 - Dry 1	0.14	18.4	473.3	0.4 - Dry 2	0.16	18.3	526.7	500.0
0.4 - Dry 1	0.15	21.1	516.7	0.4 - Dry 2	0.17	21.0	566.7	541.7
0.4 - Dry 1	0.16	24.3	546.7	0.4 - Dry 2	0.18	24.2	600.0	573.3
0.4 - Dry 1	0.17	27.3	573.3	0.4 - Dry 2	0.18	27.2	613.3	593.3
0.4 - Dry 1	0.17	28.3	553.3	0.4 - Dry 2	0.18	28.2	590.0	571.7
0.4 - Dry 1	0.17	31.3	576.7	0.4 - Dry 2	0.18	31.2	610.0	593.3
0.4 - Dry 1	0.18	34.1	593.3	0.4 - Dry 2	0.19	34.0	640.0	616.7
0.4 - Dry 1	0.19	38.3	616.7	0.4 - Dry 2	0.20	38.2	666.7	641.7
0.4 - Dry 1	0.18	40.3	593.3	0.4 - Dry 2	0.19	40.2	643.3	618.3
0.4 - Dry 1	0.18	42.1	586.7	0.4 - Dry 2	0.20	42.0	660.0	623.3
0.4 - Dry 1	0.18	45.1	583.3	0.4 - Dry 2	0.20	45.0	656.7	620.0
0.4 - Dry 1	0.18	52.3	593.3	0.4 - Dry 2	0.20	52.2	663.3	628.3
0.4 - Dry 1	0.18	55.2	610.0	0.4 - Dry 2	0.21	55.1	683.3	646.7
0.4 - Dry 1	0.18	60.2	610.0	0.4 - Dry 2	0.21	60.1	696.7	653.3

Sample Name	ΔL (mm)	Test Age (days)	Shrinkage (Microstrain, ϵ)
0.4 - Wet	0.00	0.0	0.0
0.4 - Wet	0.02	0.2	66.7
0.4 - Wet	0.00	1.0	6.7
0.4 - Wet	0.00	2.1	-16.7
0.4 - Wet	0.00	3.1	-3.3
0.4 - Wet	0.00	5.1	-13.3
0.4 - Wet	0.00	6.2	-13.3
0.4 - Wet	-0.01	10.1	-36.7
0.4 - Wet	-0.02	12.2	-73.3
0.4 - Wet	-0.02	18.3	-60.0
0.4 - Wet	-0.02	21.0	-53.3
0.4 - Wet	-0.01	24.2	-40.0
0.4 - Wet	-0.01	27.2	-43.3
0.4 - Wet	-0.01	27.2	-40.0
0.4 - Wet	-0.01	27.9	-46.7
0.4 - Wet	-0.01	28.2	-46.7
0.4 - Wet	-0.01	31.2	-23.3
0.4 - Wet	0.04	34.0	116.7
0.4 - Wet	0.05	38.2	170.0
0.4 - Wet	0.07	40.2	220.0
0.4 - Wet	0.07	42.0	236.7
0.4 - Wet	0.09	45.0	310.0
0.4 - Wet	0.11	48.2	350.0
0.4 - Wet	0.12	52.2	396.7
0.4 - Wet	0.13	55.1	426.7
0.4 - Wet	0.14	60.1	466.7

Sample Name	ΔL (mm)	Test Age (days)	Shrinkage (Microstrain, ϵ)	Sample Name	ΔL (mm)	Test Age (days)	Shrinkage (Microstrain, ϵ)	Average Shrinkage (Microstrain, ϵ)
0.5 - Dry 1	0.00	0.0	0.0	0.5 - Dry 2	0.00	0.0	0.0	0.0
0.5 - Dry 1	0.01	0.3	33.3	0.5 - Dry 2	0.01	0.3	40.0	36.7
0.5 - Dry 1	0.01	1.0	20.0	0.5 - Dry 2	0.01	1.0	40.0	30.0
0.5 - Dry 1	0.03	2.1	86.7	0.5 - Dry 2	0.03	2.1	103.3	95.0
0.5 - Dry 1	0.05	3.1	150.0	0.5 - Dry 2	0.05	3.1	160.0	155.0
0.5 - Dry 1	0.07	5.1	243.3	0.5 - Dry 2	0.08	5.1	260.0	251.7
0.5 - Dry 1	0.09	6.2	293.3	0.5 - Dry 2	0.10	6.2	320.0	306.7
0.5 - Dry 1	0.13	10.1	420.0	0.5 - Dry 2	0.14	10.1	456.7	438.3
0.5 - Dry 1	0.13	12.2	440.0	0.5 - Dry 2	0.14	12.2	480.0	460.0
0.5 - Dry 1	0.16	18.3	530.0	0.5 - Dry 2	0.17	18.1	576.7	553.3
0.5 - Dry 1	0.17	21.1	566.7	0.5 - Dry 2	0.19	20.8	616.7	591.7
0.5 - Dry 1	0.18	24.2	593.3	0.5 - Dry 2	0.20	24.0	653.3	623.3
0.5 - Dry 1	0.18	27.2	610.0	0.5 - Dry 2	0.20	27.0	673.3	641.7
0.5 - Dry 1	0.18	28.2	596.7	0.5 - Dry 2	0.20	28.0	660.0	628.3
0.5 - Dry 1	0.18	31.2	613.3	0.5 - Dry 2	0.20	31.0	676.7	645.0
0.5 - Dry 1	0.19	34.0	626.7	0.5 - Dry 2	0.21	33.8	700.0	663.3
0.5 - Dry 1	0.20	38.2	656.7	0.5 - Dry 2	0.22	38.0	723.3	690.0
0.5 - Dry 1	0.19	40.2	616.7	0.5 - Dry 2	0.21	40.0	706.7	661.7
0.5 - Dry 1	0.19	42.1	620.0	0.5 - Dry 2	0.21	41.8	703.3	661.7
0.5 - Dry 1	0.19	45.0	616.7	0.5 - Dry 2	0.21	44.8	706.7	661.7
0.5 - Dry 1	0.19	52.2	643.3	0.5 - Dry 2	0.22	52.0	733.3	688.3
0.5 - Dry 1	0.20	55.1	656.7	0.5 - Dry 2	0.22	54.9	743.3	700.0
0.5 - Dry 1	0.20	60.1	656.7	0.5 - Dry 2	0.22	59.9	746.7	701.7

Sample Name	ΔL (mm)	Test Age (days)	Shrinkage (Microstrain, ϵ)
0.5 - Wet	0.00	0.0	0.0
0.5 - Wet	-0.06	0.3	-210.0
0.5 - Wet	-0.03	1.0	-106.7
0.5 - Wet	-0.05	2.1	-173.3
0.5 - Wet	-0.05	3.1	-160.0
0.5 - Wet	-0.05	5.1	-153.3
0.5 - Wet	-0.02	6.2	-63.3
0.5 - Wet	-0.03	10.1	-100.0
0.5 - Wet	-0.04	12.2	-133.3
0.5 - Wet	-0.05	18.3	-166.7
0.5 - Wet	-0.04	21.1	-143.3
0.5 - Wet	-0.05	24.3	-153.3
0.5 - Wet	-0.03	27.3	-116.7
0.5 - Wet	-0.04	27.3	-150.0
0.5 - Wet	-0.05	28.0	-156.7
0.5 - Wet	-0.04	28.3	-143.3
0.5 - Wet	-0.04	31.2	-133.3
0.5 - Wet	0.03	34.1	106.7
0.5 - Wet	0.03	38.3	96.7
0.5 - Wet	0.05	40.3	173.3
0.5 - Wet	0.03	42.1	103.3
0.5 - Wet	0.08	45.0	263.3
0.5 - Wet	0.08	48.3	263.3
0.5 - Wet	0.08	52.3	266.7
0.5 - Wet	0.10	55.2	340.0
0.5 - Wet	0.10	60.1	316.7

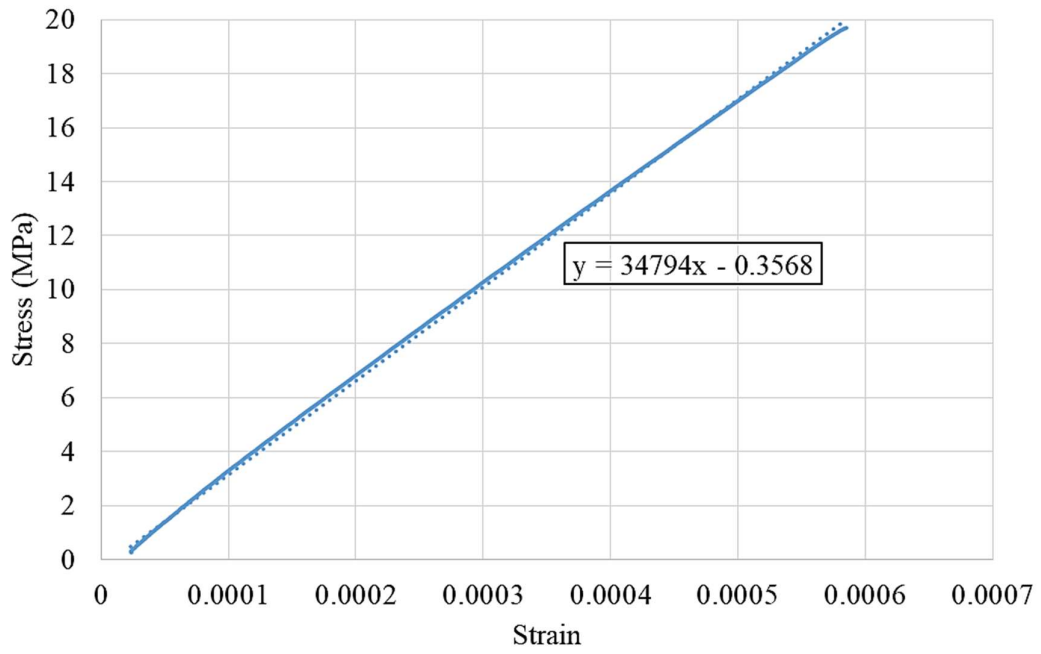
Sample Name	ΔL (mm)	Test Age (days)	Shrinkage (Microstrain, ϵ)	Sample Name	ΔL (mm)	Test Age (days)	Shrinkage (Microstrain, ϵ)	Average Shrinkage (Microstrain, ϵ)
0.6 - Dry 1	0.00	0.0	0.0	0.6 - Dry 2	0.00	0.0	0.0	0.0
0.6 - Dry 1	0.01	0.3	30.0	0.6 - Dry 2	0.02	0.3	60.0	45.0
0.6 - Dry 1	0.01	1.0	40.0	0.6 - Dry 2	0.02	1.0	70.0	55.0
0.6 - Dry 1	0.04	2.1	146.7	0.6 - Dry 2	0.05	2.1	170.0	158.3
0.6 - Dry 1	0.05	3.1	166.7	0.6 - Dry 2	0.06	3.1	186.7	176.7
0.6 - Dry 1	0.09	5.1	296.7	0.6 - Dry 2	0.09	5.1	303.3	300.0
0.6 - Dry 1	0.10	6.2	333.3	0.6 - Dry 2	0.11	6.2	353.3	343.3
0.6 - Dry 1	0.13	10.1	433.3	0.6 - Dry 2	0.14	10.1	470.0	451.7
0.6 - Dry 1	0.13	12.2	436.7	0.6 - Dry 2	0.14	12.2	480.0	458.3
0.6 - Dry 1	0.16	18.3	516.7	0.6 - Dry 2	0.17	18.3	566.7	541.7
0.6 - Dry 1	0.16	21.1	536.7	0.6 - Dry 2	0.18	21.1	600.0	568.3
0.6 - Dry 1	0.17	24.2	550.0	0.6 - Dry 2	0.19	24.2	623.3	586.7
0.6 - Dry 1	0.17	27.2	580.0	0.6 - Dry 2	0.19	27.2	633.3	606.7
0.6 - Dry 1	0.18	28.3	583.3	0.6 - Dry 2	0.19	28.2	626.7	605.0
0.6 - Dry 1	0.18	31.2	593.3	0.6 - Dry 2	0.20	31.2	650.0	621.7
0.6 - Dry 1	0.18	34.1	596.7	0.6 - Dry 2	0.20	34.0	653.3	625.0
0.6 - Dry 1	0.18	38.3	613.3	0.6 - Dry 2	0.20	38.3	680.0	646.7
0.6 - Dry 1	0.17	40.3	570.0	0.6 - Dry 2	0.19	40.3	640.0	605.0
0.6 - Dry 1	0.18	42.1	590.0	0.6 - Dry 2	0.20	42.1	653.3	621.7
0.6 - Dry 1	0.18	45.0	583.3	0.6 - Dry 2	0.20	45.0	653.3	618.3
0.6 - Dry 1	0.18	52.3	600.0	0.6 - Dry 2	0.20	52.2	666.7	633.3
0.6 - Dry 1	0.19	55.2	616.7	0.6 - Dry 2	0.21	55.1	690.0	653.3
0.6 - Dry 1	0.19	60.1	630.0	0.6 - Dry 2	0.21	60.1	700.0	665.0

Sample Name	ΔL (mm)	Test Age (days)	Shrinkage (Microstrain, ϵ)
0.6 - Wet	0.00	0.0	0.0
0.6 - Wet	-0.01	0.3	-30.0
0.6 - Wet	-0.02	1.0	-76.7
0.6 - Wet	-0.03	2.1	-83.3
0.6 - Wet	-0.02	3.1	-80.0
0.6 - Wet	-0.03	5.1	-86.7
0.6 - Wet	-0.03	6.2	-90.0
0.6 - Wet	-0.04	10.1	-120.0
0.6 - Wet	-0.04	12.2	-116.7
0.6 - Wet	-0.05	18.3	-153.3
0.6 - Wet	-0.04	21.1	-146.7
0.6 - Wet	-0.04	24.2	-140.0
0.6 - Wet	-0.04	27.2	-143.3
0.6 - Wet	-0.04	27.3	-136.7
0.6 - Wet	-0.04	28.0	-130.0
0.6 - Wet	-0.04	28.2	-123.3
0.6 - Wet	-0.01	31.2	-33.3
0.6 - Wet	0.04	34.0	143.3
0.6 - Wet	0.06	38.3	210.0
0.6 - Wet	0.07	40.3	243.3
0.6 - Wet	0.08	42.1	253.3
0.6 - Wet	0.09	45.0	310.0
0.6 - Wet	0.10	48.2	326.7
0.6 - Wet	0.11	52.2	353.3
0.6 - Wet	0.12	55.1	393.3
0.6 - Wet	0.12	60.1	416.7

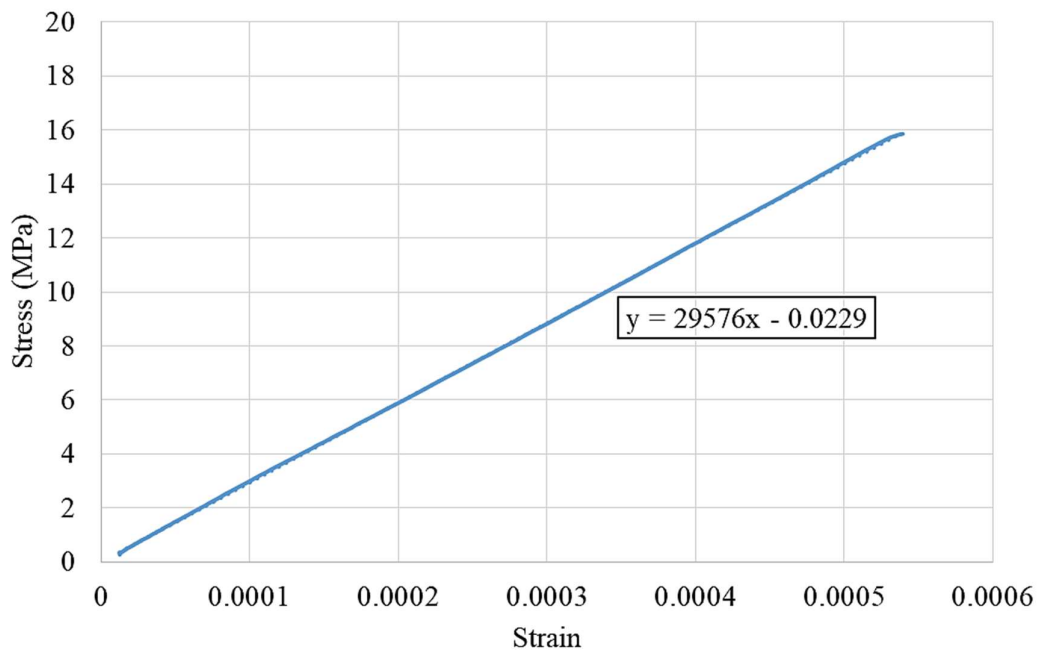
Sample Name	ΔL (mm)	Test Age (days)	Shrinkage (Microstrain, ϵ)	Sample Name	ΔL (mm)	Test Age (days)	Shrinkage (Microstrain, ϵ)	Average Shrinkage (Microstrain, ϵ)
0.7 - Dry 1	0.00	0.0	0.0	0.7 - Dry 2	0.00	0.0	0.0	0.0
0.7 - Dry 1	0.03	0.3	100.0	0.7 - Dry 2	0.04	0.3	121.2	110.6
0.7 - Dry 1	0.05	1.0	160.6	0.7 - Dry 2	0.04	1.0	115.2	137.9
0.7 - Dry 1	0.08	2.2	245.5	0.7 - Dry 2	0.07	2.2	221.2	233.3
0.7 - Dry 1	0.10	3.2	300.0	0.7 - Dry 2	0.09	3.2	275.8	287.9
0.7 - Dry 1	0.13	5.1	384.8	0.7 - Dry 2	0.11	5.1	345.5	365.2
0.7 - Dry 1	0.15	6.2	454.5	0.7 - Dry 2	0.13	6.2	384.8	419.7
0.7 - Dry 1	0.19	10.2	569.7	0.7 - Dry 2	0.12	10.2	372.7	471.2
0.7 - Dry 1	0.21	12.2	624.2	0.7 - Dry 2	0.18	12.2	536.4	580.3
0.7 - Dry 1	0.18	18.3	530.3	0.7 - Dry 2	0.22	18.3	669.7	600.0
0.7 - Dry 1	0.23	21.1	700.0	0.7 - Dry 2	0.22	21.1	669.7	684.8
0.7 - Dry 1	0.26	24.2	784.8	0.7 - Dry 2	0.23	24.2	690.9	737.9
0.7 - Dry 1	0.26	27.2	800.0	0.7 - Dry 2	0.23	27.2	690.9	745.5
0.7 - Dry 1	0.25	28.2	769.7	0.7 - Dry 2	0.22	28.2	675.8	722.7
0.7 - Dry 1	0.26	31.2	775.8	0.7 - Dry 2	0.23	31.2	684.8	730.3
0.7 - Dry 1	0.24	34.1	730.3	0.7 - Dry 2	0.21	34.1	645.5	687.9
0.7 - Dry 1	0.27	38.3	830.3	0.7 - Dry 2	0.25	38.3	751.5	790.9
0.7 - Dry 1	0.28	40.3	839.4	0.7 - Dry 2	0.26	40.3	800.0	819.7
0.7 - Dry 1	0.28	42.1	845.5	0.7 - Dry 2	0.25	42.1	751.5	798.5
0.7 - Dry 1	0.28	45.0	854.5	0.7 - Dry 2	0.26	45.0	800.0	827.3
0.7 - Dry 1	0.30	52.3	906.1	0.7 - Dry 2	0.27	52.3	815.2	860.6
0.7 - Dry 1	0.30	55.1	906.1	0.7 - Dry 2	0.27	55.1	830.3	868.2
0.7 - Dry 1	0.29	60.1	875.8	0.7 - Dry 2	0.27	60.1	830.3	853.0

Sample Name	ΔL (mm)	Test Age (days)	Shrinkage (Microstrain, ϵ)
0.7 - Wet	0.00	0.0	0.0
0.7 - Wet	-0.01	0.3	-16.7
0.7 - Wet	-0.03	1.0	-103.3
0.7 - Wet	-0.02	2.2	-60.0
0.7 - Wet	-0.01	3.2	-16.7
0.7 - Wet	-0.01	5.1	-43.3
0.7 - Wet	-0.01	6.2	-43.3
0.7 - Wet	0.02	10.2	66.7
0.7 - Wet	0.01	12.2	50.0
0.7 - Wet	-0.01	18.3	-16.7
0.7 - Wet	0.01	21.1	43.3
0.7 - Wet	0.01	24.2	26.7
0.7 - Wet	0.00	27.2	6.7
0.7 - Wet	0.01	27.3	26.7
0.7 - Wet	0.01	28.0	50.0
0.7 - Wet	0.02	28.3	60.0
0.7 - Wet	0.05	31.2	160.0
0.7 - Wet	0.08	34.1	270.0
0.7 - Wet	0.13	38.3	440.0
0.7 - Wet	0.14	40.3	450.0
0.7 - Wet	0.15	42.1	516.7
0.7 - Wet	0.16	45.0	540.0
0.7 - Wet	0.15	48.3	516.7
0.7 - Wet	0.15	52.3	516.7
0.7 - Wet	0.16	55.1	520.0
0.7 - Wet	0.16	60.1	523.3

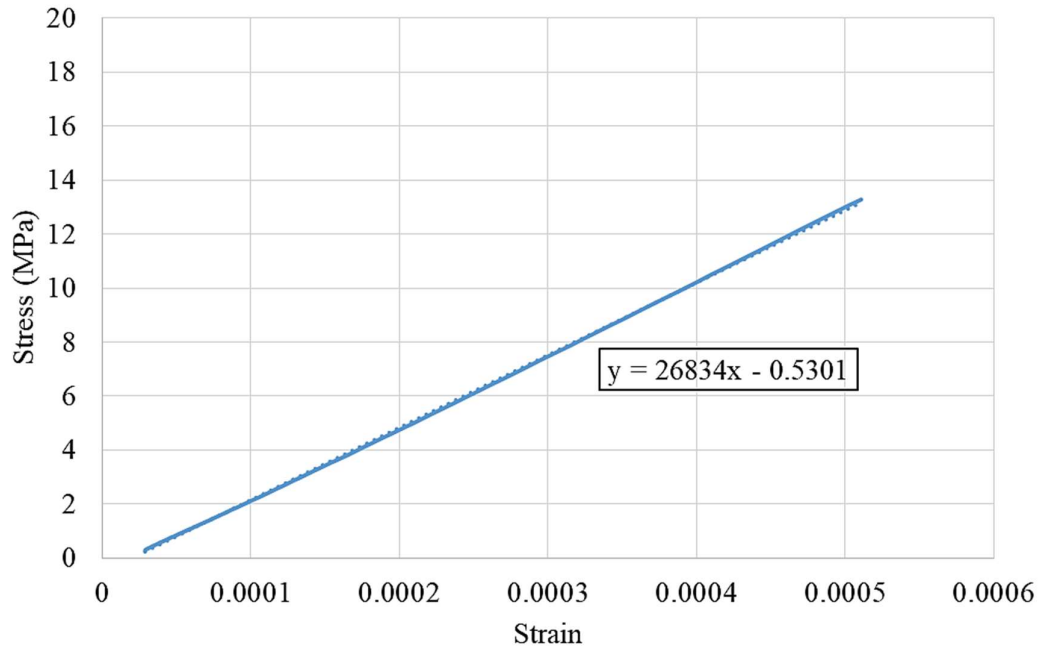
APPENDIX J
GRAPHS ILLUSTRATING
THE E-VALUES



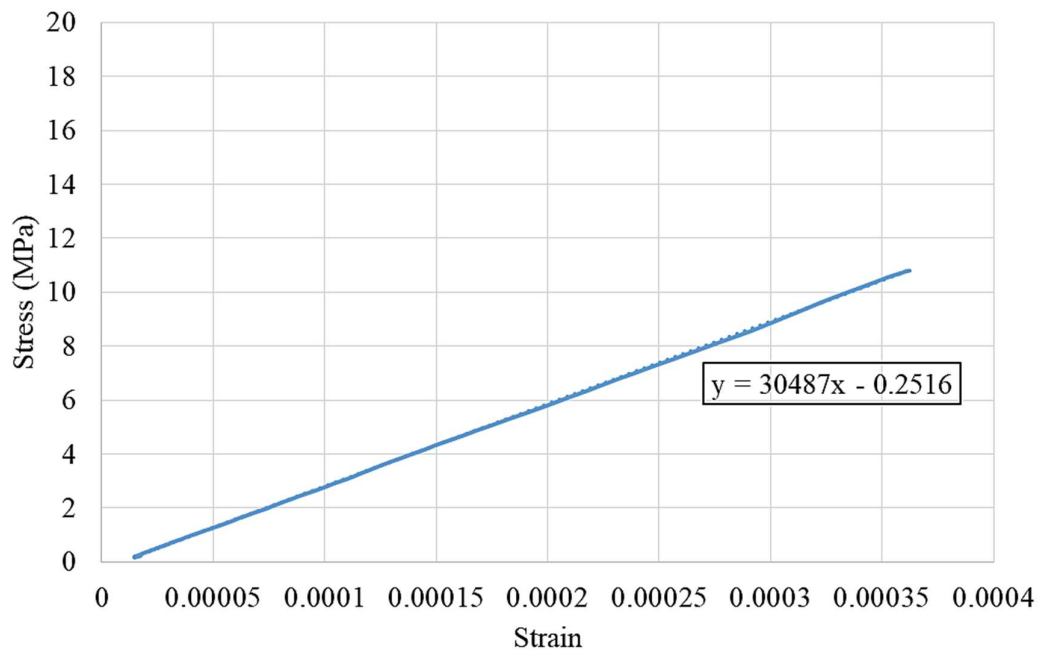
E-value Graph for the 0.3 W/C Ratio Dry Sample.



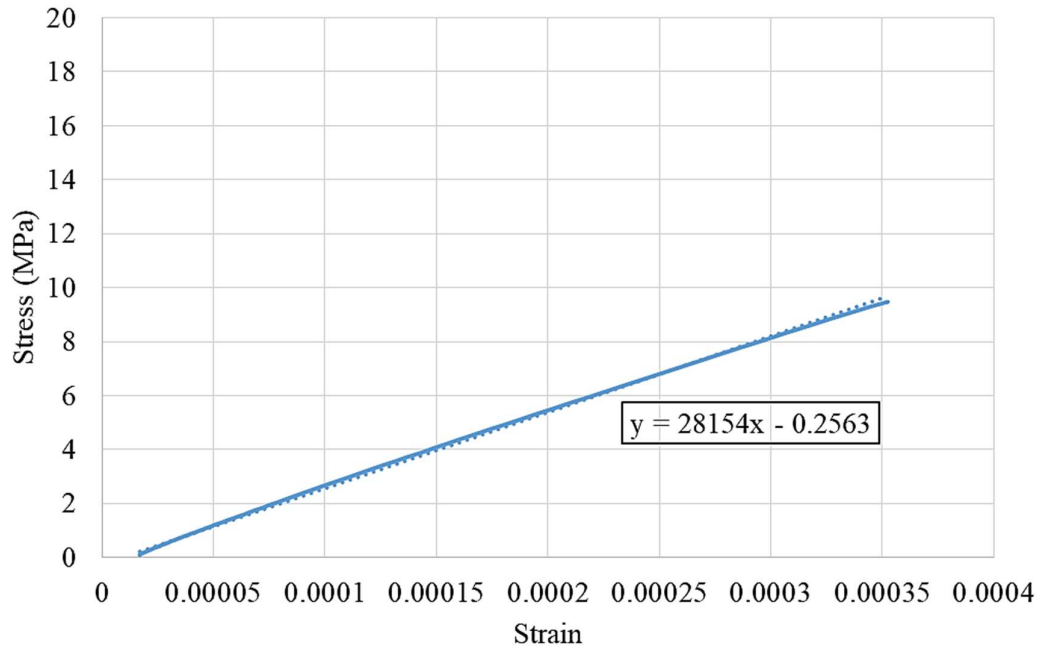
E-value Graph for the 0.4 W/C Ratio Dry Sample.



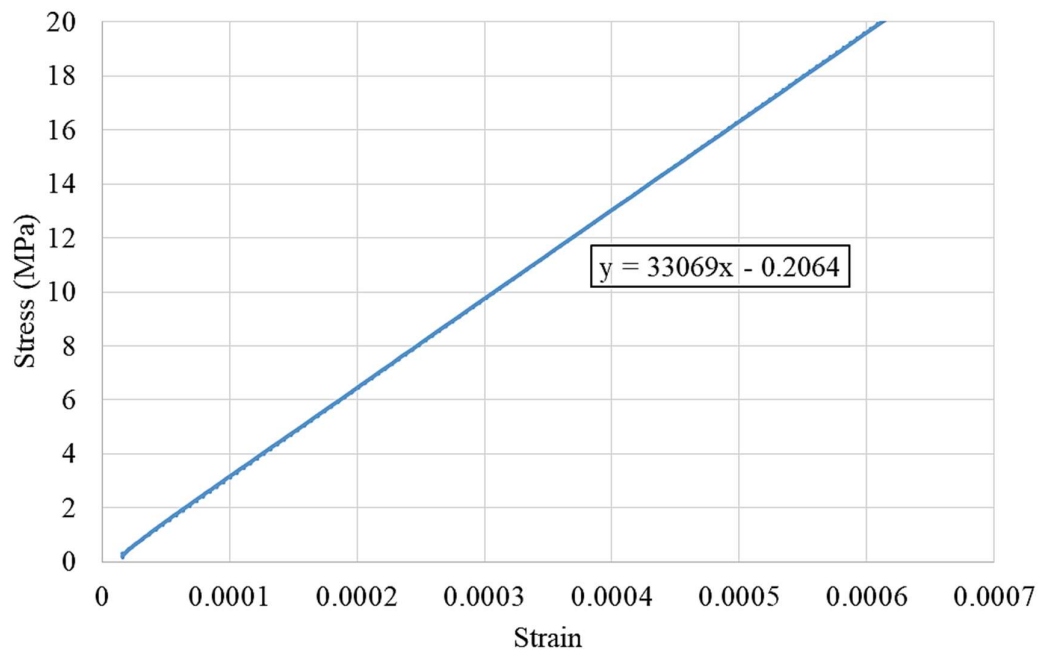
E-value Graph for the 0.5 W/C Ratio Dry Sample.



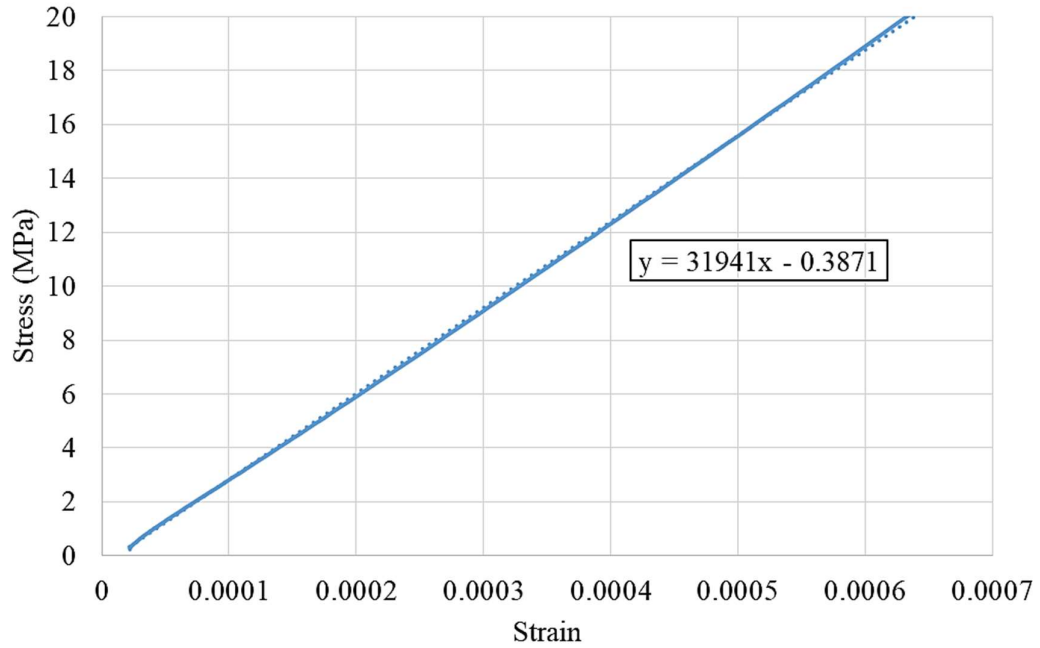
E-value Graph for the 0.6 W/C Ratio Dry Sample.



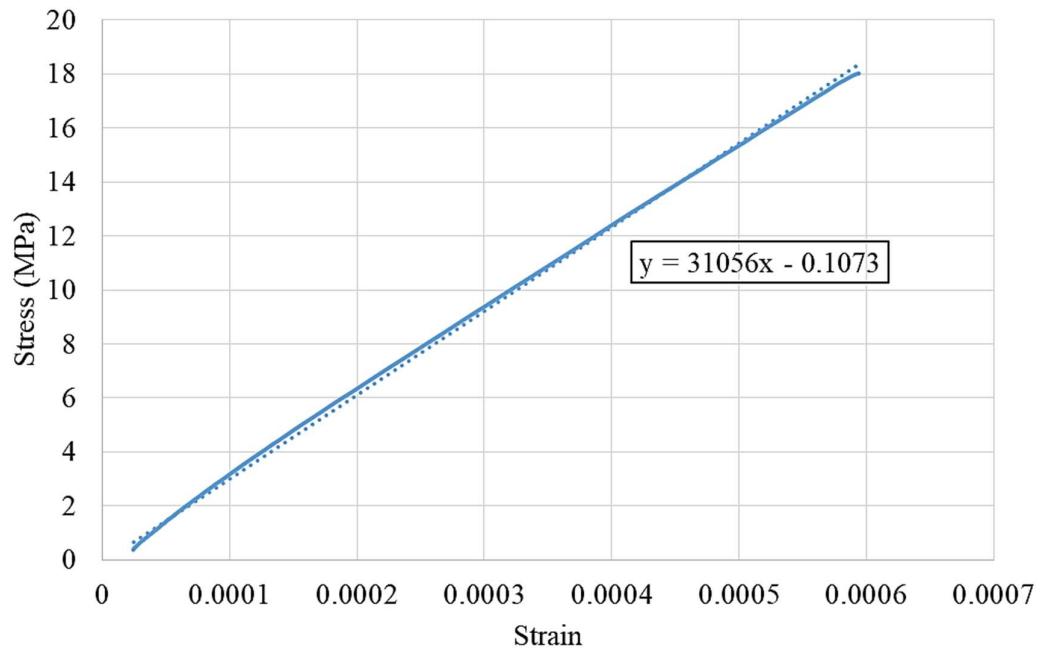
E-value Graph for the 0.7 W/C Ratio Dry Sample.



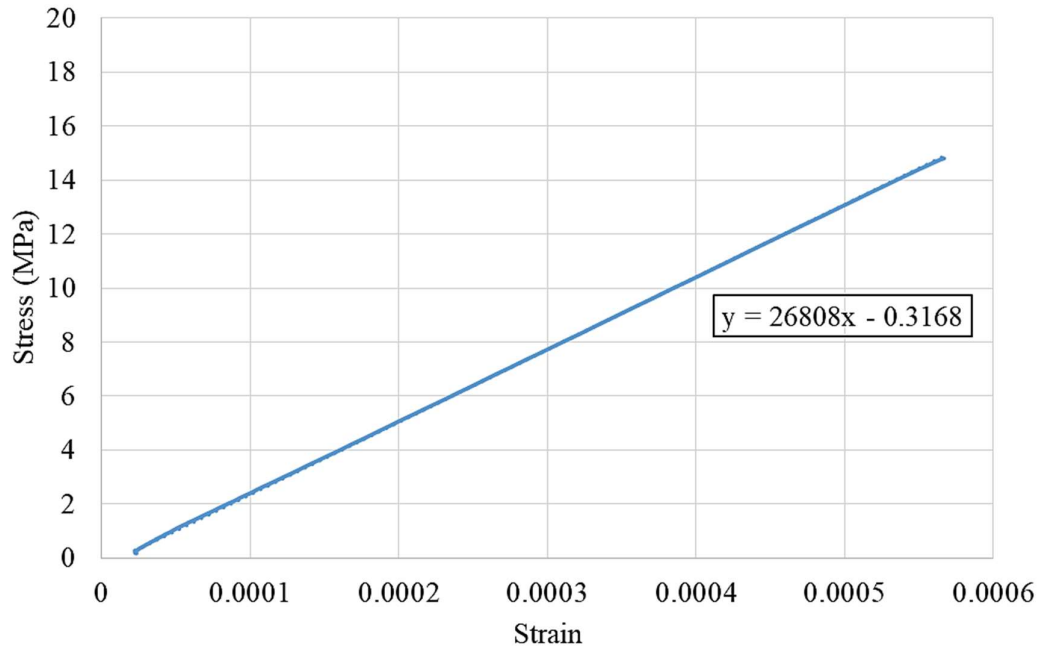
E-value Graph for the 0.3 W/C Ratio Wet Sample.



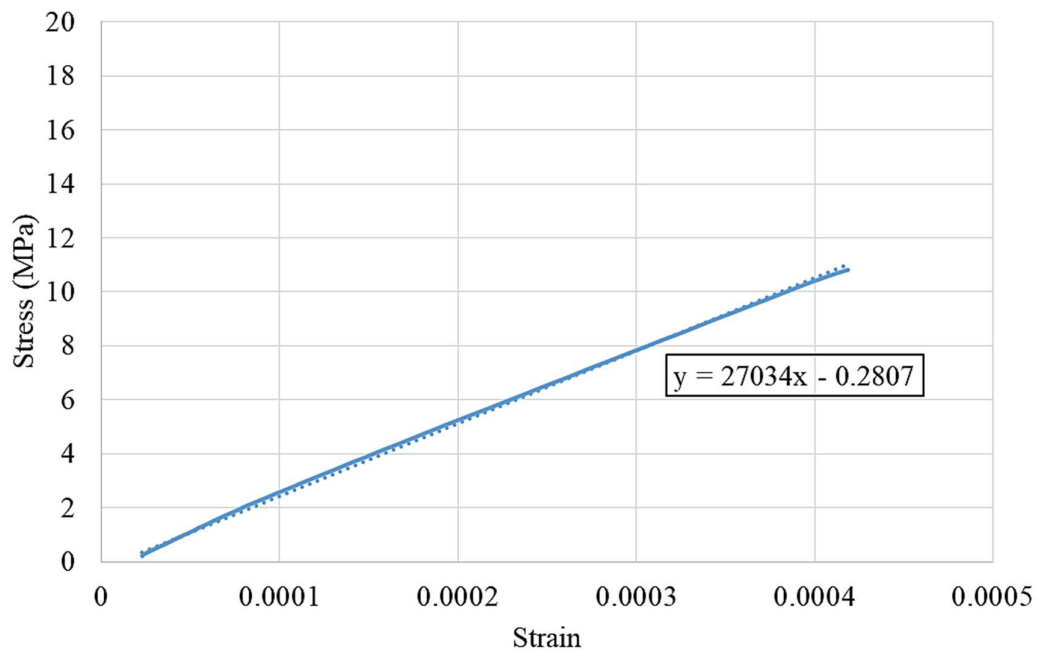
E-value Graph for the 0.4 W/C Ratio Wet Sample.



E-value Graph for the 0.5 W/C Ratio Wet Sample.



E-value Graph for the 0.6 W/C Ratio Wet Sample.



E-value Graph for the 0.7 W/C Ratio Wet Sample.